UNIVERSITÉ DE MONTRÉAL

DESIGN, OPTIMIZATION, AND EVALUATION OF A FUSIONLESS DEVICE TO INDUCE GROWTH MODULATION AND CORRECT SPINAL CURVATURES IN ADOLESCENT IDIOPATHIC SCOLIOSIS

MARK DRISCOLL

INSTITUT DE GÉNIE BIOMÉDICAL

ÉCOLE POLYTECHNIQUE DE MONTRÉAL

THÈSE PRÉSENTÉE EN VUE DE L'OBTENTION

DU DIPLÔME DE PHILOSOPHIAE DOCTOR (Ph.D.)

(GÉNIE BIOMÉDICAL)

JUIN 2011

UNIVERSITÉ DE MONTRÉAL

ÉCOLE POLYTECHNIQUE DE MONTRÉAL

Cette thèse intitulée:

DESIGN, OPTIMIZATION, AND EVALUATION OF A FUSIONLESS DEVICE TO INDUCE GROWTH MODULATION AND CORRECT SPINAL CURVATURES IN ADOLESCENT IDIOPATHIC SCOLIOSIS

présentée par : DRISCOLL Mark
en vue de l'obtention du diplôme de : Philosophiae Doctor
a été dûment acceptée par le jury d'examen constitué de :

Mme. VILLEMURE Isabelle, Ph.D., présidente
M. AUBIN Carl-Éric, Ph.D., membre et directeur de recherche
M. MOREAU Alain, Ph.D., membre et codirecteur de recherche
M. PARENT Stefan, M.D., Ph.D., membre et codirecteur de recherche
M. LAVIGNE Patrick, M.D., Ph.D., membre
Mme. LANGELIER Ève, Ph.D., membre

ACKNOWLEDGEMENTS

It is my pleasure to extend my most sincere thank you to my research director Dr. Carl-Eric Aubin for having proposed the research project described herein. Dr. Aubin`s vast expertise and confidence guided the progression of my studies. In addition, Dr. Aubin was never hesitant to spend time to structure my experience as to ensure a high degree of professionalism while moulding me into a well-rounded researcher.

In addition, I would like acknowledge and thank the efforts from my research co-directors Dr. Alain Moreau and Dr. Stefan Parent. Both these gentleman always found the time to discuss and guide my research project while providing novel and insightful recommendations.

The research project described in this dissertation is the result of a team effort provided by a diverse area of expertise oriented under the amicable and skilful words from these distinguished professionals.

I also extend thanks to my lab partners, notably Drs. Christopher Driscoll, Julien Clin, and Hui Lin. Moreover, I thank my family, particularly my wife Jennifer, for encouraging me to pursue my ambitions in biomedical engineering.

Finally, I thank our financial partners the Natural Science and Engineering Research Council of Canada and Medtronic of Canada for their support.

RÉSUMÉ

La scoliose est une déformation musculo-squelettique complexe et tridimensionnelle de la colonne vertébrale. Les mécanismes de progression de la scoliose sont liés au principe de Hueter-Volkmann. Selon cette théorie, les chargements asymétriques des plaques de croissance altèrent la croissance du rachis (cunéiformisation des vertèbres). Une courbure scoliotique présentant un angle de Cobb supérieur à 50° nécessite généralement une intervention chirurgicale avec fusion rachidienne. Cette chirurgie implique des procédures particulièrement invasives et coûteuses, ce qui a incité plusieurs chercheurs à tenter de développer d'autres alternatives.

Des techniques minimalement invasives et sans fusion ont ainsi été élaborées pour contrôler et corriger un mauvais alignement de la colonne vertébrale avant qu'une progression trop importante des déformations scoliotiques ne se produise. Ces techniques tentent d'exploiter la croissance vertébrale résiduelle afin de corriger la cunéiformisation locale et d'aboutir à un réalignement progressif du rachis. Les traitements sans fusion semblent également mettre en péril la santé du disque intervertébral à long terme et se limitent à une correction 2D (plan frontal) de déformations intrinsèquement 3D. Mieux comprendre biomécaniquement la progression des déformations scoliotiques permettrait de développer des dispositifs sans fusion plus efficaces. Cela serait une contribution importante et innovatrice à l'amélioration du traitement de la scoliose idiopathique adolescente (SIA).

L'objectif global de cette thèse était le développement, l'optimisation, et l'évaluation expérimentale d'implants sans fusion afin de moduler la croissance et de corriger les déformations scoliotiques.

Les objectifs spécifiques étaient de 1) développer un modèle par éléments finis (MEF) de la colonne vertébrale intégrant une modélisation de la croissance; 2) exploiter ce MEF pour étudier les facteurs biomécaniques impliqués dans les mécanismes de progression de la SIA; 3) exploiter le MEF pour analyser la biomécanique des dispositifs sans fusion existant actuellement et repérer les améliorations pouvant être apportées à ces dispositifs; et 4) exploiter la plate-forme de conception conçue (analyses *in silico*, *in situ*, et *in vivo*) pour développer, optimiser, et valider de nouveaux dispositifs sans fusion modulateurs de croissance pour la correction des déformations de la SIA.

L'idée centrale de cette thèse est que le développement de nouveaux traitements sans fusion plus performants peut être réalisé en comprenant mieux les facteurs biomécaniques impliqués dans les mécanismes pathologiques de la SIA, en identifiant les lacunes des dispositifs sans fusion utilisés actuellement et en utilisant une plate-forme de conception complète incluant des analyses *in silico, in situ* et *in vivo*.

Cette idée centrale a été divisée suivant les hypothèses suivantes:

1) Des facteurs biomécaniques (différence des propriétés mécaniques entre la concavité et la convexité de la colonne scoliotique) augmentent les contraintes asymétriques sur les plaques de croissance épiphysaires de la vertèbre apicale de 25% et de ce fait augmentent la progression de la cunéiformisation vertébrale de 1° (soit 10%) sur un an de croissance à l'adolescence; 2) les dispositifs sans fusion modulateurs de croissance actuels (agrafes à mémoire de forme, agrafes en acier inox, et attaches souples) réduisent les chargement asymétriques sur les plaques de croissance de la vertèbre apicale de 35% et limitent la progression scoliotique à 10% sur deux ans de croissance adolescente; 3) un dispositif intravertébral épiphysaire amélioré permet de modifier la cunéiformisation vertébrale de 4° sans modifier la physiologie du disque intervertébral dans un modèle porcin après 12 semaines; et 4) une attache souple 3D permet de modifier la cunéiformisation vertébrale de 4° et la rotation axiale de 5° dans un modèle porcin après 12 semaines.

Afin de répondre à ces objectifs et d'évaluer ces hypothèses, un MEF a été conçu pour être utilisé comme plate-forme initiale de développement. A ce MEF a été intégré un système de contrôle itératif permettant de simuler la croissance physiologique en fonction de la variation de contraintes en se basant sur des données obtenues *in vivo*.

Premièrement, le MEF a étudié l'influence de facteurs biomécaniques (différences entre la concavité et la convexité des courbures scoliotiques: migration du nucléus vers la convexité, augmentation de la densité minérale osseuse et dégénérescence des disques sur la concavité) sur la progression de la SIA. Cette modélisation suggère que ces différences concavité-convexité augmentent les contraintes asymétriques de 37% et, par conséquent, augmentent la cunéiformisation vertébrale de 1° (10-20%) en moyenne. Les méthodes et découvertes

expérimentales de cette étude ont ensuite été étendues à l'analyse des dispositifs sans fusion actuellement utilisés.

Deuxièmement, le MEF a été utilisé pour explorer de façon critique les dispositifs sans fusion modulateur de croissance actuellement utilisés pour le traitement de la SIA. Les résultats de cette analyse ont démontré que ces dispositifs permettaient de réduire les chargements asymétriques sur la plaque de croissance à l'apex de la courbe de près de 50% (attache souple) et permettaient de réduire la progression scoliotique à 11% (agrafes inox et ancrage flexible). Cette analyse a également mis en évidence plusieurs limites qui pourraient être dépassées. Les concepts explorés réduisent seulement la croissance au niveau de la convexité des courbures, réduisent l'espace du disque, et négligent les déformations scoliotiques sagittales et transverses.

Suite à cette analyse, deux nouveaux dispositifs ont été proposés: un dispositif intravertébral épiphysaire (dispositif rigide qui stoppe localement la croissance sans réduire l'espace des disques) et une attache souple 3D permettant un contrôle de la scoliose dans les plans frontaux et sagittaux mais aussi une correction dans le plan transverse.

Le dispositif intravertébral épiphysaire a réussi à moduler la croissance sans fusion tout en conservant l'espace du disque. En outre, la santé du disque intervertébral est sauvegardée si le dispositif est inséré de façon appropriée. Les porcs utilisés dans nos expériences ont présenté une cunéiformisation vertébrale de 4.1°±3.6°, ce qui a permis d'obtenir une déformation vertébrale cumulative allant jusqu'à 25° sur seulement quatre niveaux instrumentés. Au niveau du point d'insertion du dispositif, la hauteur du disque a augmenté de 0,8 mm ± 0,2. La zone hypertrophique de la plaque de croissance et la hauteur de ses cellules ont été réduites par un facteur deux. La viabilité du disque a été confirmée par des classifications radiographique et histologique et via l'absence de collagène type X. Ce dispositif est le premier du genre à obtenir une modulation de croissance dans un modèle animal avec des dimensions de vertèbres semblables à ceux des adolescents sans réduire l'espace du disque intervertébral.

L'attache souple 3D a également entraîné une modulation de croissance locale dans les modèles porcins. Elle a produit une cunéiformisation des vertèbres de 3° et une correction dans le plan coronal allant jusqu'à 10°. Les effets dans les plans transverses et sagittaux ont été confirmés en utilisant des plateformes *in silico* et *in situ*, mais les limites expérimentales n'ont pas permis de

confirmer ces effets *in vivo* en toute objectivité. Ce dispositif sans fusion est le premier à tenter activement de fournir une correction dans les trois plans anatomiques.

Plusieurs avancées notables ont été réalisées dans le cadre de cette thèse. Le MEF développé offre un moyen novateur d'explorer différentes hypothèses biomécaniques liées à la progression de la SIA. En outre, dans le cadre de la conception d'un dispositif modulateur de croissance sans fusion, ce MEF a permis de réaliser des analyses préliminaires avant de poursuivre avec des essais *in situ* et *in vivo* coûteux. Deux nouveaux dispositifs sans fusion avec modulation de croissance (dispositif intravertébral épiphysaire et attache souple 3D) ont été développés et optimisés selon une approche de conception utilisant des analyses successives *in silico*, *in situ* et *in vivo*. Le MEF, les éléments biomécaniques associés à la progression de la SIA qui ont pu être identifiés, et enfin les instruments chirurgicaux conçus au cours de cette thèse constituent un pas prometteur vers l'amélioration des traitements des adolescents atteints de scoliose idiopathique.

ABSTRACT

Scoliosis is a spinal musculoskeletal deformity defined by a 3D deformity of the spine. The pathomechanism of scoliotic progression may be in part explained by the Hueter-Volkmann principle. This theory describes how increased loading of growth plates will reduce regular growth rates while the converse is also accurate. Further, when extended to the pathogenesis of scoliosis, it defines how asymmetric loading of the vertebral bodies leads to the progression of the deformity via vertebral wedging. Currently, a scoliotic curve reaching a magnitude of 50° Cobb deformation requires surgical intervention involving instrumentation and spinal fusion. The process of fusion is among the most invasive and expensive procedures, which has motivated several researchers to develop other alternatives.

The development of a less invasive technique, to control and correct a spinal misalignment before undesirable progression occurs, has subsequently been explored. Several fusionless devices have been developed that attempt to manipulate vertebral growth to correct vertebral wedging and, consequently, realign the spine. However, to date, these approaches have yet to be adopted in a clinical context. Moreover, devices actively pursued seemed to imperil the long term health of the intervertebral disc while corrective attempts are restricted to the unilateral manipulation of a 3D deformity. Therefore, enhanced biomechanical understanding of AIS pathomechanism in conjunction with the development of early and less invasive interventions would offer an important contribution to the improved treatment of AIS.

The global objective of this thesis was to design, optimize, and evaluated experimentally fusionless device concepts to induce growth modulation and correct spinal curvatures in adolescent idiopathic scoliosis (AIS). The specific objectives were to: 1) develop a FEM of the spine with integrated growth dynamics; 2) exploit the FEM to explore biomechanical factors involved in the pathomechanism of AIS; 3) exploit the FEM to analyze biomechanically current fusionless growth sparring devices to identify available avenues of improvement; and 4) exploit the devised developmental platform (*in silico*, *in situ*, and *in vivo* analyses) to develop, optimize, and validate novel and improved fusionless growth modulating devices for AIS.

The central theme addressed in this thesis is that: improved fusionless treatments for AIS may be developed subsequently to understanding biomechanical factors in its pathomechanism,

identifying shortcomings of previous fusionless devices, and utilizing a comprehensive design platform that include *in silico*, *in situ*, and *in vivo* analyses. This central theme was divided into the following hypotheses:

This doctoral thesis aims to verify the hypothesizes that: 1) biomechanical factors (concave-convex mechanical biases) of the scoliotic spine increases apical asymmetrical growth plate loading by 25% and, concomitantly, augment coronal vertebral wedge progression by 1° (10%) over 1 year of adolescent growth in a scoliotic spine; 2) current fusionless growth sparring methods (shape memory alloy staple, stainless staple, and flexible tether) reduce asymmetrical growth plate loading by 35% and restrict coronal scoliotic progression to 10% over 2 years of adolescent growth; 3) a refined intravertebral epiphyseal device will modify vertebral wedging by 4° without altering the intervertebral disc in a porcine model after 12 weeks; and 4) a 3D tether will modify vertebral wedging by 4° and axial rotation by 5° in a porcine model after 12 weeks.

The foremost undertaking of this thesis was the FEM platform development. This self-adjusting computer model was integrated with an iterative control system that simulated physiological growth as a function of stress variation respecting *in vivo* correlations. First, the FEM explored biomechanical factors (physiological stress shielding in the form of concave-convex mechanical biases: migration of nucleus to convexity and increased bone mineral density and local disc degeneration on concavity) in the pathomechanism of AIS. This interpretation suggests that concave-convex mechanical biases increased apical asymmetrical stress distribution by 37% and effectively augmented vertebral wedging by up to 1° (10-20%). Deductions and experimental methods were then extended towards the biomechanical analysis of current fusionless methods. Second, the FEM was utilized to critically explore current fusionless growth modulation devices tailored to AIS. Results from this analysis demonstrated the biomechanical ability of these devices to reduce asymmetrical growth plate loading by up to 50% (flexible tether) and decrease scoliotic progression to 11% (stainless steel staple and flexible tether). Conversely, this analysis highlighted several limitations that could be improved. The explored concepts simply reduce convex growth, span the disc space, and neglect sagittal and axial implications of the scoliotic deformity.

Two devices were proposed for development: an improved intravertebral epiphyseal device (rigid device that locally halts growth without spanning the disc space – feasibility reported in a previous in-house study using a rat tail) and a 3D tether (tethered configuration that targets axial correction in addition to coronal and sagittal control).

The intravertebral epiphyseal device successfully demonstrated its ability to provide fusionless growth modulation without the need to cross the disc space. Moreover, its influence on intervertebral disc health is insignificant pending accurate insertion of the device. Experimental pigs achieved vertebral wedging of 4.1°±3.6°, resulting in a cumulative vertebral deformity of up to 25° over only 4 instrumented levels. Adjacent to device, disc height increased 0.8mm±0.2 and growth plate hypertrophic zone and cell height reduced by a factor of two. Positive disc viability was confirmed by radiographic and histological grading and the lack of collagen type X. This device is the first of its kind to achieve growth modulation in an animal model with vertebral dimensions similar to adolescents without spanning the disc space.

The 3D tether also achieved local growth modulation resulting in vertebral wedging of up to 4° and coronal manipulation of up to 10° in porcine models. Axial and sagittal manipulations were confirmed using *in silico* and *in situ* platforms but experimental limitations restricted their objective *in vivo* confirmation. This is the first fusionless device to seek and demonstrate 3D correction of AIS.

Several notable advances have been achieved in the context of this thesis. The developed finite element platform provides an innovative way to explore biomechanical factors involved in the progression of AIS. In addition, in the context of device design, this FEM platform allows preliminary analyses and optimization to be performed prior to moving forth with expensive *in situ* and *in vivo* testing. Two novel fusionless growth modulating devices (intravertebral epiphyseal device and 3D tether) were refined and developed using a complete engineering design approach making use of *in silico*, *in situ*, and *in vivo* analyses. The developed FEM, the identified biomechanical factor in AIS pathomechanism, and the surgical devices conceived over the course of this thesis provide a hopeful step towards the improved management of adolescents with idiopathic scoliosis.

CONDENSÉ EN FRANÇAIS

La scoliose est une déformation musculo-squelettique caractérisée par une déviation latérale et une torsion de la colonne vertébrale. Elle affecte 3 à 4% de la population et 80% des cas de scoliose sont idiopathiques. Il existe plusieurs théories tentant de décrire son étiologie [1], mais aucune n'est encore prouvée.

Les mécanismes pathologiques impliqués dans la progression des déformations scoliotiques sont en partie reliés au principe de Hueter-Volkmann [2]. Selon cette théorie, une augmentation de la compression sur les plaques de croissance aboutit à une diminution du taux de croissance. Dans le cadre de la pathogenèse de la scoliose, cette théorie explique que le chargement asymétrique des corps vertébraux dû à la présence des courbures scoliotiques entraîne la progression des déformations scoliotiques [3].

Lorsque l'angle de Cobb est inférieur à 20°, les patients scoliotiques sont habituellement considérés en observation. Pour un angle de Cobb compris entre 20° et 50°, un traitement par corset est généralement appliqué. Des controverses existent encore sur l'efficacité de ce traitement [4]. Pour un angle de Cobb supérieur à 50°, une intervention chirurgicale consistant en une fusion rachidienne est nécessaire. Toutefois, cette intervention est particulièrement invasive et coûteuse et n'est donc réalisée qu'en cas d'absolue nécessité.

Le développement de techniques minimalement invasives et sans fusion permettant de contrôler et de corriger les déformations scoliotiques ou d'empêcher leur progression, offre des perspectives intéressantes pour éviter de réaliser ces interventions chirurgicales avec fusion qui sont particulièrement lourdes de conséquences. Cette perception, en parallèle avec le succès de l'agrafage des plaques de croissance des os longs, a conduit à l'élaboration de plusieurs dispositifs qui tentent de faire usage de la croissance vertébrale résiduelle pour corriger la cunéiformisation locale et donc de rétablir l'alignement de la colonne vertébrale. Certains dispositifs de ce type avaient déjà été développés dès les années 1950, avec toutefois un succès très limité. Les progrès réalisés depuis au niveau des techniques chirurgicales et des matériaux ont récemment permis de développer de nouveaux et prometteurs dispositifs de traitement dénommés 'dispositifs de modulation de croissance sans fusion'. Toutefois, à ce jour, ces approches n'ont pas encore été validées dans un contexte clinique. Il est enfin clair que mieux

comprendre biomécaniquement la progression des déformations scoliotiques permettrait de développer des dispositifs sans fusion plus efficaces. Cela serait une contribution importante et innovatrice à l'amélioration du traitement de la SIA.

L'objectif global de cette thèse était donc le développement, l'optimisation, et l'évaluation expérimentale d'implants sans fusion afin de moduler la croissance et de corriger les déformations scoliotiques

Les objectifs spécifiques étaient de :

Objectif 1: développer un modèle par éléments finis (MEF) de la colonne vertébrale intégrant une modélisation de la croissance;

Objectif 2: exploiter ce MEF pour étudier les facteurs biomécaniques impliqués dans les mécanismes de progression de la SIA;

Objectif 3: exploiter le MEF pour analyser la biomécanique des dispositifs sans fusion existant actuellement et repérer les améliorations pouvant être apportées à ces dispositifs;

Objectif 4: exploiter la plate-forme de conception conçue (analyses *in silico*, *in situ*, et *in vivo*) pour développer, optimiser et valider de nouveaux dispositifs sans fusion modulateurs de croissance pour la correction des déformations de la SIA.

L'idée centrale de cette thèse est que le développement de nouveaux traitements sans fusion plus performants peut être réalisé en comprenant mieux les facteurs biomécaniques impliqués dans les mécanismes pathologiques de la SIA, en identifiant les lacunes des dispositifs sans fusion utilisés actuellement et en utilisant une plate-forme de conception complète incluant des analyses *in silico*, *in situ*, et *in vivo*.

Cette idée centrale a été divisée suivant les hypothèses suivantes:

Hypothèse 1: Des facteurs biomécaniques (différence des propriétés mécaniques entre la concavité et la convexité de la colonne scoliotique) augmentent les contraintes asymétriques sur les plaques de croissance épiphysaires de la vertèbre apicale de 25% et de ce fait augmentent la

progression de la cunéiformisation vertébrale de 1° (soit 10%) sur un an de croissance à l'adolescence;

Hypothèse 2: Les dispositifs sans fusion modulateurs de croissance actuels (agrafes à mémoire de forme, agrafes en acier inox et attaches souples) réduisent les chargements asymétriques sur les plaques de croissance de la vertèbre apicale de 35% et limitent la progression scoliotique à 10% sur deux ans de croissance adolescente;

Hypothèse 3: Un dispositif intravertébral épiphysaire amélioré permet de modifier la cunéiformisation vertébrale de 4° sans modifier la physiologie du disque intervertébral dans un modèle porcin après 12 semaines;

Hypothèse 4: Une attache souple 3D permet de modifier la cunéiformisation vertébrale de 4° et la rotation axiale de 5° dans un modèle porcin après 12 semaines.

Les objectifs et les hypothèses de cette thèse de doctorat ont été examinés et résolus suivant la séquence décrite à la figure 0.1. Le développement de la plateforme *in silico* (MEF) a permis de réaliser les objectifs 1, 2 et 3 et de confirmer les hypothèses 1 et 2. Les analyses complémentaires *in situ* et *in vivo* ont permis d'atteindre l'objectif 4 et de confirmer les hypothèses 3 et 4. Par conséquent, quatre articles ont été soumis et publiés dans des revues scientifiques. Une étude de faisabilité supplémentaire est présentée ainsi qu'une discussion générale de ces études et les conclusions.

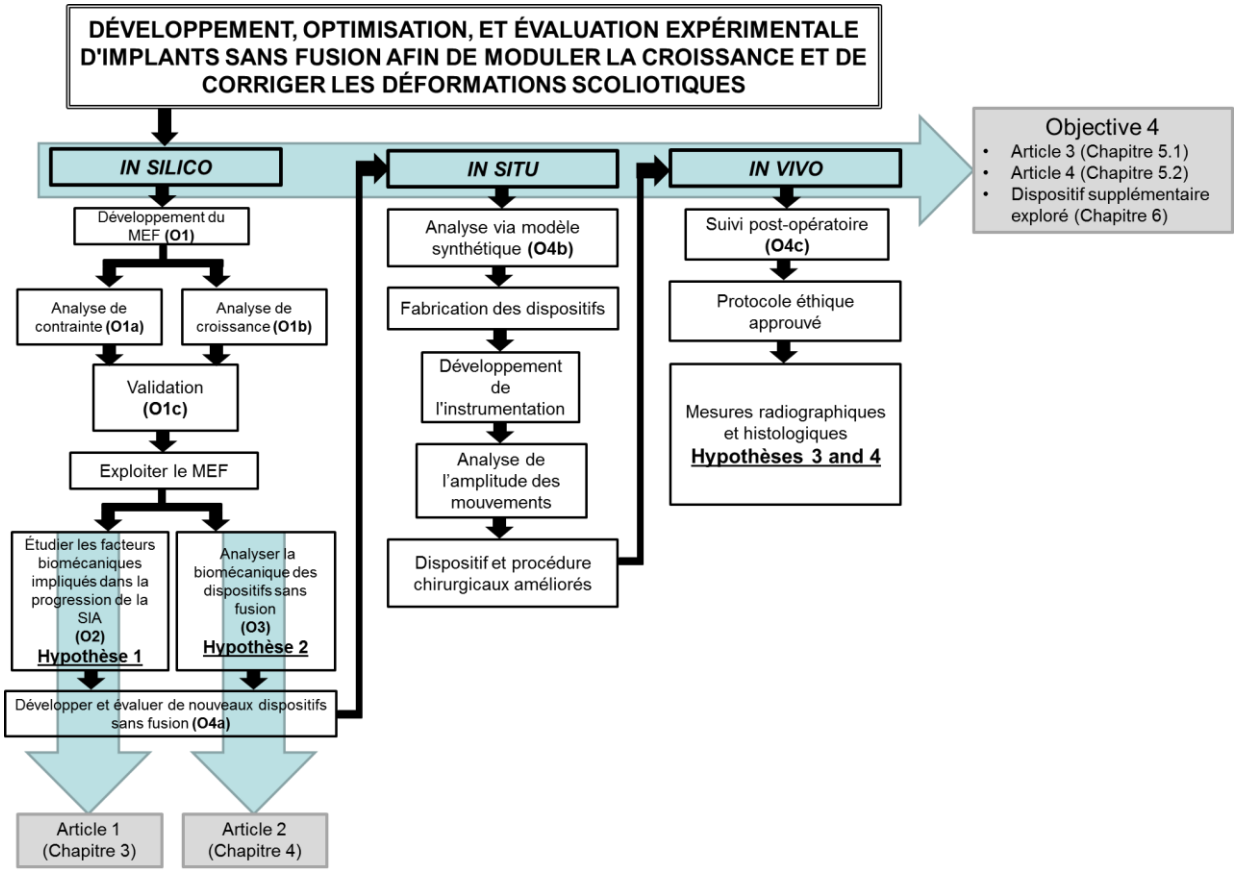

Figure 0.1: Schéma méthodologique

Objectif 1: Développement du MEF

Un modèle par éléments finis (MEF) volumique de la colonne vertébrale thoracique et lombaire antérieure a été développé. La géométrie du modèle correspond aux caractéristiques spécifiques du patient obtenues selon une technique de reconstruction stéréo-radiographique [5]. Une géométrie paramétrique a également été introduite afin de modéliser différentes configurations de colonne vertébrale. Les divisions physiologiques internes du modèle respectent les données provenant d'études publiées (Fig. 0.2).

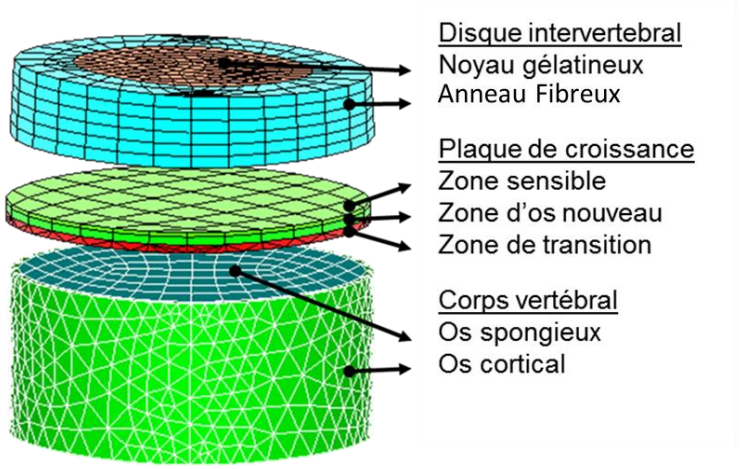

Figure 0.2: Vue éclatée du MEF d'un niveau vertébral (modifié de [6])

Analyse de contraintes (O1a)

Les mesures de contraintes sur les plaques de croissance des vertèbres sont d'un grand intérêt dans le cadre de l'analyse de la progression de la SIA mais aussi pour l'analyse des implants sans fusion qui cherchent à corriger les déformations scoliotiques. Pour analyser et quantifier ces contraintes, la zone sensible (couche supérieure de la plaque de croissance qui répond au chargement) a été divisée en différentes zones d'intérêt. Les contraintes longitudinales moyennes sur chaque zone sont calculées pour les modèles de scoliose, que ce soit avec le facteur de risque étudié ou avec les implants analysés. Par la suite, ces mesures sont comparées et les différences relatives ont permis de tirer des conclusions pertinentes.

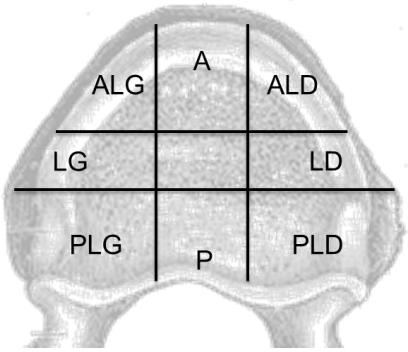

Figure 0.3: Plaque de croissance divisée en zone d'intérêt (A: antérieure, ALD: antérieure latérale droite, LD: latérale droite, PLD: postérieure latérale droite, P: postérieure, PLG: postérieure latérale gauche, LG: latérale gauche, et ALG: antérieure latérale gauche)

Analyse de la croissance (O1b)

L'évolution à long terme de la scoliose liée à un facteur biomécanique ou à un implant particulier a été mesurée en termes de modifications de l'angle de Cobb dans les plans frontaux et sagittaux. La croissance de la colonne vertébrale a été simulée sur une période comprenant une à trois année(s). Le système de contrôle itératif commence par l'analyse des contraintes résultant d'un chargement physiologique. La réponse en termes de modulation de croissance est ensuite calculée pour la couche d'os nouvellement formée au niveau des plaques de croissance. Par la suite, la géométrie du modèle est mise à jour. Ce processus en boucle prend place durant le nombre d'années simulées. Cette technique provient d'études publiées avec d'autres modèles [7, 8]. L'équation régulant le taux de croissance longitudinale des os en fonction des contraintes est basée sur des corrélations *in vivo* acquises en quantifiant les taux de croissance dépendamment des forces externes pour différentes espèces animales [9]. En bref, l'équation fournit les taux de croissance longitudinale en fonction de la variation de l'ampleur des contraintes par rapport aux conditions physiologiques ordinaires.

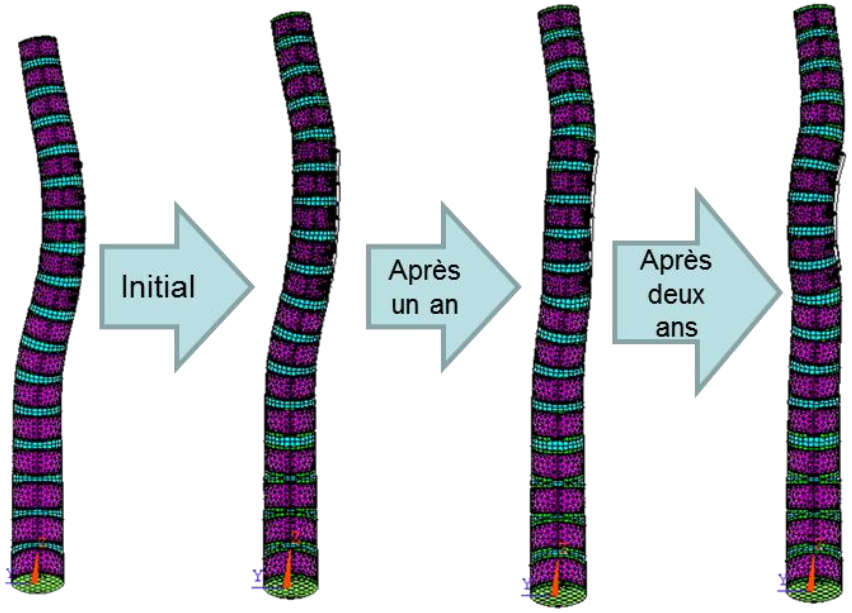

Figure 0.4: Exemple de simulation de correction initiale et à long terme dans une colonne scoliotique instrumentée

Diverses améliorations sur les modèles de croissance précédemment développés [7, 10-12] ont été introduites. Une approche plus détaillée pour la plaque de croissance a été incluse. Les

dimensions proviennent désormais d'études *in vivo*. Les variations cumulées de la taille de la plaque de croissance sont prises en considération lorsque la réponse en termes de croissance est calculée. L'algorithme pour déterminer la correspondance entre les éléments de la zone sensible et la couche d'os nouvellement formée a été amélioré. L'efficacité de l'algorithme de croissance a été optimisée afin de réduire le temps de calcul par un facteur 5. Enfin, la simulation de croissance a été effectuée pour un modèle volumétrique des régions thoraciques et lombaires complètes, modèle composé de 34 plaques de croissance fonctionnelles.

Validation (O1c)

Bien qu'il soit très difficile de valider un tel modèle, les mesures suivantes ont été prises pour assurer à la fois une corroboration qualitative et quantitative avec les valeurs expérimentales publiées. Puisque le MEF développé fournit une plate-forme pour prédire la répartition des contraintes dans la colonne vertébrale antérieure, les mesures de contraintes disponibles au sein de la littérature ont été comparées aux résultats du MEF (contraintes entre 0.15 et 0.8 MPa, tableau 1.4).

Le comportement du modèle de croissance développé a été comparé à d'autres simulations utilisant un algorithme similaire pour prédire la progression scoliotique [7, 13]. Plusieurs dossiers cliniques présentant des types de colonnes scoliotiques différents (Lenke Type 1A, Type 2A and Type 3C) ont été sélectionnés pour simuler les profils progressifs observés. Les critères de sélection pour cette phase étaient les suivants: le traitement par corset du patient n'a montré aucune influence sur la progression de la courbure scoliotique et le patient avait une progression négligeable dans le plan sagittal. Les résultats de cette étape de validation ont permis de prédire la géométrie des colonnes scoliotiques progressives à 5 degrés d'angle de Cobb près (Fig. 0.5).

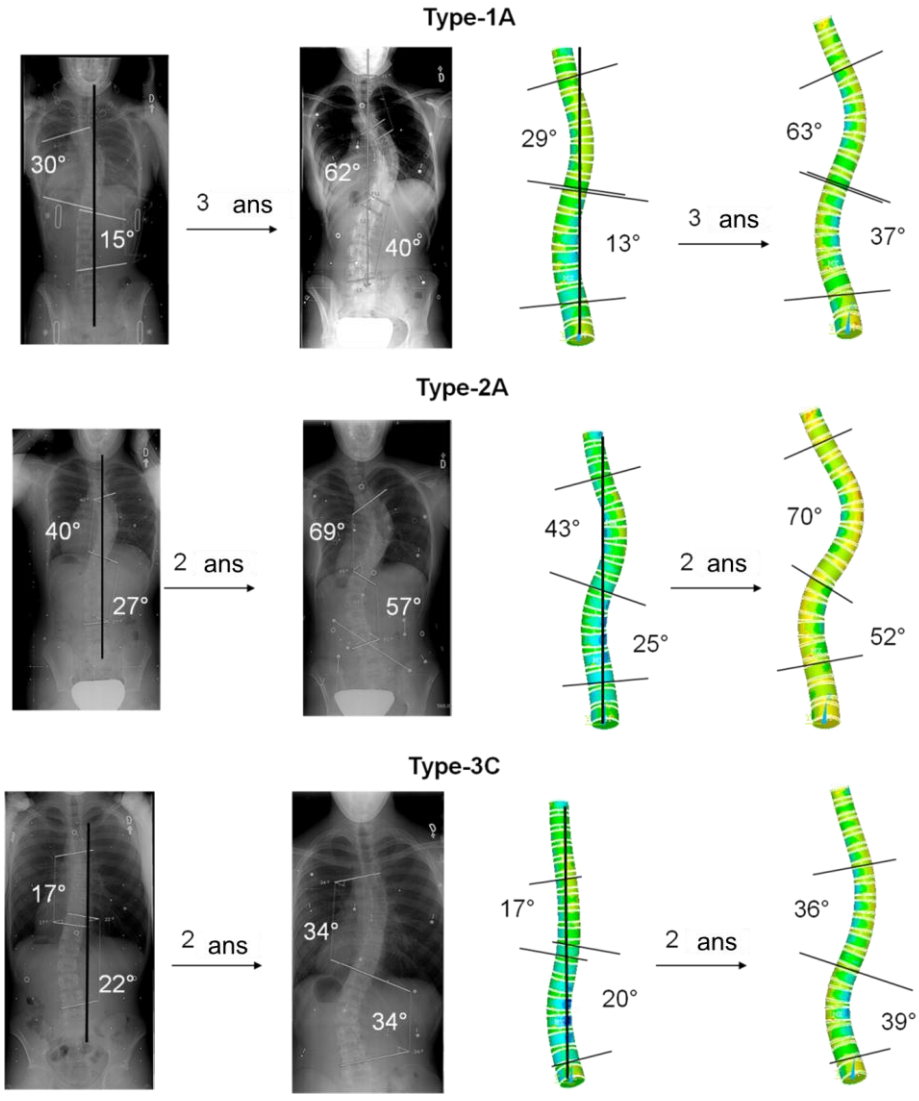

Figure 0.5: Exemple de validation du MEF prédictif (modifier de [6])

Il est toutefois important de noter qu'environ 80% des cas de scoliose ne progressent pas. Il est donc impossible de prédire avec précision les niveaux de progression en utilisant un algorithme basé sur des valeurs moyennes. En raison de cette limitation, la sensibilité des modèles (β équation 1.1) doit être ajustée pour que la progression scoliotique issue de l'interprétation numérique corresponde à celle des patients. Par conséquent, il est nécessaire de commencer par simuler un cas idéal où la progression scoliotique pose un problème clinique. Un MEF spécifique a donc été développé pour une patiente immature présentant une colonne thoracique de type 1 selon la classification Lenke [14] avec un angle de Cobb initial dans le plan coronal de 28 degrés. La courbure thoracique de cette patiente a progressé d'environ 10 degrés par année. Une

instrumentation postérieure impliquant la fusion est intervenue après deux ans de suivi. Selon les études publiées, ce cas clinique aboutit à une intervention chirurgicale dans 100% des cas [15]. Cela en fait une candidate idéale.

Objectif 2: Exploiter le modèle pour analyser divers facteurs biomécaniques (chapitre 3, article 1)

Cette partie de la thèse vise à analyser l'influence d'un facteur biomécanique dans le mécanisme pathologique de progression de la SIA. Essentiellement, l'hypothèse suggère que le remodelage des tissus dans les colonnes scoliotiques (au niveau des régions situées dans la concavité et la convexité des courbures scoliotiques Fig. 0.6) influence la distribution des contraintes internes et, par conséquent, encourage la progression scoliotique selon le principe de Hueter-Volkmann.
Trois MEF ont été développés: un modèle sain et des modèles scoliotiques incluant et excluant des différences entre les régions concave et convexe (augmentation de la rigidité de l'os trabéculaire et de l'annulus fibrosus, migration du noyau vers la convexité de la courbure dans le plan frontal). La croissance de la colonne a été simulée pour les deux modèles et les profils progressifs à long terme ont été comparés.

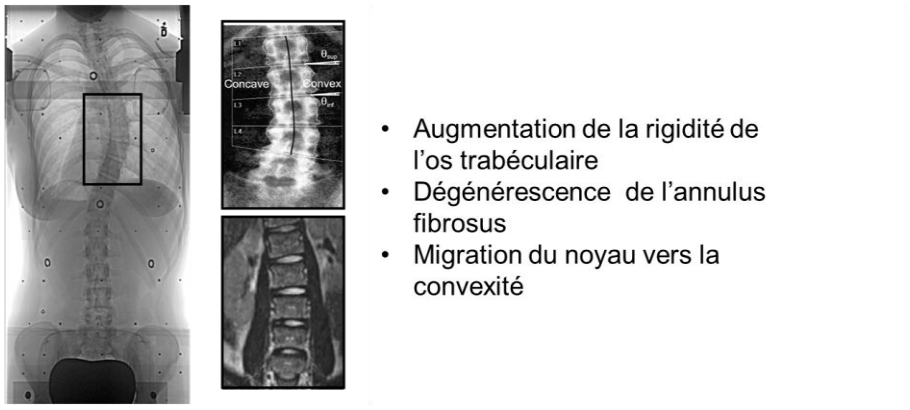

Figure 0.6: Facteur de risque analysé

Les résultats de cette interprétation suggèrent que ces différences mécaniques, entre les régions concave et convexe de la colonne, ont légèrement modifié la répartition des contraintes sur les plaques de croissance et ont modifié efficacement la progression de la déformation scoliotique. La quantification de ces paramètres chez un patient avec une scoliose pourra fournir une meilleure évaluation clinique du risque de progression.

Objectif 3: Exploiter le modèle pour explorer les dispositifs sans fusion modulateur de croissance existant actuellement (chapitre 4, article 2)

Cette section de la thèse a comparé les dispositifs sans fusion existant actuellement dans le traitement de la SIA. L'objectif implicite de cette tâche est d'identifier les défauts des concepts existant, afin de proposer de nouveaux dispositifs sans fusion améliorés. Ces dispositifs seront ensuite étudiés dans des modèles *in situ* et *in vivo*.

Trois implants (agrafe en acier inoxydable, agrafe en alliage à mémoire de forme, et attache souple en polyéthylène) ont été analysés avec le MEF. Ces implants ont été modélisés selon les descriptions fournies dans les brevets [16-18] et les études publiées [19, 20] (Fig. 0.7). Les implants ont été installés dans la modélisation au niveau des cinq corps vertébraux entourant l'apex (T7), couvrant ainsi quatre disques intervertébraux.

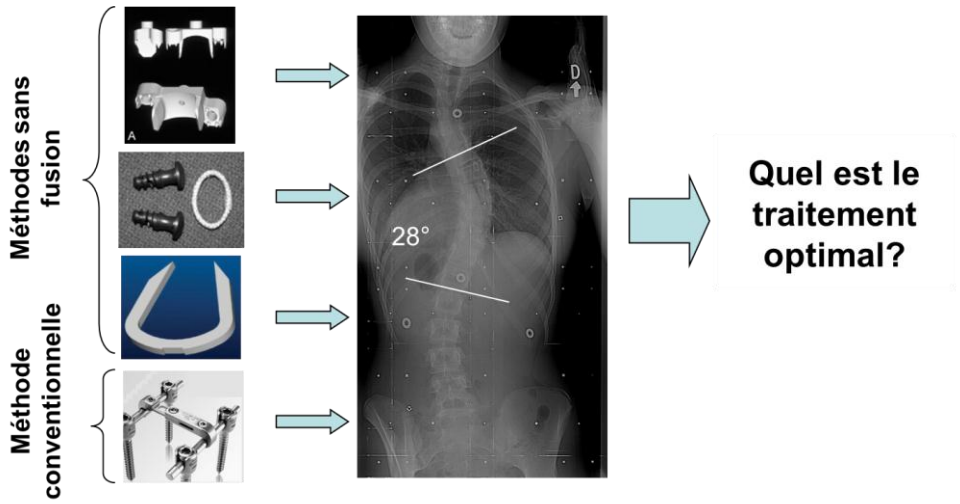

Figure 0.7: Dispositifs analysés

Deux années de croissance ont été simulées avec et sans la présence des implants décrits. La capacité des implants à altérer les contraintes (au niveau de la partie sensible de la plaque de croissance) a été quantifiée et comparée. L'effet initial et à long terme des différent implants sur les configurations scoliotiques a également été évalué.

Les résultats de cette analyse ont démontré que ces dispositifs permettaient de réduire les chargements asymétriques sur les plaques de croissance jusqu'à 50% et d'obtenir une modulation de croissance aboutissant à un réalignement du rachis. Cette analyse a aussi mis en évidence plusieurs faiblesses qui pourraient être améliorées. Tout d'abord, les implants analysés réduisent seulement la croissance dans les régions situées dans la convexité des courbures scoliotiques. La croissance n'est pas arrêtée ce qui serait souhaitable pour davantage réduire la cunéiformisation.

Deuxièmement, les implants analysés agissent purement dans le plan frontal et ne corrigent pas les déformations scoliotiques dans les plans sagittaux et transverses. Enfin, ces implants réduisent systématiquement l'espace du disque.

Objectif 4: Développement et évaluation de nouveaux dispositifs sans fusion modulateurs de croissance (chapitres 5 et 6, articles 3 et 4)

Tests in silico(O4a)

Comme mentionné précédemment, les analyses réalisées ont permis d'identifier certaines lacunes des méthodes sans fusion existant actuellement. Cette interprétation a permis la conception de nouveaux dispositifs améliorés visant un traitement précoce de la SIA. Ces nouveaux concepts ont été analysés avec la plate-forme numérique décrite précédemment selon des méthodes identiques (analyse de la capacité des dispositifs à corriger le chargement asymétrique des plaques de croissance, à induire une correction initiale, et à générer une correction à long terme par modulation de croissance). Tous les dispositifs explorés ont été comparés selon ces méthodes. Dix concepts originaux sans fusion ont été simulés à l'aide de la plate-forme MEF. Les deux les plus prometteurs ont été sélectionnés. Une optimisation *in silico* a été effectuée et des tests supplémentaires via des analyses *in situ* et *in vivo* ont été réalisés.

Tests in situ (O4b)

Une colonne vertébrale synthétique (S*awbones*) a été utilisée afin d'analyser les dispositifs choisis. Ceci constitue une étape intermédiaire avant de réaliser des expérimentations *in vivo*. Cela a permis d'obtenir un aperçu qualitatif de la correction initiale et de l'amplitude des mouvements de la colonne vertébrale après introduction de l'implant. La région thoracique du modèle physique (dimensions similaires à la région thoracique d'un modèle porcin immature et d'un adolescent humain) a été instrumentée avec les dispositifs et différentes conditions de chargement ont été qualitativement analysées. Cette méthode d'investigation a permis de développer, de vérifier et d'améliorer la procédure d'instrumentation et les outils chirurgicaux, cela dans le but de faciliter la chirurgie *in vivo*.

Tests in vivo (O4c)

Des porcs femelles immatures (âgés de 3 mois) de race Landrace/Yorkshire ont été utilisés pour tester la faisabilité des implants. Tous les groupes de porcs ont été suivis pendant 12 semaines suivant les chirurgies. Des radiographie postéro-antérieures (en position de décubitus ventral avec les pattes postérieures repliées et les pattes antérieures étirées vers l'extérieur) et latérales (position de décubitus latéral) ont été prises immédiatement après la chirurgie, puis toutes les deux semaines jusqu'à l'euthanasie sous anesthésie générale. Après sacrifice, les colonnes de porc ont été soumises à des analyses immunohistochimiques. Cette plateforme d'analyse a permis l'évaluation complète du dispositif intravertébral épiphysaire et l'analyse préliminaire du dispositif souple 3D (pas de groupes sham ni témoin).

Dispositif intravertébral épiphysaire

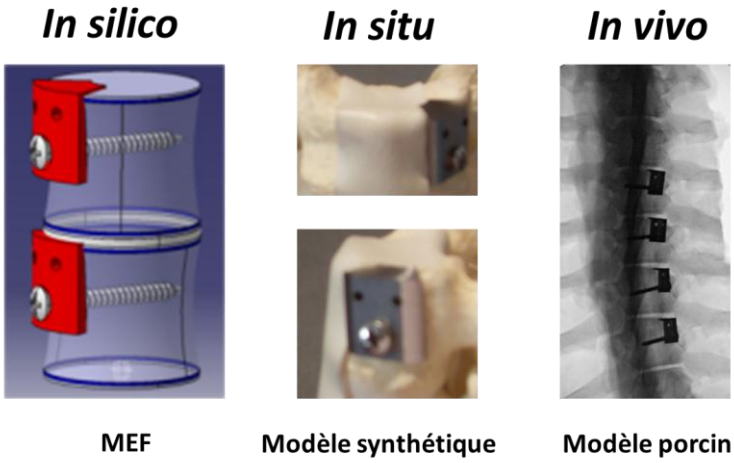

Figure 0.8: Conception du dispositif épiphysaire intravertébral

Tous les animaux ont pu subir l'analyse post-opératoire sans complications. Les groupes de témoin et de sham n'ont montré aucun changement significatif dans l'alignement des vertèbres. Le groupe test a montré un angle de Cobb frontal final de 6.5°±3.5° et une cunéiformisation cumulative allant jusqu'à 25° (limitée à 4 niveaux instrumentés). Aucune modification significative du profil sagittal n'a eu lieu. Le groupe expérimental a montré une cunéiformisation des vertèbres de 4.1°±3.6° et une différence de hauteur (hauteur droite vs gauche) de 1,24mm±1.86 dans le plan frontal. Aucune cunéiformisation ou différence de hauteur n'a été détectée dans les groupes témoin et sham.

Les données radiographiques ont montré une cunéiformisation des disques inverse à celle des vertèbres (hauteur du disque supérieure du côté du dispositif) dans les segments instrumentés. Les études histologiques ont confirmé que le dispositif générait une modulation de croissance via une réduction significative de hauteur de la zone hypertrophique et des cellules de cette zone. La santé du disque était variable et fonction de l'emplacement d'insertion de l'implant.

Dispositif attache souple 3D

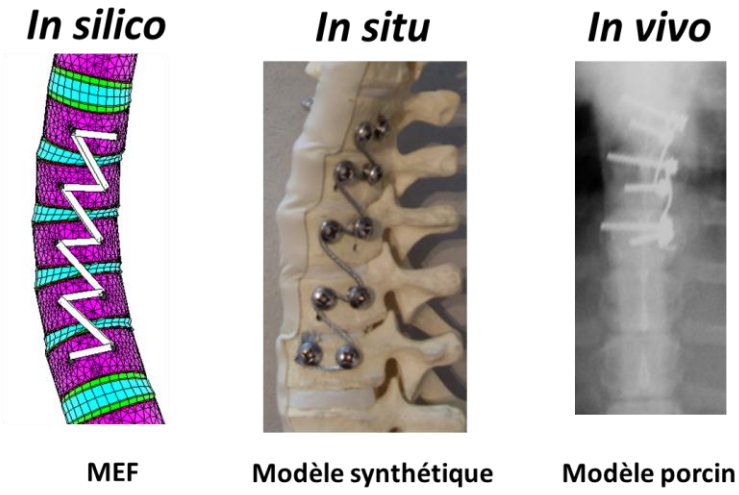

Figure 0.9: Conception du dispositif souple 3D

Les analyses *in silico* et *in situ* ont clairement démontré la capacité de ce dispositif à corriger les déformations scoliotiques rachidiennes dans les trois plans anatomiques. De plus, ces investigations ont confirmé la capacité de ce dispositif à agir sur les vertèbres adjacentes de façon indépendante. Le dispositif n'a causé aucun problème dans les quatre porcs instrumentés durant le suivi de 12 semaines. Cette étude *in vivo* a montré une cunéiformisation des vertèbres jusqu'à 4° (3°±1.5) et des corrections dans le plan coronal allant jusqu'à 10°. Cependant, les limitations expérimentales (méthodes inadéquates pour la quantification de la rotation axiale et problèmes de fixation des vis à long terme) rendent difficile une confirmation objective de l'action dans les trois plans comme démontré dans les analyses *in silico* et *in vivo*. Ce dispositif sans fusion est le premier à tenter activement de fournir une correction dans les trois plans anatomiques.

Conclusions et recommandations

Cette thèse apporte une meilleure compréhension biomécanique des mécanismes de progression de la SIA et des méthodes correctives à l'œuvre dans les dispositifs sans fusion. Deux nouveaux dispositifs sans fusion ont été élaborés et optimisés en utilisant des analyses *in silico*, *in situ* et *in vivo*.

Le MEF développé a permis l'analyse de facteurs biomécaniques impliqués dans la progression scoliotique. La présence d'un biais mécanique entre les régions concaves et convexes de la colonne vertébrale augmente le chargement asymétrique et par conséquent encourage la progression scoliotique. Ces facteurs biomécaniques sont considérés comme un facteur de risque secondaire impliqué dans la progression scoliotique. Des études supplémentaires utilisant une analyse prospective de patients scoliotiques devra être menée afin d'étayer ces conclusions et, au besoin, de concevoir des méthodes de dépistage clinique.

Le MEF élaboré confirme la capacité des dispositifs sans fusion actuels (agrafe en alliage à mémoire de forme, agrafe en acier inoxydable, et attache flexible en polyéthylène) à réduire le chargement asymétrique des plaques de croissance dans un rachis scoliotique et à réduire la progression scoliotique via une modulation de croissance convexe unilatérale Plusieurs améliorations potentielles restent toutefois à prendre en considération. Cette plate-forme MEF et des méthodes expérimentales constituent un moyen efficace d'explorer, de critiquer, et d'améliorer les dispositifs sans fusion pour le traitement de la SIA.

Le dispositif intravertébral épiphysaire a été optimisé via des analyses *in silico* et *in situ*. Le dispositif amélioré a permis de manipuler l'alignement du rachis en réalisant une modulation de croissance locale sans inclure le disque intervertébral dans le montage de fixation dans un modèle porcin. En outre, des analyses de la morphologie et de la santé du disque intervertébral et de la plaque de croissance ont montré que ces structures physiologiques restaient saines si un positionnement précis du dispositif était effectué. Un dernier essai préclinique est conseillé afin d'inclure des améliorations sur le dispositif et la technique chirurgicale. Le dispositif pourra ensuite éventuellement être adapté à l'être humain et un essai clinique pourra être effectué.

Le dispositif attache souple 3D a démontré des résultats prometteurs qui confirment son potentiel comme méthode de correction efficace pour la SIA. Sa capacité à corriger les déformations scoliotiques dans tous les plans anatomiques a été démontré à l'aide d'analyses *in silico* et *in situ*.

Les limitations expérimentales ont cependant amoindri la portée de l'évaluation *in vivo*. Néanmoins, la correction obtenue dans les trois plans anatomiques constitue une innovation importante et des expérimentations *in vivo* supplémentaires méritent d'être poursuivies.

Les deux dispositifs 'intravertébral épiphysaire' et 'attache souple 3D' offrent un espoir d'amélioration du traitement précoce de la SIA. Les essais précliniques ont été réussis et les inconvénients mineurs semblent pouvoir être résolus. Le dispositif intravertébral épiphysaire fournit une méthode intéressante pour atteindre une correction sans fusion sans inclure le disque intervertébral dans le montage de fixation. Le dispositif d'attache souple 3D offre un meilleur contrôle dans les trois plans anatomiques. Les deux dispositifs présentent des nouveautés par rapport aux traitements disponibles et répondent aux exigences des nouveaux traitements sans fusion adaptés aux patients avec la scoliose idiopathique adolescente progressive.

TABLE OF CONTENTS

LIST OF TABLES

LIST OF FIGURES

LIST OF EQUATIONS

LIST OF SYMBOLS AND ABBREVIATIONS

3D	Three dimensional
AIS	Adolescent idiopathic scoliosis
CAD	Computer-aided design
EMG	Electromyography
FEA	Finite element analysis
FEM	Finite element model
Hz	Hertz: unit of frequency
in silico	Experiment performed via computer simulation
in situ	Experiment performed in artificial environment out of organism
in vivo	Experiment performed in living organisms
MEF	Modèle d'éléments finis
ml	Millilitre
mm	Millimetre
MPa	Maga-Pascals ($kg/m.s^2$)
Mx, My, Mz	Moment in x, y, and z in Cartesian reference plane
N	Newtons ($kg.m/s^2$)
ng	Nanogram
OPN	Osteopontin
Pa	Palcals ($kg/m.s^2$)
ROM	Range of motion
SIA	Scoliose idiopathique de l'adolescent
SMA	Shape memory alloy
SS	Stainless steel

Ux, Uy, Uz	Translation in x, y, and z Cartesian reference plane
WRT	With respect to
σ	Mechanical stress ($kg/m.s^2$)
ε	Mechanical strain (elongation ratio)
Σ	Sum of

INTRODUCTION

Scoliosis is a three dimensional deformity of the spine which may progress and necessitate treatment. Conventional management successively includes bracing of moderate deformities and surgical instrumentation involving fusion of advanced spinal curvatures. The influence of orthotics on the natural history of scoliosis seldom results in deformity reduction while its utility continues to be debatable irrespective of optimal compliance. Scoliotic surgery is amongst the most invasive and expensive procedures. Spinal instrumentation coupled with fusion realigns the spine while concurrently sacrificing spinal flexibility and intrinsic segmental function. Thus, these shortcomings continue to inspire researchers to develop and explore improved alternative treatments.

Fusionless growth modulation proposes an early treatment of spinal deformities by making use of residual spinal growth in order to manipulate local vertebral morphology and, consequently, realign the spine over time. More specifically, this method exploits the Hueter-Volkmann principle of bone growth. This principle distinguishes how non physiological loading over vertebrae will alter regular growth rates. Therefore, fusionless devices seek to locally manipulate vertebral loading in an attempt to impede of reverse scoliotic progression. Consequently, fusionless treatment offers the benefit of preserving axial growth, spinal motion, and function. Initially proposed and evaluated in the 1950s, fusionless treatments of spinal curvatures were abandoned as a result of poor performance and device fixation problems. Refinements of surgical techniques and material sciences have reaffirmed fusionless growth modulation techniques as a promising alternative treatment of AIS over the last ten years. Notwithstanding, to date, fusionless devices are neither approved for use nor adopted in a clinical context; however, the current consistent emergence of registered patents, scientific publications, and preclinical and clinical trials insinuate its inevitable implementation.

Conceivably, fusionless treatments for scoliosis may be improved subsequently to gaining improved understanding of biomechanical factors involved in its pathomechanism, characterizing limitations of previously attempted fusionless devices, and utilizing a comprehensive design platform that include *in silico, in situ,* and *in vivo* analyses.

The general objective of this doctoral project is to design, optimize, and experimentally evaluate novel fusionless devices to induce growth modulation and correct spinal curvatures in adolescent idiopathic scoliosis. To achieve this endeavour, spinal anatomy, spine biomechanics and numerical modeling, scoliosis, and fusionless treatments was methodically reviewed and evaluated.

This thesis is composed of eight chapters represented in figure 0.10. Following a review of relevant literature, research objectives and corresponding hypotheses were systematically devised. Completion of the former and investigation of the latter led to four scientific manuscripts found in chapter's three to five. Chapter six reports the details of an important unpublished study. Chapter seven binds the explored themes under a general discussion while chapter eight closes with this dissertations conclusions and perspectives.

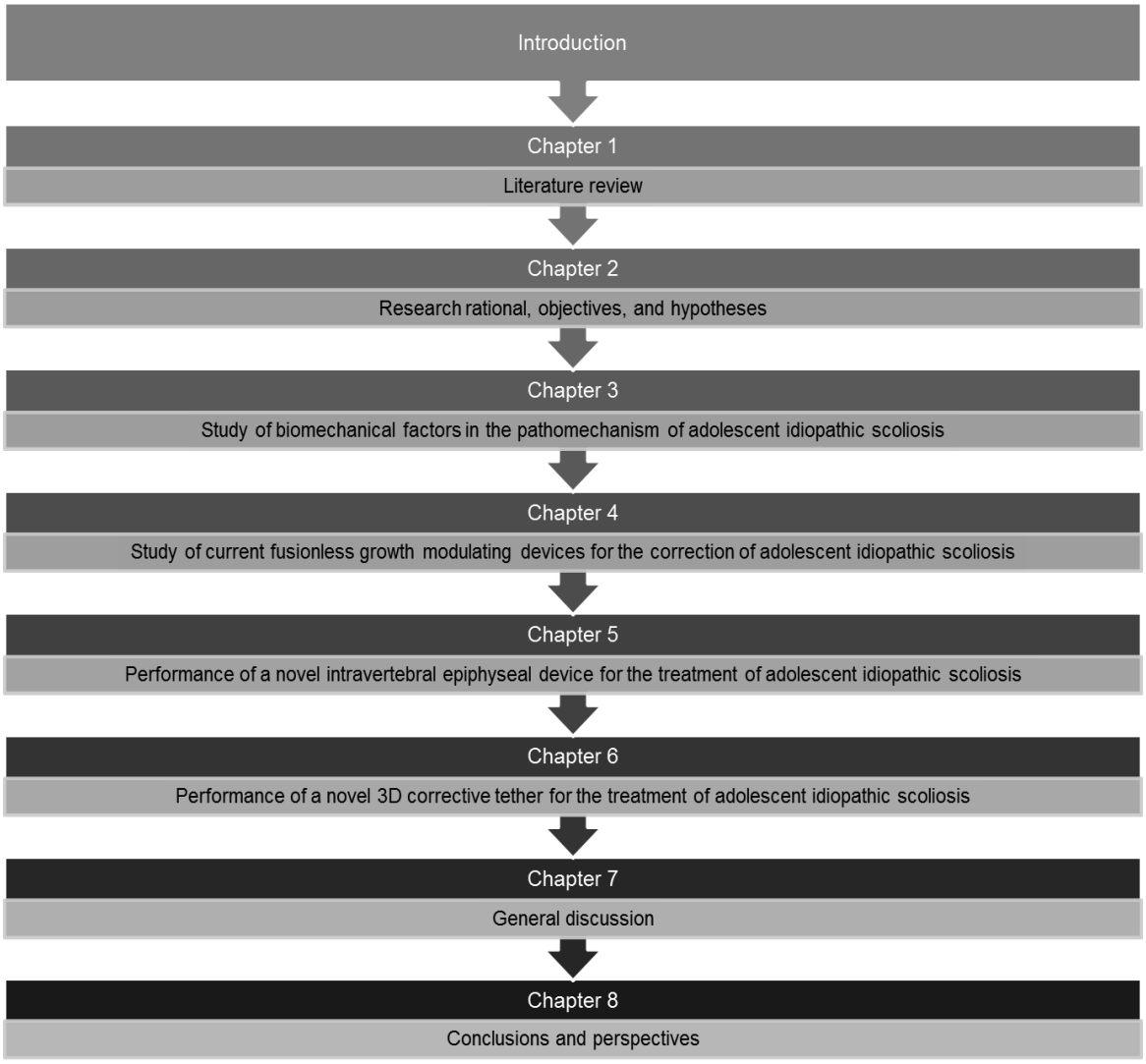

Figure 0.10: Thesis organization

CHAPTER 1 : LITERATURE REVIEW

1.1 Spinal Anatomy

The spinal column is a multifaceted structure whose morphology is uniquely defined in all three anatomical planes. Such complexity allows the spine to provide adequate support while remaining flexible under a plethora of configurations. Everything considered the spines main functions are to: provide support while bearing loads that arise from the upper body and active musculature, offer degrees of freedom in all anatomical planes and, perhaps most importantly, house and protect the spinal cord and provide a passage for nerve rootlets. In order to effectively perform the aforementioned tasks, the spine has evolved while adopting different physiological entities which are easily differentiated by their distinct characteristics.

The first and most superior division is described as the cervical spine and consists of seven vertebrae labelled C1 – C7. Due to reduced loading, when compared to its inferior members, the cervical spine is smaller than the other vertebrae in the spinal column. The shape of the cervical section is defined by an anterior convex curve in the sagittal plane which ends at the second thoracic vertebra, also known as lordosis.

The second section within the spinal column is titled the thoracic spine and is generally composed of 12 vertebrae labelled T1 – T12. The thoracic spine is coupled with the rib cage by costal facets which permit the articulation originating at the rib heads. The curvature of the thoracic spine is defined by a natural forward concave curvature from the middle of T2 until the middle of T12 – a geometry also referred to as a kyphotic profile in the sagittal plane.

The most inferior section is known as the lumbar spine and is generally comprised of five large vertebrae from L1 – L5. The lumbar curve runs from the midline of T12 until the sacrovertebral angle. Similar to the cervical spine, it assumes an anterior convexity that leads into the concave pelvic curve. Following the lumbar spine, the spinal column inferiorly ends with five fused vertebrae that make up the sacral elements (S1 – S5) leading into four more fused vertebrae (Co1 – Co4) of the coccygeal.

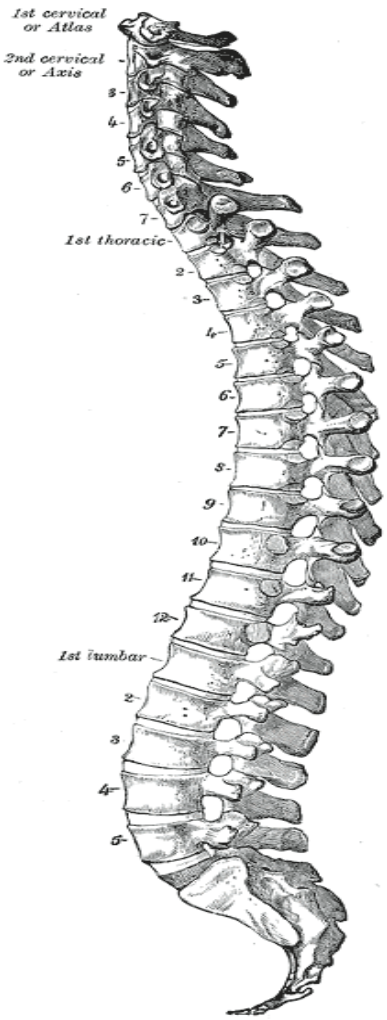

Figure 1.1: Spinal Column (obtained on January 25th 2011 from http://commons.wikimedia.org/wiki/File:Gray_111_-_Vertebral_column.png)

1.1.1 Vertebrae

Although the morphology of the vertebral bodies varies throughout the spine, they possess the same structured landmarks (excluding the atlas and axis due to their specific functions while the rib facets are implicitly reserved to the thoracic region). The vertebral bodies moulded into a complex geometry in order to effectively integrate nerve pathways, muscle insertion sites and ligaments attachments while providing sufficient load bearing.

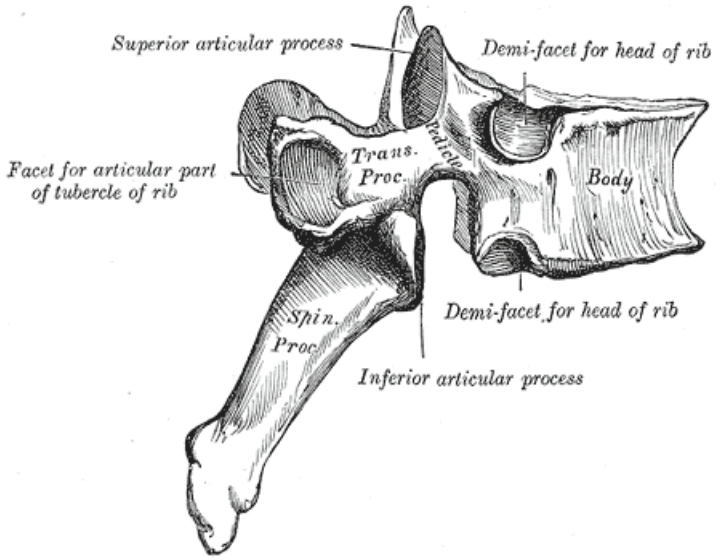

Figure 1.2: Thoracic vertebral landmarks (obtained on January 25th 2011 from http://commons.wikimedia.org/wiki/File:Gray90.png)

The structure of the vertebral body is enclosed by a thin cortical shell of about 0.64 mm in thickness [21] while the interior of the vertebral body is made up of cancellous bone (otherwise known as trabecular or spongy bone) defined by trabecular columns oriented towards the axial line of loading. The superior and inferior portions are bordered by endplates (formerly the growth plate in immature vertebra) with a thickness of approximately 0.62mm [22]. The posterior elements vary in morphology and size throughout the spine as a result of their respective functions.

1.1.2 Epiphyseal plate

The epiphyseal endplate, also known as the growth plate, is found between the vertebral body and the intervertebral discs in the spine. It is within this epiphysis that new bone is laid down in a successive fashion.

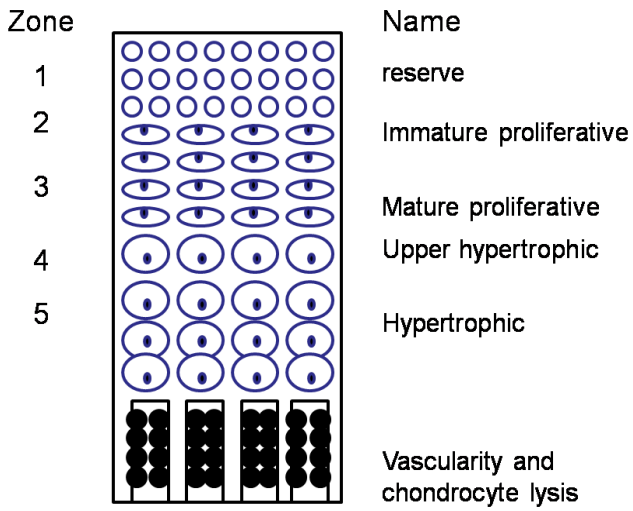

Figure 1.3: Vertebral growth plate anatomical divisions

The resting or reserve zone contains disordered chondrocytes that do not proliferate rapidly. These cells exist singly or in pairs and are surrounded by an extracellular matrix. It has been shown that this region has a high vacuole and lipid content, suggesting nutritional storage [23]. The proliferating zone consists of two distinct sections. The immature and mature portions essentially allow for new cartilage growth. The flattened chondrocytes also show signs of multiplication and become arranged in a column configuration. The hypertrophic zone begins at the sign of an abrupt increase in chondrocyte dimension [24]. The metabolic activities of these cells increase significantly when compared to the behaviour of the chondrocytes in the proliferating zone. The upper section includes matrix calcification which serves as a scaffold for new bone deposition. Also, this section has been shown to be involved with the synthesis of collagen type X and II [25]. The final section is detailed by the junction of the metaphysis and the growth plate. In this section, death of the hypertrophic chondrocytes occurs via apoptosis and the lacunae are invaded by blood vessels. This vascular region is where the osteoblast lay down osteiods or unmineralized bone. In vertebra, vascularisation is reserved below the hypertrophic zone. This leaves the hypertrophic zone avascular as no blood supply crosses into this zone of the growth plate [26]. Adjacent to the epiphyseal plates, are the intervertebral discs.

1.1.3 Intervertebral discs

The intervertebral discs provide and restrict motion that takes place between functional segments of the spine. As a primary role, the discs act as “shock absorbers” between the vertebrae which,

in turn, protects the nerves that span from the spinal cord form being compressed between adjoining vertebrae. The intervertebral discs are composed of two distinguishable structures. The inner structure, named the nucleus pulposus, is responsible for resisting compression via hydrostatic forces. Such important near incompressibility is achieved by the constraints offered by the surrounding annulus fibrosus combined with the inferior and superior endplates. The nucleus makes up roughly 45% of the discs cross sectional area upon analysis in the transverse plane [27]. In contrast to the disorderly composition of the nucleus, the outer annulus is a highly organized dense structure of collagen fibrils. The intervertebral discs are considered avascular and they must derive their nutrients via diffusion through the enclosing endplates or surrounding solution. These discs play an essential role in maintaining the integrity of the spinal column. Conversely, under a distorted environment, they may become paralysing and problematic [28]. Degeneration of the intervertebral disc can be induced in two ways: by overloading or through immobilization. The development and the associated biological alterations that arise from these two criteria are well defined in a review performed by Stokes [29]. In short, degenerative alterations within the disc may be linked to cell mediated changes that occur in relation to mechanical stimulus. More specifically the chondrocytes, who are responsible for producing the extracellular matrix along with proteoglycans and collagen, are less likely to proliferate under altered or non-optimal mechanical conditions (overloading or immobilization). While the intervertebral discs are responsible for providing compression resistance to the spine, the ligaments and passive spinal musculature (fascia) are responsible for maintaining stability and resisting tensional forces.

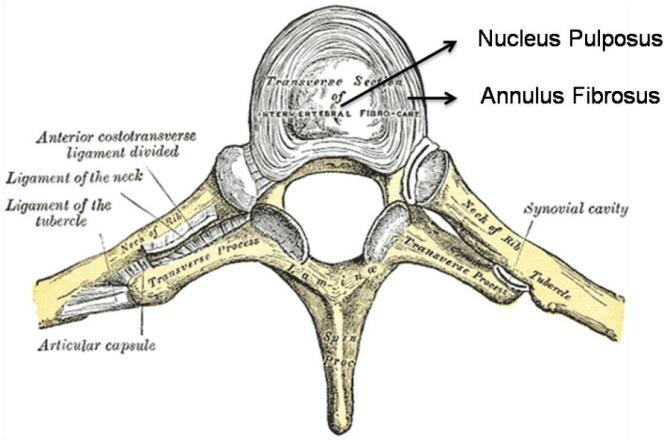

Figure 1.4: Intervetebral disc cross section (obtained on January 25th 2011 from http://commons.wikimedia.org/wiki/File:Gray313.png)

1.1.4 Ligaments

The ligaments implicated in the spinal column are numerous and their heavy presence is justified by their important roles. Their tensional restrictions begins when the range of motion of functional spinal segments surpass a certain threshold. Ligaments are fibrous structures made of tough connective tissue composed mainly of collagen type I fibres. They provide a hyperelastic (non-linear) behavior with a near exponential increase in tensional resistance as a vertebral segment attempts to move further away from its normal range of motion. In a similar manner to the intervertebral discs, ligaments are essentially avascular therefore upon undergoing injury these tissues require extensive recovery time as they derive their nourishment via diffusion which is a very slow process.

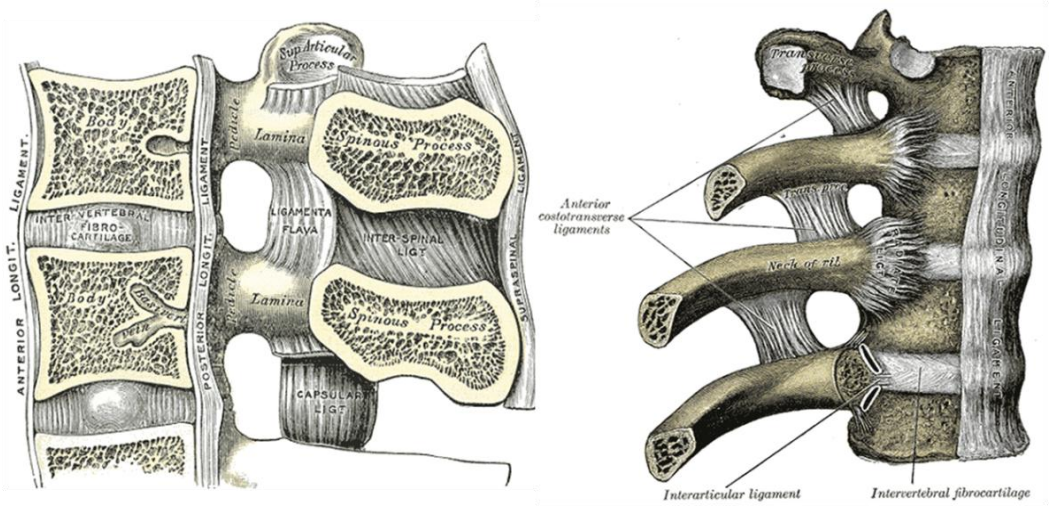

Figure 1.5: Spinal ligaments (obtained on January 25th 2011 from http://commons.wikimedia.org/wiki/File:Gray301.png and http://commons.wikimedia.org/wiki/File:Gray312.png)

1.1.5 Spinal muscles

The primary function of the spinal muscles is to provide adaptive support and stability to the vertebral column. These functions are performed by striated muscles stimulated by nerve impulses originating from the brain. This muscular system is very complex and involves high magnitudes of force transitions. Another purpose of spinal muscles is to provide controlled spinal flexion, extension and rotation. Various muscular activation strategies have been explored in order to understand the complexity that governs spinal stability. The general consensus is that

muscle activation is controlled in a matter to optimize mechanical efficiency (*i.e.* expend the less amount of energy) [30]. This notion explains that stability will be obtained under the most energy or stress efficient combinations of muscular stimulation. Other theories introduced and explored the use of a multi-criteria cost functions to explore spinal muscle activation [31]. Despite these findings, one must keep in mind that attempts to map muscular contributions to spinal stability involve several simplifications and assumptions required to solve an otherwise redundant problem.

1.2 Spine biomechanics and numerical modeling

Spine biomechanics has always been an area of great interest for researchers. Perhaps propagated by the economic burden of back pain, or driven by the importance of the enclosed spinal cord, this field has captivated popular interests throughout history while certain characteristics continue to elude today's leading scientists. The first analyses of human spine biomechanics were performed using *in vivo* and cinematography coupled with electromyography (EMG) measurement mechanisms that allowed for preliminary conclusion to be drawn with regards to spinal stability, muscular activation, and spinal forces. Over the years, the introduction of improved experimental platforms permitted *ex vivo* experimentation to be performed under "physiological like" conditions. Today, advanced computing power allows for the diversity of the spine to be explored under *in silico* conditions – a format otherwise known as numerical modeling or finite element modeling. The combination of the above mentioned methods of spinal investigation allowed for researchers to extract valuable information with regards to the following topics: spinal range of motion, mechanical properties, spinal loading, spinal growth, spinal growth modulation and spinal bone remodelling.

1.2.1 Spinal range of motion

The spine is a complex mechanical structure. Although locally confined, each vertebral segment contains six degrees of freedom consisting of three rotational and three translational. The spinal column is constantly under compressive force even when in a supine position. These forces exceed many times over what may be contributed by body weight alone. Each spinal segment has its own range of motion that is controlled and confined by its unique surroundings. The cervical section contains the largest range of motion followed by the lumbar and finally the thoracic region. The specifics of these varying degrees of freedom are estimated in figure 1.6.

Each vertebra possesses a neutral zone which allows movement requiring very little muscular input. This neutral zone has been quantified to be roughly two degrees in lateral bending, flexion/extension, and axial rotation [32]. Once this neutral range is surpassed, the motion encounters an increased resistance defined as the elastic zone regulated by the surrounding tissues.

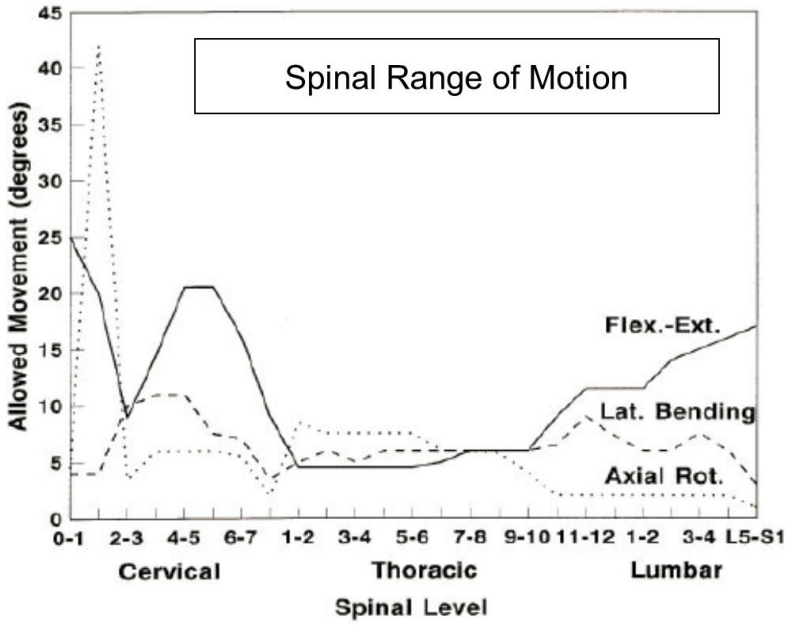

Figure 1.6: Spinal range of motion (obtained and adapted on June 25th 2011 from http://wings.buffalo.edu/academic/department/eng/mae/courses/417-517/Orthopaedic%20Biomechanics/Lecture%2012.pdf)

1.2.2 Mechanical properties

Spine biomechanics is a complex phenomenon governed by unique mechanical characteristics. Its physiological tissues have the distinct characteristic of being anisotropic (mechanical property varies with the direction of force), hyper-elastic (mechanical property varies non-linearly according to its magnitude of stretch), and visco-elastic (mechanical property will vary depending on the speed and history at which it is deformed). Nevertheless, following several justified assumptions one may extract relevant mechanical properties of spinal tissues from the available spectrum of values in order to further explore spinal mechanics.

Intervertebral discs clearly behave in a non-linear and viscoelastic manner (annulus [33, 34], nucleus [35]). Nonetheless, as a simplification, this behaviour may be summarized using Young's modulus (mechanical property) with a simplified linear value. Moreover, stiffness may be used to characterize its resistance in a given degree of freedom as summarized in table 1.1. These values are generally accepted anisotropic stiffness of the intervertebral discs commonly adopted in rigid body models. It is however important to note that the details of the stress distribution within the intervertebral discs are influenced by age, degeneration [36-38], and adjacent vertebral health [39].

Table 1.1: Material properties of lumbar intervertebral discs

Direction	**Stiffness**	**Reference**
Compression	0.7-2.5 MN/m	[40, 41]
Tension	1.0 MN/m	[42]
Shear	0.26 MN/m	[42]
Torsion	2.0 Nm/deg	[41]

Vertebral trabecular bone is a porous structure oriented axially [43] with a mechanical modulus that measures between 375-2000 MPa [44]. The outer shell of the vertebrae are made up of solid cortical bone which is believed to have a stiffness of around 8-14 GPa in the longitudinal direction and 2-8 GPa in the transverse direction [45]. Combination of these two bone types provides a mechanically efficient configuration to handle the subjected loads. In addition to mechanical properties, the vertebral size also plays an important role in its structural integrity as previously identified during *ex vivo* experimentation [46].

Ligaments of the spine have an important contribution to spinal stability as foreshadowed by its dominating presence. The mechanical implications of each ligament vary due to position,

morphology and biological makeup. These tissues are made of tough connective tissues with varying percentages of collagen and elastin which regulate their non-linear tensile resistance. Each ligament demonstrates high resistance to tension and large failure strength. In addition, during *ex vivo* analyses, it was recorded that ligament strength increases as one moves inferiorly within the spinal column [47, 48] - a phenomenon likely due to the increased cumulative forces in the lower spine sections.

As a complementing tool to *ex vivo* experimentations, attempts to improve understanding of spinal biomechanics has been performed via FEMs by various researchers [7, 10, 12, 49-60]. In brief, FEMs utilize mechanical properties, geometry, and boundary conditions (forces and constraints) in order to calculate the strain (elongation per unit length) and stress (force per unit area) of a system. The ability to extract explicit information about internal stress distribution within the spinal column is not possible under *ex vivo* and *in vivo* conditions. Thus, FEMs provide an attractive method to further the knowledge of spine biomechanics. However, these numerical interpretations include several assumptions regarding the mechanical properties of the physiological tissues under consideration. In order to insure the convergence of numerical analyses (difficulties in the computational analysis may arise and solution may diverge from reality) it is a great advantage, from a mathematical view point, to use a linear modulus to represent the behaviours of the tissue under load. As described above, such assumptions commonly take place to define properties of the intervertebral discs, the bone of the vertebral bodies and the spinal ligaments. Table 1.2 summarises the values most often used in FEMs of the spine (missing values represent neglected contribution or the use of non-linear properties) as reviewed by Jones and Wilcox [61].

Table 1.2: Summary of published material properties of spine used in numerical modeling ((ALL) anterior longitudinal ligament, (PLL) posterior longitudinal ligament, (LF) ligamentum flavum, (CL) capsulary ligament, (ISL) interspinous ligament, (SSL) supraspinous ligament, (TL) interspinous ligament)

	Linear Material Properties (Elastic Modulus in MPa)											
	Vertebra (compression)		Intervertebral Disc (compression)			Ligaments (tension)						
Author	Cortical	Trabecular	Annulus	Fibers	Nucleus	ALL	PLL	LF	CL	ISL	SSL	TL
Bellini et al. [55]	12 000	340	8	-	1	-	-	-	-	-	-	-
De Visser et al. [62]	5 000	74	4	450	1	12	13	2.4	7.7	3.4	3.4	3.4
Fantigossi et al. [63]	12 000	3 500	4.2	500	1	-	-	-	-	-	-	-
Hato et al. [64]	10 000	750	-	7.5	-	20	20	10	10	10	10	
Ivano et al. [65]	12 000	100	4.2	175	1	-	-	-	-	-	-	-
Kim [66]	120 000	100	4		-	7.8	10	17	7.5	10	8	10
Lafange et al. [67]	12 000	100	2	500	4	10	10	10	10	10	10	10
Rohlmann et al. [68]	10 000	200	-	-	-	-	-	-	-	-	-	-
Schmitt et al. [69]	22 000	200	-	-	-	-	-	-	-	-	-	-
Sylvestre et al. [11]	8 000 - 14 000	375 - 2000	8	550	2	20	70	50	20	28	28	50
Williams et al. [30]	12 000	100	-	-	-	-	-	-	-	-	-	-

1.2.3 Spinal loading

Spinal loading has yet to be fully understood. The general consensus is that considerably more compressive loads are supported in the anterior spine (vertebral body) when compared to the posterior elements. More specifically, the anterior portion of the spine supports a convincing majority (~90%) of compressive loads supported within the spinal column [70, 71]. In addition, load allocation within the anterior body was explored and it was demonstrated that roughly 50% (34%-64%) of compressive stresses were concentrated in the cortical shell [72].

Several methods to define spinal loading have been proposed and explored to date. Villemure [7, 12, 73] modeled loading of the spinal elements by using load allocation rations derived from works by Schultz [74]. This was achieved by placing 14% of body weight on the superior surface of T1 while each inferior vertebra was loaded with an additional 2.6% of body weight.

This loading was applied in a perpendicular manner over the center of the superior portion of each vertebral body. Other notable studies have reported similar load allocation rations within the spinal column demonstrated in table 1.3.

Table 1.3: Estimation of load allocation in spinal column

Vertebra	Body weight %[75]	Body weight %[74]	Body weight %[76]	Average [75,74]
T1	-	14		**14**
T2	-	16.6		**16.6**
T3	-	19.2		**19.2**
T4	-	21.8	15.2	**21.8**
T5	21	24.4		**22.7**
T6	25	27		**26**
T7	29	29.6		**29.3**
T8	33	32.2		**32.6**
T9	37	34.8		**35.9**
T10	40	37.4		**38.7**
T11	44	40		**42**
T12	47	42.6		**44.8**
L1	50	45.2		**47.6**
L2	53	47.8		**50.4**
L3	56	50.4	61.9	**53.2**
L4	58	53		**55.5**
L5	60	55.6		**57.8**

Another numerical method attempted to integrate respective moments between functional elements of the spine to more accurately emulate physiological loading provided by gravity. Clin et al. used the same load allocation ratios as defined above (Schultz) but introduced a lateral offset of the loading in the sagittal plane. This was performed to more accurately define the geometric center of mass of the patient [77]. This particular model included the ribcage and soft tissues (skin) thus allowing for stability and numerical convergence to be obtained more effectively.

Force vectors provided by spinal muscles were not included in the above mentioned models. In 1999, Pathwardhan and colleagues pointed out that perpendicular and thus gravitational loading of an *ex vivo* spines continuously provoked buckling if placed under loads of 80-100 Newtons, while under physiologic conditions our spine is known to support up to 1000 N. They then demonstrated that if loading of the spinal elements was maintained tangential to the curvature of the spine it supported up to 1200 Newtons [78]. Hence, it is suggested that the presence of

gravity and muscle forces ensures that the resulting force vectors within the spine would be maintained tangential its natural curvature [79]. Despite such novel findings, only the lumbar spine was utilized for these analyses and therefore this theory has yet to be demonstrated on a full spinal column. Another restrictive inference of this *follower load* approach is that this form of loading would not trigger alterations that occur in the sagittal plane when moving from a standing to a prone position. This has been quantified to invoke an average kyphosis reduction of 11°or 19% or a lordosis decrease of 8°or 12% [80]. A final inconsistency of the *follower load* or pure compression theory is that it does not agree with other research findings is that asymmetric spinal stress distribution via pressure transducers [81, 82] and computational analysis have been previously quantified suggesting non-congruent local segmental compression [76, 83]. Nevertheless, this *follower load* concept was adopted by Shirazi-Ald and modified to further improve the stability of the spine [84]. That is, resulting force vectors were maintained tangential to the curve while the location of loading was changed from the center of the vertebral bodies, as suggested by Pathwardhan et al., to the sides of the vertebral bodies on a FEM. However, as the individual contributions and location of active forces are unknown, it is currently a safer assumption to impose vertebral loading on successive endplates when using numerical modeling to represent a loaded spine as performed by several authors [7, 12, 31, 73, 77-79, 85].

There are several methods used to estimate the *in vivo* loads experienced within the spine. The first uses a free body diagram with the necessary assumptions to make the solution possible. These assumptions, as previously stated, include a level of ignorance that jeopardizes the accuracy of this method. Nevertheless, results that include quasi-static forces show that a compressive force of up to 10 times body weight is present in the spine. Another method uses EMG to measure muscle activity to determine their contribution to this dynamic environment. Results suggest that magnitudes of up to 50 times one's body weight may be present within the spine. The last and most accurate method requires an invasive procedure. This consists of inserting micro pressure transducers into the intervertebral discs in order to get a direct reading from its native environment [86].

The results of several experimental methods to quantify the forces present in the intervertebral disc are summarized in the table 1.4. This table includes *in silico* (computational), *in situ*, and *in*

vivo results. Although findings vary, they complement each other and give a general consensus of what magnitude of compressive stresses (FEM) or hydrostatic pressure (*in vivo* and *ex vivo*) are present within the intervertebral discs.

Table 1.4: Intervertebral disc stress distribution

Author	Method	Disc	Section	Mean Stress (MPa)
Adams 1996 [13]	*Ex vivo*	L4-5	Nucleus	1.6
			Anterior	2
			Posterior	2.6
Wilke 1999 [14]	*In vivo* standing	L4-5	Nucleus	0.5
Schultz 1982 [15]	*In vivo* standing	L4-5	Nucleus	0.27
Nachemson 1964 [16]	*In vivo* standing	L4-5	Nucleus	0.87
Andersson 1974 [17]	Computational	L4-5	Nucleus	0.3-0.5
Meir 2007 [18]	*In vivo* lateral decubitus	Apex	Concave	0.8-0.4
			Convex	0.15
Sato 1999 [19]	*In vivo* prone	L4-5	Nucleus	0.15
Shrzypiec 2007 [20]	*Ex vivo*	C7-T1	Nucleus	1
			Anterior	1.35
			Posterior	1.1
Steffen 1998 [21]	*Ex vivo*	L3-4	Nucleus	0.8
Schroeder 2006 [22]	FEM	L4-5	Nucleus	0.6-0.85
			Anterior	0.6-1
			Posterior	0.8-1.2

1.2.4 Spinal growth

Ossification Centers

Several ossification centers are present in vertebral bodies (Fig. 1.7). Each center contributes to a unique aspect of spinal growth. Further, each growth center fuses at different stages during infantile or adolescent growth while growing at a different rate. Vertebral growth is composed of a complex biological process known as endochondral or intramembrous ossification. The neuro-central canal growth plate consists of a bi-lateral growth plate as it contributes to both pedicle and vertebral body growth. Growth in this region has been shown to take end and thus

fuse prior at an average age of 9 years [87]. Expansion and growth of the vertebral processes is linked to growth plates located at their anatomical extremities. Growths in these regions are relatively small and have been shown to take end around the age of 12 years. Appositional growth of the vertebral bodies is the only form of intramembrous ossifications in the vertebrae as it involves local messemchyme cells that secrete osteoblasts into intracellular spaces on the periosteum thus differencing from regular endochondral ossification which is latter defined by a more complex phenomenon. Appositional growth may also be considered as a form of remodelling which continues to take place throughout our life. The final ossification center present in the spinal column governs longitudinal growth of the vertebral bodies. Each vertebra has an epiphyseal plate on its superior and inferior portions responsible for vertebral body height.

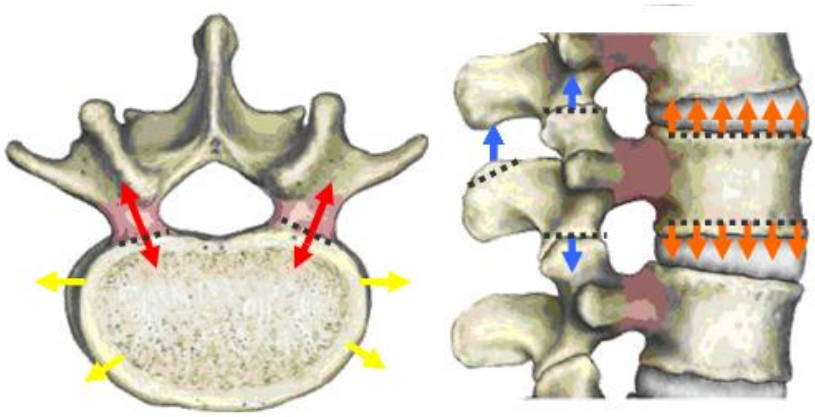

Figure 1.7: Ossification centers on vertebral bodies (red: neuro-central canal, bleu: vertebral processes, yellow: appositional growth, orange: epiphyseal plate)

Longitudinal Growth

There are three distinct longitudinal growth periods in the human spine. These include infantile, juvenile, and adolescent growth phases. At the end of infantile growth, around five years of age, sitting height is about 66% of the final value with about 30 cm of growth remaining. Between 5 and 10 years of age, there is a small increase of about 2 cm occurs in sitting height. During puberty, around 11 years of age for girls and 13 for boys, the growth rates of the sexes diverge. At this moment it is believed that the remaining growth of sitting height is 12 cm for girls and 13 cm for boys. A growth peak occurs between 11 and 13 for girls and 13 and 15 for boys. During this period the limb growth essentially comes to an end while the sitting height is left to increase about 4.5 cm [88]. Dimieglio and Bonnel performed a more accurate follow up of spinal growth [61]. Vertebral growth rates in the thoracic and lumbar regions were measured at six month

intervals. It is estimated by Dimieglio and Ferran that the thoracic and lumbar region growth 0.8 and 1.1mm per year respectively during adolescence [89]. Based on these measures, it may be assumed that a residual vertebral growth around the magnitude of 2mm per vertebra remains during adolescent growth.

Little is known about the growth of the discs. This process is believed to occur through matrix synthesis and cell proliferation. Taylor measured the growth of both the vertebrae and the intervertebral disc in different sections of the spine [90]. Results agreed with those of Stokes (Fig. 1.8), which demonstrate disc growth to conclude around 12 years of age [91].

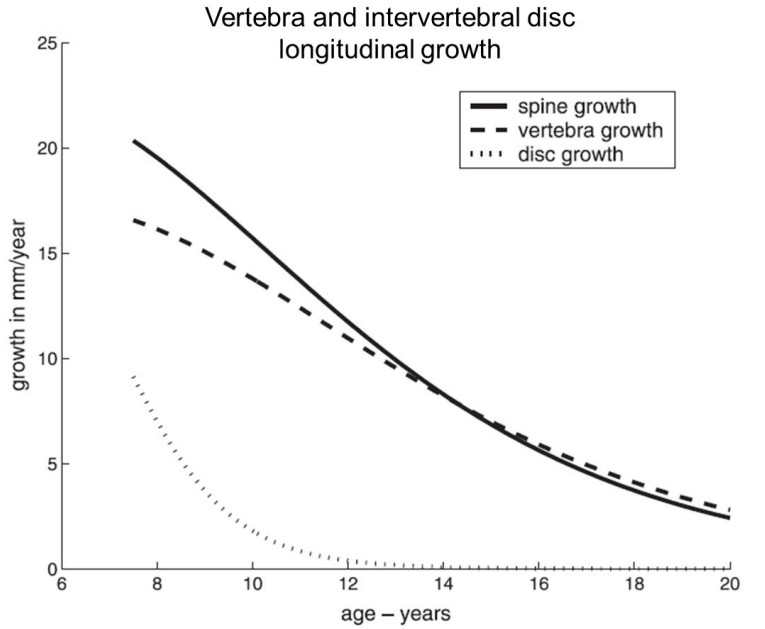

Figure 1.8: Growth of vertebral body and intervertebral disc (modified from [91])

Once bone growth has come to an end, the epiphyseal plate ossifies and fuses leaving an epiphyseal line. This occurs between 12 to 25 years of age (on average occurs at 14 years), depending on sex and other hormonal and environmental factors. The ring apophysis, which surrounds the outer portion of the growth plate, first appears about 6 years of age, begins to ossify around the age of 13, and after 16 and 18 years it fuses to the vertebral body [92].

In order to estimate to onset of peak growth velocities, the iliac crest may be observed via radiograph in order to determine the level of ossification and draw a conclusion on remaining growth. A Risser sign of 0-1 would provide knowledge that the growth spurt has yet to occur

while, once the Risser sign is between 1 and 5, it is safe to conclude that there is little remaining spinal growth [93].

1.2.5 Spinal growth modulation

The elaborate process of bone growth is known to be influenced by several factors which include: level of circulating hormones, nutritional intake, disease, and mechanical environment. The process of growth is a very difficult phenomenon to study since, at the cellular level, it involves a rapid transition between proliferation, hypertrophy and apoptosis. Nevertheless, several in-vitro studies were able to identify various growth factors that play an important role in endochondral bone ossification. The biological implications of bone growth are effectively summarized by two well written reviews from which the following interpretations arise [26, 94]. These include insulin-like growth factors, transforming growth factors, fibroblast growth factors, platelet-derived growth factors, and bone morphogenic proteins. Cytokine concentration has also been identified as influencing growth rates, these include interleukins (1, 6, and 8), tumour necrosis factors, interferons, colony stimulating factors, parathyroid hormone related peptide, and calcitonin gene related peptide. All of the above constituents have been linked to moderate bone proliferation and differentiation at different stages of growth. Although, to date no *in vivo* studies have effectively isolated and explored these factors, there is a clear biological influence regulating bone growth. What is known with respect to these listed growth rate contributors is that the growth plate's mechanical environment may invoke and, in part, govern their behaviour via the appropriate method of mechanotransduction. Several theories attempt to characterize and define the specifics of mechanotransduction (mechanosensitive ion channels as molecular transducers, enhanced membrane diffusion, microtubule ruptures, conformational change of intracellular proteins, and altered transcription of the stimulated nuclear envelope); however, limitations of the above outlined theories include the possibility that cellular response is altered by in-vitro growth factors required to maintain cell life and cell isolation procedures.

A retracted interpretation of growth modulation involves its mechanical input. The Hueter-Volkmann principal describes how growth plates under tension or compression respectively result in accelerated or hindered growth rates. Numerous *in vivo* experiments, which verify this theory, have been conducted to show the effect of loading and its ability to regulate bone growth [9, 95-105]. Additional studies suggest that dynamic loading further inhibits the growth rate in

comparison to static loading [106, 107]. Others have demonstrated that stress, in the form of shear (force parallel to surface), affects the direction of growth [103] - a result speculated to be the result of forceful realignment of cellular arrangement within the growth plate. Additionally, the longitudinal growth rate in bones has been successfully correlated to the local stresses experienced within the growth plate. These experiments involve both compression and extraction forces placed across the growth plates of various species while documenting growth [3, 95, 108]. The results from such experiments can be summarized in figure 1.9.

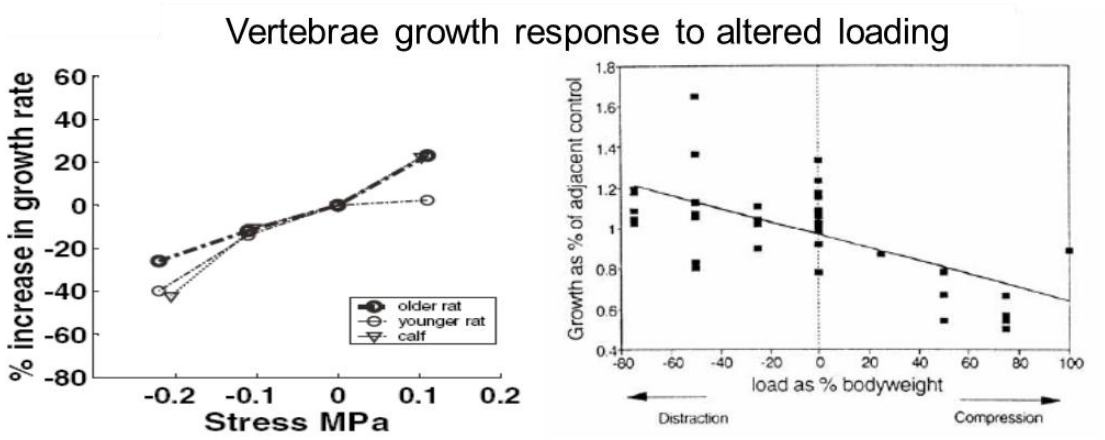

Figure 1.9: Growth response to induced static loads (modified from [9, 109])

These experimental findings were then translated into a numerical correlation that defines the growth rate as a function of altered stress.

$$\beta = 1.71\,\mathrm{MPa}^{-1}$$
$$G = G_m\,[1 - \beta\,(\sigma - \sigma_m)]$$

Equation 1.1: Correlation between longitudinal bone growth and local stress [3]

Where G is the actual growth rate (usually listed in mm per year) on the bone under consideration, G_m is the mean baseline growth, σ represents the stress on the growth plate, and σ_m is the mean stress on the growth plate. Also, the results from this stress input experiments seem to be consistent regardless of species, thus making the results extendable, with limits, to predict the behaviour of human bone growth under compression and distraction. A factor that varies slightly is the scaled parameter β [0.4 – 1.7 MPa^{-1}] depending on the species and growth plate location. This growth/stress correlation does not include a "lazy zone" in a similar manner to which bone remodelling is only responsive to abnormally high or low stresses [110]. As

speculated by Lerner et al., it would appear that natural selection would favour such a zone in order to avoid oversensitive bone growth that may result in potentially harmful or restricting morphologies [98]. Nevertheless, the aforementioned correlation is widely accepted and its utility has been extended to pose as a leading hypothesis explaining the pathomechanism of various musculoskeletal deformities that progress in conjunction with patient growth.

Growth Plate Modulation numerical modeling

The first attempt of incorporating the effect of vertebral growth modulation into a computational algorithm was to predict scoliotic curvature progression performed by Stokes. However, the results did not represent the behaviour of a true scoliotic curve. Curvatures of about 3° where obtained, but no axial rotations of the vertebrae, a phenomenon often associated with spinal deformities, presented themselves in the results [111]. Later, Villemure et al. successfully demonstrated similar results that included axial rotation by the use of a FEM using beam elements. This was achieved by anteriorly offsetting the patient's gravity line and modeling the growth plate under the growth/stress correlation previously derived by Stokes. Also, results from these simulations returned the presence of vertebral wedging, from irregular growth patterns, in addition to the axial rotation progressing towards the convexity of the curve, two concepts observed in the progression of scoliosis [7]. Both the models explored and incorporated longitudinal growth of the vertebral body utilizing equation 1.1 without the presence of a muscle bias. Huynh made a model that included the growth modulation in the longitudinal direction as well as muscles forces within the control process. Upon simulating asymmetric muscle degeneration at different levels, the weaker muscles found their way onto the convex side of the developing scoliotic curvature. These results emphasized the role of both the obliquus internus and the rectus abdominis in maintaining spinal stability [10].

1.2.6 Spinal bone remodelling

Bone is a very dynamic tissue, its ability to restructure as the result of mechanical stimuli has been recognized for approximately a century. However, most of the findings that are widely accepted have been reported in the last 30 years. These accepted discoveries have been verified to exhaustion and have thus become second nature in the field of bone biomechanics. Moreover, they acknowledge and highlight the ability of bone to alter its morphology with the objective to

handle efficiently local inputs (stresses/strains). In contrast to bone growth modulation which responds to both static and dynamic loading, dynamic inputs are responsible solely for triggering bone remodelling. Further, such dynamic stimuli are only required for short durations in order to generate an adaptive response [112]. With this in mind, several authors attempted to derive and adequately map the details of this complex process.

Within the spinal column, bone remodelling may be observed to take place at several locations. Vertebral bodies adapt to altered loading conditions in order to adequately handle their mechanical environment. This is observed as the posterior region of the lumbar spine has denser cancellous bone than the anterior region [113] leading to the educated hypothesis that this region undergoes increased loading. A similar phenomenon may be observed in scoliotic spines. Increase bone mineral density has been quantified in the concave portion of the coronal curve [114] corroborating with the understanding that this region is also attributed with increased loading. Furthermore, with regards to anterior and posterior remodelling, it has been demonstrated that the posterior endplate in the lumbar spine exhibit increased mechanical properties when compared to the anterior portions [115]. It is therefore plausible that the irregular mechanics of the endplates are, in a similar fashion to altered cancellous density, due to remodelling as a result of increase loading. Moreover, with regards to scoliotic patients, it has been shown that AIS has a persistently lower bone mineral density than age- and sex-matched controls suggesting irregular remodelling related abnormal bone metabolism [116].

1.3 Scoliosis

Scoliosis is a spinal musculoskeletal deformity with a prevalence between 2-3% if defined by an inclusion criterion of a 20 degrees Cobb angle measured in the coronal plane [117]. Due to the vast complexity of this phenotype, several categories have been defined to better describe its aetiology and associated side effects. Such classifications include: congenital, functional, neurological and idiopathic scoliosis. Idiopathic scoliosis, defines approximately 80% of all scoliotic cases. As the name implies, the origin of idiopathic scoliosis continues to elude researchers.

Clinical measures of scoliosis

The primary measure is the Cobb angle (Fig. 1.10) following guidelines developed by Dr. Cobb in 1948 [118]. Secondary measures include axial rotation of the spine by measuring the deviation between transverse plane and the associate angle gained from their back referenced from a posterior view as the patient leans forward. A more accurate means of this axial measurement may be achieved using a radiograph and observing the offset of the pedicles from the vertebral body center. Clinical measures may use 2D radiographs to construct 3D models of the spine, rib cage, and pelvis in order to better accurately characterize the deformity [5]. Perhaps the most sophisticated 3 dimensional interpretation of scoliotic deformities are defined by the plane of maximum curvature. Such a measure represents the overall deformity in an easy to use radar chart and effectively classifies patients according to their 3 dimensional curves[119].

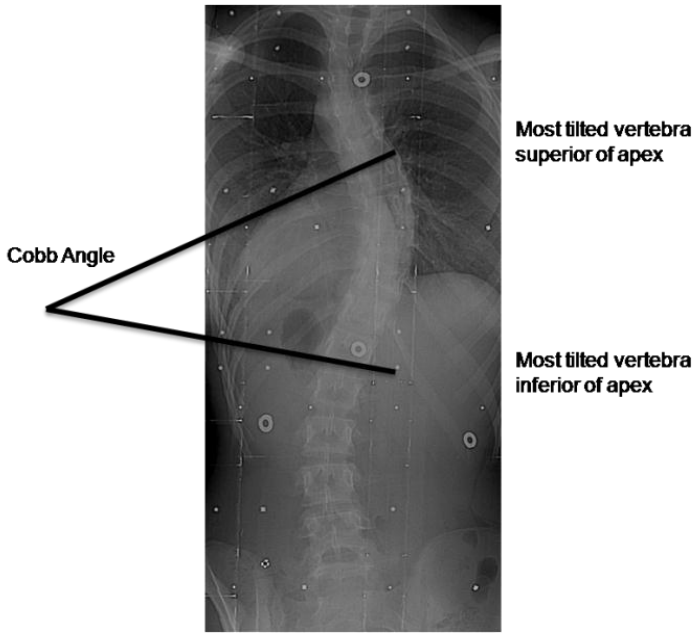

Figure 1.10: Measurement of Cobb angle

Further complicating this 3D deformity is development of a rib hump (Fig. 1.11). As the curvature progresses axial rotation often follows and, in turn, alters ribs alignment. Rib hump often leads to the breast asymmetry discontent in female patients [115]. It has been speculated that rib hump correction would limit AIS progression [120]. Moreover, rib length modulations have been shown to be capable both inducing and correcting scoliosis in animals [121]. In an attempt to better understand the biomechanical impact of this possible correctional avenue, FEMs were utilized. Results supported and confirmed the potential applicability of this method

as a means to correct scoliosis [50, 51]; however, it has yet to be adopted as a conventional intervention suggesting such reluctance must be justified.

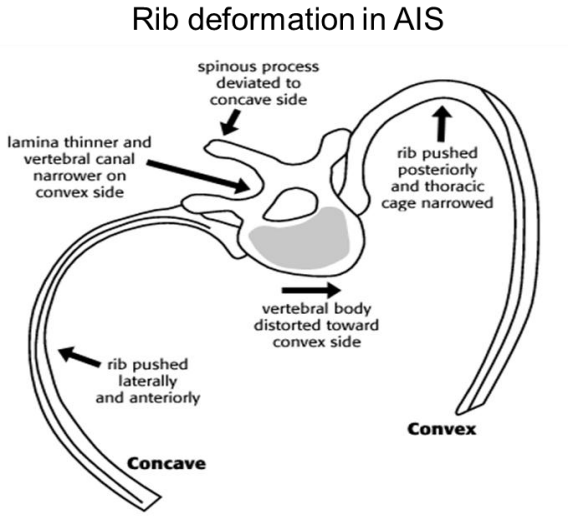

Figure 1.11: Scoliotic rib deformation (obtained and modified on January 25th 2011 from http://www.rad.washington.edu/staticpix/mskbook/RibHump.gif)

1.3.1 Etiology of idiopathic scoliosis

Over the years several scientists and clinicians have proposed various hypotheses related to idiopathic scoliosis. Despite such efforts, to date, most etiological theories are described as secondary rather than causative factors.

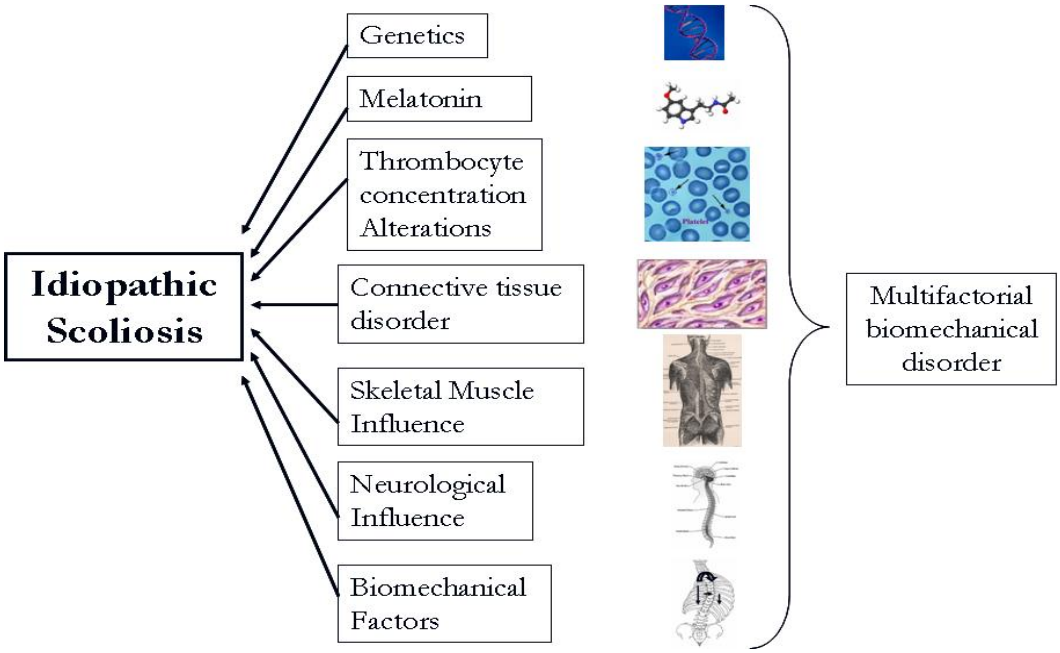

Figure 1.12: Leading etiological hypotheses of scoliosis

Genetics have long been explored as a possible trigger of AIS. This concept was propagated by the observation that 11% of direct siblings of a scoliotic parent had AIS while 2.4% of secondary siblings were affected. Moreover, monozygous twins had a 73% scoliotic correspondence rate while dizygous twins had a rate of 36% [122]. Evidently, such observations led to genetic linkage analyses and complex segregation analyses in order to obtain the loci responsible for AIS. Nevertheless, these studies are often restricted by complications in family history (migration and mating patterns), differing theoretical analyses, and non-negligible environmental influences. Therefore, the general consensus suggests various genetic inheritance patterns while the responsible gene(s) has yet to be identified.

Pinealectomized chickens (removal of pineal gland and elimination of melatonin production) develop scoliotic deformities shortly after they hatch [123-125]. This is believed to be the result of a melatonin deficiency. Moreover, when attempted in rats, this method only impacted bipedal and not quadruped rats. In contrast, Cheung reported conflicting evidence as non-human primates did not developed any sign of scoliosis [126]. Furthermore, most studies report no alterations in melatonin level in AIS patients while melatonin injections in pinealectomized chickens did not always counter the onset of scoliosis. Recently, Moreau showed that melatonin signalling impairment was a factor and impaired in osteoblasts cultured from patients with AIS [127]. Although some contradictions and further development is required, these findings show positive progress in understanding the development of AIS [128].

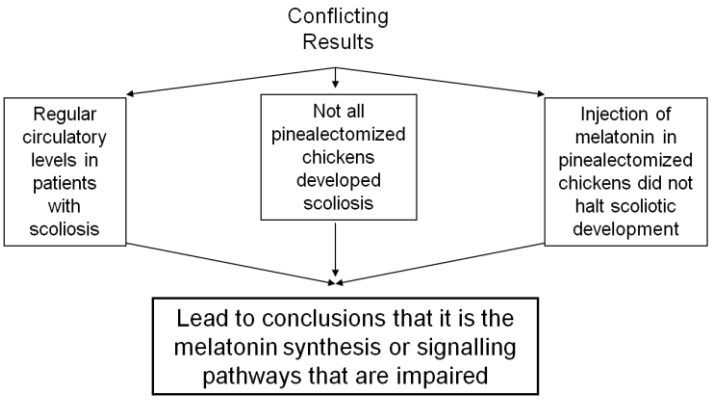

Figure 1.13: Influence of melatonin on AIS

Others explored the shape, size, charge, and function of platelets (thrombocyte influence) in AIS patients compared to control groups. A significant variation was uncovered. Moreover, elevated calmodulin (a calcium receptor regulating contractile behavior) was found in progressive

scoliotic curves when compared to stable curves. The protein contractile systems of platelet (i.e. actin-myosin regulating platelet shape change) and skeletal muscle are related, thus the discovery of irregularities within the platelets would suggest a secondary effect from the contractile system.

Scoliosis is also related to many disorders of connective tissues (ex. Marfan syndrome) thus stimulating etiological hypotheses related to this tissue. This stimulated further research into this avenue with findings summarized below (Fig. 1.14). Despite these findings, altered tissues are also believed to be secondary.

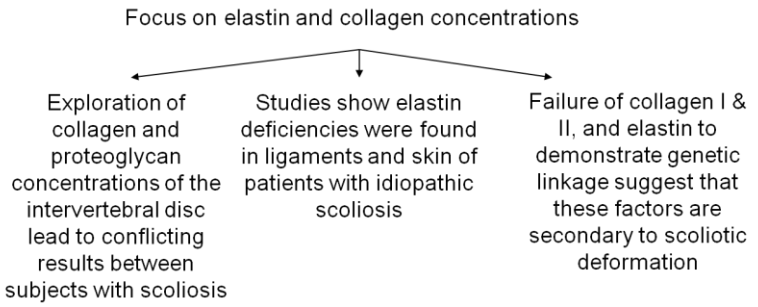

Figure 1.14: Altered connective tissue in AIS

Irregular paravertebral muscle development has also been perceived as a possible etiological factor of AIS. Many findings demonstrated differences between the concave and convex portions of the spine. However, this was quickly identified as a secondary factor. This offset of muscle activity may however be a player in the progression as demonstrated via FEM simulations [10, 85].

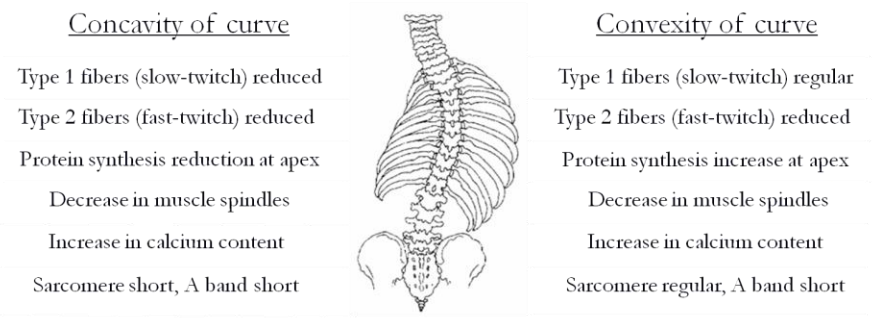

Figure 1.15: Altered paraspinal muscles in AIS patients

The central nervous system has also been believed to play a role in the development of scoliosis. Damage to the central nervous system in animals provoked scoliotic deformities. Also, when this concept was tested on primates through selective resection of spinal nerves it lead to the

formation of curvature with the severed nerves taking to the convex side [129]. As a result, balance disruption was believed to be linked to offset of the spinal alignment [130]. Despite these findings, progressive forecasting or pre-development diagnosis is not yet possible via neurological analysis; however, results lack convincing reproductive significance to support this potential prognostic avenue.

Finally, although speculated as an etiological factor, biomechanical factors are most often attributed to the pathomechanism or progression of scoliosis. Nevertheless, it may still be plausible that biomechanical factors have a partial role in its etiology through the same pathways used to explain its implication in the pathomechanism of AIS.

1.3.2 Pathomechanism

Scoliotic progression, is generally confined during adolescence [131]. More specifically, the greatest risk resides during the peak growth velocity occurring between the ages of 11 to 13 in girls and 13 to 15 in boys [132]. Curve patterns, curve degree at onset of puberty, curve progression velocity, and gender are amongst to most reliable progressive risk factor to date [133]. In this retrospective study of 205 patients with idiopathic scoliosis, the more severe the deformity at the onset of puberty the greater the progressive risk. Furthermore, double thoracic curves proved to most frequently necessitate surgical intervention as a result of scoliotic progression. Finally, this study confirmed the well accepted notion that females are for more susceptible to scoliotic progression when compared to males. Regardless of these insightful prognostic tools, there remains no consistent method to identify patients at risk of progression. Nonetheless, biomechanical interpretations offer clarifications to the obscure field of AIS progression.

Under the Hueter-Volkman principle, asymmetric loading over the vertebral growth plates, coupled with the phenomenon of growth modulation, leads to the adoption of vertebral wedging. Normal pressures acting on a human vertebral endplate is between 0.8 to 0.9 MPa [134], whereas in scoliosis the convex pressure is measured at 0.7 MPa and the concave side pressure measured at 1.3 MPa under a compressive force of 1010N laterally offset by 2mm [135]. This pressure differential applied during a growth phase will induce a vertebral wedging in the coronal plane with the greatest influence observable at the apex as shown in figure 1.16. However, in the sagittal plane no presence of significant pathological wedging is observed [136] suggesting that

intervertebral disc wedging to be a more dominant player in kyphotic and lordortic curves or vertebral forces to be perpendicular to growth plate in sagittal plane. In turn, this wedging adds to the overall deformity of the coronal curve and is believed to partially describe the progression of idiopathic scoliosis as described by the "vicious cycle" [3].

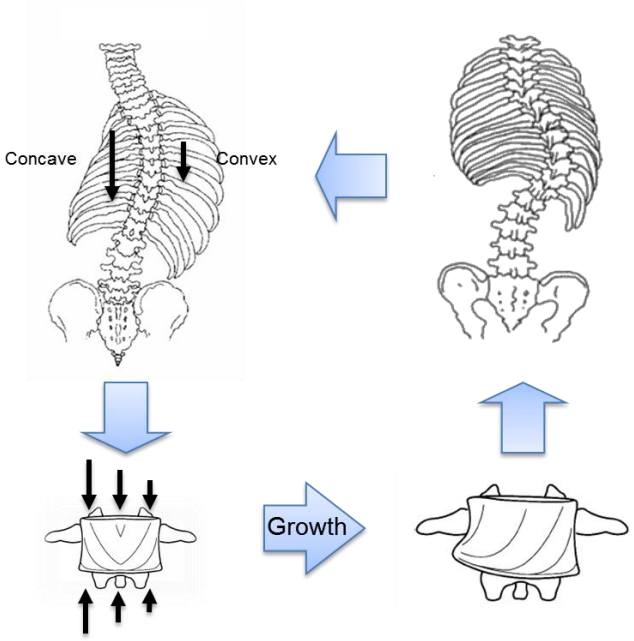

Figure 1.16: Scoliosis progressive cycle from a biomechanical perspective (in part modified from [136])

In light of the knowledge spanning from vertebral growth modulation, it was previously hypothesised that neurocentral canal growth was a contributor to AIS progression. Experiments on an immature pigs showed that halting growth in one of these posterior regions led to convincing scoliotic deformities [137]. Furthermore, this theory was additionally explored by implanting pedicle screws in order to restrict its growth locally in an animal model resulting in scoliotic curves [138]. However, further investigation of the role of pedicle growth in the progression of curvature was performed with finite element analysis and concluded that asymmetrical pedicle geometry was not sufficient to produce scoliosis, vertebral wedging, or axial rotation [52]. Moreover, neurocentral canal growth ends at 10 years of age [87, 139] and, thus, prior to AIS progression. Consequently, it is more realistic to characterize irregular pedicle morphology secondary and resulting from bone remodelling. The current reflection remains that epiphyseal growth modulation is the leading contestant in AIS progression.

The manner in which this asymmetrical loading affects the intervertebral disc may also be of interest. As previously noted, intervertebral disc growth ends prior to AIS progression. However, discs are compressible and thus assume wedge configurations when placed under asymmetrical loading. The importance of the disc wedging in the progression of scoliotic curves was significant in a cross sectional study of 150 patients as it progressed consistently with the deformity [140]. However, it is difficult to draw a direct line of causation from disc wedging to scoliotic progression.

With the aforementioned biomechanical alterations in mind, it is no surprise that upon developing treatments for AIS, these side effects have been exploited in the attempt to restore spinal alignment. Otherwise said, if one could rectify the phenotypic shortcoming of AIS they would, theoretically, solve the problem.

1.3.3 Conventional treatments

The treatment of scoliosis sequentially includes: observation, bracing and surgery as defined in figure 1.17. Suggested treatments depend on the maturity of the patient's bone structure in addition to the degree of curvature.

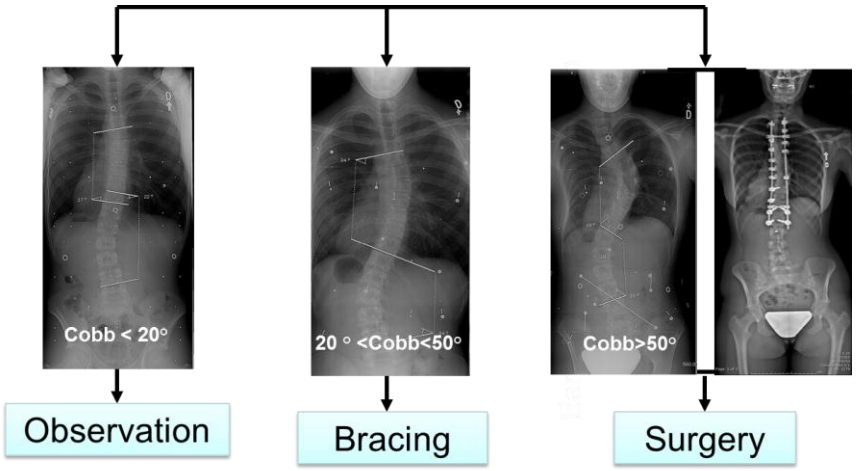

Figure 1.17: Conventional treatment protocol as a function of Cobb's angle

In the quest to develop the best brace, several models have been developed over the past decades. Introduction of the first Milwaukee brace in 1958 seemed to provide a favourable treatment and was quickly adopted by clinicians [141]. Variations of this design later came to market under Boston [142] and Wilmington braces [143]. In the early 1990's, this treatment method was well

established within the medical community making it difficult to follow sufficient control subjects in order to truly test the legitimacy of bracing. Many have proposed that minimal structural corrections gained by bracing are perhaps outweighed by the heavy psychological impact of its application [144]. Further studies suggest that the effectiveness of this treatment is limited to flexible curves (conventionally identified through bending tests) [145]. Others report that the frequency of surgical intervention in braced patients is the same as without bracing [4, 146]. However, good results from bracing appear to be restricted to, and are frequently observed in, children who have advanced in skeletal maturity and possess low Cobb angles [146]. But, upon further reflection, these are the cases which should not significantly progress regardless of such an intervention, once again bringing to question the true effectiveness of bracing. Despite these limitations, important work in biomechanical interpretation of bracing and its optimization provides promise to improve this treatment avenue in the future [77, 147-150].

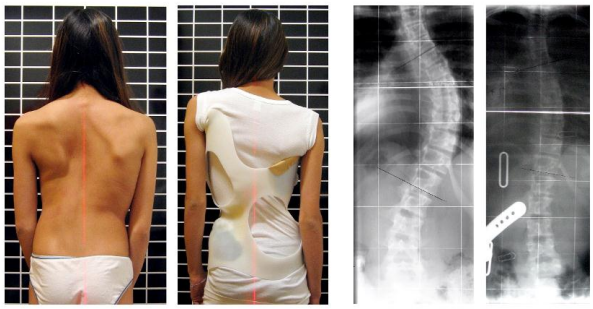

Figure 1.18: Cheneau brace management of scoliosis (obtained on January 25th 2011 from http://commons.wikimedia.org/wiki/File:Scoliosis_patient_in_cheneau_brace_correcting_from_56_to_27_deg.png)

Up to the present time, surgical intervention is the last resort of scoliotic treatment. This method leads to an effective curvature correction that may be selectively varied throughout the procedure [151]. Rods are used in conjunction with fusion to realign the spine. Fixed to the vertebrae with screws, they provide the forces required to reduce dangerous AIS curves. Spinal fusion is the surgical technique used to join two or more vertebral bodies by introducing supplementary bone tissue as to become one solidified structure. It is recommended that this form of intervention be reserved after adolescent growth is terminated. However, if the identified risk factors suggest dangerous progression, intervention may precede skeletal maturity. In such event, anterior growth arrest must be performed in order to avoid the crack shaft phenomenon or a severe imbalance caused by potential growth under fixation [152].

1.4 Scoliosis treatment via fusionless growth modulation

In the search for effective and attractive means to correct idiopathic scoliosis, several novel approaches have been attempted. Fusionless growth sparring instrumentation in particular has received growing attention resulting in a noticeable industrial push, an influx in registered patents, and a rise in scientific publications. This appealing approach consists of using residual spinal growth to correct vertebral wedging to realign the spine. These devices provide an alternative to conventional treatments for AIS.

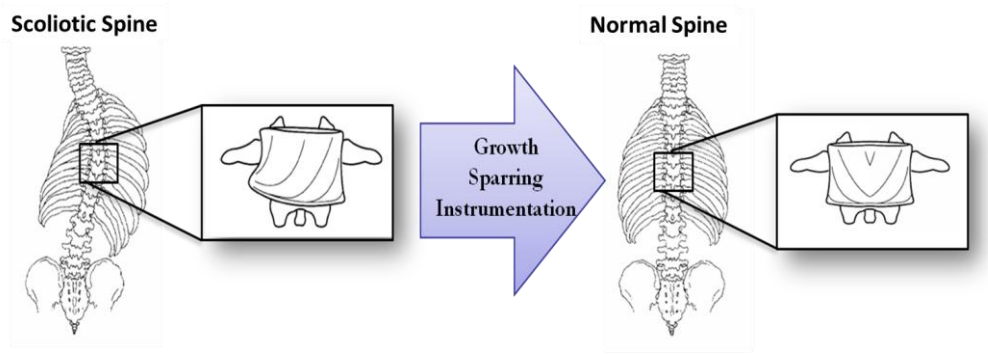

Figure 1.19: Corrective mechanism of growth sparring devices in AIS

Despite optimism and theoretical benefits offered by the method, physiological limitations somewhat hinder the initial enthusiasm surrounding this approach. The axial direction on bone deposition, via chondrocyte calcification, restricts the possibilities for pressure or tension application through mechanical devices. Furthermore, in order to maintain a minimal level of surgical invasiveness, corrective instrumentation should target the anterior portion of the vertebral bodies, while avoiding the anterior vasculature and longitudinal ligament along with the posterior muscles and nerves. Nevertheless, over the years several notable approaches have been attempted as summarize below in table 1.5.

1.4.1 Previous fusionless growth sparring attempts

Table 1.5: Historical summary of published growth modulation for the treatment of AIS

Author	Year	Implant	Subject	Technique	Objective	Measures	Results
Wittek H. [153]	1924	-	Humans	Removed epiphysis plate with a chisel	Correct deformity	Qualitative	Observed realignment of the spine
Nachlas and Borden [154]	1951	Staple	Dogs	Staple spanning 2 discs	Inverse approach (induce deformity)	Qualitative X-ray analysis	Successfully induced curvature. Development of secondary curves
Smith et al. [155]	1954	Staple	3 Humans	Lateral concave stapling spanning disc	Correct deformity	Qualitative X-ray analysis	Progression halted but compensation curves developed
Roaf R. [102, 156]	1963	Staple	188 Humans	Lateral concave stapling spanning discs	Correct deformity	Cobb angle	95 required second operation; 44 improved by ≥ 20°; 69 improved by 10° to 19°; 75 no improvement
Carpintero and Coll [157]	1997	Cable	Rabbits	Wrapping around the concave transverse process and the above spinous processes	Inverse approach (induce deformity)	Cobb angle	Induced an average Cobb of 29° after 2 months with an associated axial rotation
Rumpf [158]	1999	Laser	Foxhounds	Destroy the epiphysis plate on one side	Inverse approach (induce deformity)	Cobb angle	Induced scoliosis curvatures in 75% of cases with 30° max. Laser caused local tissue damage.
Newton and Coll [159, 160]	2002	Flexible Tethers	Cow	Lateral concave implant spanning disc	Inverse approach (induce deformity)	Cobb, ROM, backout, and disc wedging	Showed control of Cobb but induced kyphosis

Author	Year	Implant	Subject	Technique	Objective	Measures	Results
Braun and Olgilvie [19, 161]	2005	Bone anchors with ligament tethers	Goats	Lateral concave implant spanning disc	Correct deformity on progressive model	Cobb, backout, histology, and mechanics	Corrected curvature, impacted disc. Bone density concavity drift.
Betz R. [162, 163]	2003-2005	Shape memory alloy staples	Humans	Lateral concave stapling spanning the disc	Correct deformity	Complete spinal alignment	Fusion required in 2 of 39 patients; 80% showed control of progression[1]
Wall E. [20]	2005	Rigid stainless steel staple with screw fixation	Pig	Lateral concave stapling spanning disc	Inverse approach (induce deformity)	Coronal and sagittal curvatures, fixation, and backout	Steady control of Cobb with some signs of kyphosis. No backout problems due to screw
Newton et al. [164]	2008	Flexible Tethers	Pig	Lateral concave tether spanning disc	Inverse approach (induce deformity)	Coronal and sagittal curvatures, vertebral height, and disc health	1 year post-operative follow up provided impressive growth modulation and no signs of disc degeneration
Schmid et al. [165]	2008	Mini staple	Rat tail	Growth plate compression exclusive of disc	Inverse approach (induce deformity)	Coronal curvature and disc wedging	Consistent control of vertebral wedge and presence of deformity
Newton et al. [166]	2011	Flexible Tethers	Pig	Lateral concave tether spanning disc	Inverse approach (induce deformity)	Coronal and sagittal curvatures, vertebral height, and disc health	Pre-tensioning had no long term benefit in curvature control

[1] Progression control defined as scoliotic deformity not progressing by more the 10 degrees

Several mechanical avenues have been explored with the purpose of effectively restoring regular spinal loading to segmental units. However, thus far, methods most often undertaken span the intervertebral disc whose adjacent vertebrae are showing signs of wedging. This is achieved by introducing a rigid or flexible fixture onto the convexity of the anterior vertebral bodies, thus applying pressure on both the caudal section on the superior segment and the cephalad section of the inferior segment. The most recent and most promising methods utilizing this method apply corrective pressures directly and indirectly in order to restrict unilateral growth on the convexity of the spine. These include a shape memory alloy (SMA) staple, a stainless steel (SS) staple, and a flexible tether.

The SMA staple consists of two or four prongs which, upon reaching its austenite phase through temperature transition, will provide a local compression (Fig. 120). This was presented by Braun and Olgilvie [167] and then later put into practice in a clinical trial by Betz et al. on adolescents with idiopathic scoliosis [162, 163]. Although long term results are pending, the performances of preliminary results are debatable. The bar of success was not placed high as the SMA declares itself successful if following instrumentation, patient progression is limited to 10 degrees. Over the trial, this was achieved in 80% of cases [168] – a statistic very similar to the progressive risk of non-instrumented patients.

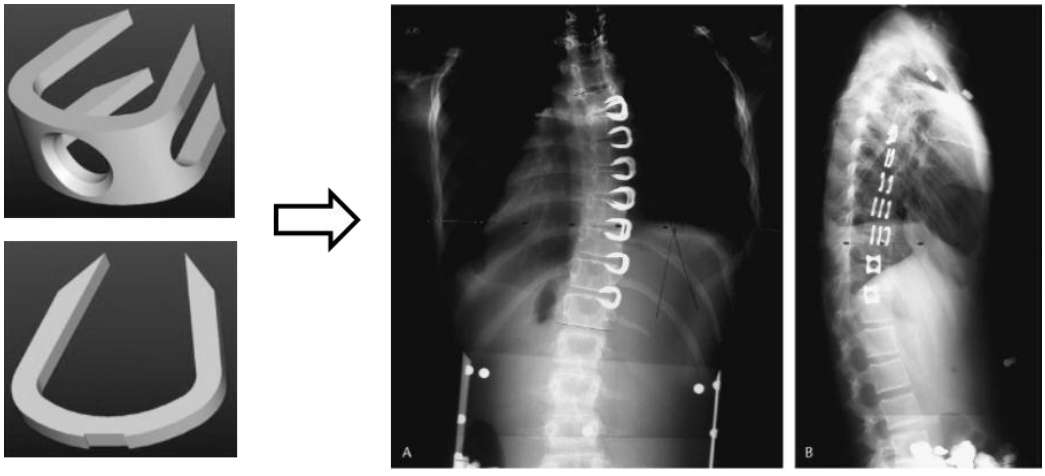

Figure 1.20: Shape memory alloy staple implant (modified from [162, 163])

Braun et al. performs a more complete analysis of the effect of shape memory alloy staples on immature goats. He evaluated the implants Cobb angle effect but also performed backout rate

tests, qualitative histology, and biochemical analyses on the intervertebral discs. This study successfully demonstrated the ability of the SMA staple to provide a mild correction of an experimentally induced, and otherwise progressive, scoliotic model. Studies of the intervertebral discs returned no significant difference between experimental groups; however, differences in disc histology (fibrosis and annulus disorganization) between experimental and control groups existed [169].

Similarly to the SMA approach, a SS staple was proposed in an attempt to achieve greater fixation and perhaps improved correction (Fig. 1.21). Upon being fixed into the vertebrae with the aid of a screw, the inserted wedge is believed to provide an initial pressure while the presence of the staple body spanning the disc will provide the passive resistance required to limit vertebral growth. Results from this study demonstrated the ability of the device to induce a spinal curvature in the coronal plane of an immature pig and had diverse effect on the sagittal plane. Moreover, after 8 weeks the device induced a coronal curvature of 16.4°±5.4° using the inverse approach (creation of scoliosis) [20]. This was further verified by local measurements of growth plate region heights and cell size in various regions of the targeted epiphysis [170]. The device succeeded in chondrocyte hypertrophy suppression under the implant indicating growth modulation. To explore the local mechanical influence of this device, experimental studies using a Wheatstone bridge (calibrated as a stress sensor) in a porcine model suggest that his method increased the local baseline stress by 0.1 MPa immediately post-operatively. However, in contrast, this method proved to reduce mean peak dynamic compressive stress [171].

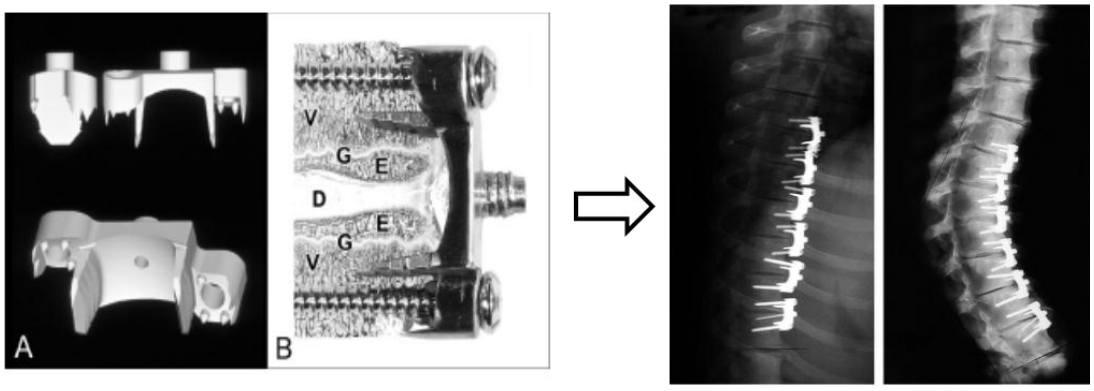

Figure 1.21: Stainless steel staple with screw (modified from [20])

Newton and later Lowe, explored a similar method, however used tethering over a vertebral segment to modify local growth. This method inserted pre-tensioned tethers fixed to adjacent vertebra with bone screws and spanning the corresponding disc (Fig. 1.22). Included in their analysis was the impact on Cobb and kyphosis angles, disc wedging, range of motion, sectional vertebral height, and back out rate [159, 160, 172]. Results suggested this method as an effective means of manipulating vertebral growth in the coronal plane. After 12 weeks, the tether induced a coronal curvature of 11.6°±4.8° via the inverse approach. Later, analyses of instrumented discs returned increased proteoglycan synthesis and collagens II and X were upregulated in instrumented segments. These findings may indicate the occurrence of degenerative changes [173].

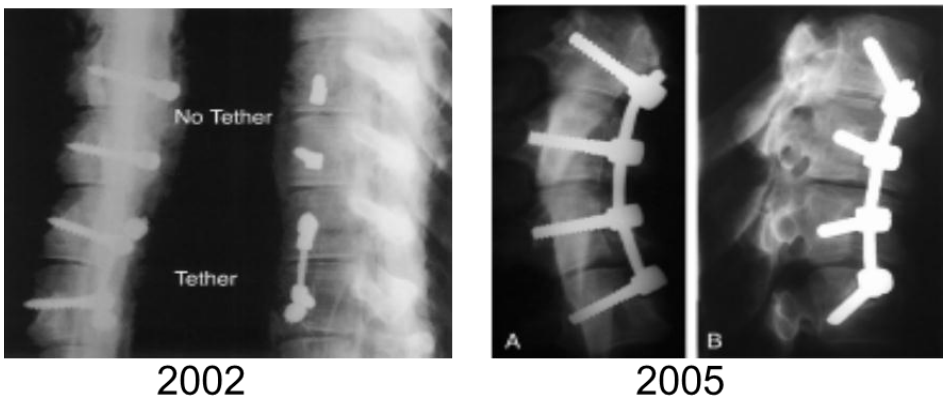

Figure 1.22: Bone anchor with tether (modified from [159, 160])

Later, Braun et al. performed experiments to analyse the effects of both SMA staples and bone anchor tethers. He defined their efficacy by the ability to control progression of the Cobb angle and their integrity as the potential to maintain fixation. Also, the osseointegration index, bone proximity index, bone ingrowths, and pullout strength were examined [19]. The results suggest that bone anchor tethering corrects more effectively the initial deformity and controls progression when compared to SMA staples [174]. Finally, Newton et al. repeated the tether study in a porcine model to find that tether pre-tensioning to provide improved initial correction whereas no significant long term correction benefits were achieved [166].

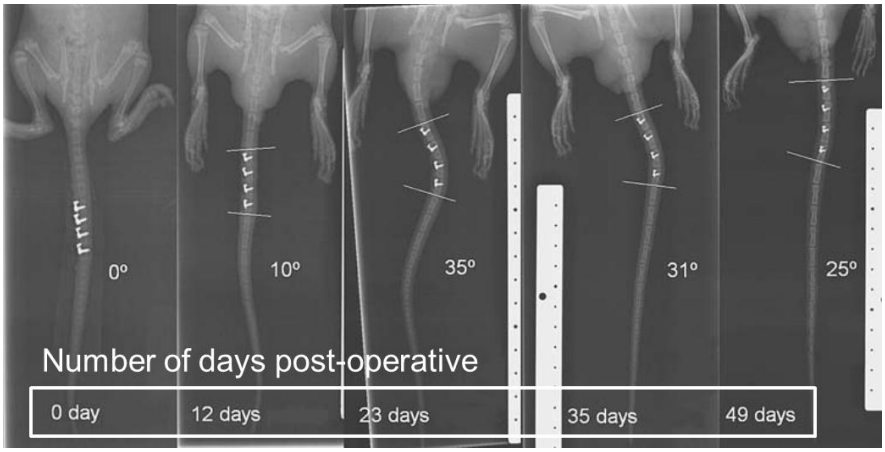

Figure 1.23: Mini staple device in a growing rat tail (modified from [165])

Schmid et al. explored a novel fusionless device that does not span the disc space in a rat tail model [165]. A maximum coronal Cobb angle of 30° and vertebral wedging of 10° was achieved between 23 and 35 days post-operative (Fig. 1.23). However, problems of device fixation and the use of a small animal model with relatively unimportant loads restricted the translation of results towards a potential human application.

Although each of these devices focuses on coronal correction it is worth noting their influence on other anatomical planes. The current consensus amongst authors is that a restriction of coronal plane progression would succeed in limiting additional vertebral axial derotation [19, 20, 162, 173]; however, this hypothesis has yet to be verified. Moreover, the impact on sagittal spinal alignment is not controlled nor does any attempt to manipulate this anatomical plane become apparent through the endless claims found in active patents. The passive influence on this plane is described as follows: a stainless steel staple suggested negligible sagittal influence [20], a stainless steel tether provided important hyperkyphosing effect (5° to 38° for a double tether) [159], a flexible tether and SMA staple produces a mild hypokyphosing or lordotic influence in sheep [19], and a SMA staple was speculated to control its impact on the sagittal plane by placing the staple more posteriorly or anteriorly with respect to the midline of the anterior vertebral body [162].

Each of these devices provides an interesting novelty to the early treatment of AIS. It is no surprise, knowing their market value, that a plethora of patents exist that claim to alter spinal mechanics in a manner that may provide helpful modification to the spine by means of growth

modulation. Nonetheless, to date, none of these devices have been approved by the Food and Drug Administration (USA). In addition, as these devices target adolescents, there is a residing uncertainty of their long term influence on the intervertebral disc.

1.4.2 Patent review

The act of registering patents does not require scientific support thus many more concepts have been devised that seek to alter vertebral dynamics. Patents reviewed in table 1.6 claim to alter the endplate loading and are therefore relevant to methods that seek to induce local growth modulation for AIS treatment.

Mechanically, many methods exist to alter loads on the vertebral endplates. These methods attempt to manipulate the geometry of the spine in order effectively redistribute body weight and spinal loading. Figure 1.24 summarizes these different attempts of which encompass the forces introduced by the selected patents reviewed in table 1.6. That is, spinal realignment and consequential regular spinal load distribution may be achieved by: introducing lateral forces over displaced spinal segments, providing compression to the convexity or expansion/distraction forces to the concavity of the spine, delivering rotational torque to derotated segments, and granting local growth arrest over deformed or wedged vertebrae.

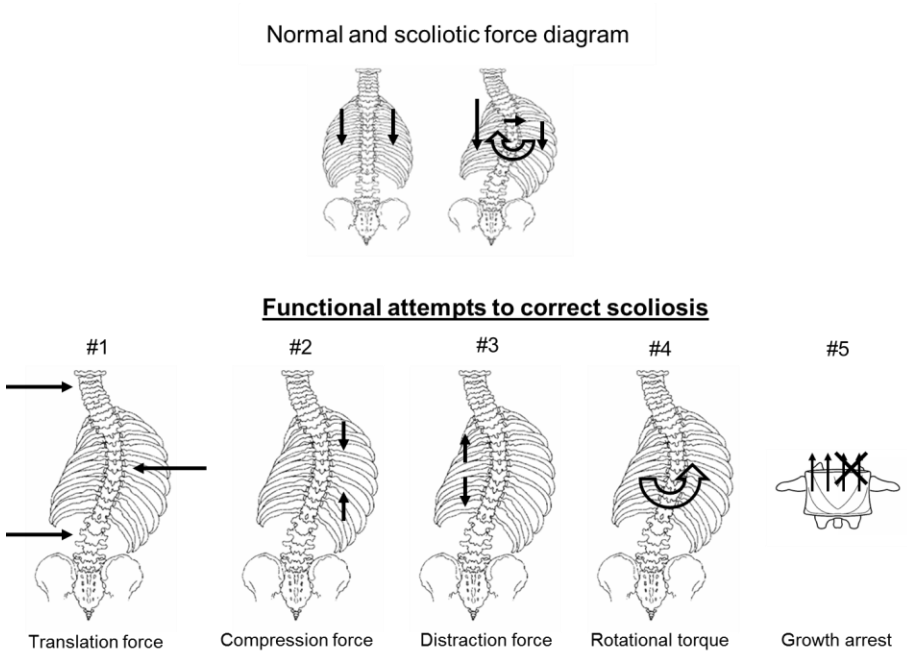

Figure 1.24: Functional attempts to correct scoliosis

Table 1.6: Analysis of current patents pertaining to innovative methods to alter loading within the adjacent vertebral bodies

Patent Type & Number [Ref.]	**Date**	**Inventor(s)**	**Assignee(s)**	**Image(s)**	***In vivo* Test**	**Summary**	**Critique**
US_5053005_A1 [175]	Oct. 1,1991	Gary E. Borodic	Gary E. Borodic, Edmund Pitcher		Rabbit	Uses botox injections to block selective muscle stimulation and alter spinal loading	Attempted to integrate with bracing treatment however interrupts regular muscular behaviour of patients
US_5951553_A1 [176, 177] [177]	Sept. 14,1999	Randal Betz, Michael Sherman, Troy Drewry	SDGI Holdings, Inc Medtronic	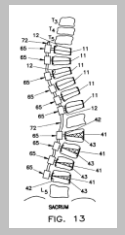	Human	Performs vertebral osteotomies and fixes with removable rigid rod	Interruptions of nutrient transfer within vertebral body and creation of kyphosis in patients
US_20030088251_A1 [178]	May 8, 2003	John T. Braun, Fred J. Molz, Troy Drewry, Sherman Michael	John T. Braun, Fred J. Molz, Troy Drewry, Sherman Michael Medtronic	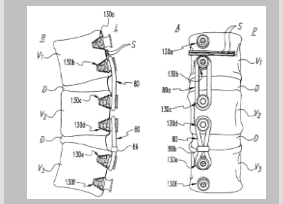	Goat	Method to correct spinal deformities without fusion via growth reduction over convexity	Alters disc mechanics and has been quantified as inducing degeneration
US_20040199219_A1 [179]	Oct. 7, 2004	George R. Dodge, Richard Bowen	George R. Dodge, Richard Bowen	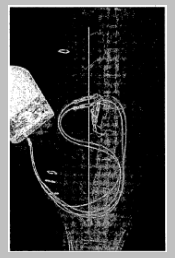	Rabbit	A device to inhibit local bone growth using electrical currents	Requires exterior power source and thus open wounds; difficult to induce local electric field

Patent Type & Number [Ref.]	Date	Inventor(s)	Assignee(s)	Image(s)	*In vivo* Test	Summary	Critique
US_20050171539_A1 [180]	Aug. 4, 2005	John T. Braun, Fred J. Molz, Jeff R. Justis	John T. Braun, Fred J. Molz, Jeff R. Justis Medtronic	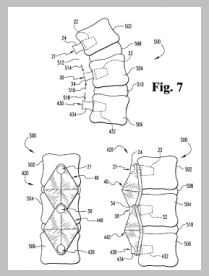	-	Distract vertebrae on concave portion of spine using flexible implant to maintain motion	No *in vivo* test to support claims and force would still remain on the concave portion but relocated at bottom of fixtures; rigid body does not allow growth of concave spine
US_20050177240_A1 [181]	Aug. 11, 2005	Jason Blain	Jason Blain	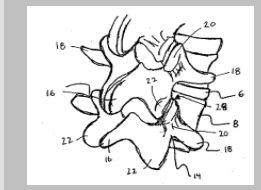	-	Replacing articular facets joint that are degenerated while maintaining a degree of motion	No *in vivo* test to support claims and would alter balance of forces over vertebral bodies
US_20060009767_A1 [182]	Jan. 12, 2006	Douglas Kiester	Douglas Kiester	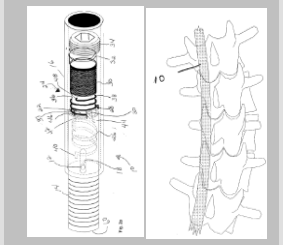	-	Rod to be implanted on concavity of curve to provide controlled expansive forces	Basis that scoliosis is induced by a tight ligamentum flavum which is an refuted hypothesis

Patent Type & Number [Ref.]	Date	Inventor(s)	Assignee(s)	Image(s)	*In vivo* Test	Summary	Critique
US_20060217714_A1 [183]	Sept. 28, 2006	Hassan Serman, Micheal Slivka, Methew Hannen, Peter Newton, Michael Nilson	DePuy Spine, Inc.	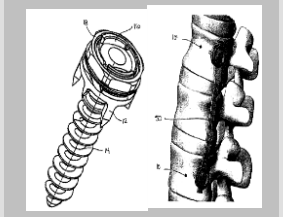	-	A locking mechanism to be used with tethering of the vertebral bodies on the convexity of the curve	Well-developed surgical instruments based on using tethering method which is shown and speculated to induce disc degeneration
US_20070055373_A1 [184]	March 8, 2007	Robert G. Hudgins, Micheal E. Lancial, Hugh D. Hestad	Zimmer Spine, Inc.	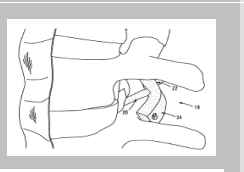 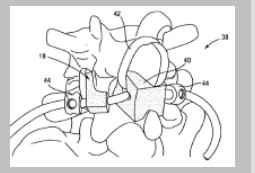	-	Reduce back pain by reducing loading in the intervertebral discs by providing spacing between processes	Fixations of articular facets will immobilize the instrumented segments
US_20070173832_A1 WO_2007075788_A2 [185-187]	July 26, 2007 July 5, 2007	Shawn Tebbe, Moti Altarac, Daniel H. Kim	Vertiflex, Inc.	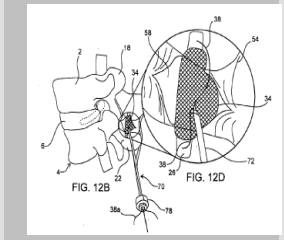	-	Reduce back pain by reducing loading in the intervertebral discs by spacing between processes	No precautions to oppose flexion with the absence of healthy interspinous ligament (resected)

Patent Type & Number [Ref.]	Date	Inventor(s)	Assignee(s)	Image(s)	*In vivo* Test	Summary	Critique
US_20070179493_A1 [188]	Aug. 2, 2007	Richard C. Kim	Richard C. Kim	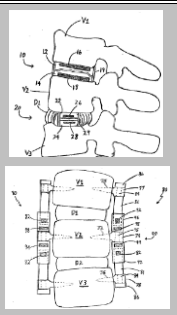	-	Using magnetic force to alter dynamics with the spine	No studies performed to analyse impact of magnetic field nor do any methods exist to minimize spread of field; loss of magnetic power is greatly dependent on magnet proximity
US_20070233084_A1 [189]	Oct. 4, 2007	Randal R. Betz, Edward Miller, Rebeccah Brown, Guilhem Denoziere	SpineMedica Corporation	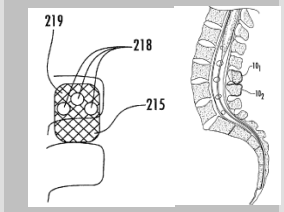	-	Reduce back pain by reducing loading in the intervertebral discs via spacing between processes	No precautions to oppose flexion with the absence of healthy interspinous ligament
US_20070270836_A1 [190]	Nov. 22, 2007	Aurelien Bruneau, Thomas Carls, Eric C. Lange, John D. Pond, Kent Anderson, Henry Bonin	SDGI Holdings, Inc	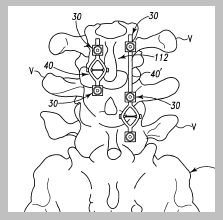	-	Provide posterior dynamic spinal stabilization via controled forces	No field testing and posterior instrumentation will alter force distribution over vertebral bodies

Patent Type & Number [Ref.]	Date	Inventor(s)	Assignee(s)	Image(s)	*In vivo* Test	Summary	Critique
US_20070276380_A1 [191]	Nov. 27, 2007	Tae-ahn Jahng, Jason Yim, Brian Bowman	Tae-ahn Jahng, Jason Yim, Brian Bowman	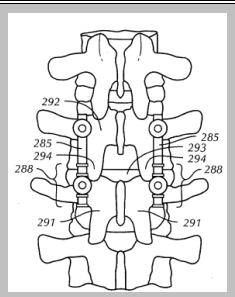	-	Provide posterior dynamic spinal stabilization via controled forces introduced by device	No field testing and posterior instrumentation will alter force distribution over vertebral bodies
US_20070276500_A1 [192]	Nov. 29, 2007	James Zucherman, Ken Hsu, Henry Klyce, Charles Winslow, John Flyn, Steven Mitchell, Scott Yerby, John Markwart	St. Francis Medical Technologies, Inc.	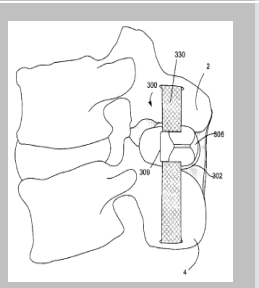	-	Reduce back pain by reducing loading in the intervertebral discs by spacing between processes	No studies performed to analyse the effect of device on segmental dynamics
WO_1990012553_A1 [193]	Nov.1, 1990	Robert Campbell	Robert Campbell	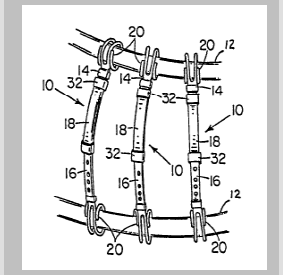	Humans	Provide regular pulmonary function and provide corrective torque for the correction of scoliosis via costovertebral joint	Because ribs are not secured on vertebral body forces provided by device are in part loss through the translation of the instrumented ribs; studies show not effective to correct scoliosis

Patent Type & Number [Ref.]	Date	Inventor(s)	Assignee(s)	Image(s)	*In vivo* Test	Summary	Critique
WO_2000064360_A9 [16, 17]	Nov. 2, 2000	James Ogilvie, Christoph Hopf, Mickael Sherman, Troy Drewry, Jean Suarat	SDGI Holdings, Inc. Medtronic	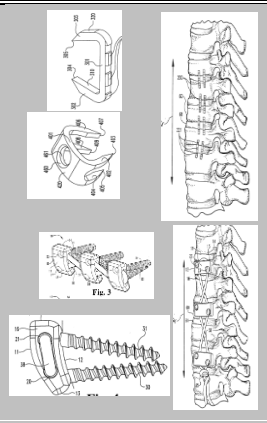	Goat, Human	Method to correct spinal deformities without fusion via growth reduction on convexity of spine	Alters disc mechanics and has been quantified as inducing degeneration; scoliotic corrections are modest an irregular
WO_2001003570_A2 [18, 194]	Jan. 18, 2001	Eric Wall, Donita Bylski-Austrow	Eric Wall, Donita Bylski-Austrow	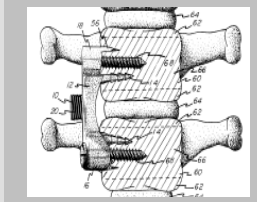	Porcine	Correct scoliosis by reducing growth on convexity of curve	Very rigid implant alters regular disc behaviour and restricts motion as in conventional posterior instrumentation with rods
WO_2002043602_A1 [195]	June 6, 2002	Robert Gaines	Robert Gaines	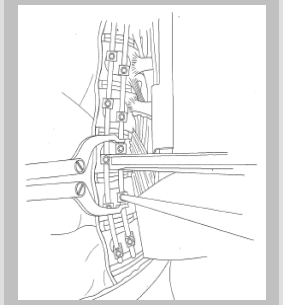	-	Anterior rod technique less invasive than posterior approach using an original spinal staple that requires vertebral body modification	Still requires fusion of implicated segments

Patent Type & Number [Ref.]	Date	Inventor(s)	Assignee(s)	Image(s)	*In vivo* Test	Summary	Critique
WO_2002045765_A2 [196]	June 13, 2002	Daryl Sybert, Lawrence Shimp, Todd Boyce, John Boyle	Osteotech, Inc.	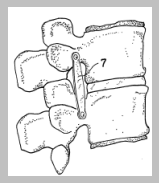 	-	Claims to correct kyphosis, scoliosis, slipped disc, and pain via altering segments dynamics	No studies to support claims; force provided by device is unidirectional and confined to the posterior region
WO_2003003901_A2 [197]	Jan. 16,2003	Isador Lieberman	The Cleveland Clinic Foundation	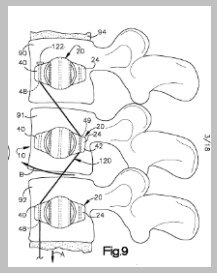	-	Method to provide tension of convexity of spine and the option of providing a corrective torque	Never tested; patent covers a concept that has no supportive research; similar to tethers previously patented (WO2000064360A9)
WO_2005023090_A2 [198]	March 17, 2005	Hong Zang, Charles Johnson, William Pierce, Richard Ashman	Texas Scottish Rite Hospital for Children	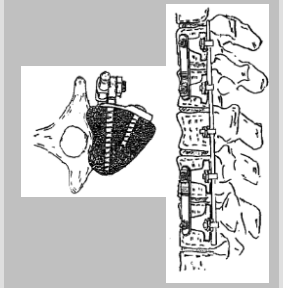	-	More elaborate method of spinal fixation over several site to reduce strains placed on hardware as with regular methods	Even more invasive than regular methods and its requirement is questionable

Patent Type & Number [Ref.]	Date	Inventor(s)	Assignee(s)	Image(s)	*In vivo* Test	Summary	Critique
WO_2007075788_A2 [199, 200]	Feb. 6, 2006	Alan Carl, Dan Sachs, Meir Rosenberg	Vertech Innovations L.L.C.	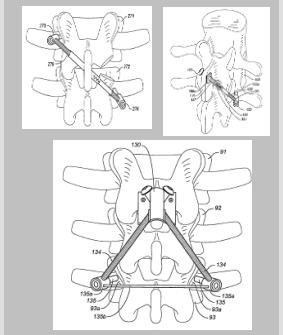	-	Control dynamics of posterior spine in order to provide stability and reduce pain	Requires invasive penetration of posterior muscles and no field tests to support claims
WO_2006110767_A1 [201]	Oct. 19, 2006	Roy Lim, Micheal Sherman	SDGI Holdings, Inc	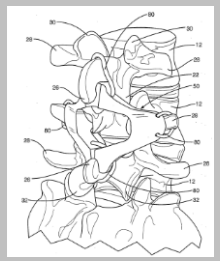	-	Posterior spacer that spans a vertebral segment and replaces a process to eliminate pain.	May halt mobility, invoke wear at site, and induce a kyphotic displacement
WO_2007089979_A1 [202]	Aug. 9, 2007	Aurelien Bruneau, Eric Lange, Randall Allard, Kent Anderson	Warsaw Orthopedic, Inc.	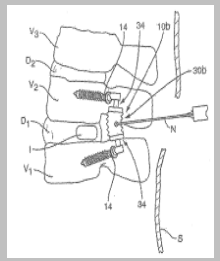	-	Purpose to reduce incision required to insert rod and to increase loading of adjacent constructs	No studies on its impact nor to support claims and no real innovation over current methods

Patent Type & Number [Ref.]	Date	Inventor(s)	Assignee(s)	Image(s)	*In vivo* Test	Summary	Critique
WO_2007090021_A1 [203]	Aug. 9, 2007	Jeff Justis, Hai Trieu	Warsaw Orthopedic, Inc.	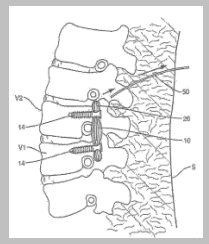	-	Purpose to reduce incision required to insert rod and to increase loading of adjacent constructs	No studies on its impact nor to support claims and no real innovation over current methods
WO_2007109470_A2 [204]	Sept. 27, 2007	John Dawson	Zimmer Spine, Inc.	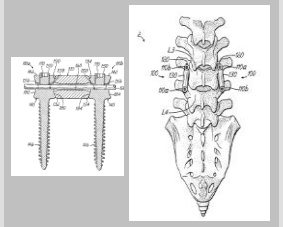	-	A dynamic spine stabilizer that provides both tensional and compressive resistance	No studies on its impact nor to support claims and no real innovation over current methods
WO_2007111795_A1 [205]	Oct. 4, 2007	Gene Dipoto, Alan Shluzas	Endius, Inc,	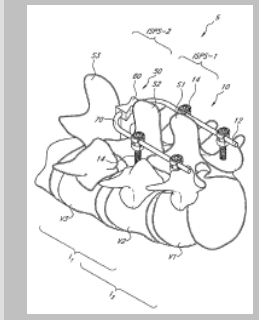	-	To reduce pain by restraining motion in a segment and/or reducing loading on another vertebral body	No studies; supporting a lower vertebra from above would however effectively redistribute the load over the implicated segments

Patent Type & Number [Ref.]	Date	Inventor(s)	Assignee(s)	Image(s)	*In vivo* Test	Summary	Critique
WO_2007147093_A2 [206]	Dec. 21, 2007	Hugues Malandain, Avrain Edidin, Andrew Kohm	Kyphon Inc.	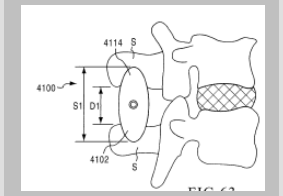	-	Reduce back pain by reducing loading in the intervertebral discs by spacing between processes	No precautions to oppose flexion with the absence of healthy interspinous ligament
US_20090030518_A1 [207]	Jan 29, 2008	Carl-Eric Aubin John Sawark Eliane Schmid Stefan Parent	Carl-Eric Aubin John Sawark Eliane Schmid Stefan Parent	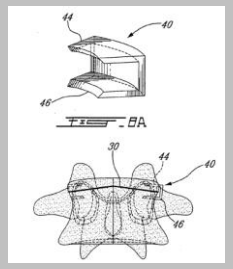	Rats	Provide scoliotic correction without spanning the intervertebral discs	Preliminary analyses in a rat tail model proved positive as an important curvature was induced (reverse method)

CHAPTER 2 : RESEARCH RATIONAL, OBJECTIVES, AND HYPOTHESES

Surgical treatment including fusion is currently the gold standard employed for the correction of scoliotic deformities in adolescents. A reassessment of spinal anatomy, biomechanics, and scoliotic pathomechanism in combination with modern medical device technologies has reaffirmed fusionless growth modulation as a plausible alternative treatment for this cohort. Fusionless devices involve harnessing residual spinal growth as a means of correction rather than progression. Over the past decade, numerous scientific publications have emerged to support fusionless devices for the improved treatment of adolescent idiopathic scoliosis (AIS). Moreover, a growing number of registered patents in conjunction with recurrent pre-clinical and clinical trials further strengthen their future adoption.

However, to date, fusionless devices struggle to demonstrate consistent corrections of scoliotic deformities. Moreover, fusionless treatments actively pursued, appear to imperil the long term health of the intervertebral disc and are restricted to the unilateral correction of a 3D deformity. Improvements in the understanding of scoliotic progressive and corrective biomechanics and the consequent development of enhanced fusionless devices would offer a sizable and innovative contribution towards the improved treatment of AIS.

The general objective of this doctoral project was the: Design, optimization, and experimental evaluation of a fusionless device to induce growth modulation and correct spinal curvatures in adolescent idiopathic scoliosis.

In order to address this general objective, a finite element model (FEM) was to be devised and utilized as the initial developmental platform. This would allow the investigation of biomechanical factors involved in AIS pathomechanism, the analysis of current fusionless devices, and the elaboration of improved fusionless devices for the treatment of AIS. Thereafter, realization of this general objective would require supplementary *in situ* and *in vivo* experimentations. Thus, a comprehensive device development platform was devised that makes use of subsequent *in silico*, *in situ*, and *in vivo* analyses. Consequently, the general objective was divided into the following 4 specific objectives:

Objective 1: Develop a custom FEM of the spine with integrated growth dynamics;

Objective 2: Exploit the FEM to explore new biomechanical factors involved in the pathomechanism of AIS;

Objective 3: Exploit the FEM to analyze biomechanically current fusionless growth modulating devices; and

Objective 4: Exploit the devised developmental platform (*in silico*, *in situ*, and *in vivo* analyses) to develop, optimize, and validate novel and improved fusionless growth modulating devices for AIS.

The central theme addressed in this thesis is:

Improved fusionless treatments for AIS may be developed subsequently to understanding biomechanical factors in its pathomechanism, identifying shortcomings of previous fusionless devices, and utilizing a comprehensive design platform that include *in silico*, *in situ*, and *in vivo* analyses. This central theme was divided into the following hypotheses:

Hypothesis 1: Biomechanical factors (concave-convex mechanical biases) in scoliotic spines increase apical asymmetrical growth plate loading by 25% and, concomitantly, augment coronal vertebral wedge progression by 1° (10%) over 1 year of adolescent growth;

Hypothesis 2: Current fusionless growth sparring methods (shape memory alloy staple, stainless staple, and flexible tether) reduce asymmetrical growth plate loading by 35% and restrict coronal scoliotic progression to 10% over 2 years of adolescent growth;

Hypothesis 3: A refined intravertebral epiphyseal device will modify vertebral wedging by 4° without altering the intervertebral disc in a porcine model after 12 weeks; and

Hypothesis 4: A 3D tether will modify vertebral wedging by 4° and axial rotation by 5° in a porcine model after 12 weeks.

The objectives and corresponding hypotheses of this doctoral thesis were explored and resolved in the sequence depicted in figure 2.1. Development of *in silico* platform allowed objectives 1 and 2 to be attained and hypotheses 1 and 2 to be explored. Complementing *in situ* and *in vivo* platforms accorded a means to accomplish objective 4 and investigate hypotheses 3 and 4. As a result, 4 manuscripts were submitted and published in peer reviewed journals detailed in chapters 3 to 5. An additional feasibility study is reported in Chapter 6. Finally, to resume and integrate

these studies, a general discussion is found in chapter 7 followed by conclusions proclaimed in chapter 8.

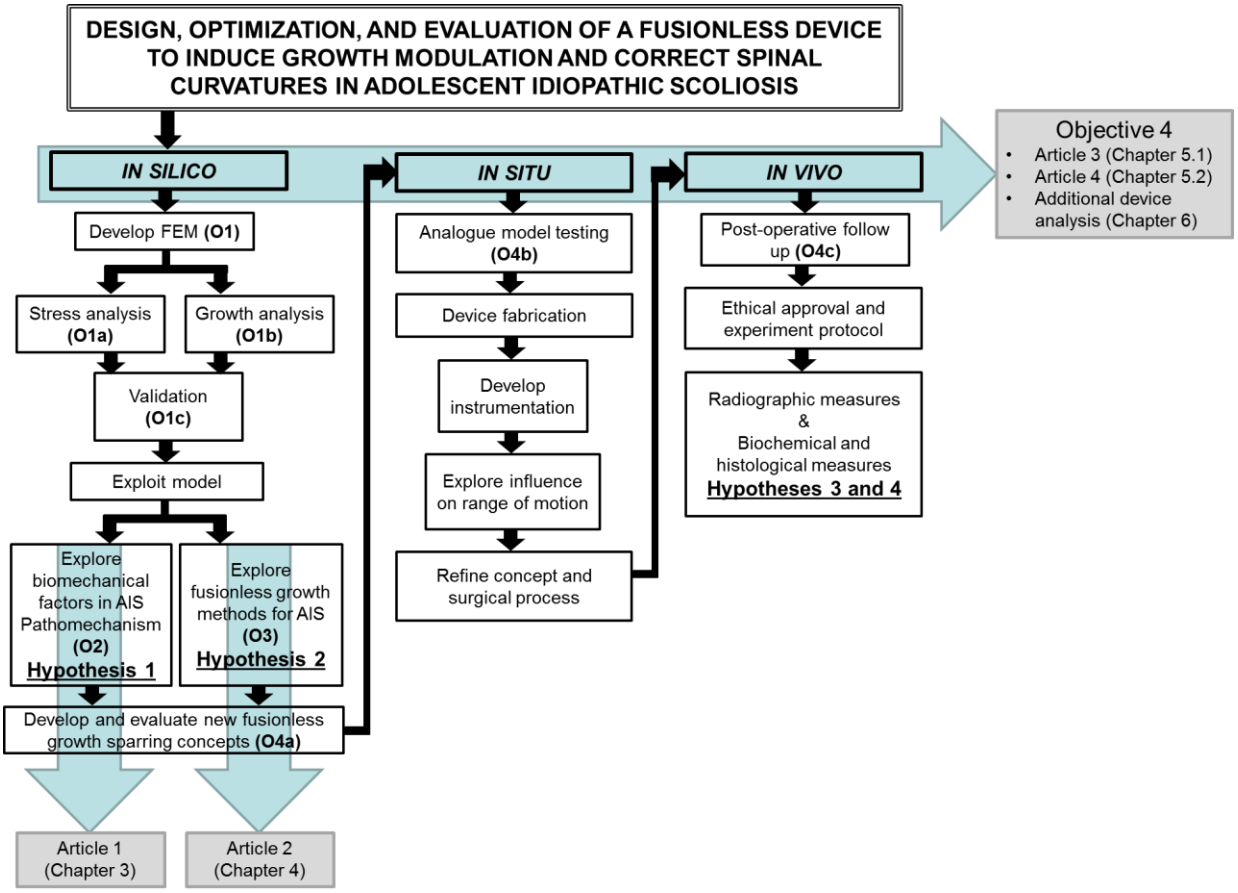

Figure 2.1: Thesis objectives (O), hypotheses, and associated manuscripts

CHAPTER 3 : Study of biomechanical factors in the pathomechanism of adolescent idiopathic scoliosis

3.1 Framework of first article

This study was an important step towards the general objective of this thesis as many features discussed herein are reliant on methods adopted in this manuscript while improved understanding of scoliotic biomechanics was gained from its conclusions. Asymmetrical loading of vertebral growth plates and consequent growth modulation are the foundations upon which biomechanical progression of scoliosis and corrective methods of fusionless devices are governed. This manuscript explores a novel biomechanical factor hypothesized to manipulate growth plate stress distribution utilizing detailed measures of asymmetrical vertebral growth plate loading and predictions of the long term scoliotic progression. The realizations of objectives 1 and 2 with the exploration of hypothesis 1 are presented in the manuscript entitled "The Role of Spinal Concave-Convex Biases in the Progression of Idiopathic Scoliosis," for which the contribution of the first author is considered to be 85%. This manuscript was published in the *European Spine Journal* on January 8, 2009.

3.2 Article 1: The role of spinal concave-convex biases in the progression of idiopathic scoliosis

The Role of Spinal Concave-Convex Biases in the Progression of Idiopathic Scoliosis

Mark Driscoll, J. Eng.[1,2]; Carl-Eric Aubin, Ph.D., Eng. [1,2]; Alain Moreau, Ph.D. [3,4,5]; Isabelle Villemure, Ph.D., Eng.[1,2]; and Stefan Parent, MD, Ph.D.[2]

1 - École Polytechnique de Montréal, Biomedical Engineering Institute, Montreal,Canada

2 - Research Center, Sainte-Justine University Hospital Center, Montreal, Canada

3 - Laboratory in Molecular Genetics of Musculoskeletal Diseases, Sainte-Justine University Hospital Research Center, Montreal, Canada

4 - Department of Stomatology, Faculty of Dentistry, Université de Montréal, Montreal, Canada

5 - Department of Biochemistry, Faculty of Medicine, Université de Montréal, Montreal, Canada

Address for notification, correspondence, and reprints:
Carl-Éric Aubin, Ph.D., P.Eng, Full Professor
Canada Research Chair, ‘‘CAD Innovations in Orthopedic Engineering,’’ & NSERC/Medtronic Industrial Research Chair in Spine Biomechanics
École Polytechnique de Montréal
Mechanical Engineering Department
P.O. Box 6079, Station ‘‘Centre-ville,’’
Montreal, QC, H3C 3A7, Canada
Phone: 514-340-4711, extention 4437
Fax: 514-340-5867
Email: carl-eric.aubin@polymtl.ca
Phone: 1 (514) 340-4711 ext. 4437

3.2.1 Abstract

Introduction: Inadequate understanding of risk factors involved in the progression of idiopathic scoliosis restrains initial treatment to observation until the deformity shows signs of significant aggravation. The purpose of this analysis is to explore whether the concave-convex biases

associated with scoliosis (local degeneration of the intervertebral discs, nucleus migration, and local increase in trabecular bone-mineral density of vertebral bodies) may be identified as progressive risk factors.

Materials and Methods: Finite element models of a 26° right thoracic scoliotic spine were constructed based on experimental and clinical observations that included growth dynamics governed by mechanical stimulus. Stress distribution over the vertebral growth plates, progression of Cobb angles, and vertebral wedging were explored in models with and without the biases of concave-convex properties.

Results: The inclusion of the bias of concave-convex properties within the model both augmented the asymmetrical loading of the vertebral growth plates by up to 37% and further amplified the progression of Cobb angles and vertebral wedging by as much as 5.9° and 0.8° respectively.

Conclusions: Concave-convex biases are factors that influence the progression of scoliotic curves. Quantifying these parameters in a patient with scoliosis may further provide a better clinical assessment of the risk of progression.

Keywords: scoliosis, growth modulation, hemiepiphysiodesis, finite element model

3.2.2 Introduction

Scoliosis is a musculoskeletal deformity defined by a lateral and rotational curvature of the spine. This affects 3% to 4% of the population of which 80% are idiopathic. There are several theories that attempt to describe its etiology, however no individual or exclusive cause has yet to emerge from this ongoing investigation. Notwithstanding, it is generally accepted that an important factor in the progression of such deformity is founded on the Hueter-Volkmann principle [19]. This principle distinguishes how non physiological loading of epiphyseal plates will modify regular growth patterns. When extended to the pathomechanism of scoliosis, it essentially defines how asymmetric loading of the vertebral bodies leads to the progression of the deformity. This phenomenon is further supported by the frequent clinical observation of local vertebral deformations in the form of wedging within scoliotic spines [3,26,39]. The dynamics responsible for such alteration has been verified by several authors and has been quantified through the process of *in vivo* experimentation on various species [34]. The resulting

growth/force relationships have then been integrated into finite element models in order to forecast progression of selected spinal configurations [33,38]. The predictive ability of these simulations highlights the importance of maintaining physiological loading conditions within the spine during pubertal growth.

Although spinal loads are induced by muscular activity, body weight, and subject dynamics, the morphology and mechanical properties of tissues surrounding the vertebral growth plates nonetheless manipulate local stress distribution. More specifically, the health of the intervertebral disc, the migration of the nucleus pulposus, and the trabecular bone mineral density (BMD) have each been identified as factors involved in local stress elevations [11,14,18]. Adams et al. have shown that a degenerated disc becomes the main source of load transfer against the adjacent endplate (formerly the growth plate in immature vertebra) [1]. Also, they have demonstrated that damaged trabecular arcades lead to high stress concentrations in the opposing annulus [2]. Keller et al., among others, have shown a close correlation between intervertebral disc degeneration and underlying trabecular BMD [15]. Degenerated discs and increased trabecular BMD undergo an increase in mechanical modulus [9,21]. These mechanical biases may then generate local increase in the stress levels of the surrounding growth plate. Such concept of stress shielding, due to altered mechanical properties, has been recognized to play a role in the etiology of posttraumatic osteoarthritis of knee articular cartilage [13]. This is propagated by a local increase in BMD, which allows for a greater load support and thus the associated increased rate of cartilage wear. Within the spinal column, the described concave-convex biases are known to cause elevated risk levels of failure in endplates [25] but their role in the progression of idiopathic scoliosis has never been explored.

The geometric configuration of a scoliotic spine entails remodeling of both the discs and the trabecular bone due to unbalanced loading between the concave and convex sides of the curve. Elevated levels of BMD have been quantified to occur in the concave side of the curvature when compared against measurements taken from the convex side [31]. The annulus of adolescent scoliotic spines have been reported to show signs of degeneration on the concave portions [10,37]. Also, an offset of the geometric centre of mass in vertebral bodies, due to altered BMD, was correlated to the degree of nucleus migration in adolescents with idiopathic scoliosis [28,29].

The objective of this article is to test the hypothesis that the lateral concave-convex biases of scoliotic spines play a role in the progression of the deformity by altering stress distribution over the growth plates.

3.2.3 Material and methods

The geometry of two finite element models (FEM) was constructed on the bases of patient specific characteristics obtained from a stereo-radiographic reconstruction technique, which provided 3D coordinates of seventeen points per vertebra [4]. The patient under consideration had a right thoracic curve of 26° Cobb (apex at T7) with a normal sagittal profile. The resulting FEM consisted of approximately 35,000 elements governed by linear elastic behaviour (Fig 1). The models were composed of seventeen anterior vertebral bodies from T1 to L5 and 16 intervertebral discs, while including nine anatomical partitions with material properties that reflect findings from published studies (Table 1). These partitions include: the cortical shell; two trabecular portions dividing lateral concave and convex sections; two divisions for the annulus fibrosus, also with a concave-convex division; nucleus pulposus; and the vertebral growth plates constructed in 3 sections, as previously explored [36]. In this study, the zones of the vertebral growth plates were constructed in 3 sections, namely a sensitive zone, a newly formed bone layer, and a transition zone. The sensitive zone includes the physiological reserve, proliferative and upper hypertrophic regions of the growth plate. The newly formed bone area includes the lower hypertrophic region in which bone calcification occurs. The rate at which local bone growth occurs in this section is governed by the stress levels experienced in the above sensitive layer [30]. The transition region links the above sensitive and newly formed bone regions to the underlying trabecular bone and its cortical shell (Fig. 1). The applied spinal forces are based on load distribution, as reported by Schultz [32], and defined by a body weight (BW) distribution of 14% on T1 with an addition of 2.6% on the following vertebral bodies, ending at L5 with 57% of BW. A “follower load” of a magnitude of 20%BW, with force vectors tangential to curvature profile, was also added to BW to emulate the forces and stability provided by the surrounding muscles [27]. The boundary conditions of the model were provided by a restraint on the inferior extremity of L5 in all degrees of freedom during loading and growth simulations.

The nucleus within the disc remained laterally centered in the model without biases, while its position was governed by a correlation derived from MRI analyses that determined the nucleus position in patients with idiopathic scoliosis in the model including the discussed concave-

convex biases [29]. Its displacement from the lateral geometric center was defined as a function of its wedge angle. However, the mechanical properties of the nucleus were homogenous throughout the spine in both models. The Young's modulus of both the annulus and the trabecular regions were uniform in the model without biases whereas different concave-convex moduli were programmed to be representative of their location within the curvature of the spine in the model with biases. The elastic modulus distribution within the discs respect experimental results from complementing studies [17,42]. The local concave stiffness of the annulus was attributed a modulus associated with discs of grade 2 degeneration (Nachemson score) whereas the modulus of the convex portion was considered that of a healthy disc. The modulus of the concave section of the trabecular bone was acquired by following correlations describing the offset of the geometric center of mass [28], while the convex portion was maintained at 400 MPa. Equilibrium relations were then used, while assuming a lateral 50-50 division, to achieve the ratio of BMD between the concave and convex regions. These ratios were then converted into BMD magnitudes respecting statistical CT measurements taken from vertebral bodies of stage II tanner subjects [6]. Finally, a local modulus bias was achieved by converting the difference in BMD to a bias in mechanical properties within the trabecular region using correlations obtained from pig vertebrae [24].

The analysis of the modulus bias impact was performed in two parts. The first part was achieved by executing a detailed stress analysis of the sensitive layer of the vertebral growth plates of the models with and without the concave-convex biases (trabecular bone and annulus moduli with nucleus migration). Results were then compared and the differences in growth plate stress distribution were quantified. This interpretation consisted of acquiring the longitudinal stress, perpendicular to the growth plate, on the 7000 nodes of the sensitive layers in each spine model. Because it is the sensitive layer that responds to stress and regulates the level of growth in the vertebra [30], it was divided into 9 zones of interest: flex zone (FZ), lateral left (LL), lateral right (LR), anterior (A), posterior (P), anterior lateral left (ALL), anterior lateral right (ALR), posterior lateral left (PLL), and posterior lateral right (PLR) (Fig. 1). The mean stress across each zone of the growth plates was determined by taking the average longitudinal stress acting on all nodes within the division. This simulation was then repeated while individually including the nucleus migration, annulus stiffness bias, and trabecular bone stiffness bias, in order to interpret the influence each factor has on altering stress distribution over the growth plates.

The second part of the analysis performed iterative computations in order to simulate the growth of an adolescent spine for both models (Fig. 2). A progression of one year was simulated at three-month intervals where each iteration consisted of four sub-steps. First, loading was applied followed by evaluation of the stress levels (σ) registered in the growth plates' sensitive zone. The scaled (β) difference, between these stress levels (σ) and those measured under regular conditions (σ_m), were converted into a thermal loading and applied on the adjoined elements in the newly formed bone layer. The thermal expansion (G) of the elements in this layer simulated the respective mechanical growth modulation as a ratio of the otherwise uniform growth (G_m).

$$G = G_m(1 - \beta(\sigma - \sigma_m))[34]$$
$$\beta = 1.7MPa^{-1}$$
$$\sigma_m = 0.1 - .02MPa$$
$$G_m = 0.8 - 1.1\frac{mm}{year}[5]$$

Equation 3.1: Article 1 equation 1 Dynamic growth equation and constants

Stress analysis, which included assessment of sagittal and coronal Cobb angles as well as vertebral wedging, was performed after each growth iteration.

Prior to the analysis, the model was validated through several steps. The stress profile, measured within the intervertebral disc of the L4-L5 functional unit, was compared to the magnitude and distribution of those measured *in vivo* by Wilke in various positions [40]. Also, load sharing between the cortical and trabecular regions in the vertebral body, was compared with ratios acquired via compression testing of excised thoracic vertebra [16]. In addition, a sensitivity analysis was performed in order to explore the relative contribution to the loading assumption compared to the explored concave-convex biases. This was achieved by simulating different loading applications (gravitational load, follower load, and a scaled combination of both gravitational and follower loads) and quantifying the change in stress distribution relative to those imposed by the explored concave-convex biases. Finally, in order to isolate the influence of the concave-convex biases from spinal configuration, the calculated concave-convex inequalities (Table 1) for the right-thoracic model were integrated into a third FEM. This model was attributed a normal alignment, thus perfectly aligned in the coronal plane with a sagittal profile matching the other models, and the described growth simulation was performed.

3.2.4 Results

The concave-convex biases for the spine model with a right thoracic Cobb of 26° were determined to be a 2 MPa increase of the modulus in the concave portion of the annulus, up to 29.6 MPa increase in the concave section of the trabecular bone when compared to convex portion, and a nucleus migration of up to 2 mm towards the convexity of the spine. Stress distribution in the right thoracic model without these biases showed the presence of asymmetrical loading on the growth plates. Figure 3 shows how the coronal curvature creates non-uniform stress distribution between the lateral left (concave) and right (convex) subdivisions. The greatest difference occurred in the apex T7 at 0.46 MPa, with the lateral left section measuring 0.68 MPa and the lateral right showing 0.22 MPa. Results from running identical simulations, in the model that included the effect of a migrating nucleus and mechanical concave-convex biases in the trabecular and annulus, are also displayed in figure 3. The analysis returned very similar stress profiles for the anterior and posterior zones of interest in the growth plates. However, it returned a stress increase on the concavity of the curve (LL) and a stress reduction on the convexity (LR) of the thoracic region, while the opposite effect was observed in the lumbar region. This difference is most prominent at the apex of the curvature T7 at 0.63 MPa, with lateral left and right stresses of 0.78 MPa and 0.15 MPa respectively. Therefore the relative difference at the apex imposed by including the biases was found to be 0.17 MPa or a 37% increase over regular stress distribution without the presence of the biases. This increase in asymmetric stress caused by the concave-convex biases varied in the thoracic curve between 18% at T4 and 29% at T9 whereas stress manipulation was less prominent in the lumbar region. The individual contribution of the concave-convex biases, to the increase in asymmetrical loading of T7, was calculated to be 43% due to annulus stiffness bias, 22% from the trabecular stiffness bias, and 35% evolved from nucleus migration.

Results from growth simulations performed under the above conditions further highlighted the influence of concave-convex biases. There was negligible progression of lordosis and kyphosis defined by insignificant vertebral wedging in the sagittal reference plane. However, the Cobb angles and vertebral wedging in the coronal plane progressed over the length of the simulations. Figure 4 displays the vertebral wedging in the coronal plane after one year of progression for the models with and without the integration of the concave–convex biases. The wedge angles for both cases share the same pattern with a slight discrepancy at T11-T12, which becomes the

inflexion point of the new spinal configuration. The sum of vertebral wedging in the thoracic and lumbar regions are 33.0° and –15.3° respectively for the simulation performed with uniform mechanical properties, i.e. where no discrepancies between concave and convex portions were included. The same simulation performed with the presence of concave-convex biases yielded vertebral wedging sums of 36.6° at the thoracic level and -21.4° in the lumbar region.

Results from the sensitivity analysis of the concave-convex stress distribution showed prominent reliance on the loading condition as expected. However, for each loading condition the relative difference in stress distribution, as a result of including the biases, showed little variation. Finally, results from uniquely simulating the concave-convex biases in the spine model without the presence of a scoliotic curvature were obtained. Under a healthy spine configuration these biases were responsible in providing an average stress difference of 0.04 MPa between what was previously convex and concave sections. When a growth simulation was performed on this model, results included a vertebral wedge sum of $2.7°$ and $-3.1°$ in the thoracic and lumbar regions respectively along with a vertebral wedge pattern that followed results observed in the model with a right thoracic curve (Fig. 4).

3.2.5 Discussion

The mechanical influence of increased vertebral BMD, annular degeneration, and nucleus migration in scoliotic spines was explored. These biases were included in a finite element model and modified stress distribution over the growth plate as well as played a moderate role in the progression of scoliotic deformities. For a spine model with an initial right thoracic Cobb angle of 26°, inclusion of these biases increased the difference in concave-convex growth plate stress distribution by up to 37% (0.17 MPa) at the apical vertebra. The recorded differences in lateral stress distribution agreed with *in vivo* measurements taken from the discs of patients with scoliosis [20]. Although this reported study obtained hydrostatic pressure measurements from patients positioned laterally with loading conditions unlikely simulated in this study, this close agreement demonstrates the qualitative corroboration of the model in terms of stress prediction. This increase in asymmetrical stresses, caused by the inclusion of the concave-convex biases, provoked an additional progression of 3.6° in the thoracic region and 5.9° in the lumbar portion when compared with simulations without the integration of the curvature biases.

These results support the hypothesis that the explored biases alter the force transmission path within the spine. The remodeled and more rigid concave portion assumes dominance over the

load distribution and thus increases asymmetrical stresses within the vertebral growth plates. This, in a sense, provides stress shielding of the convexity of the vertebral growth plates in scoliotic spines. The notion of this load stress shielding in the spinal column is further supported by the close correlation found between local annulus degeneration and elevated levels of trabecular BMD in the underlying vertebral body [23]. Grant et al. also demonstrated this phenomenon by quantifying increased endplate strength in areas of degenerated discs and elevated trabecular BMD [8]. Such correlations demonstrate that these factors complement each other by increasing the weight bearing capacity due to internal remodeling. The bone remodeling process, once initiated, becomes a dynamic cycle governed by Wolf's Law [41], where the concave portion becomes stiffer, while the convex portion weakens. This model does not include algorithms that control the level of internal remodeling as a function of stress stimulus. The present model interprets the level of degeneration of the disc and the remodeling of the trabecular bone to be constant, as a function of initial configuration. As mentioned, these parameters were obtained by following *in vivo* correlations derived from adolescents with idiopathic scoliosis. These internal biases would increase with time, and thus the inclusion of these adjustments would augment the magnitude of their impact on the progression of the deformity.

The elevated stiffness of the concave annulus accounted for 43% of the increase in asymmetrical loading of the vertebral growth plates as compared to 22% for bone remodeling and 35% for nucleus migration, suggesting that annulus remodeling primarily contributes to the increase of growth plate compressive stresses and consequent growth modulation on the spine. The significance of this factor respects previous predictions by Nachemson [22] and is supported by the works of Adams et al. [1], who described that a degenerated disc would entail a transfer of compressive stresses from the nucleus to the degenerated annulus. In a scoliotic spine, it is likely that nucleus migration occurs foremost, while degenerative remodeling of the annulus precedes trabecular apposition. Hence, the prominent stress altering role of the annulus (observed in this analysis) would have greater impact in the later stages of scoliosis progression. However, the onset and early stages of scoliosis would evolve without the presence or influence of the explored biases as they develop as a result of the condition in its advanced stages rather than suggest causative factors. Therefore the investigated biases are not speculated to have a role in

the etiology of scoliosis, alternatively their progressive influence on the pathomechanism was hypothesized and demonstrated.

The loading of the spine has been integrated into the model without any prejudice from its configuration. Other authors have explored the impact of muscle activation strategies [35] or muscle weakening [12] in the progression of the deformity. However, in this analysis, loading was not altered during iterations. Results from the sensitivity analysis provided evidence of the importance of loading conditions on the stress distribution. However, simulations with and without the presence concave-convex biases were performed on identical models in order to isolate and explore the role of these biases while excluding the influence of loading techniques on the results. Therefore this study explores the relative difference imposed by the concave-convex biases and upon examination this difference proved robust under a variety of loading conditions. When the spine model with a healthy configuration, was submitted to the mild bias in properties associated with a right thoracic Cobb angle of 26°, progression of the deformity prevailed and followed the patterns that would have otherwise occurred in the scoliotic spine. These findings further support the unconditional impact that the presence of concave-convex biases has on stress distribution over the vertebral growth plate and, in conjunction, longitudinal vertebral growth rates in scoliotic progression.

The model was limited to the anterior portion of the spine as this study aimed to explore the variation in axial stress distribution over the growth plate. Moreover, roughly 90% of axial compressive loads are believe to be transmitted within the anterior section of the spine [7] thus supporting the models as suitable and relevant platforms for the explored analyses. The correlations used in this analysis represent the mean values of concave-convex biases as a function of spinal configuration. Patient specific values of these parameters, although difficult to obtain, would yield a more personalized investigation of the progressive influence of these biases. However, the developed model may be used to identify spinal configurations in which the differences in concave-convex properties become significant progressive risk factors.

3.2.6 Conclusions

This novel analysis provides evidence that the presence of concave-convex biases is a secondary risk factor that influences the progression of established and advanced scoliotic curves by augmenting the magnitude of asymmetrical stresses in the vertebral growth plates. Quantifying these parameters in a patient with scoliosis may improve progression forecasting.

3.2.7 References

[1] Adams M, McNally D, Dolan P (1996) 'Stress' Distribution Inside Intervertebral Discs. The Effects of Age and Degeneration. J. Bone Joint Surg 78: 965-972

[2] Adams M, McNally D, Wagstaff J, Goodship A (1993) Abnormal Stress Concentrations in Lumbar Intervertebral Discs Following Damage to the Vertebral Bodies: a Cause for Disc Failure? Eur Spine J 1: 214-221

[3] Aubin CE, Dansereau J, Petit Y, Parent S, De Guise J, Labelle H (1998) Three-Dimensional Measurement of Wedged Scoliotic Vertebrae and Intervertebral Discs. Eur Spine J 7: 59-65

[4] Delorme S, Petit Y, De Guisse J, Aubin CE, Dansereau J (2003) Assessment of the 3-D Reconstruction and High-Resolution Geometrical Modeling of the Human Skeletal Trunk from 2-D Radiographic Images. IEEE Trans Biomed Eng 50: 989-998

[5] Dimeglio A, Ferran J (1990) Three-Dimensional Analysis of the Hip During Growth. Acta Orthop Belg 56: 111-114

[6] Gilsanz V, Boechat M, Roe T, Loro M, Sayre J, Goodman W (1994) Gender Difference in Vertebral Body Sizes in Children and Adolescents. Radiology 190: 673-677

[7] Goel K, Clausen J (1998) Prediction of Load Sharing among Spinal Components of a C5-C6 Motion Segment using the Finite Element Approach. Spine 23(6): 684-691

[8] Grant J, Oxland T, Dvorak M, Fisher C (2002) The Effects of Bone Mineral Density and Disc Degeneration on the Structural Property Distribution in the Lower Lumbar Vertebral Endplates. J of Orthop Res 20: 1115-1120

[9] Guerin H, Elliott D (2006) Degeneration Affects the Fibber Reorientation of Human Annulus Fibrosus under Tensile Load. J Biomech 39: 1410-1418

[10] He Y, Qiu Y, Zhu Z (2006) Quantitative Analysis of Types I and II Collagen in the Disc Annulus in Adolescent Idiopathic Scoliosis. Studies in Health Technology and Informatics 123: 123-128

[11] Horst M, Brinckmann P (1981) Measurement of the Distribution of Axial Stress on the End-Plate of the Vertebral Body. Spine 6(3): 217-232

[12] Huynh A, Aubin CE, Mathieu P, Labelle H (2007) Simulation of Progressive Spinal Deformities in Duchenne Muscular Dystrophy using a Biomechanical Model Integrating Muscle and Vertebral Growth Modulation. Clin Biomechanics 22: 392-399

[13] Kamibayashi L, Wyss U, Cooke T, Zee B (1995) Trabecular Microstructure in the Medial Condyle of the Proximal Tibia of Patients with Knee Osteoarthritis. Bone 17(1): 27-35

[14] Keller T, Hansson T, Abram A, Spengler D, Panjabi M (1989) Regional Variations in the Compressive Properties of Lumbar Vertebral Trabeculae. Effects of Disc Degeneration. Spine 14(9): 1012-1019

[15] Keller T, Ziv I, Moeljanto E, Spengler D (1993) Interdependence of Lumbar Disc and Subdiscal Bone Properties: a Report of the Normal and Degenerated Spine. J Spinal Disord 6(2): 106-113

[16] Kilincer C, Inceoglu S, Sohn M, Ferrada L, Bakirci N, Benzel E (2007) Load Sharing within a Human Thoracic Vertebral Body: An In Vitro Biomechanical Study. Turkish Neurosurgery 17: 167-177

[17] Li S, Patwardhan A, Amirouche F, Harvey R, Meade K (1995) Limitations of the Standard Linear Solid Model of Intervertebral Disc Subject to Prolonged Loading and Low-Frequency Vibration in Axial Compression. J Biomech 28: 779-790

[18] McNally D, Adams M (1992) Internal Intervertebral Disc Mechanics as Revealed by Stress Profilometry. Spine 17(1): 66-73

[19] Mehlman C, Araghi A, Roy D (1997) Hyphenated History: the Hueter-Volkmann Law. Am J Orthop 26: 798-800

[20] Meir A, Fairbank J, Jones D, McNally D, Urban J (2007) High Pressures and Asymmetrical Stresses in the Scoliotic Disc in the Absence of Muscle Loading. Scoliosis 2: 4

[21] Mitton D, Rumelhart C, Hans D, Meunier P (1997) The Effects of Density and Test Conditions on Measured Compression and Shear Strength of Cancellous Bone from the Lumbar Vertebrae of Ewes. Med Eng Phys 19: 464-474

[22] Nachemson A (1965) In Vivo Discometry in Lumbar Discs with Irregular Nucleograms. Some Differences in Stress Distribution Between Normal and Moderately Degenerated Discs. Acta Orthop Scand 36: 418-434

[23] Nanjo Y, Morio Y, Nagashima H, Hagino H, Teshima R (2003) Correlation Between Bone Mineral Density and Intervertebral Disc Degeneration in Pre- and Postmenopausal Women. J Bone Miner Metab 21: 22-27

[24] Nielson D, McEvoy F, Madsen M, Jensen J, Svalastoga E (2007) Relationship Between Bone Strength and Dual-Energy X-Ray Asorptiometry Measurements in Pigs. J Anim Sci 85: 667-672

[25] Oshia R, Tencer A, Ching R (2003) Effect of Loading on Endplate and Vertebral Body Strength in Human Lumbar Vertebrae. J Biomech 36: 1875-1881

[26] Parent S, Labelle H, Skalli W, De Guise J (2004) Vertebral Wedging Characteristics Changes in Scoliotic Spines. Spine 29(20): E455-E462

[27] Patwardhan A, Havey R (1999) A follower Load Increases the Load-Carrying Capacity of the Lumbar Spine in Compression. Spine 24(10): 1003-1009

[28] Perie D, Curnier D, De Gauzy J (2003) Correlation Between Nucleus Zone Migration within Scoliotic Intervertebral Discs and Mechanical Properties Distribution within Scoliotic Vertebrae. Magn Reson Imaging 21: 949-953

[29] Perie D, De Gauzy J, Curnier D, Hobatho M (2001) Intervertebral Disc Modeling Using a MRI Method: Migration of the Nucleus Zone within Scoliotic Intervertebral Discs. Magn Reson Imaging 19: 1245-1248

[30] Price J, Oyajobi B, Russell R (1994) The cell biology of bone growth. Eur J Clin Nutr 48: 131-149

[31] Rumancik S, Routh R, Pathak R, Burshell A, Nauman E (2005) Assessment of Bone Quality and Distribution in Adult Lumbar Scoliosis: New Dual-Energy X-ray Absorptiometry Methology and Analysis. Spine 30: 434-439

[32] Schultz A, Andersson G, Ortengren R, Nachemson A (1982) Loads on the Lumbar Spine. Validation of a Biomechanical Analysis by Measurement of Intradiscal Pressures and Myoelectric Signals. J Bone Joint Surg 64: 713-720

[33] Stokes I, (2007) Analysis and Simulation of Progressive Adolescent Scoliosis by Biomechanical Growth Simulation. Eur Spine J 16: 1621-1628

[34] Stokes I, Aronsson D, Dimock A, Cortright V, Beck S (2006) Endochondral Growth in Growth Plates of Three Species at Two Anatomical Locations Modulated by Mechanical Compression and Tension. J Orthop Res 24(6): 1327-1333

[35] Stokes I, Gardner-Morse M (2004) Muscle Activation Strategies and Symmetry of Spinal Loading in the Lumbar Spine with Scoliosis. Spine 29: 2103-2107

[36] Sylvestre P, Villemure I, Aubin CE (2007) Finite Element Modeling of the Growth Plate in a Detailed Spine Model. Med Bio Eng Comput 45: 977-988

[37] Urban M, Fairbank J, Bibby S, Urban J (2001) Intervertebral Disc Composition in Neuromuscular Scoliosis: Changes in Cell Density and Glycosaminoglycan Concentration at the Curve Apex. Spine 26(6): 610-617

[38] Villemure I, Aubin CE, Dansereau J (2002) Simulation of Progressive Deformities in Adolescent Idiopathic Scoliosis using a Biomechanical Model Integrating Vertebral Growth. J of Biomedical Engineering 124(6): 784-790

[39] Villemure I, Aubin CE, Grimard G, Dansereau J, Labelle H (2001) Progression of Vertebral and Spinal Three-Dimensional Deformities in Adolescent Idiopathic Scoliosis: a Longitudinal Study. Spine 26(20): 2244-2250

[40] Wilke H, Neef P, Caimi M, Hoogland T, Claes L (1999) New In Vivo Measurements of Pressures in the Intervertebral Disc in Daily Life Spine 24(8): 755-762

[41] Wolff J (1892) "*Das Gesetz der Transformation der Knoche*," Hirshwald, Berlin.

[42] Yerramalli C, Chou A, Miller G, Nicoll S, Chin K, Elliot D (2007) The Effect of Nucleus Pulposus Crosslinking and Glycosaminoglycan Degradation on Disc Mechanical Function. Biomechan Model Mechanobiol 6: 13-20

3.2.8 Figures and tables

Table 3.1: Article 1 table 1 Material properties of different anatomical structures of the FEM

		Model w/out biases		Model w/ biases		
Tissue	**Zone**	**Young's Modulus (MPa)**	**Poisson's Ratio**	**Young's Modulus (MPa)**		**Poisson's**
				Concave	**Convex**	**Ratio**
Growth Plate	Sensitive	12	0.4	12	12	0.4
	Newly Formed Bone	100	0.3	100	100	0.3
	Transition	300	0.3	300	300	0.3
Intervertebral Disc	Nucleus	2	0.49	2	2	0.49
	Annulus	8	0.45	8 to 10	8	0.45
Vertebral Body	Cortical Bone	14 500	0.3	14 500	14 500	0.3
	Cancellous Bone	400	0.3	400 to 429.6	400	0.3

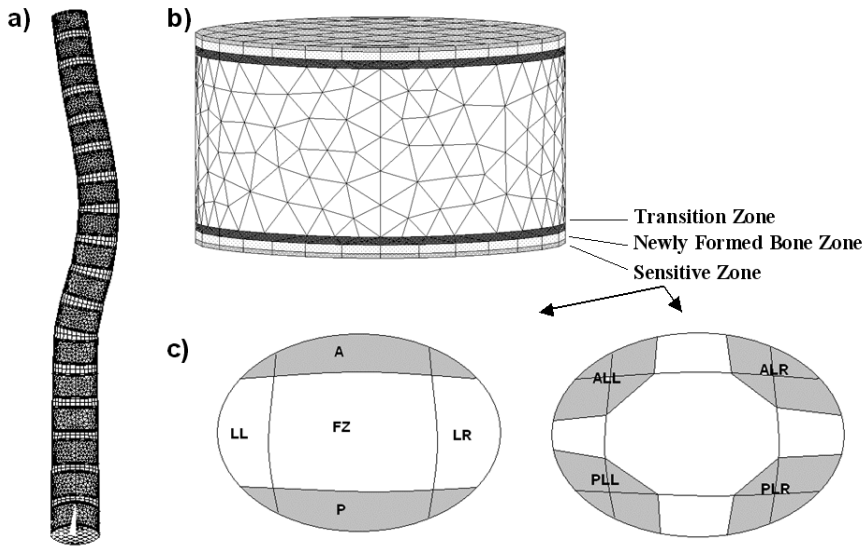

Figure 3.1: Article 1 figure 1 a) Posterior view of FEM; b) Vertebral body with growth plate divisions; c) Stress zones of interest on vertebral growth plate

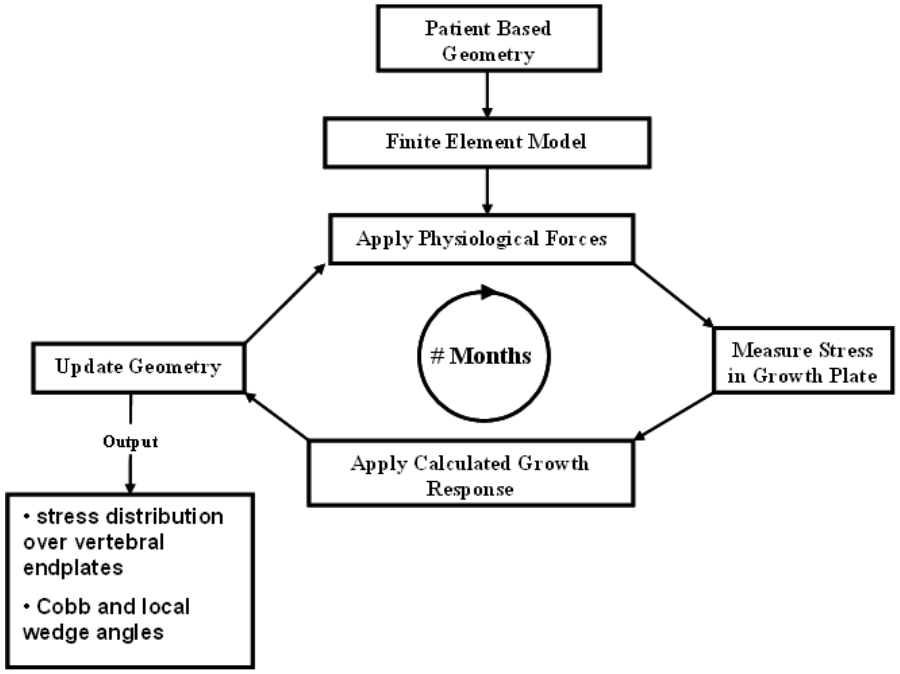

Figure 3.2: Article 1 figure 2 Block diagram of algorithm pattern controlling growth simulation

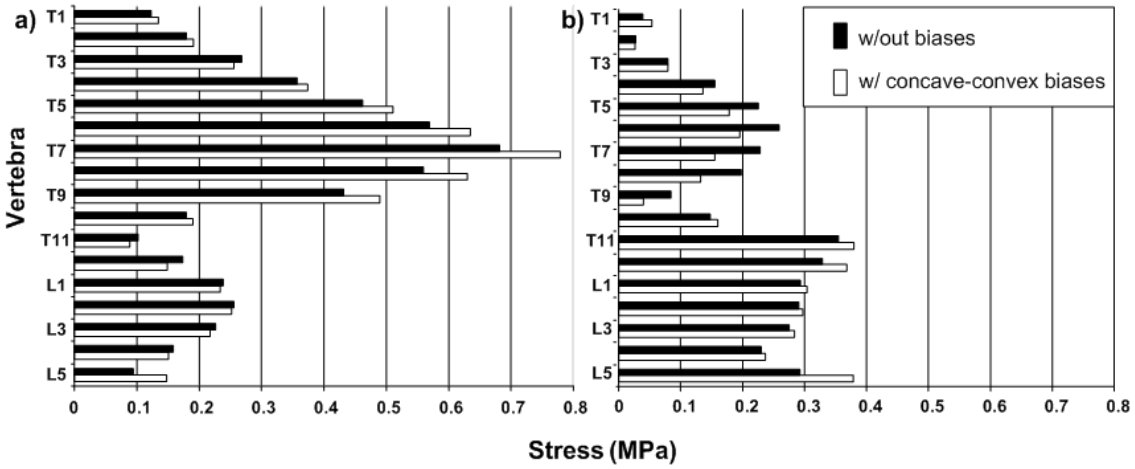

Figure 3.3: Article 1 figure 3 a) Lateral left and b) lateral right stress distribution across vertebral growth plates of spine model with and without concave-convex factors

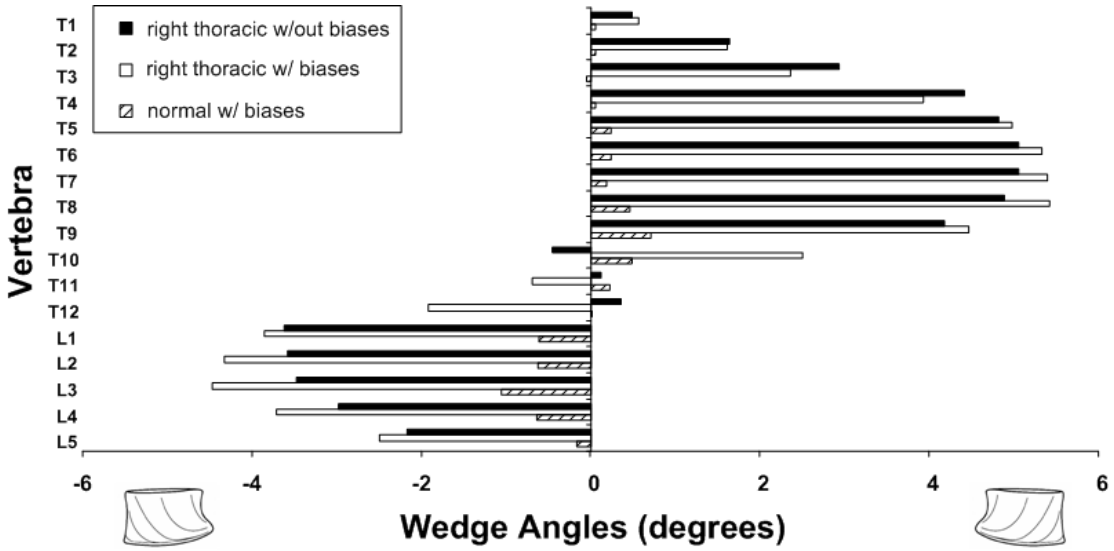

Figure 3.4: Article 1 figure 4 Magnitudes of coronal vertebral wedge angles after 1 year scoliotic progression with and without biases as well as for a normal spinal configuration with biases

3.2.9 Additional studies related to finite element methods

3.2.9.1 Sensitivity analysis of spinal loading method applied to the FEM

Additional sensitivity analyses were performed in order to explore the robustness of the reported and discussed results in article 1 section 3.2. These analyses explored three different methods of simulating spinal loading in the FEM. The first method explored is a follower type load which relies qualitatively on description provided by early works by Pathwardhan and coworkers [78]. That is, each new load introduced over the superior endplates of the vertebral bodies is maintained tangential to the curvature of the spine in both the coronal and sagittal planes. This is performed without taking into account the cumulative effect from the loads provided on superior vertebral bodies. The second loading method is a gravitational load which solely applies axial loading over each successive vertebra. The third loading application, the one applied in article 1, uses a combination of the above techniques illustrated in figure 3.5. This combination consisted of a gravitation load and an additional 20% of segmental load allocations used in article 1 section 3.2.3 that respected the follower type load described above.

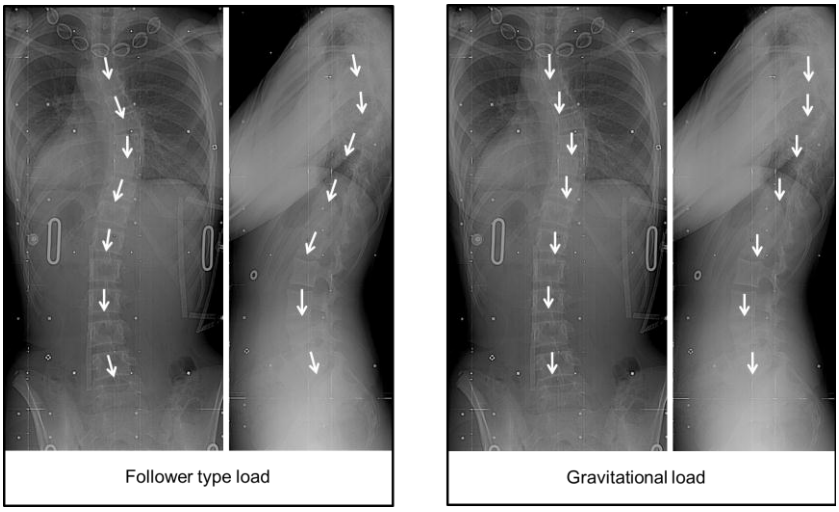

Figure 3.5: Types of spinal loading explored

As briefly discussed in the above article 1 section 3.2.4, different loading techniques altered the absolute difference in asymmetrical loading as one may expect. However, the relative difference imposed by different methods of loading varied lightly [31-42%] but remained comparatively robust.

Results from this analysis further supported the governing hypothesis that the presence of concave-convex biases in mechanical properties would influence internal stress distribution as conclusions were derived from relative interpretations. Thus, reported conclusions are not a function of the experimental assumptions regarding spinal loading. Conclusions of the influence of biomechanical factors (concave-convex biases) as a promoter of asymmetrical loading and consequent scoliotic progression proved consisted under a variety of loading techniques.

3.2.9.2 Sensitivity analysis of spinal alignment of FEM

This sensitivity analysis was to explore the influence of the initial spinal configuration on the reported results. Results reported in article 1 section 3.2.4 arise from a FEM of a scoliotic spine with a Cobb angle of 26 degrees. To further explore the influence of the biomechanical factors (concave-convex biases), the mechanical biases used in the scoliotic FEM were translated into a healthy model (no curve in coronal plane) with no coronal curvature and an identical sagittal profile. The model was loaded and both asymmetrical stress and scoliotic progression were calculated.

A healthy FEM with no concave-convex biases returned no asymmetrical stresses. The healthy FEM with the biases returned asymmetrical stresses in the curved region of the spine up to 0.016 MPa. As a result, this lead to a scoliotic type progression in the spine with a healthy alignment with vertebral wedging reaching a cumulative of 2.7° in the thoracic region.

Therefore, after initiating one year of spinal growth dynamics, the healthy FEM, including mechanical biases, developed vertebral wedging in a reduced but similar manner to the scoliotic. This meant that even without the presence of any scoliotic curvature the underlying mechanical properties of the vertebral segments manipulated local load distributions in a manner that lead to asymmetrical loading. These findings suggest that if a scoliotic spine, which has undergone such biomechanical remodelling (local degeneration of the intervertebral discs, nucleus migration, and local increase in trabecular bone-mineral density of vertebral bodies), may still undergo asymmetrical loading despite being forced into a normal configuration. Moreover, results support conclusions discussed in article 1 section 3.2.6 and are not solely based on the degree of deformity in the explored FEM.

3.2.9.3 Sensitivity analysis of computational methods FEM analysis

The third sensitivity analysis explored the assumptions made in the underlying computational methods applied to the finite element software. Two assumptions were made regarding the size of elements used in the cancellous bone and the underlying algorithm used to calculate deformations that take place in large elements.

The cancellous bone region made up the largest volume percentage in the FEM and, for this reason, it was advantageous to use large elements to reduce computation time. Other regions in the model had a refined mesh and were not further explored. In order to explore the influence of this decision on the results, a refined mesh size was used and results of stress distribution comparing asymmetrical levels on concave and convex stress profiles were explored. The second assumption that was explored was the underlying algorithm that deals with large element deformation. This particular model was developed with performance or computational speed in mind. Therefore special characteristics were selected in order to enhance efficiency and reduce time required for simulations. In order to achieve this, the command NLGEOM, OFF was introduced into the underlying code. When set on, this command essentially includes large deformations of the element while it will maintain pressure loads perpendicular or normal to the elements (i.e. nodal coordinate system is updated). Selecting the NLGEOM, OFF command assumes that element deflections are insignificant to be included a stress stiffening subset into the computational methods. For the purpose of the developed model presented in this dissertation such an assumption seemed to be justified by the use of elements that would undergo relatively minute deflection.

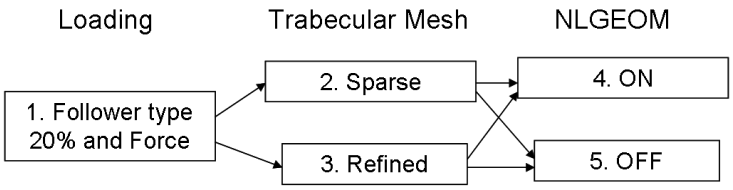

Figure 3.6: Sensitivity analysis of trabecular bone mesh size

In order to fully address the extent of this sensitivity analysis an inter-coupled study was performed as illustrated in figure 3.6. As indicated, the same spinal loading used in article 1 was utilized here.

Results from this sensitivity study are reported in table 3.2. The size of the trabecular mesh did not influence the results *i.e.*, comparison of combinations 1,2,4 with 1,3,4 and 1,2,5 with 1,3,5. The computational method named NLGEOM proved to influence the results *i.e.*, comparison of 1,2,4 with 1,2,5 and 1,3,4 with 1,3,5.

Table 3.2: Results of trabecular mesh size and computational algorithm sensitivity analysis

Concave-convex stress difference (MPa)	
1,2,4	0,61
1,2,5	0,47
1,3,4	0,63
1,3,5	0,47

Therefore, although sparse, the trabecular mesh selected in the above study does not significantly influence results. In contrast, the NLGEOM command seemed to increase the measure of asymmetrical stresses over the vertebral bodies. This is intuitive as this command would take iterative steps during its computation to rigidify elements that become heavily distorted. In other words, because the stresses over the growth plate would be, in part, dependent on reaction forces provided by the intervertebral disc which undergoes the most deformation and an increase in rigidity under the NGEOM command. Further, the elements on the concavity of the discs would become more distorted than those on the convexity thus further enhancing the presence of asymmetrical stresses. Although this computational factor proved to be significant it was neglected from the published study for three reasons. First, because the conclusions are drawn on comparing identical simulations except for the presence of the mentioned concave-convex biases, the inclusion of NLGEOM in both models provided negligible differences with respect to

conclusions drawn. Second, although this command respects stress strengthening of regular materials its relevance is somewhat debatable for physiological tissue. Further, the intervertebral disc realistically contains very complicated compression stiffness which are not taken into account in this simplified model thus the inclusion of the NLGEOM command would not be justified. Third, was a question of time. This command forces a non-linear analysis (iterative analysis which ANSYS refers to as a non-linear process) which roughly tripled the time required to solve the analysis (from 2 minutes to 6 minutes with a Duo core 2.6 GHz Processor with a maximum allocated RAM of 4 GB).

As discussed in article 1 section 3.2.5, the assumptions adopted over the course of the computational analyses were explored and verified. These additional studies supported the discussed conclusions gained from the developed FEM.

CHAPTER 4 : Study of current fusionless growth modulating devices for the correction of adolescent idiopathic scoliosis

4.1 Framework of second article

The next step of this thesis project was to explore the performance of current fusionless devices aimed at the early treatment of AIS. This was also an integral study to the completion of the general objective of this thesis. This analysis was made possible by utilizing the methods devised during the first article *i.e.*, measures of detailed growth plate asymmetrical loading and long term scoliotic progression. The underlying purpose was to acquire improved knowledge of the corrective biomechanics offered by current fusionless devices and, of greater interest, to identify their shortcomings. The realization of objectives 1, 2, and 3 and the investigation of hypothesis 2 are presented in the manuscript entitled "Biomechanical comparison of fusionless growth modulation corrective techniques in pediatric scoliosis", for which the contribution of the first author is considered to be 85%. This manuscript was submitted to the journal of *Medical & Biological Engineering & Computing* on August 26, 2010 and accepted for publication on July 2, 2011.

4.2 Article 2: Biomechanical comparison of fusionless growth modulation corrective techniques in pediatric scoliosis

Biomechanical comparison of fusionless growth modulation corrective techniques in pediatric scoliosis

Mark Driscoll, J. Eng.[1,2]; Carl-Eric Aubin, Ph.D., P. Eng.[1,2]; Alain Moreau, Ph.D. [3,4,5]; and Stefan Parent, MD, Ph.D.[2]

1 - École Polytechnique de Montréal, Biomedical Engineering Institute, Montreal, Canada

2 - Research Center, Sainte-Justine University Hospital Center, Montreal, Canada

3 - Laboratory in Molecular Genetics of Musculoskeletal Diseases, Sainte-Justine University Hospital Research Center, Montreal, Canada

4 - Department of Stomatology, Faculty of Dentistry, Université de Montréal, Montreal, Canada

5 - Department of Biochemistry, Faculty of Medicine, Université de Montréal, Montreal, Canada

Address for notification, correspondence, and reprints:

Carl-Éric Aubin, Ph.D., P.Eng, Full Professor

Canada Research Chair, ‘‘CAD Innovations in Orthopedic Engineering,’’ & NSERC/Medtronic Industrial Research Chair in Spine Biomechanics

École Polytechnique de Montréal

Mechanical Engineering Department

P.O. Box 6079, Station ‘‘Centre-ville,’’

Montreal, QC, H3C 3A7, Canada

Phone: 514-340-4711, extention 4437

Fax: 514-340-5867

Email: carl-eric.aubin@polymtl.ca

Phone: 1 (514) 340-4711 ext. 4437

4.2.1 Abstract

Fusionless growth sparing implants for the treatment of adolescent idiopathic scoliosis (AIS) attempt to manipulate vertebral growth to restore spinal alignment. This study critically explores

different implants utilizing a human spine scoliotic finite element model (FEM). Stainless steel (SS) and shape memory alloy (SMA) staples and flexible tethers were modeled and alternatively integrated around the apex of the convexity of the scoliotic model. Stress profiles over vertebral growth plates were obtained. Two years of growth was simulated with non-instrumented and instrumented models, as curvature changes were quantified. Apical asymmetrical stresses in non-instrumented and instrumented scoliotic models with SS staple, flexible tether, and SMA staple were 0.48, 0.48, 0.23, and 0.33 MPa, respectively. Patient data and non-instrumented model progressed from 28° to 62° of thoracic Cobb angle over two years. Projected long term thoracic Cobb angles of instrumented models are 31° with SS staple, 31° with flexible tether, and 34° with SMA staple. Initial implant compression achieved during instrumentation provided a significant influence on initial and long term spinal profiles. The developed FEM provides an effective platform with which to explore, critique, and perhaps enhance fusionless growth sparing techniques.

Keywords: scoliosis, growth modulation, finite element model, fusionless

4.2.2 Introduction

Adolescent idiopathic scoliosis (AIS) is characterized by a three dimensional (3D) deformity of the spine. Consequently, this results in irregular spinal loading and internal stress distribution. These asymmetrical stresses have been quantified in scoliotic afflicted spines [16], as well as having been demonstrated utilizing rigid body and finite element models (FEM) under various loading techniques [8,11,29,32]. It is generally believed that these irregular forces play a role in the pathomechanism of scoliosis under the Hueter-Volkmann principle, which identifies bone growth-rate dependence on local stress magnitudes [17]. Further, when a scoliotic deformity is coupled with the peak-growth velocity period of adolescents, the severity of the deformation is at a high risk of progression [15].

These conclusions emphasize growth plate stress distribution and remaining spinal growth as important risk factors to identify, and perhaps exploit, as a means to restore regular alignment to scoliotic spines. Bracing has attempted to address this issue, however, thus far, curve observation and bracing share similar and troubling inconsistencies in preventing the need for surgical intervention involving fusion [7]. In addition, conflicting variability in curvature

development continues to limit progressive forecasting, and thus obscures a clinician's ability to adequately select optimal or case-specific treatments.

Alternatively, new methods of intervention, which may be conceived as a form of internal bracing of the spinal column, are being developed for the early treatment of AIS. Fusionless hemiepiphysiodesis utilizing growth-sparing instrumentation provides an attractive treatment of scoliotic spines. In particular, scoliotic patients undergoing pubertal growth with Cobb angles between 20° and 30° may benefit from this novel approach, as they require surgical intervention at a rate of 70.9% or 100%, if the annual progression exceeds 6° or 10°, respectively [5]. Growth sparing instrumentation attempts to harness remaining spinal growth in order to manipulate vertebral body geometry in an effort to reverse vertebral wedging in the coronal plane. Such an approach would, in theory, maintain a degree of segmental mobility, allow for a minimally invasive surgery, and effectively impede, halt, or reverse the scoliotic progression.

There are a growing number of registered patents that document the endeavor to turn these theoretical advantages into tangible solutions for the improved treatment of idiopathic scoliosis. These patents consist of conceptual prototypes, as well as implants that have undergone rigorous animal and/or human experimental trials. Perhaps the most serious and hopeful amongst them consist of a rigid stainless steel (SS) staple [37], a flexible tether [3] and a shape memory alloy (SMA) staple [2]. Although these implants vary in rigidity, all are mechanically similar in their attempt to restrict unilateral growth on the convexity of the curvature, which is accomplished by locally increasing stress over vertebral growth plates. Preliminary results obtained with such implants appear promising. Notwithstanding such hopefulness, experimental limitations and trial differences add significant difficulty in drawing comparative conclusions concerning the various implants' performance, and therefore restrain translation of expectations and optimism for the treatment of AIS.

Thus, the purpose of this biomechanical study is to critically explore methods of fusionless growth modulation in a human scoliotic finite element model (FEM) by quantifying a selected method's ability to: manipulate stress distribution over the growth plates, provide immediate corrective influence on spinal alignment, and provide long term correction via growth modulation.

4.2.3 Methods

A normal and a scoliotic finite element model of 13 year old female anterior spines were developed utilizing ANSYS 11.0 (Canonsburg, PA). Both models possess normal sagittal profiles (kyphosis: 34°; lordosis: 44°), however, while the normal model possesses no coronal curvatures, the scoliotic model exhibits a right thoracic curve (Cobb angle of 28°). Anatomical landmarks arose from 3D reconstructive techniques using bi-planar radiographs of the two cases providing an accuracy of 3.3±3.8 mm previously validated for mechanical analysis [6]. Internal divisions of the models respect physiological proportions from published studies, specifically: 0.64 mm cortical shell [9]; 0.62 mm growth plate (immature endplate) [24]; and a nucleus cross sectional area proportion of 45% [28]. Anterior and posterior longitudinal ligaments cross sectional areas are 38 mm^2 and 20 mm^2, respectively [22]. Physiologic divisions include cortical and cancellous bone, growth plate, annulus fibrosis, nucleus pulposus, and anterior and posterior longitudinal ligaments. Linear mechanical properties attributed to each zone respect mean values of respective data from published studies [33] (Table 1). Growth plates consisted of three individual zones conforming to *in vivo* observation and previously simulated growth models [14, 33] (Fig 1). Sensitive zone includes reserve, immature proliferative and upper hypertrophic divisions, all of which are responsive to stress sensitivity [23]. Newly formed bone layer consists of lower hypertrophic region in which bone apposition and calcification occurs. Transition zone represents a gradual increase in rigidities between cartilaginous growth plates and cancellous bone.

The scoliotic model was alternately instrumented with implants over five vertebral bodies centered about the apex (T5-T9). Implant fixation within vertebral bodies was consistently maintained between trials providing each with identical insertion sites modeled as rigid beams. Stainless steel staples were provided material properties of surgical stainless steel. Flexible tethers were modeled capable of transmitting tensional force only and assigned material properties associated with 3.5 mm diameter polyethylene. Initial strain of the element (20%) was selected to mimic forces required to realign each vertebral segment under consideration, as practiced under a clinical setting. SMA staples were assigned mechanical properties respective of surgical body temperature Nitinol in its austenite phase. This staple was modeled using weight bearing tensional elements in order to emulate the initial compression force provided by

the temperature triggered phase change. Initial strain utilized (5%) followed experimental results for 8 mm staples [34].

Analyses were performed utilizing two parts. The first consisted of acquiring average longitudinal stress profiles on various areas of interest in the stress sensitive zone of growth plates (Fig 1). The inferior surface of L5 is constrained in all degrees of freedom while the superior surface of T1 is constrained to oppose transverse deflections. To simulate body loading, each vertebral body superior surface is submitted to distributed load magnitudes respecting load allocation ratios derived from Schultz [27] and previously employed in scoliotic FEMs of the spine [8, 36] (i.e. 14% body weight over T1 with an additional 2.6% per inferior vertebrae resulting in a cumulative 55.6% over L5). Spinal load vectors in the coronal plane respected gravitational direction (z-axis of global coordinate system). Loading in the sagittal plane was maintained tangential to the curve of the spine to insure spinal stability as displayed by the resultant load vectors at each level in figure 2. Stress acquisition over these zones was initially performed on the normal FEM and the non-instrumented scoliotic FEMs to collect stress profiles from which to compare the stress manipulative ability of the explored implants. Scoliotic FEM was then alternatively introduced with implants prior to initiation of loading in order to simulate the pre-operative curve reduction obtained in a clinical setting during the lateral decubitus patient positioning [13]. As a result, the scoliotic FEM was instrumented while under a thoracic Cobb angle of 16º (43% reduction over loaded non-instrumented scoliotic model). Once instrumented, the scoliotic FEM was submitted to the adopted spinal loading while new stress profiles and spinal configuration were recorded. Initial correction provided by the implant was defined by the difference in thoracic Cobb angles between the loaded non-instrumented and instrumented models.

The second part of the analysis involved simulating growth over a two year period. The integrated iterative control system begins with application of spinal loading followed by applying calculated growth response to the newly formed bone layer of the growth plates, after which the geometry of the model is updated. This process is repeated during the simulated growth phase similar to previously explored scoliotic models [8, 35, 36], which is briefly detailed below.

The governing equation, which regulates the level of longitudinal bone growth (G), is based on *in vivo* correlations acquired from quantifying growth rates under external forces for various animal species [31].

$$G = G_m(1-\beta(\sigma-\sigma_m))[29]$$

Equation 4.1: Article 2 equation 1 Base of growth algorithm

This equation provides the ratio of expected vertebral longitudinal growth rates (G_m: 0.8 – 1.1 mm/yr) [25] according to the difference in magnitudes between scoliotic stress (σ) and regular physiological stress (σ_m). Sensitivity of the growth algorithm (β) was adjusted to 1.3 MPa^{-1} in order to simulate the scoliotic progression of the selected patient, who progressed more than 10° per year for 2 consecutive years. Such corroborative calibration ensured patient specific progression which, in turn, served as a constant platform to compare devices. Finally, 2 years of spinal growth was simulated for the non-instrumented and instrumented models while changes in coronal Cobb angles were recorded.

The final step of the study consisted of performing several sensitivity analyses in order to interpret the influence of the numerical assumption adopted in the spine and implant models. This included repeating all simulations under different loading directions (tangential to curve and gravitational in both sagittal and coronal planes), initial strains or pre-tension values assigned to flexible tethers and SMA staples (modified by ± 25% of their respective values), and implant insertion sites (varied superiorly and inferiorly with respect to the intervertebral disc as shown in figure 3). Initially, the influence of these variables on growth plate stress distribution was explored. The variables that posed significant stress differences were further pursued and their manipulation of the thoracic Cobb angle following 2 years of simulated growth was investigated.

4.2.4 Results

Stress distribution over vertebral growth plate returned unique profiles for each simulation. The apex (T7) provided the most insightful depiction of the variability invoked by the presence of the explored implants (Fig 4). Standard stress profile, obtained from the normal spine model, returned symmetric lateral profiles. Lateral stresses registered in the left (LL) and right (LR) areas were 0.35 MPa collectively, while the average anterior (A, ALL, ALR) and posterior (P,

PLL, PLR) stresses obtained were 0.41 MPa and 0.16 MPa respectively. Stress profile of the non-instrumented scoliotic right thoracic model returned similar stress profiles to the normal model with respect to anterior (A) and posterior (P) zones, whereas concave (LL) and convex (LR) profiles demonstrated asymmetrical loading within the scoliotic spine. More specifically, the concave portion of the apical growth plates yielded a stress of 0.60 MPa, whereas stress in the convex section measured 0.12 MPa. This translates into an asymmetrical loading of 0.48 MPa. The instrumented right thoracic models consistently shared similar anterior and posterior profiles with both the normal and right thoracic models. In addition, lateral stress profiles (LL & LR) in instrumented models clearly displayed the implants' attempt to return stress distribution to regular conditions, as measured in the normal model. The scoliotic model instrumented with the SS staple had little influence on stress profiles, as they were similar to those observed in the non-instrumented scoliotic model. Introduction of the flexible tether into the right thoracic model reduced slightly concave stress to 0.53 MPa, and increased significantly convex stress to 0.30 MPa in comparison to the non-instrumented scoliotic model. In turn, these alterations adjusted the magnitude of asymmetrical loading to 0.23 MPa. The scoliotic FEM instrumented with the SMA staple provided similar but less effective results to the flexible tether. Apical concave and convex stresses were measured at 0.55 MPa and 0.22 MPa, respectively, thereby reducing the asymmetrical loading to 0.33 MPa.

The simulated growth of the non-instrumented scoliotic model corroborated closely with progressive sequence of the patient data, as demonstrated in figure 5 and quantitatively summarized in figure 6. The FEM proposed a Cobb angle progression from 28º to 42º in the first year, followed by an increase to 62º after 2 years — whereas the selected patient had an initial thoracic Cobb angle of 30º, which became 41º and 62º after one and two years respectively as a result of inadequate brace treatment. After this point, the patient underwent posterior fusion resulting in a final thoracic curve of 24º.

The simulated scoliotic model instrumented with the SS staple displayed a negligible initial correction over the non-instrumented model; however, growth results show the implant would establish a Cobb angle of 29º after one year, followed by 31º after two years. As a result, the SS staple confined progression to 3º (or a relative increase of 11%) over two years of growth. The scoliotic model instrumented with the flexible tether provided an initial correction that resulted

in a post-operative curvature of 23º. This value translates into a 5º (or 18%) initial reduction when compared to the original configuration of the non-instrumented model. After one and two years of simulated growth dynamics the tethered model progressed to a curvature of 27º and 31º respectively. Finally, the SMA staple provided a mild initial correction of 3º (or 10%) over the non-instrumented scoliotic model. The long term post-operative influence of this technique predicted a thoracic curve of 29º after one year and 34º after two years. To summarize (Fig 6), after 2 years, the curve of the patient under consideration and the non-instrumented scoliotic model progressed by 34° (120%) with respect to the initial scoliotic curvature, whereas the instrumented scoliotic model progressed by 3° (11%), 3° (11%), and 6° (21%) when correspondingly introduced with the SS staple, flexible tether, and SMA staple.

Results from the sensitivity analyses with regards to the implant insertion site proved to be robust and had less than 5% influence on the magnitude of asymmetrical growth plate stress. On the contrary, the direction of loading proved to have important implications on growth plate stress profiles. Namely, the gravitation loading in both planes invoked a 28% greater asymmetrical stress than reported above. However, in order to couple the progression of the FEM with the patient data, the sensitivity parameter (β) was reduced to 0.6. Due to this corroborative modification to the underlying algorithm, the long term influence of the explored implants on spinal alignment showed insignificant transformations to spinal configuration when compared to those expressed above. Finally, initial tension attributed to the flexible tether and SMA staple revealed conclusive impact in view of their correction of the scoliotic model. More specifically, using $\beta = 1.3$ with a tangential loading while varying the initial strains ± 25% led to a 2 year thoracic Cobb angle 30.6 ± 8.7º (SD) with the flexible tether and 33.3 ± 5.2º with the SMA staple. Under similar conditions, using a $\beta = 0.6$ and gravity loading, returned 31.6 ± 4.0º with the flexible tether and 33.6 ± 3.7º with the SMA staple.

4.2.5 Discussion

Fusionless growth sparing approaches for the treatment of AIS were compared utilizing a scoliotic FEM of the spine with integrated growth dynamics. Results suggest these methods as a suitable solution to effectively reduce asymmetrical loading of vertebral growth plates and provide immediate post-operative correction. Moreover, the explored methods achieved long term growth modulation resulting in reduced scoliotic progression.

Fusionless growth sparing implants should seek to eliminate, if not reverse, asymmetrical loading of vertebral growth plates. Introduction of implants into the scoliotic model confirmed the ability of the convex lateral approach to reduce asymmetrical loading of vertebral growth plates, an attribute of scoliotic spines believed to play an important role in its progressive pathomechanism [30]. However, this biomechanical analysis also demonstrated the difficulty of the tested implants to establish sufficient control over segmental stresses, which coincides with their struggle to achieve convincing long term curvature correction. In turn, these results may account for the inability of these methods to stimulate contralateral growth as previously observed during *in vivo* studies of the flexible tether and the SMA staple [4]. Reversal of vertebral wedging, by means of altered loading, has previously been achieved, suggesting vertebral growth is not permanently affected by abnormal stress conditions [18]. Therefore, adequate control of growth plate stress distribution via fusionless growth sparing methods may effectively reverse vertebral wedging, leading to long term and permanent curvature correction.

Stress predictions, provided by the developed FEM, corroborated with relevant studies. The growth plate stress profile of the normal (non-scoliotic) model in this analysis predicted an average of 0.30 MPa, a value compatible to *in vivo* human studies measuring mean standing lumbar disc (adjacent to the endplate) stresses of 0.5 MPa [38] and 0.27 MPa [27]. Scoliotic asymmetrical loading obtained herein also agree with measurements of asymmetrical stress distribution around the apical segment of laterally positioned scoliotic patients with mean concave/convex differences of 0.38±0.32 MPa [16]. Alternatively, Stokes reported concave/convex differences in the order of 0.1 MPa [29] using a rigid-body model of the lumbar spine, which may account for the differences.

The SS staple, flexible tether and SMA staple displayed the ability to significantly reduce scoliotic progression that would have otherwise occurred (Fig 6). The SS staple achieved reliable growth modulation through its high rigidity (a characteristic that dictates the passive resistance of the device toward expansion granted by vertebral growth). Similar to *in vivo* porcine trials using SS staples [37] this study reported no immediate post-operative influence on spinal curvature. Such study showed the SS staple's ability to induce an average coronal Cobb angle of 16.4° (±5.4) after 8 weeks following instrumentation. However, the inverse method (creation of scoliosis on a healthy model) was used. Therefore, no corroborative conclusions of

long term influence may be drawn, as this manuscript explored the percentage of correction achieved in a scoliotic spine. In addition to offering a passive resistance to growth, the flexible tether provided an initial force aimed at altering local segmental load distributions. The flexible tether and the SMA staple have been previously examined on experimentally induced scoliotic goat spines [3]. On average, after 12 to 16 weeks, the flexible tether provided an initial correction of 15.5% and a long term change from 73.4° to 69.9°, or a correction of 4.8%. In the same study, the SMA trial led to an average initial correction of 1.5% followed by a long term progression from 77.3° to 94.3° or a 22% increase. In a human clinical trial of the SMA staple, 13% of instrumented patients having an average pre-operative curves of 33° (20°- 41°) progressed by greater than or equal to 10° or 30%, whereas mixed results were achieved with respect to the remainder of the group, resulting in moderate or no progression [2].

An important difference between these *in vivo* studies is that, in reference to the induced scoliotic goat trial [3], a control group was used to monitor non-instrumented progression. This control group led to an average coronal Cobb angle increase from 79.5° to 96.8°, thus, establishing a progressive model upon which to analyze implants that seek to reverse this effect. Whereas human pre-pubertal curves between 21°and 30° have a high progressive variability [5], making human clinical trials a difficult platform upon which to judge the long term success of an implant. Therefore, the analysis of such methods on a controlled finite element environment provides a suitable platform to derive relative conclusions that may be used to explain previously obtained *in vivo* results and to predict the feasibility of or optimize new concepts prior to *in vivo* testing.

Limitations of this FEM study include assumptions associated with spinal loading, which is still insufficiently understood. Loading and boundary conditions were selected to best predict the resultant force vectors that arise from gravitational and muscular forces. To address these uncertainties, a sensitivity analysis was performed to explore the influence of these assumptions. This analysis supported conclusions expressed in this paper, as relative distinctions achieved by the implants proved to be consistent under different loading conditions. Only the vertebral bodies were modeled, since it is known to support a convincing majority of compressive loads [1]. Further, the relative motion between vertebrae was monitored to ensure segmental motion remained within physiologic range. Moreover, it was previously demonstrated that irregular

pedicle growth did not produce scoliotic curves in a FEM [12]. Nevertheless, the authors recognize that if a contact between posterior elements occurred it may influence local relative displacements between adjacent segments. Although the iterative control system governing growth dynamics relies on correlation derived from animal species [31], it has been previously modeled to predict realistic rates of scoliotic progression [29, 36]. This biomechanical comparison study focused on the device's ability to manipulate coronal profile while scoliotic deformities are defined by a 3 dimensional deformity. To date, fusionless devices focus on the coronal plane deformity and, perhaps, they should also seek to fully address the complexity of the deformity as observed in intermediate or advanced scoliotic curves. The reported results of this manuscript were obtained by isolating selected variables in order to draw relevant comparisons between fusionless methods. However, the authors recognize that in a clinical setting these methods may be subject to mild alterations with respect to insertion sites. In order to address this concern, implant location was varied to represent possible disparity (Fig 3) and had a minute influence on the previously reported results. Conversely, initial strains attributed to the flexible tether and SMA staple significantly influenced their impact on curvature progression. Nonetheless, the sensitivity of this parameter is not believed to encumber the reported results as its influence was mechanically instinctive. In contrast, recognition of the significance of this factor may in part described the variability observed during *in vivo* trials of these devices or perhaps be exploited to further optimize their performance.

Although not explored in this analysis, the influence on the health of intervertebral discs must not be neglected, considering that these concepts are developed for pediatric use. Such apprehension is supported by the observation of irregular stress profiles within the growth plates – a phenomenon believed to promote disc degeneration. Implicated researchers have explored this issue and found various stress induced or hypomobility related changes in the discs of instrumented segments [10, 21]. In an attempt to address this concern, a fusionless growth-sparing mini staple has subsequently been developed that does not alter the mechanical environment of the intervertebral discs [26].

The ability to identify patients at risk of progression prior to the onset of peak growth velocity (currently being pursued by Moreau et al. [19, 20]) and improved stress/growth control would justify and complement this method of early intervention that attempts to correct or limit

expected scoliotic progression. Despite the fact that the pathomechanism of scoliosis is likely multi-factorial, fusionless growth-sparing instrumentation provides many biomechanical advantages over conventional treatments. However, several potential improvements remain to be considered. The use of a finite element platform presents a valuable medium to explore, compare, and, perhaps, improve upon methods seeking to corrected spinal deformities via fusionless growth sparring instrumentation.

Acknowledgements

Funded by the Natural Sciences and Engineering Research Council of Canada (Industrial Research Chair Program with Medtronic of Canada) and the Canada Research Chair Program.

4.2.6 References

1. Adams M, Hutton W (1980) The effect of posture on the role of the apophysial joints in resisting intervertebral compressive forces. J Bone and Joint Surg Br 62(3): 358-362

2. Betz R, Andrea L, Mulcahey M, Chafetz R (2005) Vertebral Body Stapling Procedure for the Treatment of Scoliosis in the Growing Child. Clinical Orthopaedics and Related Research 434: 55-60

3. Braun, J, Akyuz E, Ogilvie J, Bachus K (2005) The efficacy and integrity of shape memory alloy staples and bone anchors with ligament tethers in the fusionless treatment of experimental scoliosis. J Bone Joint Surg Am 87(9): 2038-2051

4. Braun J, Hunt K, Sorenson S, Ogilvie J, Can Fusionless Scoliosis Surgery Reverse the Hueter-Volmann Effect? 42nd Annual Meeting Scoliosis Research Society, Edinburg, Scotland, 2007.

5. Charles Y, Daures J, de Rosa V, Dimeglio A (2006) Progression risk of idiopathic juvenile scoliosis during pubertal growth. Spine 31(17): 1933-1942

6. Delorme S, Petit Y, de Guise J, Aubin CE, Dansereau J (2003) Assessment of the 3-D reconstruction and high-resolution geometrical modeling of the human skeletal trunk from 2-D radiographic images. IEEE Transactions on Biomedical Engineering 50(8): 989-998

7. Dolan L, Weinstein S (2007) Surgical rates after observation and bracing for adolescent idiopathic scoliosis: an evidence-based review. Spine 32(19S): 91-100

8. Driscoll M, Aubin CE, Moreau A, Villemure I, Parent S (2009) The role of concave-convex biases in the progression of idiopathic scoliosis. Eur Spine J 18: 180-187

9. Edwards T, Zheng Y, Ferrara L, Yuan H (2001) Structural Features and Thickness of the Vertebral Cortex in the Thoracolumbar Spine. Spine 26(2): 218-225

10. Hunt H, Braun J, Christensen B (2007) The Effect of Two Clinically Relevant Fusionless Scoliosis Implant Strategies on the Health of the Intervertebral Disc, 42nd Annual Meeting Scoliosis Research Society, Edinburgh, Scotland

11. Huynh A, Aubin CE, Mathieu P, Labelle H (2007) Simulation of progressive spinal deformities in Duchenne muscular dystrophy using a biomechanical model integrating muscle and vertebral growth modulation. Clin Biomechanics 22: 392-399

12. Huynh A, Aubin CE, Rajwani T, Bagnall K, Villemure I (2007) Pedicle growth asymmetry as a cause of adolescent idiopathic scoliosis: a biomechanical study. Eur Spine J 16: 523-529

13. Lalonde N, Villemure I, Pannetier R, Parent S, and Aubin C (2010) Biomechanical modeling of the lateral decubitus posture during corrective scoliosis surgery. Clin. Biomech. 25(6): 510-516

14. Lin H, Aubin CE, Parent S, Villemure I (2009) Mechanobiological bone growth: comparative analysis of two biomechanical modeling approaches. Med Bio Eng Comput 47(4): 957-966

15. Little D, Song K, Katz D, Herring J (2000) Relationship of peak height velocity to other maturity indicators in idiopathic scoliosis in girls. J Bone and Joint Surgery 82(5): 685-693

16. Meir A, Fairbank J, Jones D, McNally D, Urban J (2007) High pressures and asymmetrical stresses in the scoliotic disc in the absence of muscle loading. Scoliosis 2: article 4

17. Mehlman C, Araghi A, Roy D (1997) Hyphenated history: the Hueter-Volkmann law. Am J Orthop 26: 798-800

18. Mente P, Aronsson D, Stokes I and Iatridis J (1999) Mechanical Modulation of Growth for the Correction of Vertebral Wedge Deformities. J of Orthopaedic Research 17: 518-524

19. Moreau A, Franco A, Azedine B, Rompre P, Turgeon I, Bagnall K, Poitras B, Labelle H, Rivard C, Grimard G, Ouellet J, Parent S, Larouche G, Lacroix G (2008) Elevated plasma factor P is involved in AIS onset and curve progression, SRS 43rd Annual Meeting Scoliosis Research Society, Salt Lake City, USA

20. Moreau A, Wang D, Forget S, Azeddine B, Angeloni D, Fraschini F, Labelle H, Poitras B, Rivard C, Grimard G (2004) Melatonin Signaling Dysfunction in Adolescent Idiopathic Scoliosis. Spine 29(16): 1772-1781

21. Newton P, Farnsworth C, Faro F, Mahar A, Odell T, Mohamad F, Breisch E, Fricka K, Upasani W, Amiel D (2008) Spinal Growth Modulation with an Anterolateral Flexible Tether in an Immature Bovine Model. Spine 23 (7): 724-733

22. Polikeit A, Ferguson S, Nolte L, Orr T (2003) Factors influencing stresses in the lumbar spine after the insertion of intervertebral cages: finite element analysis. Eur Spine J 12: 413-420

23. Price J, Oyajobi B, Russell R (1994) The cell biology of bone growth. Eur. J Clin Nutr 48(Suppl 1): 131-149

24. Roberts S, Menage J, Urban J (1989) Biochemical and structural properties of the cartilage end-plate and its relation to the intervertebral disc. Spine 14(2): 166-174

25. Sarwark, J, Aubin CE (2007) Growth considerations of the immature spine. J Bone Joint Surg Am 89 Suppl 1: 8-13

26. Schmid E, Aubin CE, Moreau A, Sarwark J, Parent S (2008) A novel fusionless vertebral physeal device inducing spinal growth modulation for the correction of spinal deformities. Euro Spine J 17(10):1329-1335

27. Schultz A., Andersson G, Ortengren R, Nachemson A (1982) Loads on the lumbar spine. Validation of a biomechanical analysis by measurement of intradiscal pressures and myoelectric signals. J Bone and Joint Surg 64(5): 713-720

28. Shirazi-Adl A, Shivastava S, Ahmed A (1984) Stress analysis of the lumbar disc-body unit in compression: A three dimensional nonlinear finite element study. Spine 9(2): 120-134

29. Stokes I (2007)Analysis and Simulation of Progressive Adolescent Scoliosis by Biomechanical Growth Simulation. Eur Spine J 16: 1621-1628

30. Stokes I, Spence H, Aronsson D, Kilmer N (1996)Mechanical Modulation of Vertebral Body Growth: Implications for Scoliosis Progression. Spine 21(10): 1161-1167

31. Stokes I, Aronsson D, Dimock A, Cortright, Beck S (2006) Endochondral growth in growth plates of three species at two anatomical locations modulated by mechanical compression and tension. J of Orthopaedic Research 10: 1327-1333

32. Stokes I, Gardner-Morse M (2004) Muscle activation strategies and symmetry of spinal loading in the lombar spine with scoliosis. Spine 29(19): 2103-2107

33. Sylvestre PL, Villemure I, Aubin CE (2007) Finite element modeling of the growth plate in a detailed spine model. Med Biol Eng Comput 45(10): 977-988

34. Tremblay M (2004)Caractérisation expérimentale de la modulation de croissance vertébrale à l'aide d'agrafes à mémoire de forme pour la correction de la scoliose idiopathique: étude de faisabilité. Master thesis, École Polytechnique de Montréal --> it is suggested not using such reference (difficult to find, + not in English)

35. Villemure I, Aubin CE, Grimard G, Dansereau J, Labelle H (2001) Progression of vertebral and spinal three-dimensional deformities in adolescent idiopathic scoliosis: a longitudinal study. Spine 26(20): 2244-2250

36. Villemure I, Aubin CE, Dansereau J (2002) Simulation of Progressive Deformities in Adolescent Idiopathic Scoliosis Using a Biomechanical Model Integrating Vertebral Growth. J of Biomedical Engineering 124: 784-790

37. Wall E, Bylski-Austrow D, Kolata, R, Crawford A (2005) Endoscopic mechanical spinal hemiepiphysiodesis modifies spine growth. Spine 30(10): 1148-1153

38. Wilke H, Neef P, Caimi M, Hoogland T, Claes L (1999) New In Vivo Measurements of Pressures in the Intervertebral Disc in Daily Life. Spine 24(8): 755-762

4.2.7 Figures and tables

Table 4.1: Article 2 table 1 Mechanical properties of the finite element model

		Young's Modulus (MPa)	Poisson's Ratio
Vertebral Body	Cortical Bone	14 500	0.3
	Cancellous Bone	400	0.3
Growth Plate	Sensitive	12	0.4
	Newly Formed Bone	100	0.3
	Transition	300	0.3
Intervertebral Disc	Nucleus	2	0.49
	Annulus	8	0.45
Ligaments	Anterior Longitudinal	20	0.3
	Posterior Longitudinal	70	0.3
Implants	Stainless Steel Staple	190 000	0.4
	Flexible Tether	275	0.3
	Shape Memory Alloy Staple	80 000	0.3

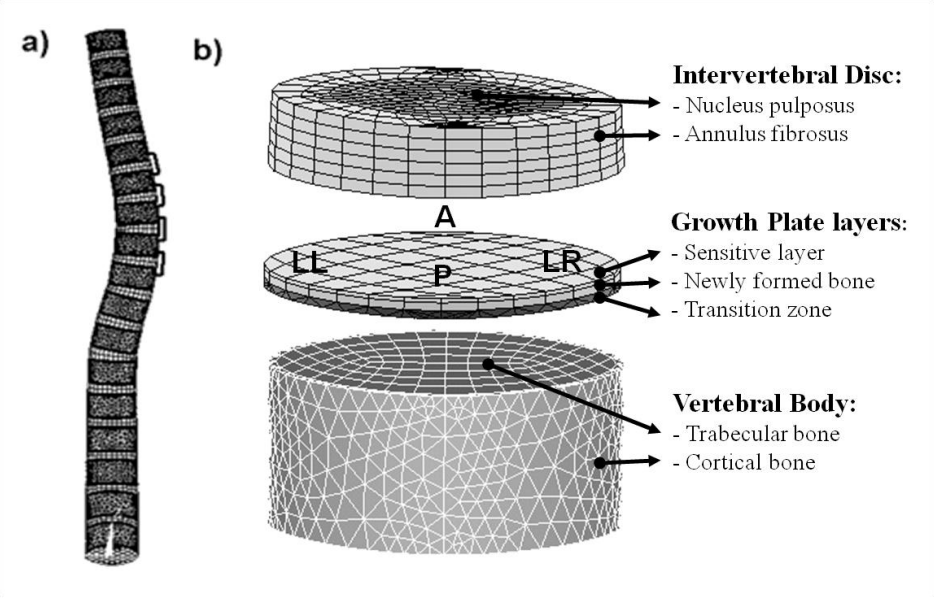

Figure 4.1: Article 2 figure 1 a) Postero-anterior view of the instrumented scoliotic finite element model b) Vertebral body, intervertebral disc, and detailed growth plate with zones of interest (A=anterior, P=posterior, LL=lateral left, and LR=lateral right)

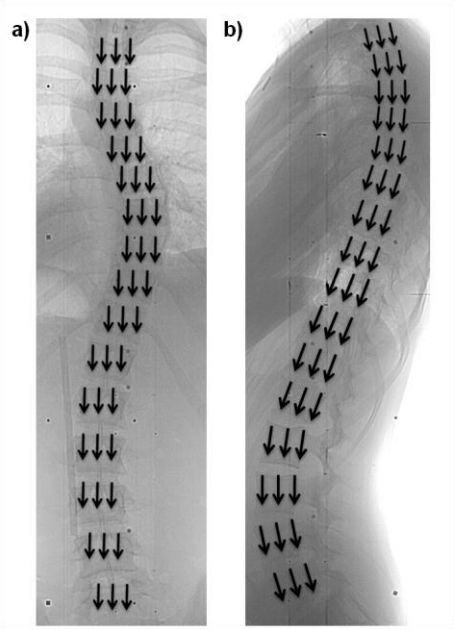

Figure 4.2: Article 2 figure 2 Representation of load vectors introduced in model with reference to a) coronal and b) sagittal planes

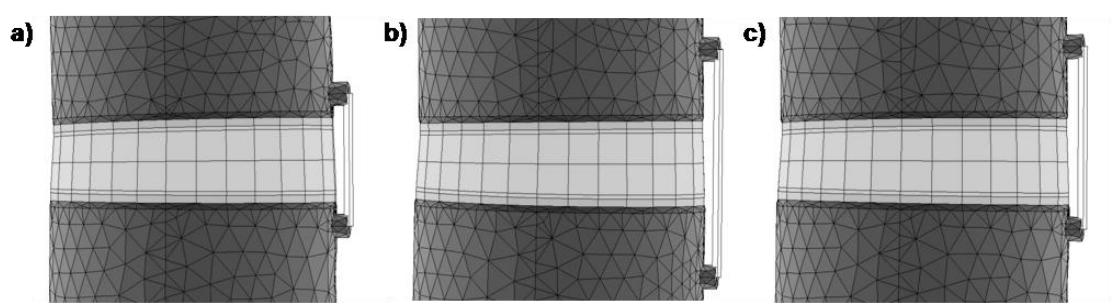

Figure 4.3: Article 2 figure 3 Explored implant insertion sites a) adjacent to growth plates, b) short distance apart from growth plates and c) superior offset with respect to intervertebral disc

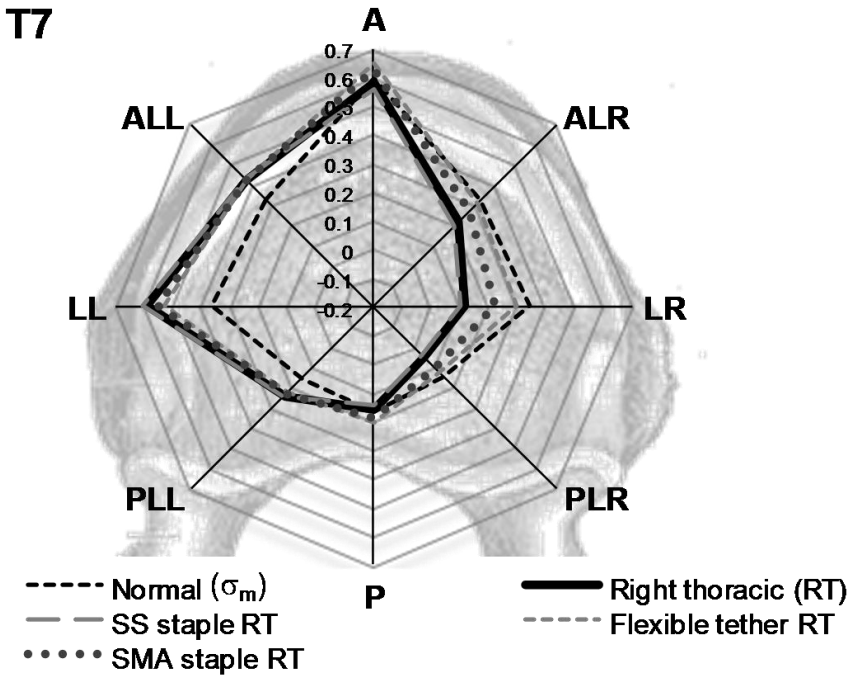

Figure 4.4: Article 2 figure 4 Longitudinal (normal) Stress in MPa profiles over apical vertebral growth plate (T7) of normal model, right thoracic scoliotic model and right thoracic scoliotic model with implants over anterior (A), anterior lateral right (ALR), lateral right (LR), posterior lateral right (PLR), posterior (P), posterior lateral left (PLL), lateral left (LL and anterior lateral left (ALL)

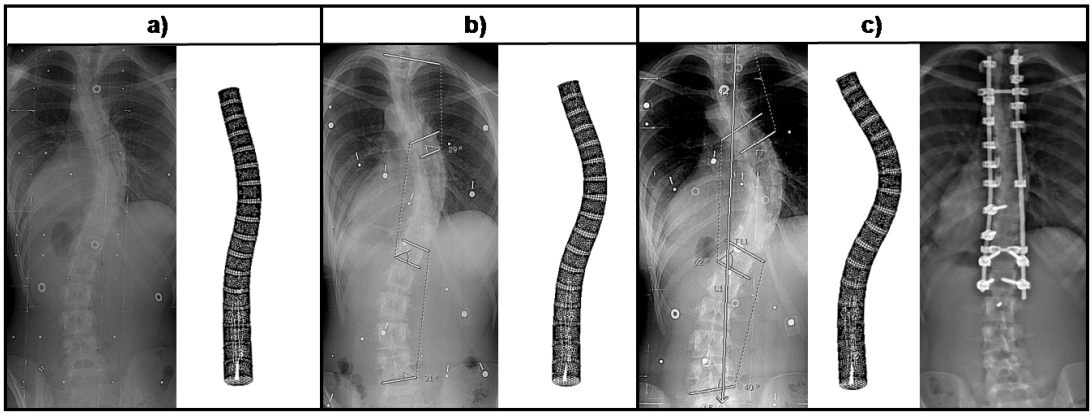

Figure 4.5: Article 2 figure 5 Patient radiographs and non-instrumented scoliotic model at a) 13 years b) 14 years and c) 15 years & post-operative radiograph following posterior fusion

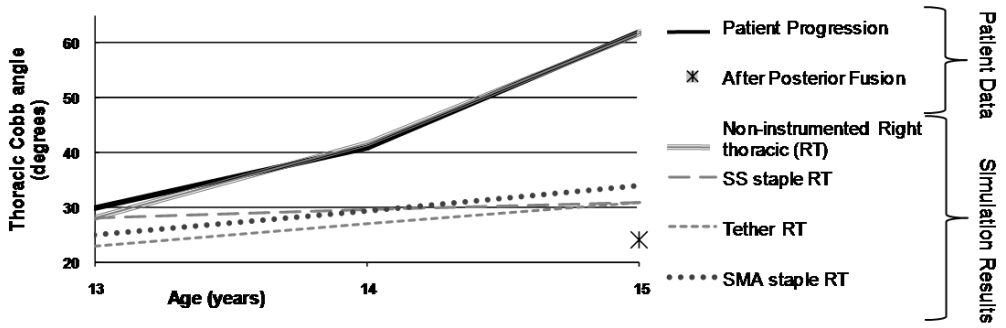

Figure 4.6: Article 2 figure 6 Progressive results of patient, non-instrumented FEM and instrumented FEMs

4.2.8 Additional studies related to finite element methods

4.2.8.1 Removal of loads for pre-operative positioning

Fusionless devices, including those explored in article 2 section 4.2, are subject to a pre-operative correction offered by patient positioning in a lateral decubitus position. This has been studied previously and demonstrated that, on average, such positioning provides a curvature reduction of 44% [208]. Therefore, for simulation purposes it is of interest to alter the FEM to provide this pre-operative correction prior to introducing the explored fusionless devices. In order to represent this via finite element analysis several methods were attempted. To begin, a first technique implied removing the expected loading was attempted *i.e.*, reversing the direction of gravitational loading. Following load removal from the scoliotic model, FEM geometry was updated and the coronal and sagittal Cobb angles were measured. A second technique involved performing the same actions describe in the first technique but included registering stresses in a text file when the spine was stretched following load removal. Geometry was updated then the stored stress file was fed in to the program, which, in theory, should return the spine to its original configuration.

The first loading technique, load removal and reapplication, did not return the FEM to its initial geometry. The second method, that attempted to make use of stresses to return the FEM to initial configuration, was also unsuccessful.

Upon revision the above observations, such geometric disagreement make sense as upon elongating the spine to emulate pre-operative positioning, elements are stretched and then updated. Therefore the elements assume a new shape and are giving the same mechanical properties as their original shape. Upon resubmitting to a new force the element will deform but not sufficiently to mimic its new configuration as it would have to deform more than it would originally. The same problem is encountered in the second technique that registered stresses. Further, the boundary conditions make it difficult to reproduce what is occurring during patient positioning. The mechanics of pre-operative positioning is a complicated phenomenon to mimic mechanically. Further, there are a number a unknown variables that cause additional complications. In order to avoid this time consuming problem the following steps were taken.

Because the model developed over the course of this thesis permits a parametric or user specific spinal configurations, original geometry does not depend on reconstructions acquired from patient specific data. Thus, methods applied in article 2 section 4.2.3 constructed a spine model with a thoracic Cobb of 16 degrees and, when loaded, adopted a scoliotic deformity of 28 degrees. Therefore implants are inserted on the scoliotic spine of 16 degrees (43 % correction from the 28 degree curve of FEM when under spinal loading). Once the implant is inserted the spine FEM was loaded the initial correction offered by the implant was coupled with pre-operative correction gained by patient positioning.

4.2.8.2 Sensitivity analysis involving spinal loading and boundary conditions applied to the FEM

Spinal loading techniques

As described within this thesis, FEM loading is a sensitive parameter and must be explored with care. Above in article 2 section 4.2.3, a sensitivity analysis regarding spinal loading is briefly described. This analysis relies on repeating the simulations under a variety of loading configurations in order to analyze their influence on the results of asymmetrical loading and scoliotic progression. While load allocation ratios remained the same, the force vector directions were varied according to their anatomical planes. Four types of simulated spinal loading was attempted (Fig. 4.7) and are described as a follower type load, a gravitational load, a real follower load, and a gravitational & follower type load.

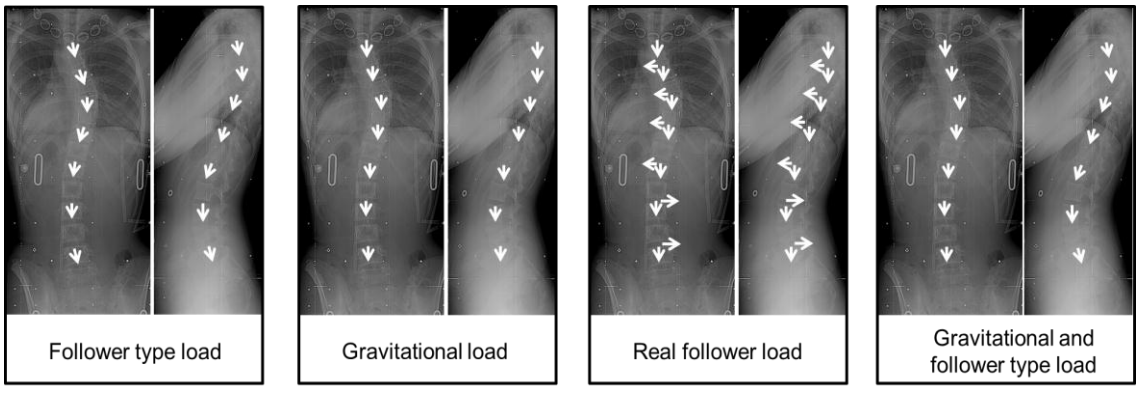

Figure 4.7: Sensitivity analysis of loading alternatives

The follower type load was developed to be representative of Pathwardhan`s first publication on the matter [78]. As explained in section 3.2.9.1, each additional force introduced on the vertebral

segments was tangential to the curvature of the spine. This was programed to hold true in both the coronal and sagittal profile. The gravitational loading format explored was strictly a gravitational loading as previously utilized in similar analyses [7, 73]. This loading method maintained all vertebral loads perpendicular to the global reference plane in both the coronal and sagittal planes. This holds true as gravity is a constant, thus, this technique neglects the role of stabilizing tissues and adopted muscle activation strategies. The real follower load relies on Pathwardhan`s second publication which identifies the cumulative influence of superior loading on each vertebral segment [79]. In other words, local muscular and ligament reactions realign vertebral force vectors tangential to the curvature in the sagittal plane. This was programmed as direction of each segmental load was attributed two vectors to assure cumulative consistency as observable in figure 4.8. More specifically, the orientation of each segmental load was determined as follows.

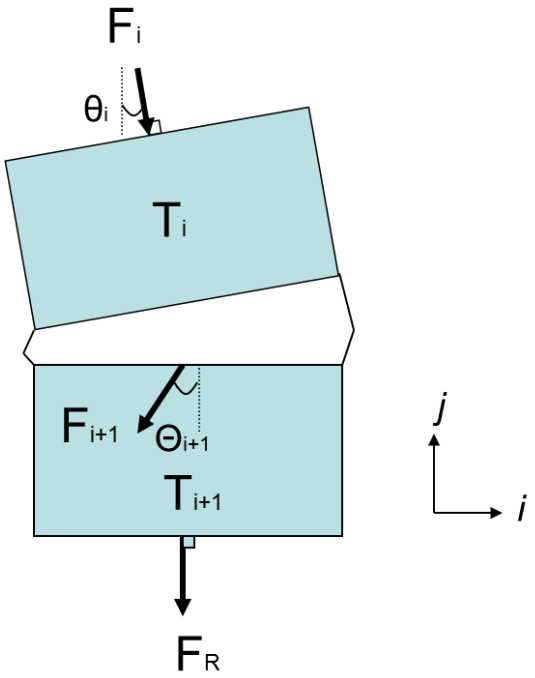

Figure 4.8: Vector diagram of real follower load

$$\overline{F}_R = \overline{F}_i + \overline{F_{i+1}}$$
$$F_R(i+j) = F_i(i+j) + F_{i+1}(i+j)$$
$$F_R \Rightarrow Tangential \therefore F_R(i) = 0$$
$$F_i(i) = -F_{i+1}(i)$$
$$F_i \sin\theta_i = -F_{i+1}\sin\theta_{i+1}$$
$$\theta_{i+1} = \sin^{-1}\left[\frac{-\left(\sum_{n=0}^{i} F_n\right)}{F_{i+1}}\sin\theta_i\right]$$

Equation 4.2: Derivation of real follower load algorithm

The final type of loading explored, gravitational & follower type load is a combination of the follower type load in the sagittal plane (successive loading is maintain tangential to spinal curvature) and a gravitational load (always in the direction of gravity) was programmed to take effect in the coronal plane.

Boundary conditions

The boundary conditions imposed on the models are another user defined variable that requires further exploration. With regards to the developed model, several boundary conditions methods on the superior endplate of T1 were explored while the inferior endplate of L5 remained constrained in all degrees of freedom as observed in figure 4.9.

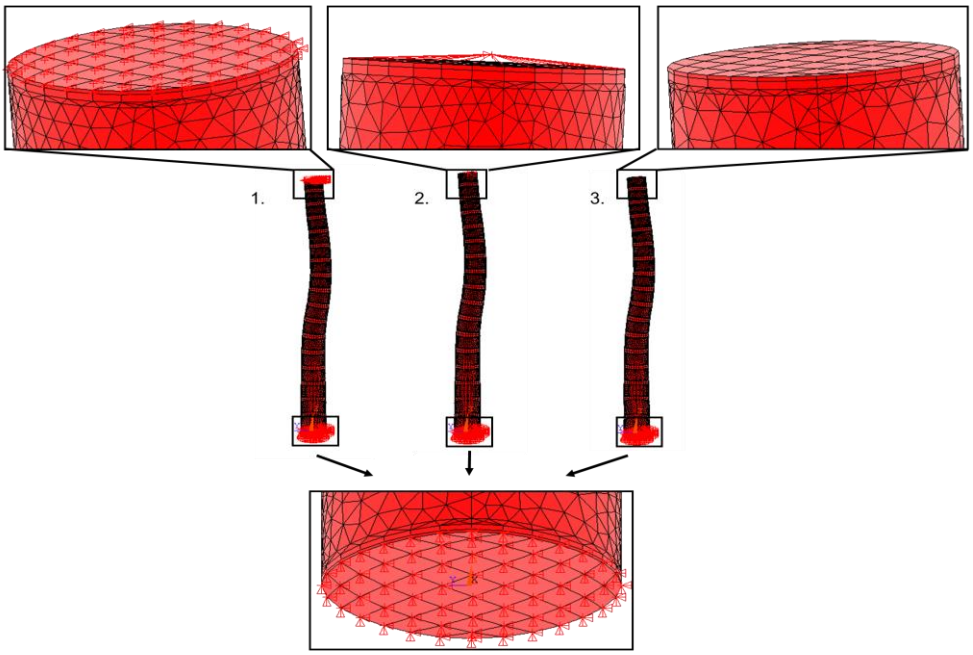

Figure 4.9: Explored Boundary Conditions (1. Top fixed in transverse plane 2. Top fixed in transverse plane with integrated pivot 3. Top free)

The first method, spine 1 in figure 4.9, consisted of a fixation in the transverse plane of T1. Every node on the superior area of the vertebra is selected and confined in both the XZ (coronal) and YZ (sagittal) planes. This method would, in theory, provide reaction forces that may be considered to be due to muscular tension stabilizing this section of the spine. Under this boundary condition such imposed stability would ensure no movement of T1 in the transverse plane while restricting its rotation. The second technique, spine 2 in figure 4.9, was explored because the first boundary condition mentioned above provides a restriction in two planes which, in turn, restricts 5 /6 (Ux, Uy, Mx, My, and Mz) degrees of freedom due of its geometric nature – a factor not believed to be relevant during spinal growth. In order to overcome this issue, a node was introduced slightly above the centroid of the most superior area of T1. This node was then fixed to the areas circumferential nodes. As a result, 2/6 (Ux, Uy) possible degrees of freedom were fixed as this method allows the free rotation of T1. The third technique, spine 3 in figure 4.9, imposed no boundary condition on T1.

Experimental plan

Prior to the setup of the experimental plan, independent preliminary analyses of loading and boundary condition techniques were performed to explore their realism. Preliminary simulations using the real follower load retuned no asymmetrical loading in the scoliotic spine between concave and convex portions as measured by others [209]. Such an observation is not realistically applied to a scoliotic spine and this method was excluded from further involvement in the sensitivity analysis. Moreover, comparative analyses using the follower type loading was also excluded from further interpretation as it was very consistent with the gravitational and follower type load. Boundary conditions that allowed complete freedom to T1 (spine 3 image 4.9) was also excluded from further analyses as it returned unrealistic asymmetrical stresses and spinal deformations when placed under spinal loading.

Following these preliminary refinements, several user defined assumptions remained to be explored interchangeably (Fig. 4.10). During this process, the growth algorithm remained the same except for the input of healthy stress distribution (σ_m: normal stress from healthy spine adapted as a function of loading) and the sensitivity parameter (β) in the governing equation (Eqn. 4.1).

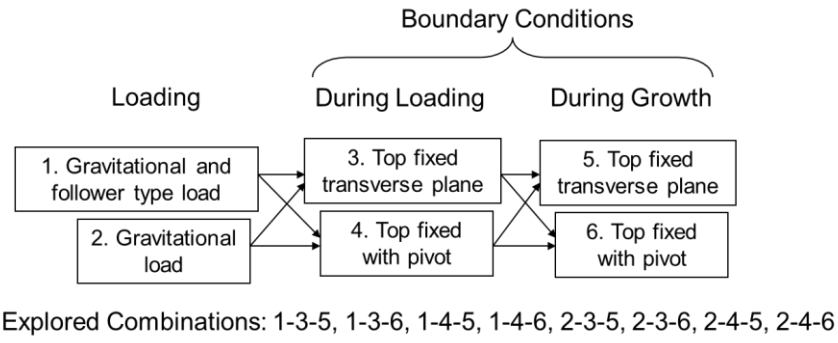

Figure 4.10: Sensitivity analysis of loading and boundary conditions

Prior to analysing the influence of the implants a corresponding progressive model was established without any instrumentation. This was achieved by selecting the loading and boundary conditions under consideration and simulating 2 years of progressive growth. Results were then compared to the actual values of patient progression from the case study and the

sensitivity variable (β) was adjusted appropriately. As later detailed, this phase of the analysis also allowed for the rejection of certain combinations.

First, the boundary condition fixing top of T1 in the transverse plane during growth was rejected as it imposed too many restrictions on the model during the growth phase. This is because the growth phase should only be restricted with reaction forces from the presence of the implants and not the boundary conditions. Another combination that was excluded from the sensitivity analysis based on preliminary results was the use of the pivot during the loading phase. This led to an under constrained model since the resulting asymmetrical stresses over the vertebral growth plates were not in the physiological range previously reported on scoliotic spines (0.1 – 0.8 MPa) [31, 210]. In addition to elevated asymmetrical stresses, this boundary condition allowed for exaggerated progression. That is, the predicted progression from the FEM was much greater than that observed in the patient and the sensitivity variable (β) would have to have been reduced below acceptable levels (0.4 -1.7 MPa^{-1}) [9, 50].

Table 4.2: Thoracic Cobb angle (degrees) results over time for the sensitivity analysis of loading and boundary conditions

		1,3,6				2,3,6		1,4,6	2,4,6,
Time	Patient	β =0,8	β =1,0	β =1,1	β =1,3	β =0,8	β =0,6	β =0,8	β =0,8
pre-op	-	16	16	16	16	16	16	16	Divergence
Simulated post-op	30	28	28	28	28	28	28	0	
Simulated 1 year	41	34,05	37,36	38,70	41,50	45,20	41,01	57,20	
Simulated 2 year	62	47,30	55,40	58,91	62,32	71,90	60,19	90,70	

These educated eliminations left two possibilities (1,3,6 and 2,3,6) that were selected and explored under the influence of the implants as represented in table 4.2. Under these two different combinations the influence of the explored implants in article 2 described in section 4.2.3 are found in tables 4.3 and 4.4.

Table 4.3: Sensitivity analysis part 1 – influence of spinal loading and boundary condition on thoracic Cobb angle of scoliotic spine with fusionless simulated devices

β = 0,6 Trial 2,3,6						
Time	Patient	Non-instrumented FEM		FEM with SS staple	FEM with SMA Staple	FEM with Tether
pre-op	16	16		16	16	16
post-op	30	28		27.52	28.02	21.25
1 year	41	41.01		29.93	30.09	29.41
2 year	62	60.19		31.85	33.6	31.57
	WRT initial Cobb angle	Relative Impact (%)	post-op	-1.7	0.0	-24.1
			1 year	6.9	7.4	5.0
			2 year	13.7	20.0	12.7
		Absolute Impact (degrees)	post-op	-0.5	0.0	-6.8
			1 year	1.9	2.1	1.4
			2 year	3.8	5.6	3.6

Table 4.4:Sensitivity analysis part 2 – influence of spinal loading and boundary condition on thoracic Cobb angle of scoliotic spine with fusionless simulated devices

β = 1,3 Trial 1,3,6 (Published results)						
Time	Patient	Non-instrumented FEM		FEM with SS staple	FEM with SMA Staple	FEM with Tether
pre-op	16	16		16	16	16
post-op	30	28		28	25	23.0
1 year	41	41.50		29.7	29.29	27
2 year	62	62.32		30.51	33.63	30.57
	WRT initial Cobb angle	Relative Impact (%)	pos-op	0	-10	-18
			1 year	6	4.6	-3.6
			2 year	10.7	21.4	10.7
		Absolute Impact (degrees)	pos-op	0	-3	-5
			1 year	1.7	1.3	-1
			2 year	3	6	3

From these results, one may observe that the magnitude (relative and absolute) of correction imposed by the implants, with respect to the predicted rate of progression, varied mildly according to the adopted sensitivity parameter (β). Despite this variation, the differences between implant performances, as discussed in article 2 section 4.2.5, remained. Therefore, the sensitivity analysis of spinal loading and boundary conditions did not alter conclusions put forth in article 2.

4.2.8.3 Sensitivity analysis of fusionless device insertion position

Another variable that required additional revision was the implants insertion location. The various implants were modeled according to descriptions provided in patents [16-18] and, to remain objective, the position of the implants within the spine of the scoliotic model were maintained consistent although insertion sites described in published studies suggested otherwise [19, 20]. The rigid stainless steel staples are described as being fixed into the vertebral bodies via screws penetrating posterolaterally next to the position of the rib head attachment. The bone anchors (screws) of the flexible tether construct are inserted into the convex lateral vertebral body, while, in a similar manner, the staple was inserted anterolaterally with the prongs positioned over the growth plates.

In order to address the concern that such variations may significantly influence the results provided by the FEM, different insertion possibilities were explored: a) standard insertion centered on intervertebral disc b) implant spacing between screw (or prong for SMA staple) and the growth plate; c) and implant geometric center offset with respect to the midline of the intervertebral disc (Fig. 4.11).

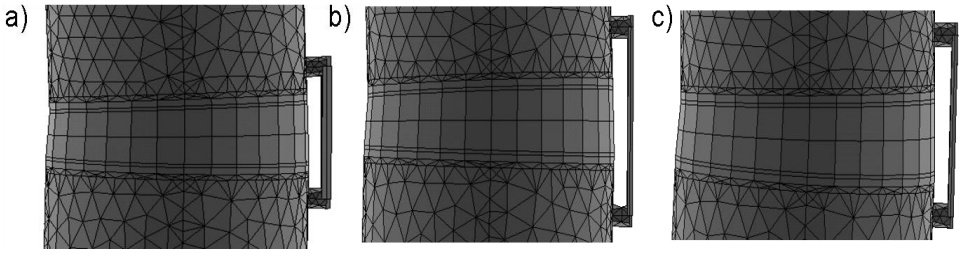

Figure 4.11: Sensitivity analysis of implant insertion site a) regular b) large gap c) offset

This analysis was performed in terms of exploring the stress distribution across the growth plates. This method of interpretation is therefore very sensitive to changes caused by the different implant insertion sites. Therefore, as previously discussed in articles 1 and 2, the sensitive zone of the growth plate was divided into 9 zones of interest for each vertebral body. In particular, the apex (T7) of the scoliotic curve was selected as it is the most representative of the asymmetrical loading that occurs in the spine.

Table 4.5:Stress (MPa) results from sensitivity analysis of implant insertion site

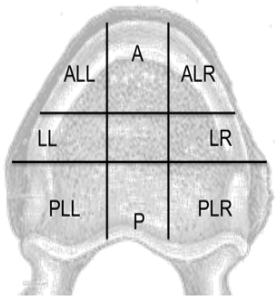

	Apical axial Stress in MPa with fusionless devices								
	SMA Staple			SS Staple			Flexible Tether		
Section	Regular	Large Gap	Offset	Regular	Large Gap	Offset	Regular	Large Gap	Offset
A	0.63	0.62	0.62	0.57	0.56	0.56	0.63	0.70	0.67
ALR	0.28	0.27	0.27	0.21	0.20	0.20	0.29	0.37	0.33
LR	0.22	0.21	0.20	0.11	0.08	0.08	0.26	0.39	0.31
PLR	0.10	0.09	0.09	0.05	0.04	0.03	0.11	0.17	0.14
P	0.19	0.18	0.18	0.15	0.15	0.15	0.19	0.23	0.21
PLL	0.23	0.23	0.23	0.24	0.24	0.24	0.23	0.21	0.22
LL	0.55	0.56	0.56	0.60	0.61	0.61	0.54	0.49	0.52
ALL	0.42	0.43	0.43	0.43	0.43	0.43	0.42	0.42	0.42

From table 4.5, it could be observed that the variation of implants insertion sites did not significantly influence the performance of the implant. Both the SMA and SS staples provide near identical stress distributions while the simulation of the tether provides a mild but still negligible variation. Explanation of this source of discrepancy may arise from irregular adjustments of the initial strain values assigned to the implant. Because the strain is a function of initial length appropriate adjustments of this value had to be made. The impact of the flexible tether is highly dependent of this variable because of its low Young's modulus therefore causes mild but noticeable alterations at different lengths. In order to eliminate further concern of the initial strain variable another sensitivity analysis was performed.

4.2.8.4 Sensitivity analysis of pre-tension in fusionless device

The final variable that led to further analyses was the initial strain programmed into the SMA and flexible tether implants. These approaches utilise this compressive characteristic to achieve one or all of the following: increased implant fixation, initial compression of the vertebral growth plates, or initial post-operative correction. However, mechanical insight suggested the FEM would be sensitive to the magnitude of programmed initial strain therefore it was varied ± 25% of the selected values. Furthermore, it was believed that the influence of the implant would be dependent on the sensitivity factor (β). Therefore, the influence initial strain in fusionless devices (SMA staple and flexible tether – SS staple provides passive resistance to growth) was explored against previously verified loading conditions and boundary conditions (combinations 1,3,6 and 2,3,6 from figure 4.10). These analyses led to the following corrective profiles of the thoracic curvature.

Table 4.6:Results of thoracic Cobb angles (degrees) from sensitivity analysis of initial implant stain (%) part 1

β = 1,3 Trial 1,3,6						
Time	Tether 15%	Tether 20%	Tether 25%	SMA Staple 3.75%	SMA Staple 5%	SMA Staple 6.25%
pre-op	16,0	16,0	16,0	16,0	16,0	16,0
post-op	22,1	23	18,8	24,7	25	23,7
1 year	29,4	27	22,1	30,9	29.3	26,2
2 year	40,4	31	23,0	35,2	34	25,4
σ(dev)	8,7			5,2		

Table 4.7:Results of thoracic Cobb angles (degrees) from sensitivity analysis of initial implant stain (%) part 2

β = 0,6 Trial 2,3,6						
Time	Tether 15%	Tether 20%	Tether 25%	SMA Staple 3.75%	SMA Staple 5%	SMA Staple 6.25%
pre-op	16	16	16	16	16	16
post-op	21,1	21,3	18,8	24,7	28,0	23,7
1 year	32,2	29,4	26,4	29,5	30,1	26,9
2 year	37,6	31,6	30,1	32,0	33,6	26,5
σ	4,0			3,7		

The programmed initial strain of both the tether and the SMA staple affected both their simulated initial and long term correction. Tables 4.6 and 4.7 confirm that the larger the initial strain the greater the correction while the converse also holds true, somewhat trivial of a conclusion. Notwithstanding, the effect of the sensitivity parameter (β) on the thoracic coronal Cobb angle may be measured when comparing tables 4.6 and 4.7. A lower β leads to a more robust model. More specifically, using β = 1.3 with a follower type loading while varying the initial strain ± 25% led to a 2 year thoracic Cobb angle with the following standard deviations: 31º ±8.7º with the flexible tether and 34º±5.2º with the SMA staple. Under similar conditions, using a β = 0.6 and force (gravity) loading returned the following: 31.6º±4.0º with the flexible tether and 33.6º±3.7º with the SMA staple.

This analysis explored the influence of initial strain (compressive forces provided by fusionless devices) on the conclusions reported in article 2 section 4.2. Based on the results in tables 4.6 and 4.7 one may reasonably derive that the devices initial compression plays an important role on its correction of the scoliotic deformity. The values used in article 2 respect published

measured of both the tether and SMA staples. Nevertheless, it is of great interest to explore alternative pre-tensions to attempt to improve implant performance. Netwon et al. explored this in porcine models and found that although augmented initial tension provided additional initial correction, over time (12 months), the differences were no longer significant [166]. Perhaps a maximum correction exist, as limited by growth modulation, perhaps surrounding tissues restrict additional compression imposed by devices, and perhaps compensatory mechanisms exist in *in vivo* models; nonetheless, initial tension in fusionless devices remains a corrective mechanism that merits further investigation.

CHAPTER 5 : Performance of a novel intravertebral epiphyseal device for the treatment of adolescent idiopathic scoliosis

5.1 Framework of third article

The final steps of this thesis project were to explore the performance of the developed devices for the treatment of AIS. A previously explored and patented device [207], the intravertebral epiphyseal staple, underwent *in silico* (objectives 1, 2, and 3) and *in situ* analyses (part of objective 4) aimed at refining and optimizing the device for improved function. Following enhancements, device effectiveness was explored using *in vivo* experimentation using a skeletally immature porcine model. This device was conceived to exclude the intervertebral disc while halting local growth modulation and, consequently, would be an improvement over current fusionless device which merely impede (slow) growth as identified through the completion of objective 2. This third manuscript explores the intravertebral epiphyseal device's ability to modify vertebral morphology and spinal alignment. The sequential realization of objectives 1, 2, 3, and 4 and the investigation of hypothesis 3 are presented in the manuscript entitled "Spinal growth modulation using a novel intravertebral epiphyseal device in an immature porcine model", for which the contribution of the first author is considered to be 85%. This manuscript was submitted to the *European Spine Journal* on February 2, 2011 and minor modifications addressing the reviewers concerns were resubmitted to the editor May, 10 2011.

5.2 Article 3: Spinal growth modulation using a novel intravertebral epiphyseal device in an immature porcine model

Spinal growth modulation using a novel intravertebral epiphyseal device in an immature porcine model

Mark Driscoll, J. Eng.[1,2]; Carl-Eric Aubin, Ph.D., Eng.[1,2]; Alain Moreau, Ph.D. [3,4,5]; Yaroslav Wakula, MD[2]; and Stefan Parent, MD, Ph.D.[b]

1 - École Polytechnique de Montréal, Biomedical Engineering Institute, Montreal,Canada

2 - Research Center, Sainte-Justine University Hospital Center, Montreal, Canada

3 - Laboratory in Molecular Genetics of Musculoskeletal Diseases, Sainte-Justine University Hospital Research Center, Montreal, Canada

4 - Department of Stomatology, Faculty of Dentistry, Université de Montréal, Montreal, Canada

5 - Department of Biochemistry, Faculty of Medicine, Université de Montréal, Montreal, Canada

Address for notification, correspondence, and reprints:
Carl-Éric Aubin, Ph.D., P.Eng, Full Professor
Canada Research Chair, ‘‘CAD Innovations in Orthopedic Engineering,’’ & NSERC/Medtronic Industrial Research Chair in Spine Biomechanics
École Polytechnique de Montréal
Mechanical Engineering Department
P.O. Box 6079, Station ‘‘Centre-ville,’’
Montreal, QC, H3C 3A7, Canada
Phone: 514-340-4711, extention 4437
Fax: 514-340-5867
Email: carl-eric.aubin@polymtl.ca
Phone: 1 (514) 340-4711 ext. 4437

5.2.1 Abstract

Purpose: Fusionless growth modulation is an attractive alternative to conventional treatments of idiopathic scoliosis. To date, fusionless devices achieve unilateral growth modulation by compressing the intervertebral disc. This study explores a device to control spinal alignment and vertebral morphology via growth modulation while excluding the disc in a porcine model.

Methods: A device that locally encloses the vertebral growth plate exclusive of the disc was introduced anteriorly over T5-T8 in 4 immature pigs (experimental) while 3 underwent surgery without instrumentation (sham) and 2 were selected as controls. Bi-weekly coronal and lateral radiographs were taken over the 12 week follow up to document vertebral morphology and spinal alignment modifications via an inverse approach (creation of deformity).

Results: All animals completed the experiment with no post-operative complications. Control and sham groups showed no significant changes in spinal alignment. Experimental group achieved a final coronal Cobb angle of 6.5°±3.5° (constrained to the 4 instrumented levels) and no alteration to the sagittal profile was observed. Only experimental group ended with consistent vertebral wedging of 4.1°±3.6° amounting to a cumulative wedging of up to 25° and a concurring difference in left/right vertebral height of 1.24±1.86mm in the coronal plane.

Conclusions: The proposed intravertebral epiphyseal device, for the early treatment of progressive idiopathic scoliosis, demonstrated its feasibility by manipulating spinal alignment through the realization of local growth modulation exclusive of the intervertebral disc.

5.2.2 Introduction

Adolescent idiopathic scoliosis (AIS) is described by a three dimensional spinal deformity that involves wedging and shape asymmetry of vertebrae and discs. Conventional treatment of AIS consists of bracing and instrumentation requiring spinal fusion. While the former has debatable effectiveness [1], the reliable corrective appeal of the later is perhaps offset by its high level of invasiveness. Although the etiology of AIS continues to elude researchers, its pathomechanism may result from local growth modulation governed by the Hueter-Volkmann principle, which identifies bone growth-rate dependence on stress magnitudes [2]. This notion is further supported by vertebral wedging observation in scoliotic spines [3] – a result of reduced vertebral

growth on the concavity due to increased loading in conjunction with the converse proceeding on the convexity. In an attempt to reverse this phenomenon, restore spinal alignment, and improve treatment options for skeletally immature patients with progressive AIS, several fusionless growth sparring instrumentation methods have been proposed [4-8]. In brief, these methods attempt to locally harness residual vertebral growth with the purpose of spine realignment.

Mechanical, morphological, kinematic, and physiological complexities of the spinal column set challenging hurdles for implicated researchers seeking to address this issue. Over the last decade, few fusionless growth modulating devices for AIS treatment have undergone experimental testing. These include a stainless steel [4] and shape memory alloy staples [5], and an anterior tether made from polyethylene [6, 7] and stainless steel [8]. Such devices attempt to locally retard convex spinal growth by enclosing and compressing the intervertebral disc and adjacent growth plates. Consequently, local convex growth retardation is believed to prevent scoliotic progression and promote spinal realignment. Feasibility of these treatments to manipulate vertebral growth has been demonstrated; however, their modification of spine kinematics and possible influence on intervertebral disc health remains an underlying concern. Assuming fixation remains, instrumentation montages utilizing rigid constructs may provoke disuse atrophy of surrounding bone [4] or ankylosis and biochemical changes in discs are alleged to occur [9]. Although no fusion is performed, success of these methods resides within the solid fixation of an otherwise mobile segment. The tether approach allows for a larger degree of freedom in instrumented segments (tether provides no compression resistance). However, this instrumentation montage may induce elevated and harmful stress levels in compressed portions of intervertebral discs. Rodent tails placed under static compression encountered accelerated degenerative changes in discs indicated by increased proteoglycan content compared to immobilized segments that underwent similar but decelerated trends [10]. Although Newton and colleagues reported an up-regulation of proteoglycan synthesis and increased collagen type II within discs adjacent to instrumented vertebrae in a bovine model, no morphological or water content alterations 6 month post-operative was measured [11]. Despite encouraging insight suggesting sustainable disc health gathered from this well performed study, a justifiable concern remains regarding long term disc health in adolescents submitted to such instrumentation techniques.

In an attempt to address the aforementioned concerns, a growth sparring intravertebral epiphyseal device that locally modifies vertebral growth without spanning the disc space was developed. The device head is inserted between growth plate and adjacent intervertebral disc annulus while the body is fixed to the respective vertebra. Feasibility of this approach was previously demonstrated using a rodent tail model [12]. Presence of device over 4 vertebrae induced a mean Cobb angle of 30º after 23 days (inverse approach – device applied to the convexity of a scoliotic spine in practice). However, translation and comparison of these results to other studies exploring growth modulating devices is encumbered by the use of a small animal tail model. The purpose of this study was to explore the performance of the intravertebral epiphyseal staple, a growth sparing device for the treatment of AIS, on an immature porcine model to verify its ability to manipulate vertebral growth and alter spinal alignment.

5.2.3 Materials and Methods

The intravertebral epiphyseal device was optimized over previous design [12] using finite element software (ANSYS, Canonsburg) and constructed through CAD applications (CATIA V5r17, Dassault Systèmes, France) (Fig. 1). Stainless steel 316L (UNS S31603) was used for device and bone screw (25mm by 2.8mm). Device head was designed for position immediately below annulus fibrosus and above growth plate (approximately 5mm penetration) and device body is secured using bone screw.

Surgical Protocol

Nine immature 3 month old hybrid female porcine (ladrace/yorkshire) weighing approximately 35 kg were utilized. Based on statistical predictions, pigs were randomly selected into following groups: 2 control (no surgery), 3 sham (surgery without instrumentation), and 4 experimental (surgery with instrumentation).

Methods adopted were approved by Institutional Committee for Animal Care in Research (ICACR) of Sainte-Justine University Hospital Centre. Pre-surgical sedation was achieved through intramuscular injection of atropine (0.04mg/kg), azaperone (4mg/kg), and ketamine (25mg/kg). Propofol (1.66mg/kg) was injected intravenously prior to intubation with a 6.5mm endotracheal tube. Automatic ventilation was provided to maintain anesthesia through a mix of

oxygen and 1-3% isoflurane. Pig was positioned in a lateral decubitus position. Insertion site was shaved and prepared with a proviodine solution. Under a sterile environment right side thoracotomy was made between 7th and 8th rib providing sufficient access to vertebrae T5 to T8. At this time, the pleura over T5-T8 were cauterized at the location of device insertion in the sham group and lesions were closed. Experimental group underwent transpleural insertion of the devices over T5-T8 prior to closure. Device was fixed unto a custom surgical instrument while insertion site was guided via fluoroscopic imaging. Device was inserted and fixed into position by means of bone screw accurately guided through custom surgical tool. Subcutaneous tissue and skin sutures were applied followed by film dressing. All surgeries were performed by the same surgeon. Pig was introduced with a fentanyl patch (7.5 mg) and intramuscular injections of antibiotics (Excenel 3 mg/kg) were administered over 3 days post-operative. All pigs were maintained in individual cages until complete healing of surgical wound after which they were allowed to interact in a communal area until euthanasia. Post-operative follow up lasted 85 days or 12 weeks.

Post-operative analysis

All test subjects underwent bi-weekly radiographs, under pre-surgical sedations, to provide coronal (postero-anterior (PA)) and lateral spine views. Digitized images provided measurements of Cobb angles of interest. Constrained thoracic Cobb angles were measured between superior endplate of T5 and inferior endplate of T8 for coronal and sagittal plane analyses. Measurements were repeated between T4 and T13 to explore influence outside region of instrumentation. Vertebral wedging measurement (angle between vertebral endplates) was made over T5-T8 for all groups in coronal plane. Measures of vertebral height in coronal plane were documented on left (non-instrumented) and right (instrumented in experimental group) extremities of T5-T8 vertebral bodies in all groups. Vertebral height differences (left-right) were calculated and compared between groups. Measures were performed on digital radiographs using Synapse® 3.1.1 (Fujifilm Medical Systems, USA, INC).

Statistical analyses

Group sample sizes were determined using a significance of α=0.05 and a power of p=0.80. Post-hoc analyses (Cobb angles, vertebral wedging, and vertebral height) were compared

between groups using values recorded pre-operatively and immediately prior to euthanasia. Successive results (Cobb vs. age, vertebral wedging vs. age, and vertebral height vs. age) were collected sequentially and thus not statistically independent. Areas under the temporal curves of these results were calculated using trapezoidal rule and results compared as single variables per subject. Non-parametric Wilcoxon tests were utilized to interpret this data. Measures (constrained Cobb angles, vertebral wedging, and vertebral heights) were repeated by two different observers.

5.2.3 Results

Minimal blood loss occurred during surgery (<30ml) and no post-operative complications occurred. Average surgery time (with standard deviation) to install all 4 devices, exclusive of opening and closure of the incision site, was 10.8±4.8 minutes. All animals underwent standard weight gains of 4.1±0.5kg/week and showed no signs of reduced physical activity.

Initial coronal radiographs showed no irregular spinal configurations in all subjects (coronal Cobb angle=0). Final coronal radiographs returned insignificant modifications to average constrained T5-T8 Cobb angles for both control and sham groups, while experimental group finished with an average angle of 6.5°±3.5° (between 3° and 12°). Measures of constrained T4-T13 Cobb angles showed no important deviation (<1°) from reported data between T5-T8 and were excluded from graph for clarity (Fig. 2). Bi-weekly radiographs in coronal plane returned negligible differences between initial and final Cobb measures in control and sham groups ($p \geq 0.44$). Such Cobb measures did not significantly diverge between control and sham groups during follow up ($p=0.56$). Experimental group showed significant modification of coronal profile (Fig. 3). Final experimental coronal Cobb angles measured were significantly modified over initial values ($p=0.01$) while temporal modifications differed significantly from both control and sham groups ($p \leq 0.05$).

Sequential measures of sagittal Cobb angles demonstrated no difference between subjects (Fig. 4). Final mean measures involving T5-T8 or T4-T13 were 4.0°±1.4° or 30.0°±1.4°, 3.6°±0.6° or 26.0°±2°, and 6.3°±0.6° or 25.8°±4.6° for control, sham, and experimental groups respectively. All possible post hoc and sequential comparisons of Cobb angles in sagittal plane provided no evidence of deviating profiles ($p \geq 0.12$).

Mean T5-T8 vertebral wedging angles measured in the coronal plane began at 0º in all groups and, following 85 days of growth, ended with 0.2°±0.4°, 0.1°±0.5°, and 4.1°±3.6° in control, sham, and experimental groups respectively. This vertebral wedging amounted to a cumulative wedging of up to 25° over only four instrumented segments. No difference regarding initial and final wedging values for control and sham groups was measured ($p \geq 0.82$) whereas experimental group showed significant change ($p=0.01$). Sequential wedging measures between groups reported no differences concerning control and sham ($p=0.56$). Experimental sequential data differed from control and sham groups ($p=0.01$) (Fig. 5).

Final differences in vertebral body heights were evident in experimental group. Vertebral left and right heights of T5-T8 were 0mm±0.5, 0mm±0.6, and 1.2mm±1.9 for control, sham, and experimental groups respectively (Fig. 6). Left and right vertebral height differences between initial and final measures did not present themselves within control and sham groups ($p \geq 0.31$). Experimental group revealed a growth reduction on instrumented portion (right) with respect to non-instrumented side (left) of the vertebra ($p=0.04$). Difference in vertebral height progressive data revealed insignificant deviations between control and sham groups ($p=0.77$) while measures of experimental diverged significantly from control and sham data ($p=0.02$). All measures (constrained Cobb angles, vertebral wedging, and vertebral heights) between observers did not alter reported statistical conclusions.

5.2.3 Discussion

A novel growth modulating device for early AIS treatment demonstrated its ability to locally modify spinal growth and alignment. Although the intravertebral epiphyseal device formerly confirmed its feasibility on a rat tail model [12], the study discussed herein is the first to demonstrate success of a fusionless instrumentation to manipulate spinal alignment without spanning the intervertebral discs in a large animal model.

The device achieved a mean coronal curvature of 6.5° after 12 weeks and a cumulative vertebral wedging of up to 25° over only 4 segments and solely targeting one of two possible growth plates per vertebra. Interestingly, coronal Cobb angle measure seemed to level at 123 days of age (Fig. 2) despite consistent progression of vertebral wedging (Fig. 5). To rationalize this, there was a trend in the development of reverse intervertebral disc wedging (discs compensated

and assumed an opposing wedged to vertebrae) which may be responsible for the Cobb measure plateau. It is possible that radiographs taken while spine is placed under compression would be prone to adopt a more pronounced scoliotic curvature than those reported under anesthetized conditions. This speculative behavior was qualitatively observed while manually imposing compression loads on excised spines. Irrespective of such experimental restrictions, the intravertebral epiphyseal device was able to effectively modify spinal curvatures. A novel and important characteristic of this approach is its ability to control spinal alignment as a direct result of inflicting local growth modulation of the vertebral body exclusive of disc compression. Accordingly, in a clinical context, this innovative approach would theoretically allow for its removal if over correction was obtained without loss of structural alignment. Nonetheless, disc wedging in scoliotic spines remains an important characteristic to progression and, correspondingly, correction.

As a result of the unassuming size and position of the intravertebral epiphyseal device, initial corrective ability offered by compression of intervertebral discs is not exploited. In scoliotic spines, comparative measures of disc and vertebral wedging suggest larger vertebral body wedging in thoracic spine; the contrary was observed in thoracolumbar and lumbar curves [13, 14]. However, a longitudinal study using progressive scoliosis patients demonstrated intervertebral disc wedging a more important constituent of scoliotic curves up until and during adolescent growth spurt followed by vertebral wedging taking precedence following growth spurt [15]. Regarding the mechanical factors in the pathomechanism of scoliosis, it is therefore reasonable to deduce that, as a result of initial curvature created by disc wedging, asymmetrical forces may encourage irregular soft tissue remodeling and/or growth and pose another progressive risk. Although the proposed intravertebral device may not actively alter and correct disc wedging, it would halt or inverse progression through its ability to manipulate vertebral wedging. As a result of improved spinal alignment, asymmetrical forces would diminish. In consequence, this system may also passively reduce AIS progression resulting from additional soft tissue deformation and/or remodeling.

The device insertion of 5mm targets resting and proliferation zone of growth plate (immediately below annulus). Theoretically, insertion in this region would not hinder intervertebral disc or growth plate health. Previous authors have demonstrated disc rim lesions as a precursor to

degeneration in a porcine model [18, 19]. However, the insertion sites in these studies takes place in the midline of the annulus at a depth of 13mm and, thus, are not analogous to those imposed by the explored device. Previous analyses of this device on rat tail model returned positive results concerning disc and growth plate viability [12]. During spinal extraction following sacrifice, the device appeared lightly covered in fibrous tissue; however, no macroscopic changes were observed. Alternatively, quantitative histological and biochemical analyses will be conducted to draw more assertive conclusions with regards to disc and growth plate health.

Limitations of this study reside with the sham group and include the use of a quadruped animal model. The sham group may be merely representative of the surgical procedure devoid of periosteal irritation related to device insertion. The putative contribution of perioseal tissue cannot be ruled-out although prior investigations of similar intravertebral epiphyseal device in a rat tail which included an incision at the site of device insertion (creating a periosteal irritation) in sham animals led to no significant growth modulation compared to controls [12]. A porcine model was selected as morphology of anterior body of pig vertebra resembles human adolescent spines. Hybrid porcine (ladrace/yorkshire) vertebrae grow at a mean rate of 20 microns/day/growth plate [18] which translates into 3.4mm (or 1.7mm per growth plate) vertebral growth over 12 weeks. Adolescents, during their 2-3 year growth spurt, grow an average of 1mm/year [19] or a total of 2-3mm per vertebra. Therefore, results achieved using porcine model may be realistically utilized to draw inferences to the early treatment of AIS. Porcine spines are submitted to 15% to 50% of human stresses [20] and have a second ossification zone whereas human vertebral growth plates are bordered by discs. Such variances are perceived not to hinder device performance. The intravertebral epiphyseal device arrests growth through rigidity and position. This mechanism would not be diminished by altered stress magnitudes and lack of subchondral bone above growth plate. Alternatively, morphological differences between growth plates challenge instrumentation techniques. Device insertion in this study was guided by fluoroscopic imaging. Currently, a custom imaging device is being developed to allow device positioning within micro meter accuracy and allow for a minimally invasive surgery [21]. Nevertheless, these mechanical and morphological differences should be acknowledged when inferring towards human application.

In conclusion, this study confirms the ability of the intravertebral epiphyseal device to locally manipulate vertebral growth and spinal alignment in a porcine model exclusive of the intervertebral disc.

5.2.4 References

1. Dolan L and Weinstein S (2007) Surgical rates after observation and bracing for adolescent idiopathic scoliosis: an evidence-based review. Spine 32(19S): 91-100

2. Mehlman C, Araghi A, Roy D (1997) Hyphenated History: the Hueter-Volkmann Law. Am J Orthop 26: 798-800

3. Parent S, Labelle H, Skalli W, et al. (2004) Vertebral Wedging Characteristics Changes in Scoliotic Spines. Spine 29(E): 455-462

4. Wall E, Bylski-Austrow D, Kolata R, et al. (2005) Endoscopic mechanical spinal hemiepiphysiodesis modifies spine growth. Spine 30(10): 1148-1153

5. Betz R, Andrea L, Mulcahey M, et al. (2005) Vertebral Body Stapling Procedure for the Treatment of Scoliosis in the Growing Child. Clinical Orthopaedics and Related Research 434: 55-60

6. Braun, J, Akyuz E, Ogilvie J, et al. (2005) The efficacy and integrity of shape memory alloy staples and bone anchors with ligament tethers in the fusionless treatment of experimental scoliosis. J Bone Joint Surg Am 87(9): 2038-2051

7. Newton P, Upasani V, Farnsworth C, et al. (2008) Spinal growth modulation with the use of a tether in an immature porcine model. J Bone Joint Surg Am 90: 2695-2706

8. Newton P, Fricka K, Lee S, Farnsworth C, et al. (2002) Asymmetrical flexible tethering of spine growth in an immature bovine model. Spine 7: 689-693

9. Braun J, Ogilvie J, Akyuz E, et al. (2004) Fussionless scoliosis correction using shape memory alloy staple in the anterior thoracic spine of the immature goat. Spine 29(18): 1980-1989

10. Iatridis J, Mente P, Stokes I, et al. (1999) Compression-induced changes in intervertebral disc properties in a rat tail model. Spine 24: 996-1002

11. Newton P, Farnsworth C, Faro F, et al. (2008) Spinal growth modulation with an anterolateral flexible tether in an immature bovine model. Spine 33(7): 724-733

12. Schmid E, Aubin CE, Moreau A, et al. (2008) A novel fusionless vertebral physeal device inducing spinal growth modulation for the correction of spinal deformities. Euro Spine J 17(10):1329-1335

13. Modi H, Suh S, Song HR, et al. (2008) Differential wedging of vertebral body and intervertebral disc in thoracic and lumbar spine in adolescent idiopathic scoliosis – A cross sectional study in 150 patients. Scoliosis; 3:11

14. Stokes I and Aronsson D (2001) Disc and vertebral wedging in patients with progressive scoliosis. J Spinal Disord 14(4)**:**317-322

15. Will R, Stokes I, Qiu X, et al. (2009) Cobb Angle Progression in Adolescent Scoliosis Begins at the Intervertebral Disc. Spine 34(25): 2782-2786

16. Kaapa E, Holm S, Han X, et al. (1994) Collagens in the injured porcine intervertebral disc. J Orthop Res 12: 93–102

17. Kaapa E, Zhang L, Muona P, et al. (1994) Expression of type I, III, and VI collagen mRNAs in experimentally injured porcine intervertebral disc. Connect Tissue Res 30: 203–214

18. Wakula Y, Parent S, and Villemure I. (2010) Characterization of In Vivo Vertebral Growth Modulation by Shape Memory Alloy Staples on a Porcine Model for the Correction of Scoliosis. Research Into Spinal Deformities 8, ed. CE Aubin, Nieuwe: IOS Press 224-225

19. Wever DJ, Tønseth KA, Veldhuizen AG, Cool JC, van Horn JR. (2000) Curve progression and spinal growth in brace treated idiopathic scoliosis. Clin Orthop Relat Res 377: 169-179

20. Bylski-Austrow D, Glos D, Sauser F, et al. (2006) Bilateral intra-annular spinal compressive stresses in vivo. Stud Health Technol Inform 123: 398-403

[21] Beaudette K, Strupler M, Driscoll M, et al. (2010) Towards a handheld probe based on optical coherence tomography for minimally invasive spine surgeries. Stud Health Technol Inform 158: 49-5

5.2.5 Figures and tables

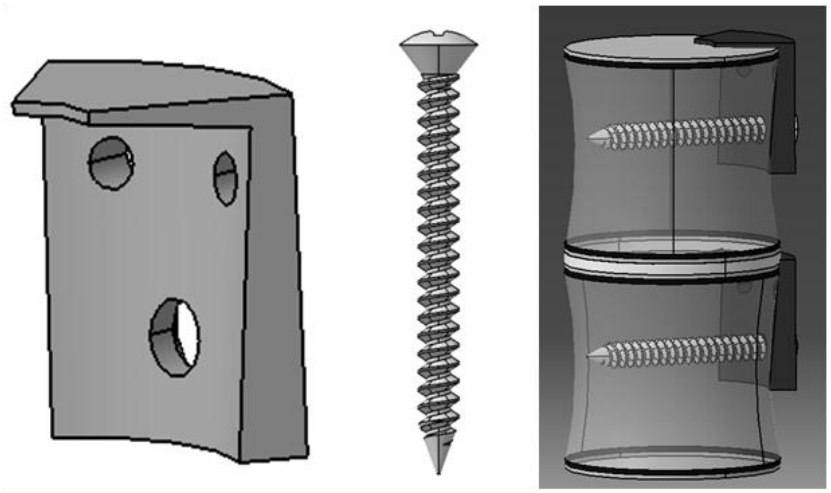

Figure 5.1: Article 3 figure 1 Fusionless **i**ntravertebral epiphyseal device

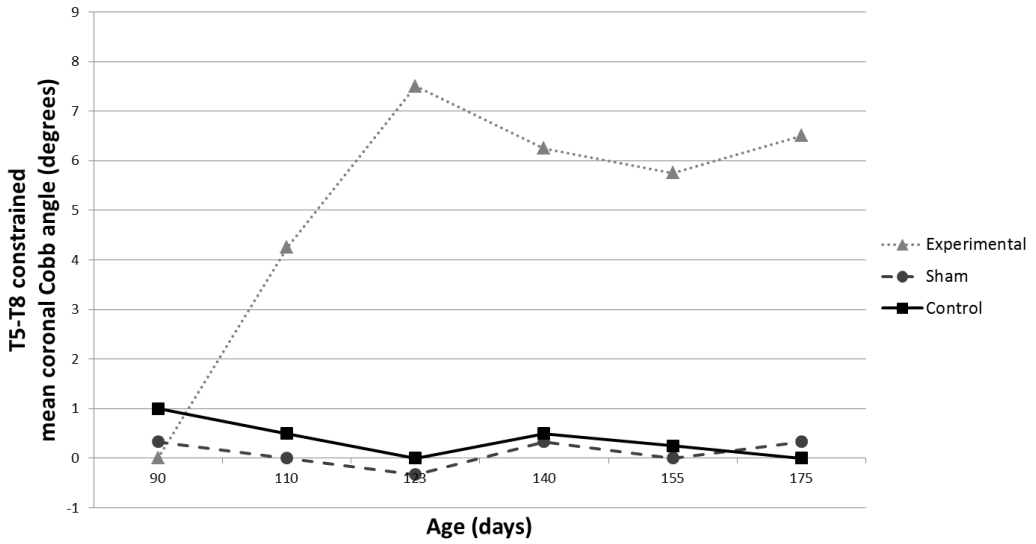

Figure 5.2: Article 3 figure 2 Progressive bi-weekly T5-T8 constrained Cobb angles from coronal plane radiographs

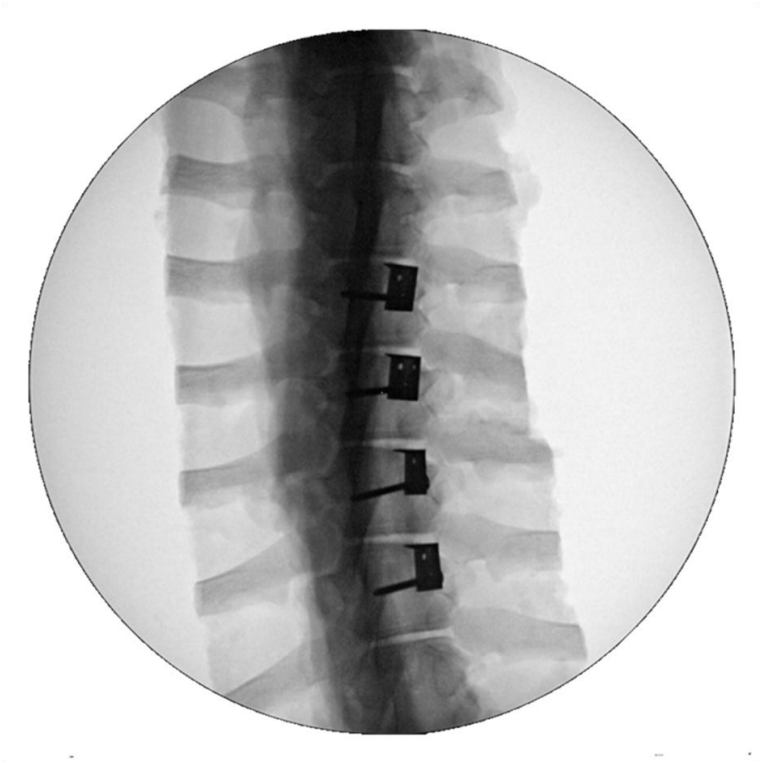

Figure 5.3: Article 3 figure 3 Example of coronal plane manipulation in excised porcine spine

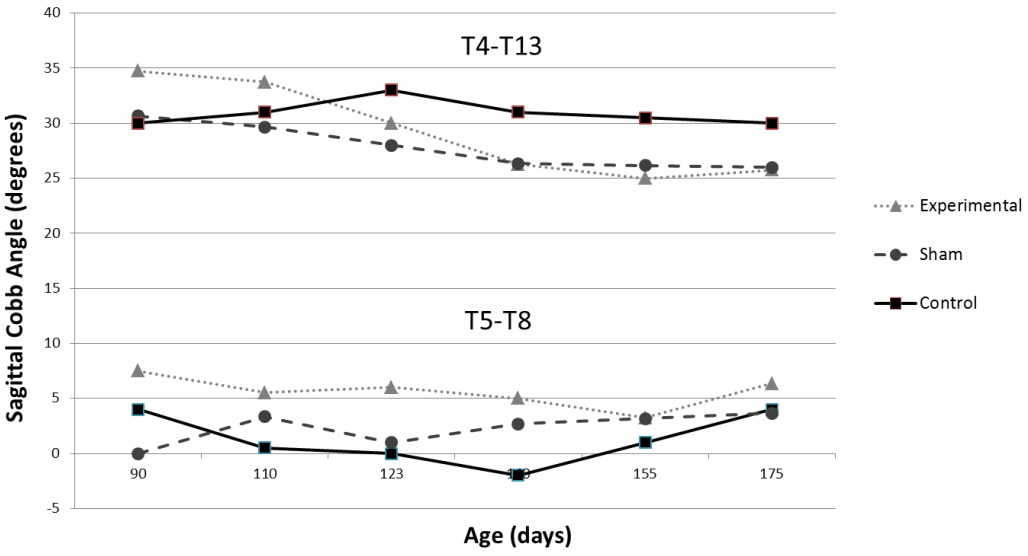

Figure 5.4: Article 3 figure 4 Progressive bi-weekly Cobb angles constrained between T5-T8 and T4-T13 measured from sagittal plane radiographs

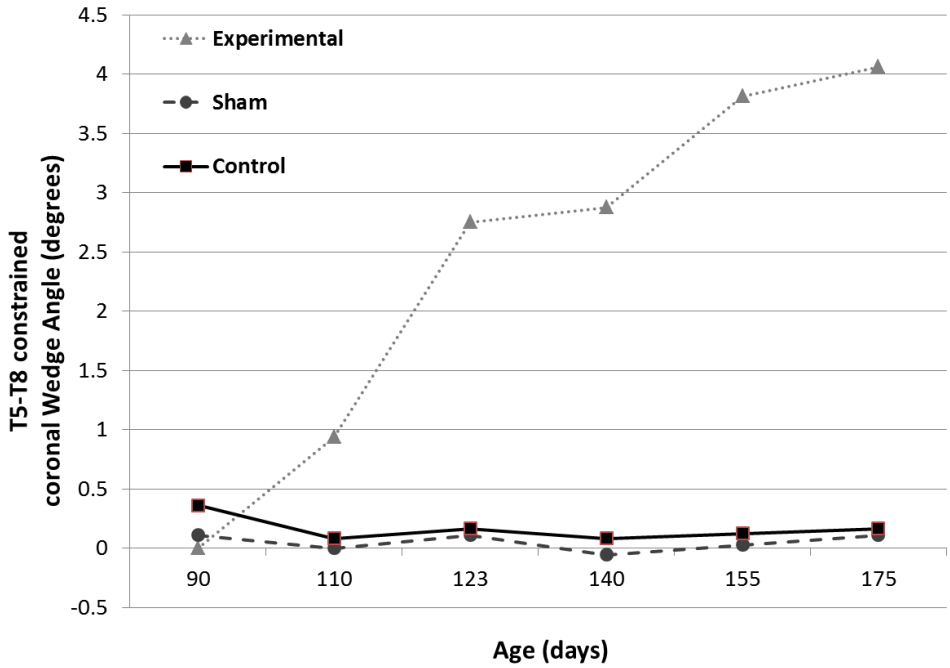

Figure 5.5: Article 3 figure 5 Progressive bi-weekly vertebral wedge angles (measured in the coronal plane)

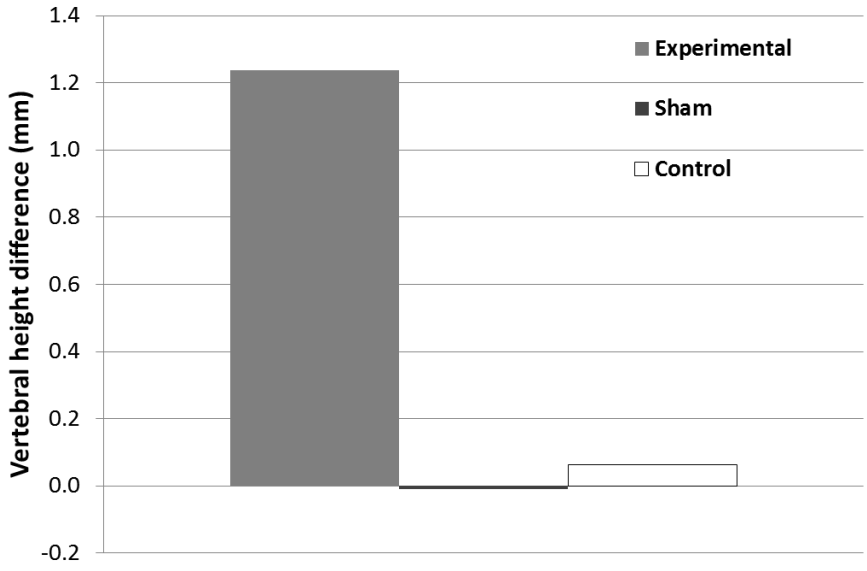

Figure 5.6: Article 3 figure 6 Difference in final left and right vertebral heights measured at 85 days post-operative

5.3 Framework of fourth article

The novel intravertebral epiphyseal device explored in the preceding manuscript (section 5.2) demonstrated its ability to induce local growth modulation while manipulating global spinal alignment. However, it is essential that the *in vivo* application of this device maintains intervertebral disc health and growth plate function as it is tailored towards adolescent use. The fourth manuscript explores the devices influence on the intervertebral disc and growth plate using radiographic and histological analyses. The realization of objective 4 and the investigation of hypothesis 3 are presented in the manuscript entitled "Novel device for the correction of paediatric scoliosis: influence on intervertebral disc and growth plate in a porcine model", for which the contribution of the first author is considered to be 85%. This manuscript was submitted to the *European Spine Journal* on May 4, 2011.

5.4 Article 4: Novel intravertebral device for the fusionless correction of paediatric scoliosis: influence on intervertebral disc and growth plate in a porcine model

Novel intravertebral device for the fusionless correction of paediatric scoliosis: influence on intervertebral disc and growth plate in a porcine model

Mark Driscoll, J. Eng.[1,2]; Carl-Eric Aubin, Ph.D., Eng.[1,2]; Alain Moreau, Ph.D. [3,4,5]; Yaroslav Wakula, MD[2]; and Stefan Parent, MD, Ph.D.[b]

1 - École Polytechnique de Montréal, Biomedical Engineering Institute, Montreal,Canada

2 - Research Center, Sainte-Justine University Hospital Center, Montreal, Canada

3 - Laboratory in Molecular Genetics of Musculoskeletal Diseases, Sainte-Justine University Hospital Research Center, Montreal, Canada

4 - Department of Stomatology, Faculty of Dentistry, Université de Montréal, Montreal, Canada

5 - Department of Biochemistry, Faculty of Medicine, Université de Montréal, Montreal, Canada

Address for notification, correspondence, and reprints:

Carl-Éric Aubin, Ph.D., P.Eng, Full Professor

Canada Research Chair, ‘‘CAD Innovations in Orthopedic Engineering,’’ & NSERC/Medtronic Industrial Research Chair in Spine Biomechanics

École Polytechnique de Montréal

Mechanical Engineering Department

P.O. Box 6079, Station ‘‘Centre-ville,’’

Montreal, QC, H3C 3A7, Canada

Phone: 514-340-4711, extention 4437

Fax: 514-340-5867

Email: carl-eric.aubin@polymtl.ca

Phone: 1 (514) 340-4711 ext. 4437

5.4.1 Abstract

Purpose: Fusionless growth modulation for the early treatment of scoliosis should insure the long term viability of the intervertebral disc and successfully reduce or arrest local growth. The influence of an intravertebral epiphyseal device, which proved effective control of coronal spinal alignment, on disc health and growth plate morphology was explored.

Methods: A novel device that inhibited local vertebral growth exclusive of the disc was introduced over T5-T8 in 4 immature porcine (experimental) while 3 underwent surgery without instrumentation (sham) and 2 had no intervention (control). Three month follow up prior to sacrifice provided radiographic (disc height and health) and histological (growth plate morphology, disc health, and type X collagen distribution) analyses.

Results: No post-operative complications were experienced. Radiographic data returned inverse disc wedging (greater disc height adjacent to device) in experimental segments and suggested disc viability. Histological data confirmed device growth modulation through significant local reduction of growth plate hypertrophic zone and cell height. A variability of disc health, dependant of device insertion location, was observed. Type X collagen was consistently identified in experimental growth plates and absent from intervertebral discs.

Conclusions: Intravertebral epiphyseal device decreased growth plate hypertrophic zone and cell height, and, reliant on device insertion site, showed positive signs of disc health sustainability. Spinal growth modulation achieved exclusive of disc compression, as practiced by this method, offers unique advantages over other fusionless techniques. This technique may provide a suitable and attractive alternative for the early treatment of idiopathic scoliosis.

Key Words

scoliosis, fusionless, surgery, growth modulation, hemiepiphysiodeisis, intervertebral disc

5.4.2 Introduction

Idiopathic scoliosis is a 3D spinal deformity whose etiology continues to escape researchers while a lack of exploitable risk factors dictating scoliotic progression restricts case specific prognostics. These restraints bound conventional scoliotic treatments to observation, brace treatment, and spinal fixation involving fusion. To improve progressive scoliosis management, fusionless growth modulation techniques have been explored. Propagated by the Hueter-

Volkmann principle [1], this method seeks to alter local forces within the spine with the purpose of correcting and/or reversing vertebral wedging – a phenomenon linked to scoliotic progression described under the "vicious cycle" [2]. This approach utilizes residual spinal growth to alter vertebral morphology (most commonly seek to halt convex vertebral growth) and, consequently, encourage spinal alignment.

Previous fusionless attempts returned both debatable and promising results. In a human clinical trial, shape memory alloy staples constrained scoliotic progression in 87% of cases (defined by progression ≤ 10°) [3]. Braun and colleagues explored the performance of both shape memory alloy staples and flexible tethers in a progressive scoliotic goat model. Although the staple showed no significant difference with untreated group, the flexible tether demonstrated considerable corrective abilities [4]. Others investigated a rigid stainless steel staple and demonstrated its ability to reduce local growth in a porcine model resulting in important deformities (reverse approach) [5].

Despite preliminary appeal of these devices, considerable scepticism remains regarding their influence on intervertebral disc health. Such cautious considerations arise from the fact that, by spanning the disc space, these methods invariably alter the discs mechanical environment, which may lead to local degenerative alterations [6]. Newton et al. demonstrated the flexible tether approach to preserve discs health through a detailed analysis [7]. Nevertheless, as these methods target skeletally immature adolescents, long term effects remain disconcerting. In an attempt to remedy such distress surrounding disc health, an intravertebral epiphyseal device that does not traverse disc space, thus preserving the disc's mechanical setting, was explored. *In vivo* testing in rodent [8] and porcine models [9] proved the devices effectiveness to control coronal spinal curvature. However, the insertion location of this device, aimed between the growth plate and the disc`s annulus, poses justified suspicion of its particular influence on discs and growth plates. The purpose of this study was to explore the influence of the intravertebral epiphyseal device on intervertebral disc health and growth plate morphology in an immature porcine model.

5.4.3 Methods

Nine immature 3 month old hybrid female pigs (ladrace/yorkshire) were utilized. Four experimental pigs underwent surgery with device introduction. Three sham pigs underwent

surgical protocol, including vertebral puncture, exclusive of device. Two pigs were maintained as control subjects.

Surgical Protocol and harvest

Study was approved by Institutional Committee for Animal Care in Research (ICACR) of Sainte-Justine University Hospital Centre. Pre-surgical sedation was achieved using intramuscular injections of atropine (0.04 mg/kg), azaperone (4 mg/kg), and ketamine (25 mg/kg). Intravenous injection of propofol (1.66 mg/kg) was introduced before intubation using a 6.5mm endotracheal tube. Ventilation and anesthesia maintenance were achieved using an oxygen and 1-3% isoflurane mix. Pig was placed in a lateral decubitus position over a heated mat. Insertion site was shaved and prepared with proviodine solution. Right side thoracotomy was made between the 7^{th} and 8^{th} rib providing access to vertebrae T5 to T8. Experimental group underwent transpleural insertion of device between vertebral growth plate and intervertebral disc. Insertion site and device were guided via fluoroscopic imaging. Device was fixed with a 25 mm bone screw through a custom guided surgical tool (Fig. 1). The pleura were cauterized at the site of insertion and lesions were closed in sham group. Subcutaneous tissue and skin sutures were applied at incision site. Film dressing was used to insure proper healing. Pig was then introduced with a fentanyl patch (7.5 mg). Post-operative intramuscular injections of antibiotics (excenel 3 mg/kg) were performed for 3 days. All pigs were maintained in individual cages until lesions were healed. Pigs were then held in a communal area until sacrifice. Post-operative follow up lasted 12 weeks.

Immediately following sacrifice, experimental cultured spinal segments with intact growth plates and discs were submerged in 4% paraformaldehyde. Segments were decalcified in RDO (Apex, Cederlane Burlington, Canada, ON.). Dehydration was performed using ethanol concentration gradients of 40%, 70%, 90%, and 100%. Lightening was achieved in Xylene. Segments were embedded in paraffin and the region of interest, which included the disc and adjacent growth plates (Fig. 2), was sectioned in slices of 5μm.

Radiographic study

All test subjects underwent final pre-sacrifice radiographs while sedated. Radiographs were digitized and intervertebral disc heights measures were performed on using Synapse® 3.1.1 (Fujifilm Medical Systems, U.S.A., Inc.). Left and right disc height measurements were taken in all groups. Intervertebral disc health of all groups was graded (between 0 and 4) as employed by Christe et al [10]. Namely, degree of disc health was projected using osteophytosis measures, narrowing disc space, and vertebral plates sclerosis.

Histological study

Two 5μm coronal slices, spaced 30 μm, apart, per experimental vertebra were taken from zone of interest and stained using safranine-O to highlight growth plate and bring into evidence surrounding tissues (Fig. 3). An optical microscope (Leika MDR) and Bioquant 6.9 software was used to measure growth plate hypertrophic zone height, hypertrophic cell height, and grade intervertebral disc degeneration. The hypertrophic zone was easily distinguishable as it begins with an abrupt increase in chondrocyte dimension and finishes with intact columns coming to an end. Under a magnification of 10, a sample of 35 measures of hypertrophic growth plate height was manually identified in left and right regions. Similarly, under a magnification of 20, a sample of 30 measures of cell height in hypertrophic region was recorded. As cell height was diverse, a range of cell sizes was selected to incorporate this variation. Mean measures of hypertrophic zone and cell heights were computed resulting in statistical comparisons of a singular value per region per vertebrae.

In parallel, experimental segments were treated for type X collagen. Two 5μm coronal slices, spaced 30μm apart, were processed for immunoperoxydase labelling with an in house type X collagen staining protocol using a monoclonal antibody anti-collagen X (Sigma C-7974). Subsequent to imunoperoxydase labelling, segments were processed with hematoxylin to bring into evidence cellular content. A control segment was also processed to accurately assess type X collagen distribution. Comparison of type X collagen and cellular dispersion was assessed between left and right utilizing an optical microscope (Leika MDR). Under a magnification of 40, device insertion region was explored thoroughly to interpret tissue morphology. To objectively interpret type X collagen dispersal and tissue characteristics, intra-observer tests were performed.

Intervertebral disc health of all groups was evaluated using a histological grading scale [10]. The scale estimates disc heath using signs of annulus fibrosus laminar orientation, nucleus pulposus clefting and necrosis, and distinction between growth plate and subchondral bone margins. The grade selected for each disc was defined by its worst characteristic observed over analysed sections.

Statistics

Comparative data were analyzed using non-parametric Wilcoxon tests. Radiographic measures compared left and right disc height and graded disc health in all groups. Disc height (left and right) and difference in height (left-right) was compared for each group. Histological analyses compared difference in left and right growth plate morphology for the experimental group. Radiographic/histological grading of disc heath, distributions of collagen type X, and tissue analyses remain qualitative and were thus reported as such. All measures were repeated by 2 observers to interpret influence on statistical conclusions.

5.4.4 Results

Device successfully induced a curvature of 6.5±3.5° under the inverse approach (creation of a scoliotic curve). No pigs experienced post-operative infection or showed altered activity. Upon processing the histological samples, it was noted that 9/16 vertebrae showed device insertion in a relevant position to explore its influence on discs and growth plates. These included samples were device presented slightly in annulus, between annulus and growth plate, and/or pierced mildly the growth plate. Other samples (7/16) had devices located inferior to growth plate. Accordingly, this position would not significantly influence disc or growth plate health and were excluded from analyses. All groups were investigated via radiographic analysis. Only experimental group was processed for histological and biochemical examinations.

Radiographic data

Experimental left and right (device) intervertebral disc mean height and standard deviations were respectively 1.8mm ±0.5 and 2.6mm ± 0.7. Correspondingly, left and right discs of shams measured 2.0 mm ± 0.4 and 2.0 mm ± 0.3 while left and right control disc zones were 2.2 mm ± 0.5 and 2.2 mm ± 0.5 (Fig. 4). Only left and right measures in experimental group suggested

significant difference ($p=0.01$). Sham ($p=0.38$) and control ($p=0.97$) measures returned no quantifiable difference. Left and right disc height difference in experimental group diverged from both sham ($p<0.01$) and control ($p<0.01$) groups while comparison of sham and control suggested measurement difference ($p=0.26$).

Sham and control discs were graded as 0, no signs of degenerative alteration (0=healthy, 5=advanced degeneration). Experimental discs demonstrated no osteophytosis or vertebral plate sclerosis signs. Disc height narrowing was not observed in experimental group compared to sham and control groups ($p>0.34$). Consequently, experimental discs received a grade 0.

Histological data

Differences in growth plate hypertrophic zone and cell height proved different over experimental vertebra (Fig. 5). Mean measures and standard deviations of hypertrophic zone height over left and right (device) portion of the growth plates were $125.64\mu m \pm 16.61$ and $61.16\mu m \pm 8.25$ respectively. Hypertrophic zone cell height measures were $16.14\mu m \pm 1.87$ over left portion and $9.22\mu m \pm 1.57$ in right (device) sections (Fig. 6). Zone and cell heights provided significant difference ($p < 0.01$) between the left and right measures in properly instrumented vertebrae.

Successful type X collagen staining was confirmed as hypertrophic zone of growth plate was brought into evidence in contrast to control slides (Fig. 7). Type X collagen was consistently observed in growth plate regions inferior to device. No evidence of type X collagen in either left or right sections of discs in all segments was observed. Correspondingly, no indication of type X collagen surrounding the inserted device head was distinguished.

Documentation of intervertebral disc health via histological grading (1=healthy, 5=advanced degeneration) returned a value of 3 (3/9 vertebrae), 2 (5/9 vertebrae) and 1 (1/9 vertebrae) for experimental group. All segments had a significant increase in cellular content distinctively observed surrounding void formerly occupied by device head. These cells were not highlighted using Safranine-O staining and had a fibroblastic morphology suggesting fibrous tissue. This tissue, under a 40x magnification, included signs of nominal vascularisation in 3/9 explored segments, resulting in a disc grade of 3. A grade of 2 was attributed to segments with laminar penetration of device into inferior portion of annulus. Such penetration disrupted laminar

orientation reserved to outer portion of annulus. Score of 1 was credited to segment whose insertion site was immediately superior to growth plate and inferior to annulus, thus had no influence on disc or growth plate health. All segments showed no signs of chronic inflammation, absence of clefting or necrosis in the nucleus, and growth plate and subchondral bone appeared consistently healthy with no indication of invading vascular channels or osteophytes formation.

5.4.5 Discussion

A novel intravertebral epiphyseal device for the treatment of paediatric scoliosis demonstrated the ability to control coronal spinal alignment in a porcine model. Objectives of fusionless techniques are to correct spinal deformities while maintaining mobility, health, and function. The intravertebral device proposes a novel instrumentation method that would tentatively respect such aspirations.

Radiographic analyses confirmed device's ability to manipulate spinal alignment. Moreover, this interpretation provided evidence of that the flexible intervertebral disc adopted an opposing configuration to vertebrae. Measurements confirm disc wedging converse to vertebral wedging previously measured [9]. Evidently, this impedes coronal profile control; however, such a restrained expense may be justifiable if spinal health and function is preserved. Moreover, as this approach targets early and immature scoliotic spines, correction magnitudes observed in this study (up to 12 degrees Cobb over 4 instrumented vertebrae) may suffice as a treatment to retard, arrest, or correct underdeveloped deformities in immature patients.

Decisive evidence significantly supported the device`s capacity to reduce growth as indicative of adjacently reduced hypertrophic zone and cell height. Others have demonstrated reduction of both hypertrophic zone and cell height in growth plates to be representative of reduced longitudinal bone growth [11, 12]. These findings support the notion that the device successfully reduces height by means of growth modulation.

In this study, 9 of 16 instrumented vertebrae had device inserted in or immediately adjacent to the annulus and/or growth plate while guided via fluoroscopy. Although radiographic examination suggested preservation of disc health, histological disc health grading reported local signs of degenerative tendencies consequential to device position. Nonetheless, histological disc

viability outside region of device insertion demonstrated no additional signs that would suggest degeneration. Absence of type X collagen distribution in disc extracellular matrix further supported disc viability remote to device. Previous works have demonstrated that type X collagen is expressed in the matrix of degenerated [13] and scoliotic [14] discs. Such differentiations may be initial indication of matrix calcifications related to degenerative adaptations. As expected, type X collagen was present in hypertrophic region of growth plates while its continued presence adjacent to device insertion suggests sustainability of growth plate function.

Intervertebral disc health remains a concern with this method. Although device does not span disc space, insertion site requires great accuracy and its position invites unrest. Insertion precision is important both for device's ability to arrest growth and avoid disc puncturing which, as indicative in this analysis, may initiate degenerative adaptations. Such precision obligations may be remedied by reduction of device head thickness and the development of a handheld probe based on optical coherence tomography that allows for a real time resolution of 10μm and a penetration up to 3mm [15]. Such a probe, allows for per-operative tissue differentiation. The current study did not utilize this probe to position device but authors are confident that, upon completion, the custom probe may be coupled with surgical instrumentation to insure exact insertion location of intravertebral epiphyseal devices.

While attempting to infer the influence of this intravertebral epiphyseal device on humans one must acknowledge differences. Adolescent human vertebrae grow at a slower pace while they differ anatomically from porcine vertebrae as they lack a second ossification zone amid epiphysis and disc. Only experimental group was processed for histological analyses. Detailed interpretation of the device influence on disc health was nevertheless assessed using common interpretative methods. Although a 12 week follow up may not suffice to deduce long term disc and growth plate viability, this study successfully identified areas necessitating improvements. Other limitations include the act of decalcifying and embedding vertebral samples which is known to alter growth plate morphology [16]. Absolute morphometric measures may be imprecise and, thus, authors reserved conjectures to measures derived from relative comparisons.

In conclusion, the intravertebral epiphyseal device provides an attractive method to achieve fusionless growth sparring instrumentation. Its minimally invasive procedure and unassuming presence may satisfy judicious requirements of aspiring new fusionless treatments tailored to progressive adolescent idiopathic scoliosis.

5.4.6 References

1. Mehlman C, Araghi A, Roy D (1997) Hyphenated History: the Hueter-Volkmann Law. Am J Orthop 26: 798-800

2. Stokes I, Spence H, Aronsson D, et al. Mechanical Modulation of Vertebral Body Growth: Implications for Scoliosis Progression. *Spine* 1996; 21(10): 1161-7.

3. Betz R, D'Andrea L, Mulcahey M, et al. Vertebral body stapling procedure for the treatment of scoliosis in the growing child. *Clinical Orthopaedics and Related Research* 2005; 434: 55-60.

4. Braun J, Akyuz E, Ogilvie J, et al. The efficacy and integrity of shape memory alloy staples and bone anchors with ligament tethers in the fusionless treatment of experimental scoliosis. *J Bone Joint Surg Am* 2005; 87(9): 2038-51.

5. Wall E, Bylski-Austrow D, Kolata R, et al. Endoscopic mechanical spinal hemiepiphysiodesis modifies spine growth. *Spine* 2005; 30(10): 1148-53.

6. Stokes I, and Iatridis J, Mechanical Conditions that Accelerate Intervertebral Disc Degeneration: Overload Versus Immobilization *Spine* 2004; 29(23): 2724-32.

7. Newton P, Farnsworth C, Faro F, et al. Spinal growth modulation with an anterolateral flexible tether in an immature bovine model. *Spine* 2008; 23(7): 724-33.

8. Schmid E, Aubin C, Moreau A, et al. A novel fusionless vertebral physeal device inducing spinal growth modulation for the correction of spinal deformities. *Euro Spine J* 2008; 17(10): 1329-35.

9. Driscoll M, Aubin C, Moreau A, et al. Novel minimally invasive device for the fusionless treatment of pediatric scoliosis by means of growth modulation. *Spine* Under review

10. Christe A, Laubli R, Guzman R, et al. Degeneration of the cervical disc: histology compared with radiography and magnetic resonance imaging. *Neuroradiology* 2005; 47:721-9.

11. Stokes I, Mente P, Iatridis J, et al. Enlargement of growth plate chondrocytes modulated by sustained mechanical loading. *J Bone Joint Surg Am* 2002; 84: 1842-8.

12. Bylski-Austrow D, Wall Em Glos D, et al. Spinal hemiepiphysiodesis decreases the size of vertebral growth plate hypertrophic zone and cells. *J Bone Joint Surg Am* 2009; 91: 584-93.
13. Boos N, Nerlich A, von der Mark I, et al. Immunolocalization of type X collagen in human lumbar intervertebral discs during ageing and degeneration. *Histochem Cell Biol* 1997; 108: 471-80.
14. Aigner T, Greskötter K, Fairbank J, et al. Variation with age in the pattern of type x collagen expression in normal and scoliotic human intervertebral discs. *Clcif Tissue Int* 1998; 63: 263-8
15. Beaudette K, Strupler M, Driscoll M, et al. Towards a Handheld Probe based on Optical Coherence Tomography for Minimally Invasive Spine Surgeries. *Stud Health Technol Inform* 2010; 158: 49-54.
16. Hunziker E, Schenk R, and Cruz-Orive L. Quantitation of chondrocyte performance in growth-plate cartilage during longitudinal bone growth. *J Bone Joint Surg Am* 1987; 69: 162-73.

5.4.7 Figures and tables

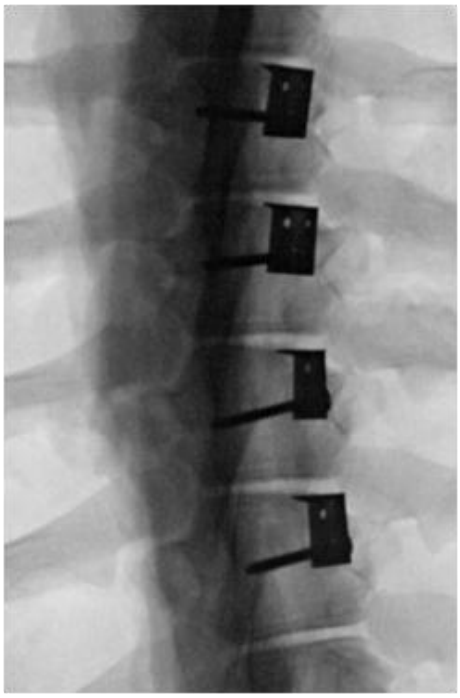

Figure 5.7: Article 4 figure 1 Fluoroscopic image of harvested instrumented porcine spine with intravertebral epiphyseal device

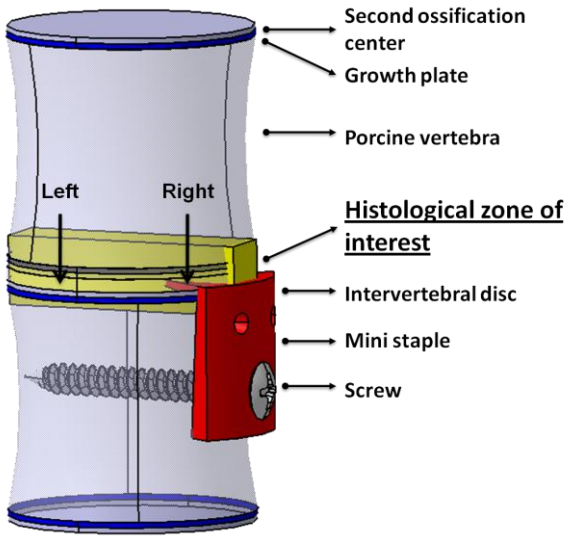

Figure 5.8: Article 4 figure 2 Scaled depiction of the zone of interest from which biochemical and histological analyses were performed

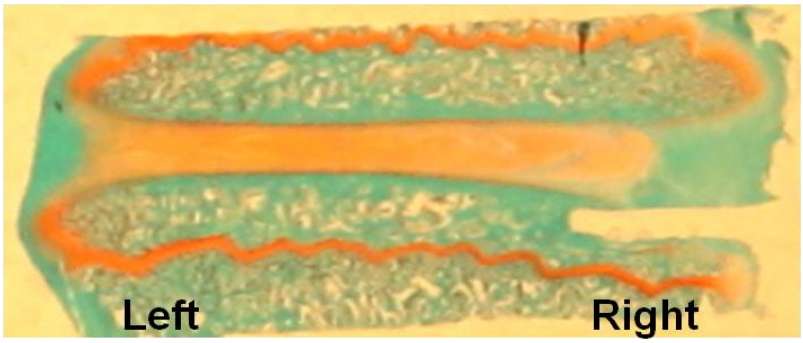

Figure 5.9: Article 4 figure 3 Section of instrumented segment (device formerly in void) stained with Safranine O

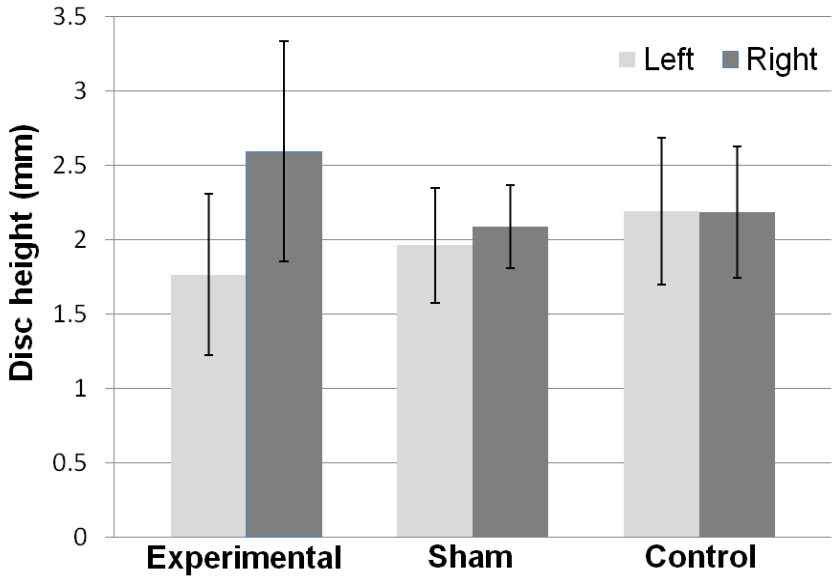

Figure 5.10: Article 4 figure 4 Left and right intervertebral disc height measurements

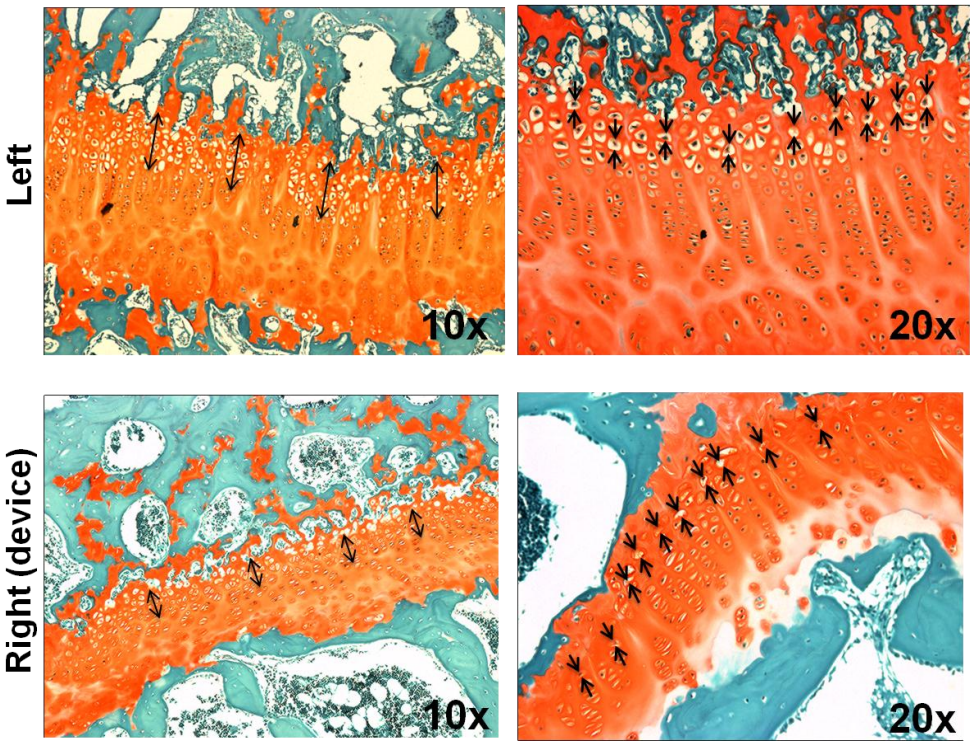

Figure 5.11: Article 4 figure 5 Left and right sections of growth plate under 10x and 20x magnification

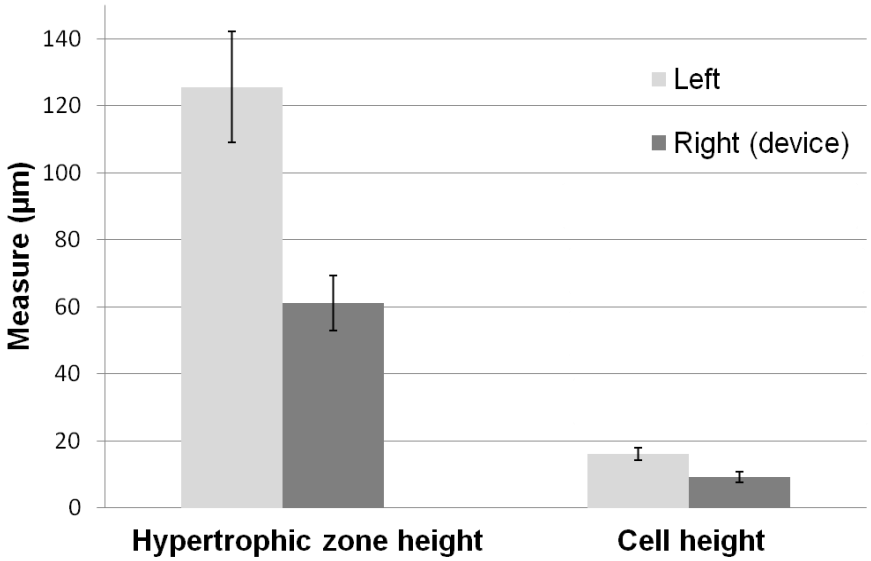

Figure 5.12: Article 4 figure 6 Measurements of left and right portions of hypertrophic zone and cell height of instrumented growth plate

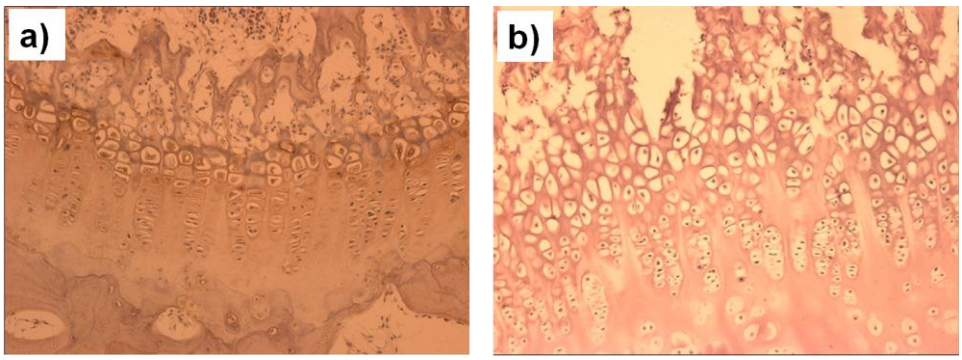

Figure 5.13: Article 4 figure 7 a) Positive immunostaining of type X collagen in hypertrophic zone of growth plate b) control segment

5.2.8 Additional studies related to the comparative measure of osteopontin

Osteopontin (OPN) is an extracellular structural protein which is biosynthesized by most physiologic tissues. Recent finding have attributed it as a potential progressive risk marker in scoliotic spines [127, 128]. More specifically, these studies suggest mutations are present that interfere with melatonin signal transduction and, thus, post transduction modifications affecting Gi protein function are speculated as a mechanism in the etiopathogenesis of AIS. Therefore, to analyze the influence of growth modulating implants (that seek to induce a scoliotic curve – reverse method) on its circulatory concentration, OPN was calculated bi-weekly during the 12 week post-operative follow up in all groups.

Blood was taken from each pig in all groups in parallel to radiograph sessions every two weeks while sedated (Stresnil, IM 2.2 mg/kg; Atropine, IM 0.1 mg/kg 4ml; Ketamine, IM 10mg/kg). A blood sample of 2ml from the ear was taken using a 5ml syringe with a number 23 needle. This took place over the 12 week post-operative follow up. Following culture, blood plasma was separated and analyzed using enzyme-linked immunosorbent assays. Statistical analyses utilizing t-student test were performed.

Detectable levels of OPN were nominal in pig plasma. Pre-operative concentrations of OPN in sham, control, and experimental groups were 11.06 ± 3.3ng/ml, 14.72 ± 0.54ng/ml, and 12.72 ± 0.08 ng/ml respectively. Successive post-operative measures were 10.80 ± 1.8ng/ml, 11.44 ± 0.44ng/ml, and 9.92 ± 1.12ng/ml and post-operative at 4 months were 11.11 ± 2.6ng/ml, 11.24 ± 1.15ng/ml, and 9.83 ± 0.82ng/ml for respective sham, control, and experimental groups. This data are represented in figures 5.14 and 5.15 below. No statistical differences were identified between groups (sham-control, sham-experimental, and control-experimental) at different times.

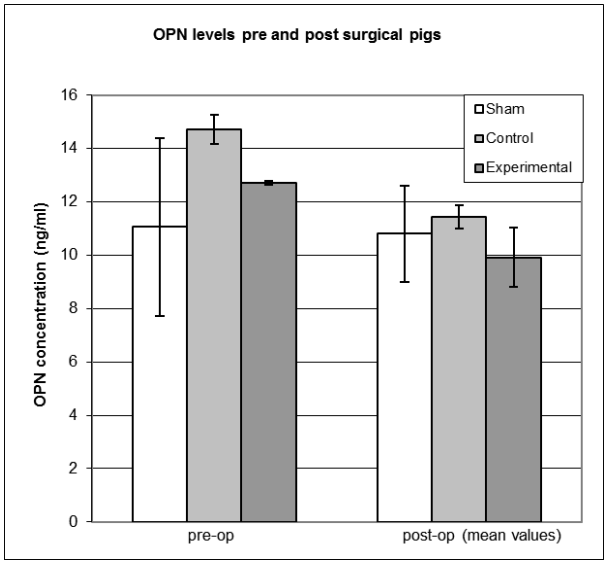

Figure 5.14: OPN result pre and post-operative in all experimental groups

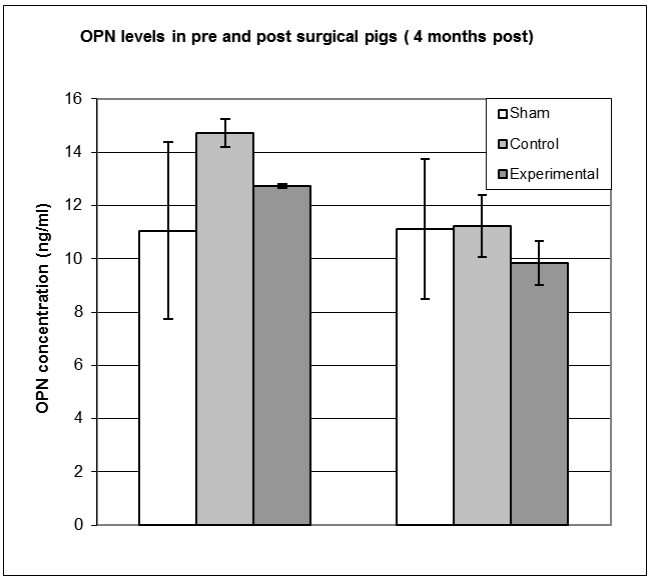

Figure 5.15: OPN result pre and 4 month post-operative in all experimental groups

This information provides inconclusive trends as statistical significance was not achieved. Possibly because a difference did not exist but this inconclusive evidence is believed to take place as processing kits used were designed with antibodies recognizing human OPN while pig plasma did not offer sufficient cross-reactivity. For future studies, a speculated alternative approach would entail measuring OPN levels (utilizing a developed in-house OPN antibody for pigs) after processing the cultured spines using immunohistochemistry and gathering OPN levels locally around the implant.

CHAPTER 6 : Performance of a novel 3D corrective tether for the treatment of adolescent idiopathic scoliosis

6.1 Framework of chapter 6

Over the course of the *in vivo* trial of the intravertebral epiphyseal device described in chapter 5, another novel device was conceived. The device, titled 3D corrective tether (initial invention disclosure made on July 29, 2009, provisional patent filed April 14, 2011 by Mark Driscoll, Carl-Eric Aubin, and Stefan Parent), was engineered to meet distinct design specifications and was developed and thoroughly explored using the platform which includes *in silico*, *in situ*, and *in vivo* analyses. This device was conceived to addresses the full 3D deformity present in scoliotic spines and, consequently, would be an improvement over current fusionless devices which act solely unilaterally (identified through the completion of objective 2). The sequential realization of objectives 1, 2, 3 and 4 and the investigation of hypothesis 4 are presented in chapter 6.

6.1.1 Design specification

To date, no corrective fusionless device for the treatment of AIS has attempted to address its three dimensional characteristic. In order to achieve this, careful planning in all anatomical planes is required to ensure proper direction and magnitude of corrective force vectors.

Coronal/Sagittal plane correction

One may manipulate coronal and sagittal planes independently from another by moving the insertion site of the screw over the vertebral body. In a healthy spine (i.e. no axial rotation), the normalized coronal and sagittal influence ratios may be summarized in figure 6.1. This interpretation is significantly modified when applied to a scoliotic spine with associated vertebral rotation. Under this consideration, the normalized coronal and sagittal correction ratios were also calculated for vertebrae under 15 and 30 degrees of axial rotation as observed in figures 6.2 and 6.3 respectively. Given this information it becomes apparent that if one was actively seeking to manipulate the coronal and sagittal planes, selection of the screw insertion site should vary according to the degree of axial rotation of the vertebra under consideration.

Notwithstanding, one should note that the projected coronal and sagittal manipulation presented in figures 6.1 to 6.3 where made under the following assumptions. First, the relations were

achieved based on the vertebral pivot occurring at the geometric center of mass of the anterior vertebral body. Second, it was considered that the magnitudes of the forces were equivalent in order to effectively compare their relative influence while the direction of the force vector was maintained normal to the displayed transverse plane. Finally, it was assumed axial rotation would remain the same.

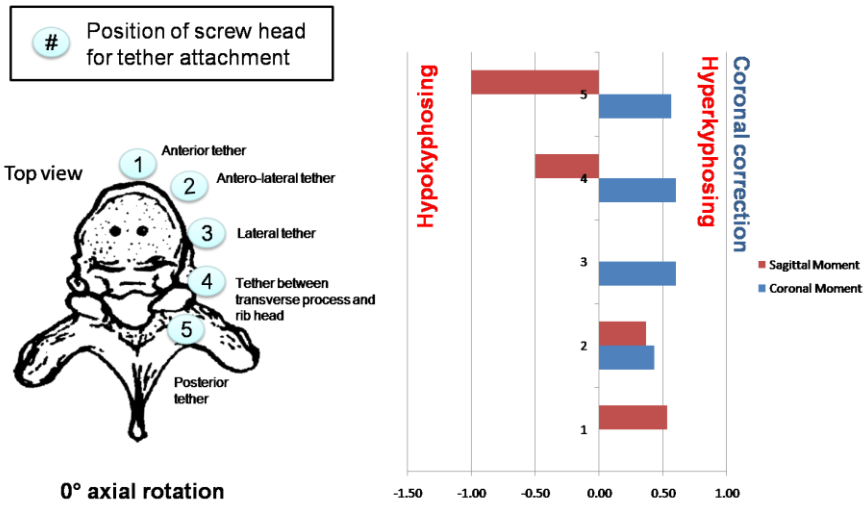

Figure 6.1: Normalized relative moments imposed on vertebra as a function of implant location

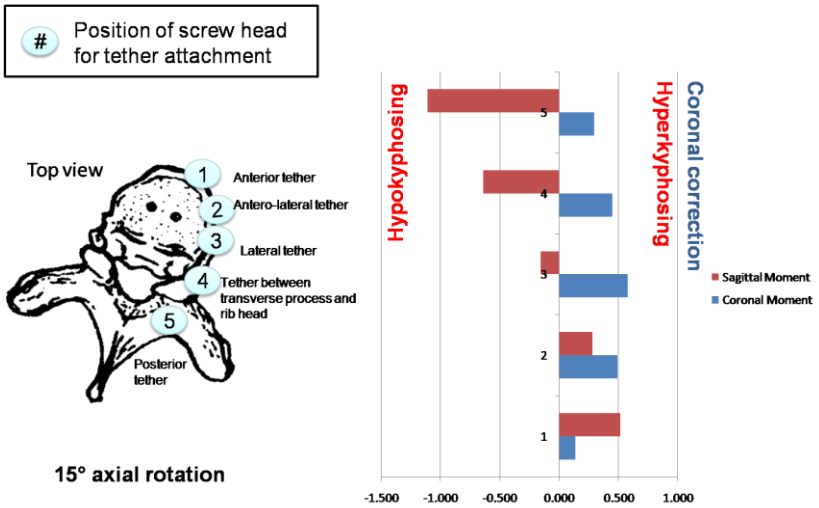

Figure 6.2: Normalized relative moments imposed on 15º axially rotated vertebra as a function of implant location

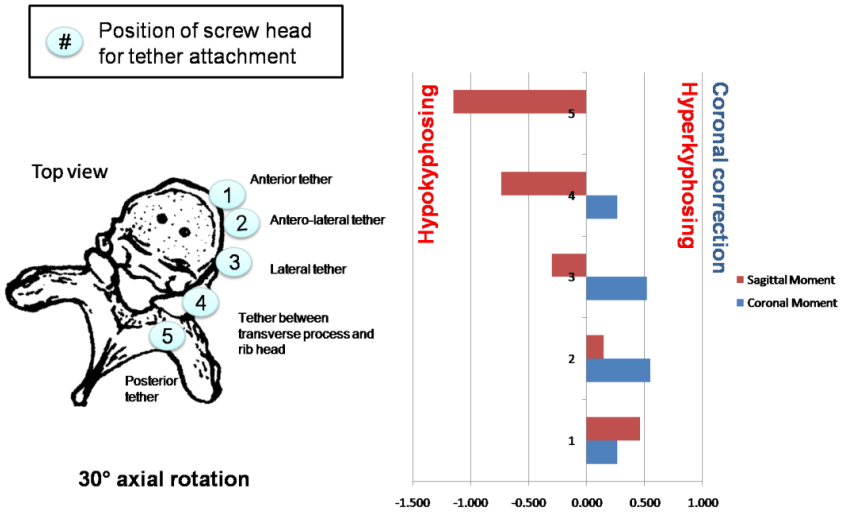

Figure 6.3: Normalized relative moments imposed on 30º axially rotated vertebra as a function of implant location

Transverse Plane Correction (axial derotation)

To interpret desired axial rotation for the correction of scoliotic spines, the average degree of rotation was acquired for a type 1 Lenke scoliotic deformity using published values from Stokes [211]. Such values and corrective angles are summarized in figure 6.4. The second graph titled *global (absolute) rotation required* demonstrates the total magnitude of vertebral derotation required during a surgical procedure in order to fully align all vertebrae of the thoracolumbar spine with respect to the transverse plane. As one would expect, around the apex of the curvature (T7-T8) larger inputs are required to achieve proper alignment. One must keep in mind that any rotational inputs induced on a vertebra will directly influence the axial position of superiorly located vertebrae (under the assumption that rotational inputs translate to superior vertebrae as L5 is considered to be the most grounded reference point). As a consequence of such interpretative assumptions, it is also important to recognize the relative axial rotations required for proper transverse arrangement as observed under *relative rotation required*. From these results it becomes apparent that if sufficient axial correction is achieved at each level, then the relative values required for an effective transverse repositioning during instrumentation are achievable under the capabilities of conventional instrumentation methods. Moreover, these values identify that the minimum relative rotation required would be present at the apex. That is, if vertebral rotation is corrected, no additional derotation forces would be required at the apex. Although the magnitude of vertebral rotation achieved under conventional scoliotic treatments

remains a debate, authors have identified that possible corrections lie between 1 and 5 degrees, [212, 213] - values within the suggested relative ranges found in figure 6.4 below. However, to date, no fusionless device has attempted nor measured axial correction.

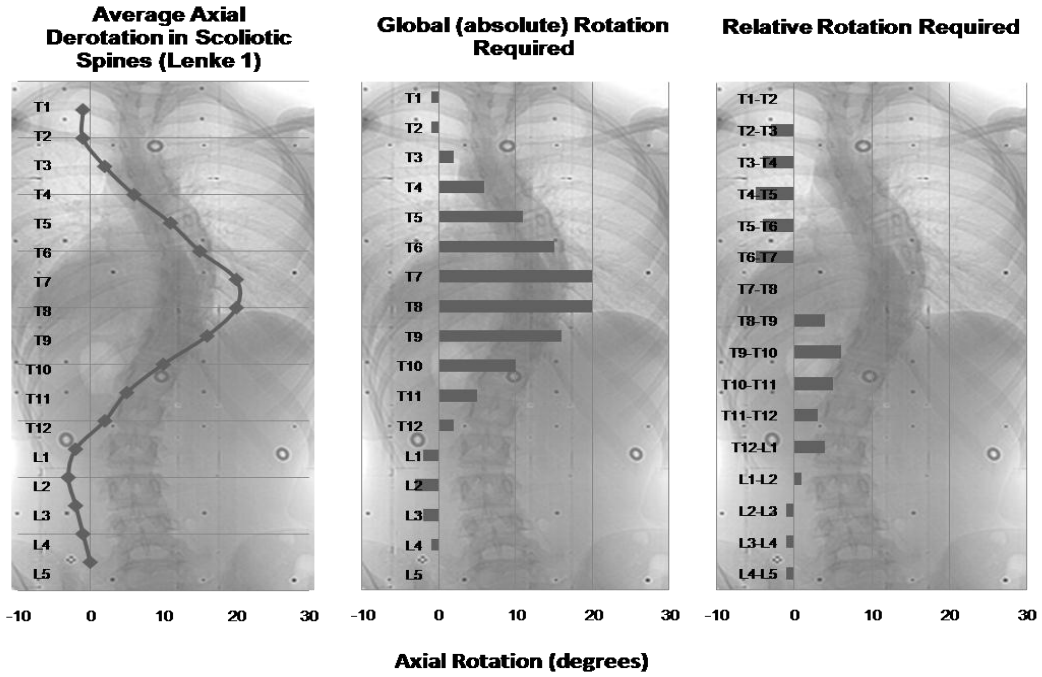

Figure 6.4: Required axial correction for Lenke Type 1 scoliotic curve

6.2 FEM conception (*in silico*)

A 3D corrective tether was devised to meet corrective requirements indicated above in section 6.1. Initial analyses were performed using the developed FEM platform to interpret growth plate stress distribution, immediate correction, and long term modifications by means of growth modulation.

6.2.1 Methods

Stress distribution using the proposed 3D tether was explored using the FEM developed through the completion of objectives 1 and 2 as reported in chapters 3 and 4. The 3D corrective tether was introduced into the same scoliotic model utilized to explore other fusionless device detailed in article 2. Once introduced, spinal loading was applied and axial stresses over the apical growth plate were measured in a healthy FEM (no coronal curve), a non-instrumented scoliotic

model, and an instrumented scoliotic model with a tether of varying initial strain (pre-tension) using different materials.

Next, the immediate impact of the device on spinal alignment (post-operative) was explored. This was achieved by comparing the final configurations of the loaded non-instrumented FEM and the FEM instrumented with the 3D corrective tether. As an additional step, the immediate axial correction was measured and compared to the desired correction previously calculated and reported in figure 6.4. In order to achieve the necessary axial correction, successive tensions in the 3D corrective tether were altered.

The final step consisted of simulating 2 years of progressive growth in the scoliotic model. Again applying methods adopted in chapter 4 section 4.2.3, the iterative growth algorithm governed this simulation.

6.2.2 Results

Figure 6.5 report the apical stress distributions. A pre-tension of 150 Newtons using stainless steel (SS) proved to be the best in terms of altering growth plate stress distribution by reducing concave and augmenting convex stresses.

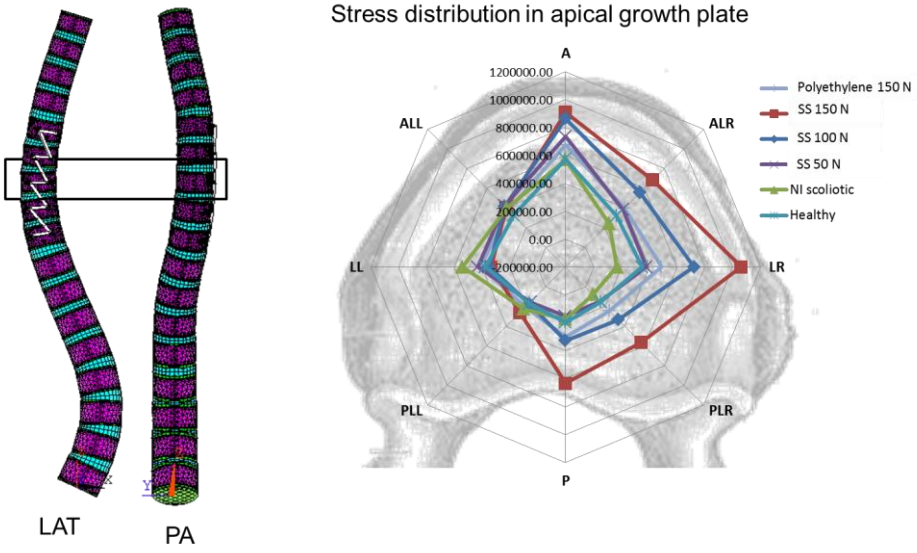

Figure 6.5: Apical (T7) axial stress (Pa) distribution in instumented scoliotic FEM with 3D corrective tether using polyethylene and stainless steel (SS) at vayring intial strains compared to non-intrumented (NI) scoliotic and healthy FEMs ((LAT) lateral, (PA) posterior anterior)

Figure 6.6 reports values of calculated immediate correction offered by the 3D tether in SS at varying initial strains. The coronal Cobb angle was reduced from 28° to 8° using about 150 Newtons. The impact on the sagittal plane was not significant under this configuration; however, it was verified that sagittal manipulation may be achieved by anterior and posterior displacement of device.

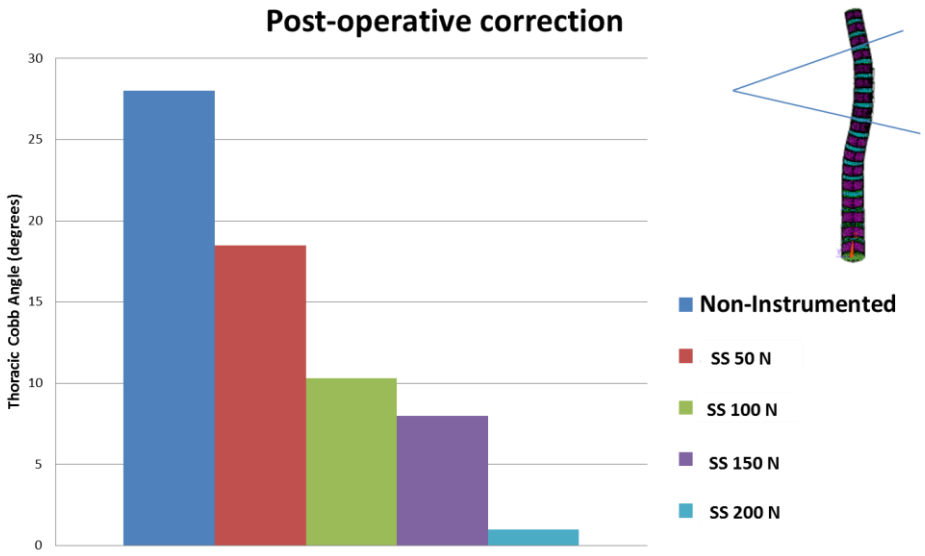

Figure 6.6: Immediate impact of 3D tether on thoracic coronal Cobb angle at different initial strains

Figure 6.7 reports the axial manipulation of the 3D tether device on a scoliotic spine. A tether configuration spanning 7 functional segments from T10 to T4 at varying tensions of 200, 200, 150, 150, 100, 50, 50 Newtons respectively (high tension to low tension) was able to achieve an absolute derotation up to 10° and a relative derotation of up to 8°. When limited to 5 functional units, a tether with successive tensions from T9 to T5 of 200, 150, 150, 100, 50 Newtons best matched required derotation for a scoliotic Lenke Type 1 as depicted in figure 6.4.

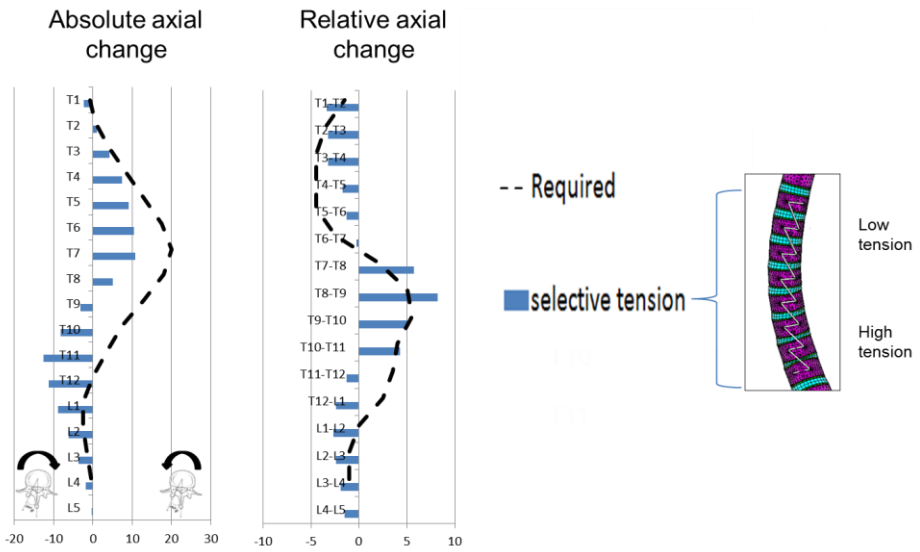

Figure 6.7: Immediate absolute and relative axial correction obtained from 3D tether compared to required value (calculated in fig. 6.4)

Figure 6.8 reports examples of spinal configurations after 2 years of simulated adolescent spinal growth when instrumented with the 3D tether at varying tensions. Based on this analysis, an initial tension of about 100 Newtons proved the most beneficial under these conditions (thoracic curve 28° and two years of adolescent growth remaining). As indicated, tensions of 150 Newtons provided a mild overcorrection at the site of instrumentation.

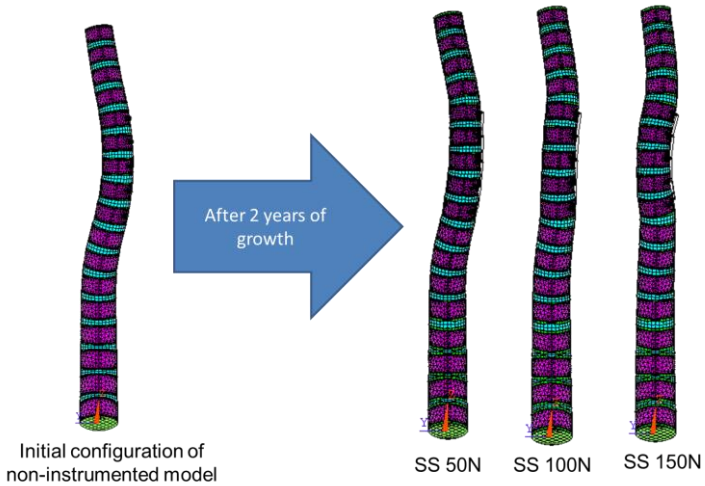

Figure 6.8: Long term correction of scoliotic curve using stainless steel 3D tether at different initial tensions

6.2.3 Discussion

Results reported are based on several optimization analyses that explore the material properties of the tether, insertion sites of bone screws, initial tensions, and a plethora of tether angles and configurations.

In a trivial manner, results agree with findings of chapter 4 article 2 and indicate scoliotic correction is, in part, dependant of initial tension in tether. However, one must be cautious and keep in mind a few additional design factors. More tension may entail more disc adaptation or degeneration. Also, greater force may place demands too great for the vertebra to handle resulting in screw plow (bone screw moving within vertebra). It is estimated that unconstrained screw plow (*i.e.* screw movement not restricted by attachment) occurred in cadaveric vertebrae at about 190 Newtons [214]. Finally, with regards to tether tension, the possibility of overcorrection must be considered.

Each tether is mechanically independent from another and, therefore, local tensional forces may vary in isolation of others. This, as demonstrated in figure 6.7, is a novel aspect to obtaining the desired absolute and relative axial rotations. Evidently, during *in vivo* instrumentation, such adjustment would be performed at the discretion of the surgeon and tailored to the patient's deformity specifics. However, as discussed in sections 6.1.2, the relative moments in the coronal and sagittal planes must be kept in mind when imposing this desired pre-tension. Finally, another factor one must consider is the available long term correction by means of growth modulation available, as patient skeletal maturity will vary.

These *in silico* analyses supported the 3D corrective tether to provide spinal manipulation in three anatomical planes. To further verify this information, additional studies using *in situ* and *in vivo* investigations were performed.

6.3 Analogue spine model analyses (*in situ*)

Once design specifications were met using the *in silico* platform, the device was fabricated from technical drawings and further explored using an analogue spine model. This analysis employed a qualitative assessment of the device`s influence on spinal alignment while providing a means to develop surgical tools and techniques. This phase of the developmental platform took place

under two iterations for the 3D tether. The first feasibility study encountered experimental problems during *in vivo* analyses. Problems were remedied and the *in situ* and *in vivo* processes were repeated.

The first trial consisted of using a screw with a large head used as a means to clamp and fix the tether between bone and screw (Fig. 6.9 left). This design provided sufficient strength to maintain the forces estimated to take place within a pig spine during *in situ* tests (100-400 Newtons). However, a few problems were encountered during the first *in vivo* trial. Bone screws had too large of a head and the fixation between the bone screw and tether was not sufficient. Moreover, bone screw threads were not sufficient and mild screw pullout appeared with time. Thus, the problem was resolved and the *in situ* and *in vivo* processes were repeated.

The second trial of the 3D tether consisted of using improved bone screws (Fig. 6.9 right). This was required to address inadequacies experienced within the first design regarding device size and fixation problems. First, a longer screw (as to achieve cortical to cortical insertion) with a larger thread was adopted to encourage osseointegration as a means to enhanced long term screw/bone fixation. Second, to address the confined space available, a lower profile head was designed and machined. This head integrated a tapered and threaded slot that allowed the tether to pass while under wedged compression in the taper. A set screw drove the tether further into the machined wedge and, thus, provided improved and effective screw/tether fixation.

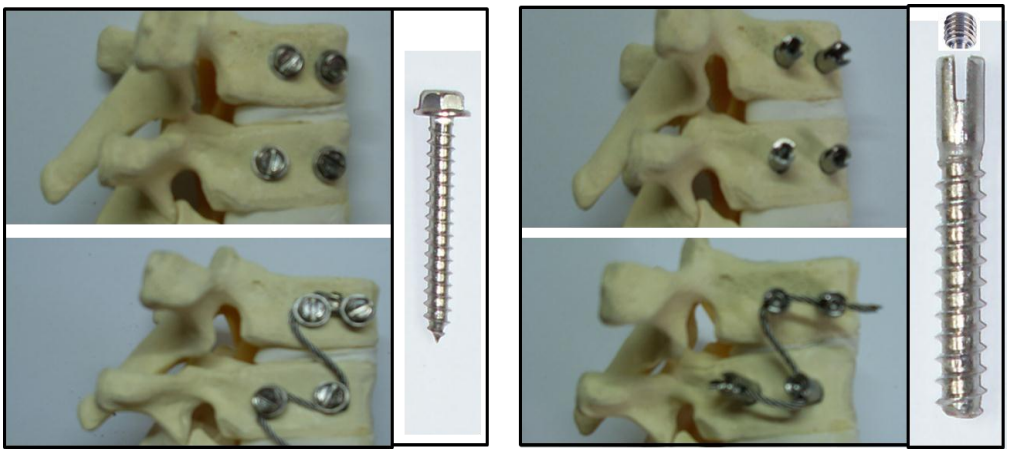

Figure 6.9: Design of first trial (left) and second trial (right) of screw/bone/tether fixation

The qualitative assessment of the 3D corrective tether agreed with the axial control measured under the *in silico* platform. Local adjustments of tether tension provided the ability to alter relative rotations of vertebral bodies independently from adjacent vertebrae (Fig 6.10).

Figure 6.10: Example of agreement between *in silico* and *in situ* manipulation of spinal alignment by the 3D corrective tether

6.4 Porcine model (*in vivo*)

The *in vivo* porcine model trial of the 3D tether construct also took place in two separate parts. Experimental methods followed those described in chapter 5 article 3. The *in vivo* analysis of the 3D corrective tether was performed as a feasibility study. Thus no control or sham pigs were used. The purpose of this analysis was to investigate if *in vivo* manipulations of spinal alignment provided by the 3D tether in a porcine spine respected those predicted by *in silico* and *in situ* analyses.

6.4.1 Methods

Part 1 of the *in vivo* tests, involved 1 three-month old pig instrumented from T6-T8. Experimentally, part 2 underwent several modifications over the first. This analysis utilized 3 four-month old pigs and instrumented T9-T12 in order to target larger vertebrae. The second trial also used an improved screw design as indicated in figure 6.9. Both groups were followed for 12 weeks. All pigs were instrumented by means of a right side thoracotomy. Bone screw insertion sites were bored prior to screw insertion using custom surgical tools. A stainless steel

tether was then joined to the bone screws via a compression fixture. Subcutaneous tissue and skin sutures were used to close the incision. Post-operative bi-weekly dorsal-ventral and lateral radiographs of sedated pigs were taken until sacrifice. Radiographic images were digitalized and measures of Cobb angles together with vertebral and disc wedging were acquired in the coronal and sagittal planes while axial rotation was also analyzed. All measured were performed using Synapse® 3.1.1 (Fujifilm Medical Systems, USA, INC).

6.4.2 Results part 1

The first pre-clinical trial manipulated the coronal plane, axial plane modifications were not sufficient to record, and sagittal plane was slightly altered (sagittal plane not targeted in this analysis but it is maintained that the 3D tether may alter the sagittal plane if desired). Following 30 days post-operative, one of the screws was loosened and pulled out at T8 and, consequently, the integrity of the screw/tether assembly suffered. Prior to the pull-out, inverse disc wedging was observed (opposing induced vertebral wedging) while the tether construct achieved a mean vertebral wedging of 3° and a mild coronal Cobb angle of 10°. Measures of the sagittal plane went from 34° to 41° after 33 days post-operative.

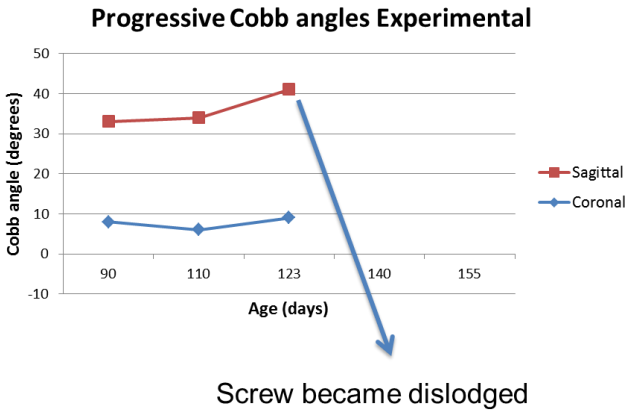

Figure 6.11: Sequential post-operative coronal Cobb angles of first *in vivo* trial using 3D tether on a porcine spine prior to screw loosening

With reference to the sagittal profile radiographs, the successive pedicle offset of adjacent vertebrae support the achievement of axial rotation. However, experimental limitations impede the objective measure of axial rotation.

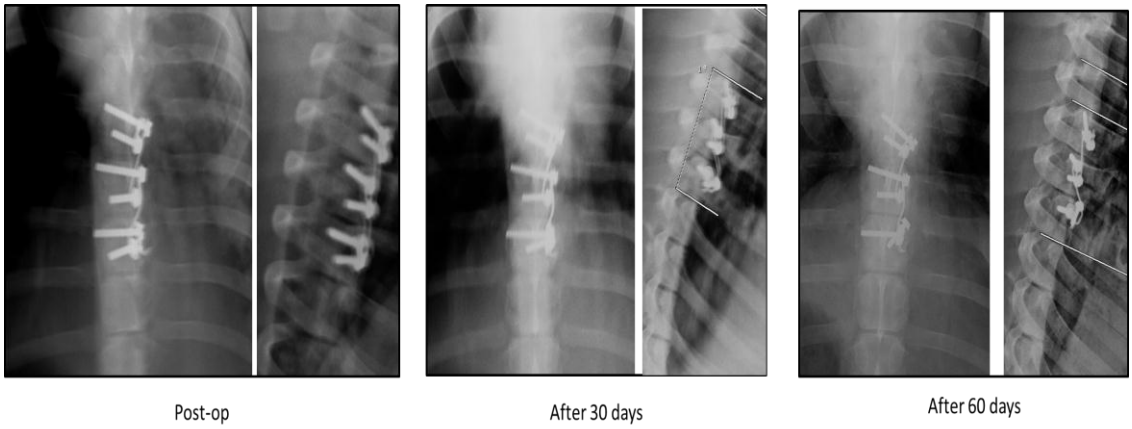

Figure 6.12: Digitized radiographic images of first *in vivo* trial of 3D tether in pig spine

6.4.3 Results part 2

Similarly to the first trial, this device design also led to vertebral wedging as a result of unilaterally compressed vertebral growth plates. Inverse vertebral wedging was also reported *i.e.*, disc height is greatest adjacent to device. Mean measures of vertebral and disc wedging was 2.6° and 1.1° after 61 days respectively. The average final post-operative Cobb angles were between 1 to 3 degrees. The sagittal profile fluctuated between 30° and 33° over the course of the post-operative follow up.

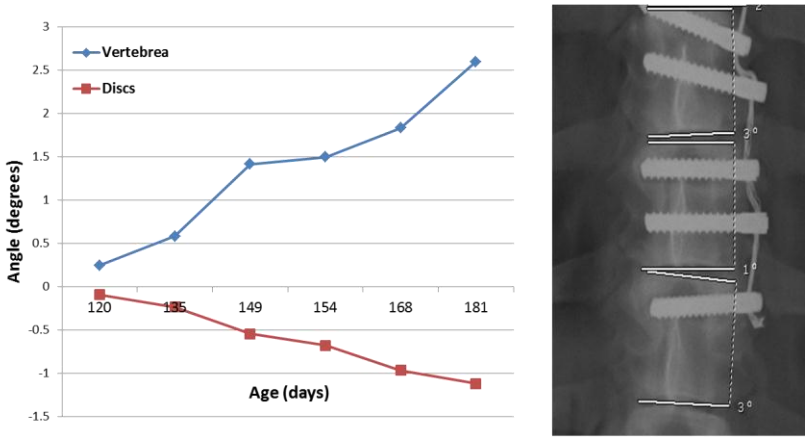

Figure 6.13: Sequential post-operative measures of vertebral and disc wedging angles in the coronal plane

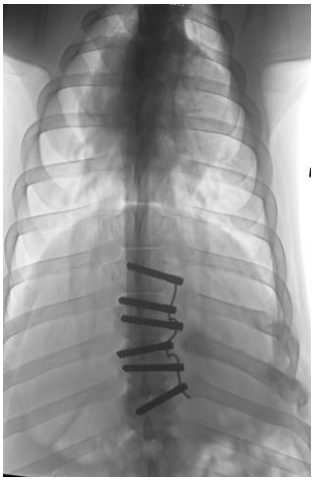

Figure 6.14: Post-operative dorsal-ventral radiograph of 3D tether after 30 days

Screw pullout and loosening occurred in 2 of 3 pigs. This loosening may be observed in the lower screw in the sequential radiographs of pig a) in figure 6.15. Other screw loosening was confirmed during spinal culture following sacrifice.

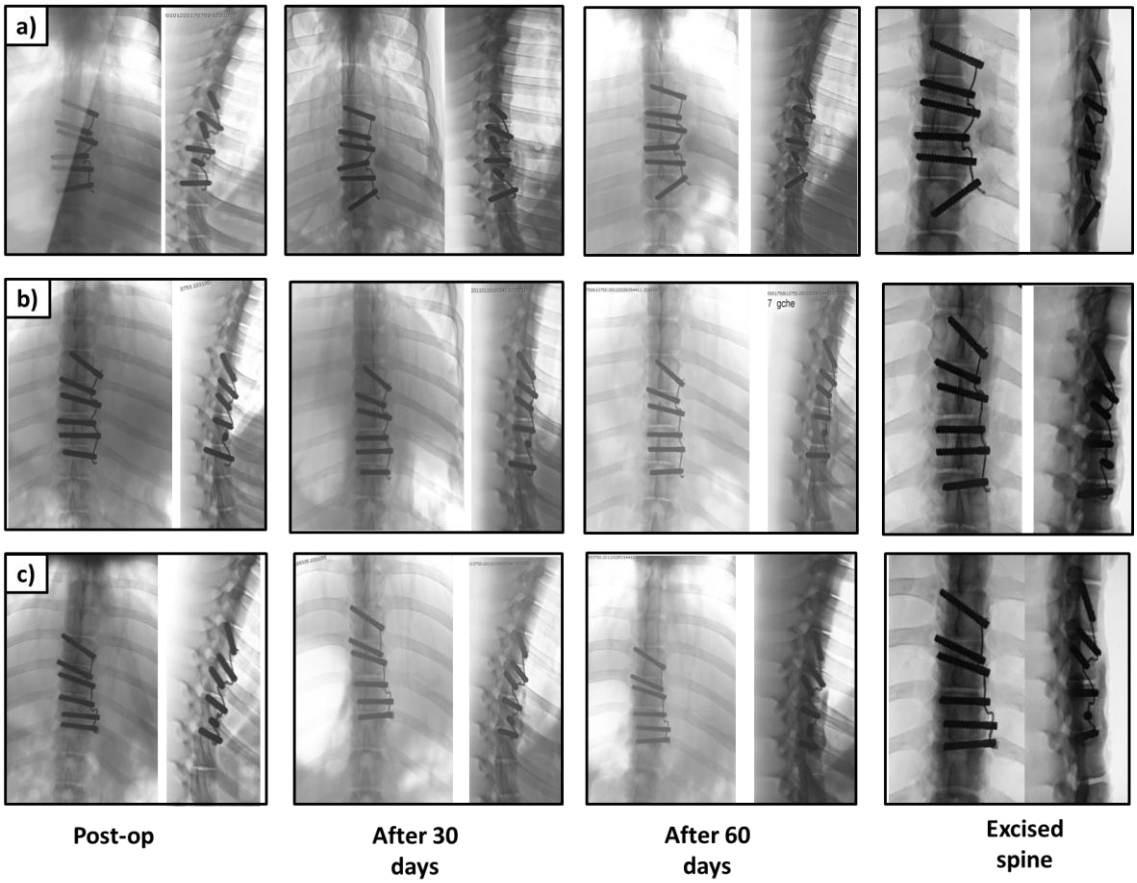

Figure 6.15: Digitized post-operative radiographs of 3D tether in pig spines

6.4.4 Discussion

Two *in vivo* trials of the 3D tether took place using skeletally immature pigs. The device proved its ability to modify the coronal profile by means of local growth modulation observed through consistent vertebral wedging. Sagittal manipulation was not targeted in this study and, correspondingly, no significant modification to the sagittal profile was observed. Axial rotation was not sufficient to conclude with confidence the devices ability to modify this vertebral orientation. Qualitatively, axial rotations (when screw fixation remained) were observable by the offset of the posterior processes (Fig. 6.14); however, insufficient data was available to realize statistical support. Moreover, the ability to objectively quantify vertebral rotation by means of 3D reconstruction was hindered by the change in position of the pig during dorsal-ventral and lateral x-ray. Although the Perdriolle torsionmeter and Cobb methods may be adopted to analyze axial rotation by means of posterior radiographs, the accuracy offered by these methods is not sufficient to conclude with confidence the presence of axial manipulation in this study [215, 216].

Both *in vivo* trials returned signs of inversed vertebral wedging. There are three reasons believed to induce this inverse local wedging of the discs which hinders the global control of the device on spinal alignment. As speculated by Newton et al., who also measured inversed wedging when exploring fusionless growth modulating devices in a porcine model [164, 166], it is believed that the devices explored herein led to intervertebral disc remodelling due to augmented asymmetrical stresses imposed by the devices. Interestingly, this assumption is not feasible to explain the inverse wedging of the discs measured in the intravertebral epiphyseal device (Chapter 5) as it does not alter the loads over the disc. Thus, although disc remodelling may lead to inverse wedging, it is also believed to be due to the dorsal-ventral position of the pig during the radiograph. This position may place a tension over the spine and remove curvatures by means of reverse disc wedging. A final possibility is that a compensatory position is adopted by the pig as to remove undesirable coronal curvatures within their spine.

A biological follow up of the spinal segments was not performed in this study. However, pig spines were cultured following sacrifice and submerged in paraformaldehyde where they are maintained at 4 degrees Celsius for future histomorphometric and histological analyses. These analyses will allow for a greater understanding on the mechanism of correction offered by the 3D

tether. In addition, further interpretation of the devices influence on the health of the intervertebral disc should be performed and, if needed, modifications should be conducted to encourage a viable disc environment.

Unfortunately, experimental limitations impeded both these investigations. Parts 1 and 2 experienced problems of screw fixation believed to be related to under sized screw threads or the lack of cortical to cortical penetration. Despite these apparent restrictions, it is still hypothesized that the 3D tether has the novelty of correcting a scoliotic spine in all three anatomical planes. Further, *in vivo* testing on a larger animal model, while ensuring adequate screw fixation, will allow one to truly analyze the innovative spinal manipulation offered by the 3D tether as revealed through *in silico* and *in situ* analyses reported in sections 6.2 and 6.3 respectively.

CHAPTER 7 : GENERAL DISCUSSION

Fusionless devices for the early treatment of AIS offer many appealing advantages over conventional surgical treatments. A literature review however indicates that uncertainties remain regarding the biomechanics of the pathomechanism of AIS and of the corrective avenues attempted by current fusionless methods.

In an attempt to address these issues and to bring an improved theoretical base to fusionless treatment, a FEM was developed. The purpose of this thesis was to develop a finite element platform of the spine with integrated growth dynamics, use the FEM to investigate biomechanical factors involved in AIS pathomechanism, use the FEM to analyse current fusionless devices, and to develop, optimize, and evaluate improved fusionless devices for the treatment of AIS using a platform that includes *in silico*, *in situ*, and *in vivo* analyses.

The development of the computational platform or FEM was an integral aspect of this thesis. The devised spinal FEM proved to be effective and corroborated with patient specific progression (Fig. 0.5) and predicted asymmetrical forces that agree with published literature (0.15 – 0.8 MPa in articles 1 and 2 correspond to stresses detailed in table 1.4). The model was designed and programmed to be utilized as a comparative platform (i.e. explore biomechanical factors and devices against the lack thereof). As a result, various assumptions were adopted in order to achieve calculations within a sensible time frame and render the evaluation of an otherwise indeterminate system possible. In spite of such simplifications, additional steps were taken to insure that reported results held true and were thus robust under variations of the selected assumptions (spinal loading, boundary conditions, and parameters of computational algorithm). Such comparative analyses allowed for engineering and clinical insight to be derived and, when suitable, further explored.

In an attempt to improve biomechanical understanding of AIS, a theory entitled physiological stress shielding was explored in the scoliotic spine FEM (such theory was later applied to develop novel implant concepts). This notion, suggested that underlying mechanical factors found within a scoliotic spine would encourage and augment the risk of scoliotic progression (hypothesis 1). More specifically, the hypothesis projected the idea that a local offset of mechanical properties in scoliotic spines, caused by remodelling, would augment asymmetrical

loading and encourage scoliotic progression. That is, the concave portion would become more rigid while the convex portion would become less rigid or remain the same. Such differences in mechanical properties are known to lead to stress shielding in the context of rigid prostheses; however, the theory of physiological stress shielding occurring within a scoliotic spine is novel. Moreover, the functional application of such a hypothesis is related to the Hueter-Volkmann principle and scoliotic progression which suggest that increased loading will lead to augmented progression. Therefore, it was believed that physiological stress shielding in a scoliotic spine, if it was to take place, may serve to identify patients with added risk of progression – a prognostic attribute required to justify an early intervention such as growth sparring instrumentation.

This first study utilizing the developed FEM explored the aforementioned theory (article 1, chapter 3). This FEM analysis affirmed hypothesis 1. That is, upon the inclusion of the offset of mechanical properties calculated to occur in AIS patients, increased asymmetrical stresses measured at the apex was greater than 25% and increased vertebral thoracic wedging of up to 1° (10-20%) occurred. However, such measures are not significant enough to identify with confidence those at risk of progression. It is important to note that the offset of mechanical factors utilized in this experiment represent the mean values. Perhaps, patients with larger mechanical offsets (greater increase in concave bone and disc rigidities and augmented convex migration of nucleus) may undergo exaggerated progression based on the explored hypothesis. Thus, the identification of an irregular distribution of spinal mechanical properties may be valuable measure to forecast progressive risks.

Hypothesis 1 was verified via computer modeling and not by means of experimental studies. Although results from the modeling simulations may be deemed objective, this notion has yet to be experimentally verified under *in vivo* conditions. At the time of this thesis, such a concept was not easily verifiable as mechanical property prediction from available medical imagery was neither achievable nor commonly practiced in a clinical context. Predictions of patient specific cancellous bone density and rigidity may be achieved via CT-scans [217]. Furthermore, a group under the supervision of Dr. Delphine Périé (Associate Professor at École Polytechnique) is working on new methods to predict intervertebral disc properties using MRI images. Therefore, a combination of this data could be used in a prospective study to further support and verify that

these mechanical biases may be adopted as an effective marker for advanced risk of scoliosis progression.

There exist various other scoliotic morphological differences between evolutive and non-evolutive AIS patients accentuated by a retrospective study [218]. These include wedging of apical disc, axial rotation of inferior junctional vertebra, torsion, and height width ratios of vertebra. The developed FEM platform would be an effective method with which to further explore the biomechanical influences of these modifications.

As for all FEM analyses one must be aware of limitations. First, as previously detailed, FEMs include assumptions that simplify reality to insure computational feasibility. These assumptions must be explored via sensitivity analyses to document their influence on the derived conclusions (chapter 3 section 3.2.9 and chapter 4 section 4.2.8). Second, FEM simulations aid greatly in advancing knowledge of mechanical aspects of the spine but, to be conservative, insight gathered should be limited to relative deduction and not absolute quantifications.

A parallel objective to exploring possible mechanical factors involved in the pathomechanism of AIS was to acquire a mechanical comfort, *per se*, regarding the manner in which loads are dispersed within the spine – a key to developing new fusionless methods that seek to manipulate spinal growth plate loading.

The next stage of this thesis was concerned with exploring the biomechanics behind current fusionless treatments of scoliosis while making use of the developed FEM and previously utilized methods of documenting comparative asymmetrical growth plate stress and scoliotic progression. To begin, the FEM was integrated with different fusionless growth sparring devices (article 2, chapter 4). The explored devices were chosen on the basis that, amongst a plethora of related devices (patent review table 1.6), they appeared the most promising and commercially driven. This included a SMA staple, SS staple, and flexible tether. These devices were critically explored on the developed FEM platform. Results supported this fusionless approach and affirmed hypothesis 2. That is, compression and passive expansion resistance focused on the convexity of the spine reduced asymmetrical loading by more than 35% and showed the ability to limit scoliotic progression by 10% in a scoliotic FEM after 2 years of simulated growth.

Although the FEM predicted the biomechanical feasibility of these devices, more importantly, it highlighted their shortcomings and provided valuable inferences into plausible methods of improvement. An important factor employed by these devices is their ability to alter loads over the vertebral growth plate. As a result of the selected approach (compressive isolation of the contralateral convex growth plate), these devices may induce an environment of hypomobility over the intervertebral disc, a phenomenon attributed to disc degeneration [29]. This undesirable influence on the disc could be avoided in two ways. First, an implant that would not span the intervertebral disc space would not alter the local mechanical environment. Second, a method that allowed for a certain degree of mobility to be maintained or introduced controlled dynamic stimulus would encourage the maintenance of a healthy disc environment. Another important characteristic identified through the use of the FEM platform showed that although convex growth was reduced, it was not arrested. Moreover, this FEM investigation confirmed the lack of initial and long term 3D control over spinal alignment offered by the explored fusionless concepts.

Subsequent to these interpretations, ten novel fusionless growth modulation devices were conceived, modeled, and explored over the course of this thesis using the *in silico* platform. Amongst them, two devices were selected for further development and investigation by means of *in situ* and *in vivo* analyses: an intravertebral epiphyseal device (seeks to arrest local vertebral growth without spanning the disc) and a 3D tether (seeks to manipulate all anatomical planes).

The intravertebral epiphyseal device previously demonstrated its feasibility on a rat tail [165]. Alterations performed to this original device were explored and achieved while using both CATIA and ANSYS (*in silico* FEM platforms with 3D design capabilities) and initially verified via *in situ* testing with an analogue spine model. Such improvements to the former device took place in order solve previously encountered problems of device post-operative migration and fixation experienced in the rate tail model. In brief, the dimensions were altered to respect the morphology of immature pig vertebra. Bone screw selection was improved and device/bone screw interface was accurately designed to include a counter sink and press fit in order to restrict degrees of freedom between the two bodies. Moreover, an important circumferential curvature, which more accurately mimicked vertebral body profile, was introduced as to eliminate fixation and device migration problems previously encountered in the rat tail study. Finally, a custom

surgical tool was designed and fabricated to guide device insertion and allow for screw fixation to be accurately achieved with ease.

In vivo result of the improved intravertebral epiphyseal device explored in a porcine model proved to be notable and affirmed hypothesis 3 (articles 3 and 4, chapter 5). This device manipulated vertebral morphology and achieved wedging greater than 4° with sustainable influence on the intervertebral disc. Inverse method was used (creation of scoliotic deformities as the goal). An important aspect of this approach, suggested by relatively small curvature control observed, is that the intravertebral epiphyseal device is perhaps best fit for early curves showing signs of progression. The accurate identification of patients at risk of early progression would thus greatly complement and further justify this device as a means of early intervention. Moreover, as the intravertebral epiphyseal device does not seek to manipulate local forces, as it seeks to passively halt growth, its applicability to advanced curves may be hindered. Advanced scoliotic curves are coupled with irregular force distribution. This factor would not be initially altered by the intravertebral device. It is believed that, with time, the intravertebral device would passively correct the deformity and thus return spinal forces to regular standards. However, another conceivable scenario under such context is that the implication of the asymmetrical forces overshadows the correction provided by the intravertebral device. Therefore, for the moment, the intravertebral epiphyseal device is tailored as an early method of intervention. Alternatively, additional studies of the influence of the intravertebral staple on a progressive animal model would further support and persuade one of its corrective abilities over a larger range of scoliotic deformities.

Following radiographic and histological analyses of the disc and growth plate, instrumented vertebrae showed positive signs of disc and growth plate viability (article 4). This analysis suggested effective growth modulation was achieved and intervertebral disc health was unhindered outside the region of instrumentation. Conversely, at times, disc health surrounding the insertion of the intravertebral epiphyseal device showed a tampering of disc space. That is, degenerative signs were identified most commonly by the adoption of fibrous tissues surrounding the device head. These encouraging results may be further enhanced through minor alterations to the device and surgical procedure.

The introduction of slits or voids into the device head (portion inserted into spine) may alleviate obstruction of disc space and further encourage the conservation of disc health. These slits would vastly reduce the amount of outer annular fibres that are incised by the device insertion (as observed in the histological analyses) – a key characteristic of the outer annulus to maintain compression resistance. Moreover, such slits would allow for a greater nutrient diffusion between vertebral body and intervertebral disc. Finally, if required, removal of the device containing these slits would induce less laminar lesions and, thus, further encourage adequate healing. Another possible improvement may be achieved by the reduction of device head thickness as to solely target the upper zone of the growth plate without hindering the disc. Finally, the development of a custom surgical endoscopic guidance system, being advanced in parallel by the team of Pr. Caroline Boudoux (Assistant Professor at École Polytechnique), would insure accurate positioning of the device [219].

The intravertebral epiphyseal device offers the novelty of excluding the intravertebral disc in its attempt to realign the spines of patients with AIS. The exploited experimental platform confirmed the intravertebral device to be a plausible early treatment for progressive AIS patients.

Conversely, AIS patents with advanced scoliotic deformities often include deformations in all three anatomical planes. This cohort would benefit from initial correction offered by disc compression and would be more effectively treated with a device that offers a 3D correction. To address these concerns, another novel device was devised during this thesis. A 3D tether was also developed, optimized and explored in this thesis. Both *in silico* and *in situ* analyses confirmed the 3D tether`s ability to effectively manipulate all three anatomical planes. *In vivo* analyses however experienced difficulties with limited anterior vertebral space (related to porcine model) for device insertion and inconsistent screw fixation. Moreover, experimental limitations restricted objective conclusions concerning axial manipulation to be derived. Nevertheless, hypothesis 4 was partially verified. The 3D tether achieved vertebral wedging of up to 4° after 12 weeks in a porcine model. Vertebral rotation greater than 5° was confirmed in *in silico* and *in situ* models but experimental limitations restricted its affirmation under the *in vivo* analysis. Inverse method was also used (creation of scoliotic deformities as the goal).

It is advisable that the 3D tether be pursued under the following modifications. First, as screw and tether dimensions were selected under a generous safety factor of 1.5 (in the absence of accurate data, worst case configuration was used), this may be reduced to adopt smaller dimensions to tailor to reduce anterior vertebral body space in pig vertebra. Alternatively, the current device may be explored on a larger animal model. A porcine model has an anterior vertebral body size (sagittal height and width) of roughly half of human vertebra [220]. In contrast, a bovine model has larger vertebral morphology to that of humans [221]. Moreover, bovine spines have previously been utilized as a pre-clinical model for fusionless devices [159, 160, 173]. Finally, cortical to cortical screw fixation must be achieved to insure that screw pullout or screw plow is avoided. These modifications will offer an attractive avenue to explore the 3D tether while maintaining improved structural and fixation integrity.

Another alternative is utilizing a material with a less aggressive stress/strain relationship as to allow for a more consistent compression of the targeted growth plates by the 3D corrective device. To elaborate, the modulus (linear relation between stress and strain) of the applied 316L stainless steel is about 190 000 MPa while polyethylene is 275 MPa. Therefore, if relative motion of the tether occurs between fixations (bone screws) stainless steel will resist this transition with 690 times more force (assuming identical cross sectional area and deformation takes place in elastic region of stress/strain curve). Such a vast increase in force may not be necessary to halt vertebral growth. Moreover, it may cause fixation problems of the screw which is predicted, in *ex vivo* vertebrae, to dislodge at between 188 and 562 Newtons [214]. Finally, polyethylene thickness may be selected as to fail at a desired tension in order to avoid dangerous screw movement due to screw/bone interface breakdown. Given the vast dynamic mobility of the spine and the large forces distributed within, polyethylene may be the more logical selection for future studies; however, as predicted under *in silico* analyses (section 6.2) a loss of corrective abilities is to be anticipated.

To date, there are no fusionless devices for the treatment of spinal deformities that claim to actively pursue 3D correction. Preliminary analyses of this device were promising and thus a provisional patent was filed (April 14, 2011) to protect the novelties of the 3D tether device.

CHAPTER 8 : CONCLUSIONS AND PERSPECTIVES

This doctoral dissertation describes improved understanding of biomechanical factors involved in the pathomechanism of AIS and in the corrective avenues exploited by fusionless treatments utilizing growth modulation. This enhanced comprehension in combination with a thorough experimental platform employing *in silico*, *in situ*, and *in vivo* analyses has led to the development and evaluation of two novel fusionless devices.

The developed FEM permitted exploration of biomechanical factors implicated in scoliotic progression. The presence of a mechanical bias between concave and convex regions in the spine mildly increases asymmetrical loading and, consequently, encourages scoliotic progression. These biomechanical factors are believed to be a secondary risk factor involved in scoliotic progression. Additional studies using a prospective analysis of scoliotic patients are advised to further substantiate these findings and, if applicable, conceive feasible clinical screening methods.

The elaborated FEM confirmed the ability of current fusionless devices (SMA staple, SS staple, and flexible tether) to reduce asymmetrical growth plate loading and decrease scoliotic progression by means of unilateral convex growth modulation; however, several potential improvements were made evident. The developed FEM platform and experimental methods provide an effective means to enhance current or devise novel fusionless devices for the treatment of AIS.

The intravertebral epiphyseal device, which was improved over preliminary designs, manipulated spinal alignment through the realization of local growth modulation exclusive of the intervertebral disc in a porcine model. Additionally, analyses of intervertebral disc and growth plate health and morphology revealed the viability of these physiological structures given accurate device positioning. A final pre-clinical trial is advised to include suggested improvements prior to adapting device to human application and moving forth with a clinical trial.

The 3D tether, which was conceived over the course of this thesis, returned promising results which confirmed its application as a plausible corrective method for AIS. Manipulation of spinal

alignment was demonstrated in all anatomical planes using *in silico* and *in situ* analyses. Although promising, *in vivo* evaluations were encumbered by experimental limitations. Nevertheless, the valuable novelty of providing correction all three anatomical planes is worth pursuing in supplementary *in vivo* experimentations over the next 12 month pendency period offered by the issued provisional patent.

Both the intravertebral epiphyseal device and the 3D tether offer hopeful expectations for the improved early treatment of AIS. Pre-clinical trials were successful and minor inconveniences appear to be resolvable. The intravertebral epiphyseal device provides an attractive method to achieve fusionless growth sparring instrumentation exclusive of the disc. The 3D tether device offers corrective control in all three anatomical planes.

Both devices offer valuable novelties over current treatments and satisfy judicious requirements of aspiring new fusionless treatments tailored to skeletally immature patients with progressive idiopathic scoliosis. The intravertebral staple is tailored towards the early treatment of relatively small curves showing no signs of complicated 3 dimensional deformities. The 3D tether is adapted to offer a complete 3 dimensional correction of primitive or advanced deformities. Together, these devices may offer improved treatments over the considerable phenotypic spectrum of deformities observed in adolescents with idiopathic scoliosis.

REFERENCES

1. Lowe T, et al., *Etiology of Idiopathic Scoliosis: Current Trends in Research.* J Bone and Joint Surgery, 2000. **82**(8): p. 1157-68.

2. Mehlman CT., Araghi A., and Roy DR., *Hyphenated history: the Hueter-Volkmann law.* Am J Orthop., 1997. **26**: p. 798-800.

3. Stokes, I.A.F., et al., *Mechnical Modulation of Vertebral Body Growth: Implications for Scoliosis Progression.* Spine, 1996. **21**(10): p. 1161-1167.

4. Dolan LA. and Weinstein SL., *Surgical rates after observation and bracing for adolescent idiopathic scoliosis: an evidence-based review.* Spine, 2007. **32**(19S): p. 91-100.

5. Delorme S., et al., *Assessment of the 3-D reconstruction and high-resolution geometrical modeling of the human skeletal trunk from 2-D radiographic images.* IEEE Transactions on Biomedical Engineering, 2003. **50**(8): p. 989-998.

6. Lin, S., et al., *Biomechanical analysis and modeling of different vertebral growth patterns in adolescent idiopathic scoliosis and healthy subjects.* Scoliosis, 2011. **6**(1): p. 11.

7. Villemure, I., Aubin C É, Dansereau J, *Simulation of Progressive Deformities in Adolescent Idiopathic Scoliosis Using a Biomechanical Model Integrating Vertebral Growth.* J of Biomedical Engineering, 2002. **124**: p. 784-790.

8. Villemure I., et al., *Progression of vertebral and spinal three-dimensional deformities in adolescent idiopathic scoliosis: a longitudinal study.* Spine, 2001. **26**(20): p. 2244-2250.

9. Stokes IA., et al., *Endochondral growth in growth plates of three species at two anatomical locations modulated by mechanical compression and tension.* J of Orthopaedic Research, 2006. **10**: p. 1327-1333.

10. Huynh A., et al., *Simulation of progressive spinal deformities in Duchenne muscular dystrophy using a biomechanical model integrating muscle and vertebral growth modulation.* Clin Biomechanics, 2007. **22**: p. 392-399.

11. Sylvestre P.L., Vilemure I., and Aubin CE., *Finite element modeling of the growth plate in a detailed spine model.* Med Bio Eng Comput, 2007. **45**: p. 977-988.

12. Villemure, I., et al., *Modelisation biomecanique de la croissance et de la modulation de croissance vertebrales pour l'etude des deformations scoliotiques : etude de faisabilite: Biomechanical modeling of vertebral growth and growth modulation for the study of scoliotic deformities : a feasibility study.* ITBM-RBM, 2002. **23**(2): p. 109-117.

13. Stokes I., *Analysis and Simulation of Progressive Adolescent Scoliosis by Biomechanical Growth Simulation.* Eur Spine J, 2007. **16**: p. 1621-1628.

14. Lenke, L.G., C.C. Edwards, 2nd, and K.H. Bridwell, *The Lenke classification of adolescent idiopathic scoliosis: how it organizes curve patterns as a template to perform selective fusions of the spine.* Spine (Phila Pa 1976), 2003. **28**(20): p. S199-207.

15. Charles, Y.P., et al., *Progression risk of idiopathic juvenile scoliosis during pubertal growth.* Spine, 2006. **31**(17): p. 1933-42.

16. Ogilvie, J., et al., *Shape memory alloy staple for use in treatment of spinal deformities e.g. scoliosis, has two pairs of prongs whose tips are made closer when staple is in memorized state*. 2000, SDGI HOLDINGS INC (SDGI-Non-standard) OGILVIE J (OGIL-Individual) SHERMAN M C (SHER-Individual) DREWRY T (DREW-Individual) SAURAT J (SAUR-Individual) DREWRY T D (DREW-Individual) WARSAW ORTHOPEDIC INC (WARS-Non-standard).

17. Ogilvie, J., et al., *Fusionless correcting method for treating abnormal alignment of spine having convex and concave sides, involves attaching tether having staples to at least two vertebral bodies of spine*. 2000, SDGI HOLDINGS INC (SDGI-Non-standard).

18. Wall, E.J., D.I. Bylski-Austrow, and J.E. Reynolds, *Spinal staple for spinal correction system, has legs with transverse cross-sectional areas that ensure adequate contact surface against vertebra and to compress sufficient endplate growth areas*. 2001, CHILDREN'S HOSPITAL MEDICAL CENT (CHIL-Non-standard) SPINEFORM LLC (SPIN-Non-standard).

19. Braun, J.T., et al., *The efficacy and integrity of shape memory alloy staples and bone anchors with ligament tethers in the fusionless treatment of experimental scoliosis.* J Bone Joint Surg Am, 2005. **87**(9): p. 2038-51.

20. Wall, E.J., et al., *Endoscopic mechanical spinal hemiepiphysiodesis modifies spine growth.* Spine, 2005. **30**(10): p. 1148-53.

21. Edwards T., et al., *Structural Features and Thickness of the Vertebral Cortex in the Thoracolumbar Spine.* Spine, 2001. **26**(2): p. 218-225.

22. Roberts, S., J. Menage, and S.M. Eisenstein, *Cartilage end-plate and intervertebral disc in scoliosis: Calcification and other sequelae.* Journal of Orthopaedic Research, 1993. **11**(5): p. 747-757.

23. Brighton, *Structure and function of growth plate.* Clin Orthop, 1978. **136**: p. 22-32.

24. Farnum, C.E., et al., *Volume increase in growth plate chondrocytes during hypertrophy: the contribution of organic osmolytes.* Bone, 2002. **30**(4): p. 574-581.

25. Kielty CM, K.A., Holmes D, Scor S, and Grant M, *Type X collagen, a product of hypertrophic chondrocytes.* J Biochem, 1985. **27**: p. 545-554.

26. Ballock T. and O'keefe R., *The biology of the growth plate.* J Bone and Joint Surgery, 2003. **85**: p. 715-726.

27. Shirazi-Ald SA., Shivastava SC., and Ahmed AM., *Stress analysis of the lumbar disc-body unit in compression: A three dimensional nonlinear finite element study.* Spine, 1984. **9**(2): p. 120-134.

28. Grunhagen T., et al., *Nutrient Supply and Intervertebral Disc Metabolism.* J Bone and Joint Surgery, 2006. **88**: p. 30-35.

29. Stokes A.F. and Iatridis J.C., *Mechanical Conditions that Accelerate Intervertebral Disc Degeneration: Overload Versus Immobilization.* Spine, 2004. **29**(23): p. 2724-2732.

30. Williams J and A.G. Natarajan R, *Inclusion of regional poroelastic material properties better predicts biomechanical behavior of lumbar discs subjected to dynamic loading.* J Biomech, 2007. **40**(9): p. 1981-1987.

31. Stokes, I.A.F. and M. Gardner-Morse, *Lumbar spinal muscle activation synergies predicted by multi-criteria cost function.* Journal of Biomechanics, 2001. **34**(6): p. 733-740.

32. Panjabi M, Goel V, and Takata K, *Physiological Strains in the Lumbar Spinal Ligaments.* Spine, 1982. **7**(3): p. 192-203.

33. Iatridis, J.C., et al., *The viscoelastic behavior of the non-degenerate human lumbar nucleus pulposus in shear.* Journal of Biomechanics, 1997. **30**(10): p. 1005-1013.

34. Kemper AR., McNally C., and Duma SM., *The influence of strain rate on the compressive stiffness properties of human lumbar intervertebral discs.* Biomed Sci Instrum., 2007. **43**: p. 176-181.

35. Leahy, J.C. and D.W.L. Hukins, *Viscoelastic properties of the nucleus pulposus of the intervertebral disk in compression.* Journal of Materials Science: Materials in Medicine, 2001. **12**(8): p. 689-692.

36. Adams M., McNally C., and Dolan P., *'Stress' Distribution Inside Intervertebral Discs. The Effects of Age and Degeneration.* J Bone and Joint Surgery, 1996. **78**(6): p. 965-972.

37. Iatridis, J.C., J.J. MacLean, and D.A. Ryan, *Mechanical damage to the intervertebral disc annulus fibrosus subjected to tensile loading.* Journal of Biomechanics, 2005. **38**(3): p. 557-565.

38. Iatridis, J.C., et al., *Degeneration affects the anisotropic and nonlinear behaviors of human anulus fibrosus in compression.* Journal of Biomechanics, 1998. **31**(6): p. 535-544.

39. Adams M., et al., *Abnormal Stress Concentrations in Lumbar Intervertebral Discs Following Damage to the Vertebral Bodies: a Cause for Disc Failure?* Eur Spine J, 1993. **1**: p. 214-221.

40. Brown T, Hansen R, and Yorra A, *Some mechanical test on the lubosacral spine with particular reference to the intervertebral discs.* JBJS, 1957. **39**(A): p. 1135-1164.

41. Virgin W, *Experimental investigation into the physical properties of the intervertebral discs.* JBJS, 1951. **33**(B): p. 607-611.

42. Markolf K, *Deformation of the thoracolumbar intervertebral joint in response to external loads: a biomechanical study using autopsy material.* JBJS, 1972. **54**(3): p. 511-533.

43. Keaveny T.M. and Yeh O.C., *Architecture and trabecular bone - Towards an improved understanding of the biomechanical effects of age, sex and osteoporosis.* J Musculoskel Interact, 2002. **2**(3): p. 205-208.

44. Hobatho M, Rho J, and Ashman R, *Mechanical properties of the lumbar spine.* Res Spinal Deformities, 1997. **1**(181-184).

45. Gibson L and Ahshby M, *Cellular solid: structure and properties*. 1998, Oxford: Pergamon Press.

46. Edmondston, S.J., et al., *In-vitro relationships between vertebral body density, size, and compressive strength in the elderly thoracolumbar spine.* Clinical Biomechanics, 1994. **9**(3): p. 180-186.

47. Pintar F, et al., *Biomechanical properties of human limbar spine ligaments.* J Biomech, 1992. **25**(11): p. 1351-1356.

48. Yoganandan N, Kumaresan S, and Pintar F, *Geometric and mechanical properties of human cervical spine ligaments.* J Biomech Eng, 2000. **122**(6): p. 623-629.

49. Aubin, C.-E., et al., *Simulation of progressive deformities in adolescent idiopathic scoliosis using a biomechanical model integrating vertebral growth modulation.* Journal of Biomechanical Engineering, 2002. **124**(6): p. 784-790.

50. Carrier, J., et al., *Biomechanical modelling of growth modulation following rib shortening or lengthening in adolescent idiopathic scoliosis.* Medical and Biological Engineering and Computing, 2004. **42**(4): p. 541-548.

51. Grealou, L., C.E. Aubin, and H. Labelle, *Rib cage surgery for the treatment of scoliosis: a biomechanical study of correction mechanisms.* Journal of Orthopaedic Research, 2002. **20**(5): p. 1121-1128.

52. Huynh A M, A.C.É., Rajwani T, Gagnall K, Villemure I, *Pedicle growth asymmetry as a cause of adolescent idiopathic scoliosis: a biomechanical study.* Eur Spine J, 2007. **16**(4): p. 523-529.

53. Kilincer C., et al., *Load Sharing within a Human Thoracic Vertebral Body: An In Vitro Biomechanical Study.* Turkish Neurosurgery, 2007. **17**(3): p. 167-177.

54. Kumaresan, S., et al., *Biomechanical study of pediatric human cervical spine: A finite element approach.* Journal of Biomechanical Engineering, Transactions of the ASME, 2000. **122**(1): p. 60-71.

55. Bellini C, et al., *Biomechanics of the lumbar spine after dynamic stabilization.* J Spinal Disord Tech, 2007. **20**(6): p. 423-429.

56. Liu, C.L., et al., *Biomechanical evaluation of a central rod system in the treatment of scoliosis.* Clin Biomech, 1998. **13**: p. 548-559.

57. Martinez J, O.O., Broom N, *Biomechanics of Load- Bearing of the Intervertebral Disc: an Eperimental and Finite Element Model.* Med. Eng. Phys, 1996. **19**(2): p. 145-156.

58. Perie, D., et al., *Personalized biomechanical simulations of orthotic treatment in idiopathic scoliosis.* Clinical Biomechanics, 2004. **19**(2): p. 190-195.

59. Pitzen, T., et al., *A finite element model for predicting the biomechanical behaviour of the human lumbar spine.* Control Engineering Practice, 2002. **10**(1): p. 83-90.

60. Skalli, W., et al., *A biomechanical analysis of short segment spinal fixation using a three-dimensional geometric and mechanical model.* Spine, 1993. **18**(5): p. 536-45.

61. Jones A and Wilcox R, *Finite element analysis of the spine: towards a framework of verification, validation and sensitivity analysis.* Med Eng Phys, 2008. **30**(10): p. 1287-1304.

62. De Visser H, et al., *The role of quadratus lumborum asymmetry in the occurrence of lesions in the lumbar vertebrae of cricket fast bowlers.* Med Eng Phys, 2007. **29**: p. 877-885.

63. Fantigrossi A, et al., *Biomechanical analysis of cages for posterior lumbar interbody fusion.* Med Eng Phys, 2007. **29**(1): p. 101-109.

64. Hatto T, et al., *Finite-element analysis on closing-opening correction osteotomy for angular kyphosis of osteoporotic vertebral fractures.* J Orthop Sci, 2007. **12**(4): p. 354-360.

65. Ivanov A, et al., *The effect of removing the lateral part of the pars interarticularis on stress distribution at the neural arch in lumbar foraminal microdecompression at L3–L4 and L4–L5: anatomic and finite element investigations.* Spine, 2007. **32**(22): p. 2462-2466.

66. Kim Y, *Finite element analysis of anterior lumbar interbody fusion. Threaded cylindrical cage and pedicle screw fixation.* Spine, 2007. **32**(23): p. 2558-2568.

67. Lafage V, et al., *New interspinous implant evaluation using an in vitro biomechanical study combined with a finite-element analysist.* Spine, 2007. **32**(16): p. 1706-1713.

68. Rohlmann A, et al., *Comparison of the effects of bilateral posterior dynamic and rigid fixation devices on the loads in the lumbar spine: a finite element analysis.* Eur Spine J, 2007. **16**(8): p. 1223-1231.

69. Schmidt H, et al., *Application of a calibration method provides more realistic results for a finite element model of a lumbar spinal segment.* Clin Biomech, 2007. **22**: p. 377-384.

70. Adams M and Hutton W, *The effect of posture on the role of the apophysial joints in resisting intervertebral compressive forces.* J Bone and Joint Surg Br, 1980. **62**(3): p. 358-362.

71. Goel, V.K., et al., *An analytical investigation of the mechanics of spinal instrumentation.* Spine, 1988. **13**(9): p. 1003-11.

72. Cao K, Grimm M, and Yang K, *Load sharing within a human vertebral body using the finite element method.* Spine, 2001. **26**(12): p. E253-E260.

73. Villemure, I., *Étude biomécanique du processus de croissance et de déformation du rachis scoliotique*. 2000, Université de Montréal.

74. Schultz A, et al., *Loads on the lumbar spine. Validation of a biomechanical analysis by measurements of intradiscal pressures and myoelectric signals.* J bone and Joint Surg, 1982. **64**: p. 713-720.

75. Ruff S, *Brief Acceleration: Less than One Second, German Aviation Medicine*, in *World War II, (I)*. 1950.

76. Keller TS. and et al., *Influence of spine morphology on intervertebral disc loads and stresses in asymptomatic adults: implications for the ideal spine.* The Spine Journal, 2005. **5**: p. 297-309.

77. Clin J., Aubin C., and Labelle H., *Virtual prototyping of a brace design for the correction of scoliotic deformities.* Med Bio Eng Comput, 2007. **45**(5): p. 467-473.

78. Patwardhan A. and Havey RM., *A follower load increases the load-carrying capacity of the lumbar spine in compression.* Spine, 1999. **24**: p. 1003-1009.

79. Patwardhan A, Meade K, and Lee B, *A Frontal Plane Model of the Lumbar Spine Subjected to a Follower Load: Implications for the Role of Muscles.* J Biomech Eng, 2001. **123**(3): p. 212-217.

80. Driscoll, C.R., et al., *Impact of Prone Surgical Positioning on the Scoliotic Spine.* J Spinal Disord Tech, 2011.

81. McNally DS. and Adams MA., *Internal intervertebral disc mechanics as revealed by stress profilometry.* Spine, 1992. **17**(1): p. 66-73.

82. Steffen T, et al., *Lumbar intradiscal pressure measured in the anterior and posterolateral annular regions during asymmetrical loading.* Clin Biomech, 1998. **13**: p. 495-505.

83. Keller TS., et al., *Regional variations in the compressive proeprties of lumbar vertebral trabeculae. Effects of disc degeneration.* Spine, 1989. **14**(9): p. 1012-1019.

84. Shirazi-Ald A and Parnianpour M, *Load-bearing and stress analysis of the human spine under a novel wrapping compression loading.* Clinical Biomechanics, 2000. **15**: p. 718-725.

85. Stokes I.A. and Gardner-Morse M., *Muscle activation strategies and symmetry of spinal loading in the lombar spine with scoliosis.* Spine, 2004. **29**(19): p. 2103-2107.

86. Ledet, E.H., et al., *Direct real-time measurement of in vivo forces in the lumbar spine.* The Spine Journal, 2005. **5**(1): p. 85-94.

87. Tulsi R, *Growth of the human vertebral column An osteological study.* Acta anat, 1971. **79**: p. 570-580.

88. Dimeglio, A., *Growth in pediatric orthopaedics.* J Pediatr Orthop, 2001. **21**(4): p. 549-55.

89. Schwab F, et al., *A porcine model for progressive thoracic scoliosis.* Spine, 2009. **34**(11): p. E397-E404.

90. Taylor J, *Growth of human intervertebral disc and vertebral bodies.* J. Anat., 1975. **120**(1): p. 49-68.

91. Stokes IA, W.L., *Vertebral Height Growth Predominates Over Intervertebral Disc Height Growth in Adolescents With Scoliosis.* Spine, 2006. **31**(14): p. 1600-1604.

92. Brick E and Copel J, *The ring apophysis of the human vertebra; contribution to human osteogeny. II.* J Bone and Joint Surg Am, 1951. **33-A**(3): p. 783-787.

93. Risser J, *The Iliac apophysis; an invaluable sign in the management of scoliosis.* Clin Orthop, 1958. **11**: p. 111-119.

94. Price J.S., Oyajobi B.O., and Russell R.G.G., *The cell biology of bone growth.* Eur. J Clin Nutr., 1994. **48**(Suppl 1): p. 131-149.

95. Stokes, I.A., et al., *Modulation of vertebral and tibial growth by compression loading: diurnal versus full-time loading.* Journal of Orthopaedic Research, 2005. **23**(1): p. 188-195.

96. Stokes IA, M.P., Iatridis J, Farnum C, Aronsson D, *Enlargement of Growth Plate Chondrocytes Modulated by Sustained Mechanical Loading.* J Bone and Joint Surgery, 2002. **84**: p. 1842-1848.

97. Stokes IA., *Mechanical effects on skeletal growth.* J Musculoskel Neuron Interact, 2002. **2**(3): p. 277-280.

98. Lerner, A.L., J.L. Kuhn, and S.J. Hollister, *Are regional variations in bone growth related to mechanical stress and strain parameters?* Journal of Biomechanics, 1998. **31**(4): p. 327-335.

99. Hall-Craggs ECB. and Lawrence CA., *The effects of epiphyseal stapling on growth in length of the rabbits tibia and femur.* J Bone and Joint Surgery, 1969. **51B**(2): p. 359-365.

100. Hall-Crags, E.C.B., *The effect of experimental epiphysiodesis on growth in length of the rabbit's tibia.* J Bone and Joint Surgery, 1968. **50-B**: p. 392.

101. McGibbon K, D.A., *Experience in growth retardation with heave vitallium staples.* J Bone and Joint Surgery, 1962. **44-B**(1): p. 86.

102. Roaf, R., *Vertebral growth and its mechanical control.* J Bone Joint Surg [Br], 1960. **42**(1): p. 40-59.

103. Arkins A, K.J., *The effect of pressure on epiphyseal growth: The mechanism of plasticity of growing bone.* J Bone and Joint Surgery, 1956. **38**: p. 1056-1076.

104. Churches A, H.C., *Functional adaptation of bone in responce to sinusoidally varying controlled compressive loading of the ovine metacarpus.* Clin Orthop, 1982. **168**: p. 265-280.

105. Rubin C T, L.L.E., *Regulation of bone formation by applied dynamic loads.* J Bone and Joint Surgery, 1984. **66**: p. 397-402.

106. Akyuz, E., et al., *Static versus dynamic loading in the mechanical modulation of vertebral growth.* Spine, 2006. **31**(25): p. E952-8.

107. Robling, A.G., et al., *Modulation of appositional and longitudinal bone growth in the rat ulna by applied static and dynamic force.* Bone, 2001. **29**(2): p. 105-113.

108. Stokes, I.A., et al., *Mechanical modulation of vertebral and tibial growth: diurnal versus full-time loading.* Stud Health Technol Inform, 2002. **91**: p. 97-100.

109. Stokes, I.A., et al., *Mechanical modulation of intervertebral disc thickness in growing rat tails.* J Spinal Disord, 1998. **11**(3): p. 261-5.

110. Wolff J., *Das Gesetz der Transformation der knoken*. 1892, Berlin:Hirshwald.

111. Stokes, I.A. and J.P. Laible, *Three-dimensional osseo-ligamentous model of the thorax representing initiation of scoliosis by asymmetric growth.* J Biomech, 1990. **23**(6): p. 589-95.

112. Turner, C.H., *Three rules for bone adaptation to mechanical stimuli.* Bone, 1998. **23**(5): p. 399-407.

113. Grant JP., et al., *The effects of bone mineral density and disc degeneration on the structural property distribution in the lower lumbar vertebral endplates.* J of Orthopaedic Research, 2002. **20**: p. 1115-1120.

114. Rumancik S., et al., *Assessment of Bone Quality and Distribution in Adult Lumbar Scoliosis: New Dual-Energy X-ray Absorptiometry Methology and Analysis.* Spine, 2005. **30**(4): p. 434-439.

115. Denoel, C., et al., *Idiopathic scoliosis and breast asymmetry.* J Plast Reconstr Aesthet Surg, 2009. **62**(10): p. 1303-8.

116. Cheng, J.C. and X. Guo, *Osteopenia in adolescent idiopathic scoliosis. A primary problem or secondary to the spinal deformity?* Spine (Phila Pa 1976), 1997. **22**(15): p. 1716-21.

117. Richardson, M., *Approches to Differentila Diagnosis in Musculoskeletal Imaging*. 2006, University of Washington School of Medicine.

118. Cobb, J.R., *Outline for the study of scoliosis.* Am Acad Orthop Surg Instruct Lect, 1948. **5**: p. 261-275.

119. Sangole, A.P., et al., *Three-dimensional classification of thoracic scoliotic curves.* Spine (Phila Pa 1976), 2009. **34**(1): p. 91-9.

120. Pratt RK, B.R., web JK. *The role of the rib-cage in infantile idiopathic scoliosis (IIS)*. in *Scientific Meeting*. 1997. Nottingham.

121. Piggott H, *Posterior rib resection in scoliosis.* J Bone and Joint Surgery, 1971. **53B**: p. 663-671.

122. Kesling, K.L. and K.A. Reinker, *Scoliosis in twins. A meta-analysis of the literature and report of six cases.* Spine (Phila Pa 1976), 1997. **22**(17): p. 2009-14; discussion 2015.

123. Bagnall K., et al., *Pineal Transplantation after pinealectomy in young chickens has no effect on the development of scoliosis.* Spine, 2001. **26**(9): p. 1022-1027.

124. Machida, M., et al., *Pathologic Mechanism of Experimental Scoliosis in Pinealectomized Chickens.* Spine, 2001. **26**(17): p. E385-391.

125. Turgut M., et al., *The effects of pineal gland transplantation on the production of spinal deformity and serum melatonin level following pinealectomy in the chicken.* Eur Spine J, 2003. **12**: p. 487-494.

126. Cheung K, e.a., *The Effect of Pinealectomy on Scoliosis Development in Young Nonhuman Primates.* Spine, 2005. **30**(18): p. 2009-2013.

127. Moreau A, W.S., Forget S, et al., *Melatonin Signaling Dysfunction in Adolescent Idiopathis Scoliosis.* Spine, 2004. **29**(16): p. 1772-1781.

128. Moreau A, et al. *Elevated Plasma Factor P is Involved in AIS Onset and Curve Progression*. in *SRS 43rd Annual Meeting*. 2008. Salt Lake City, Utah, USA.

129. Pincott JR, T.L., *Experimental scoliosis in primates: A neurological cause.* J Bone and Joint Surgery [Br], 1982. **64**: p. 503-507.

130. Yamada K, Y.H., Nakagawa Y, et al, *Etiology of idiopathic scoliosis.* Clinical Ortho, 1984. **184**: p. 50-57.

131. Duval-Beaupère G, D.J., Queneau P. , *Pour une Théorie Unique de L'Évolution des Scolioises.* Presse Med, 1970. **78**: p. 1141-1146.

132. Little DG., et al., *Relationship of peak heigth velocity to other maturity indicators in idiopathic scoliosis in girls.* J Bone and Joint Surgery, 2000. **82**(5): p. 685-693.

133. Yann Philipe Charles, J.-P.D., Vincenzo de Rossa, and Alain Diméglio, *Progression Risk of Idiopathic Juvenile Scoliosis During Pubertal Growth.* Spine, 2006. **31**(17): p. 1933-1942.

134. Nachemson, A., *Disc pressure measurements.* Spine, 1981. **6**(1): p. 93-97.

135. Stokes, I., Burnwell, R., and Dangerfield, P., *Biomechanical spinal growth modulation and progressive adolescent scoliosis - a test of the 'vicious cycle' pathogenetic hypothesis: Summary of an electronic focus group debate.* Scoliosis, 2006. **1**(16).

136. Parent S, L.H., Skalli W, and Guise J *Vertebral wedging characteristics changes in scoliotis spines.* Spine, 2004. **29**(20): p. E455-E462.

137. Beguiristian J., et al., *Experimental Scoliosis by epiphysiodesis in pigs.* Intern. Orthopaedics, 1980. **3**: p. 317-321.

138. Zhang H and Sucato D, *Unilateral Pedical Screw Epiphysiodesis of the Neurocentral Synchondrosis.* J bone and Joint Surg, 2008. **90**: p. 2460-2469.

139. Yamazaki, A., D.E. Mason, and P.A. Caro, *Age of closure of the neurocentral cartilage in the thoracic spine.* J Pediatr Orthop, 1998. **18**(2): p. 168-72.

140. Will, R.E., et al., *Cobb angle progression in adolescent scoliosis begins at the intervertebral disc.* Spine (Phila Pa 1976), 2009. **34**(25): p. 2782-6.

141. Blount WP, S.A., Keever ED, et al., *The Milwaukee Brace in the operative treatment of scoliosis.* J Bone and Joint Surgery, 1958. **40**: p. 511-525.

142. Watts HG, H.J., Stanish W, *The Boston brace system for the treatment of low thoracic and lumbar scoliosis by the use of a girdle without superstructure.* Clin Orthop, 1977. **126**: p. 87-92.

143. Basset GS, B.W., MacEwen GD, *Treatment of idiopathic scoliosis with the Wilmington brace.* J Bone and Joint Surgery, 1986. **68**: p. 602-605.

144. Noonan K, D.L., Jacobson W, et al, *Long-Term Psychological Characteristics of Patients Treated for Idiopathic Scoliosis.* Pediartr Orthop, 1997. **17**: p. 712-717.

145. Castro, J.F.P., *Adolescent idiopathic scoliosis, bracing, and the Hueter-Volkmann principle.* The Spine Journal, 2003. **3**(3): p. 180-185.

146. Goldberg, C.J., et al., *Adolescent idiopathic scoliosis: the effect of brace treatment on the incidence of surgery.* Spine, 2001. **26**(1): p. 42-7.

147. Clin, J., et al., *A biomechanical study of the Charleston brace for the treatment of scoliosis.* Spine (Phila Pa 1976), 2010. **35**(19): p. E940-7.

148. Clin, J., et al., *Biomechanical modeling of brace treatment of scoliosis: effects of gravitational loads.* Med Biol Eng Comput, 2011.

149. Clin, J., et al., *Comparison of the biomechanical 3D efficiency of different brace designs for the treatment of scoliosis using a finite element model.* Eur Spine J, 2010. **19**(7): p. 1169-78.

150. Clin, J., et al., *Correlation between immediate in-brace correction and biomechanical effectiveness of brace treatment in adolescent idiopathic scoliosis.* Spine (Phila Pa 1976), 2010. **35**(18): p. 1706-13.

151. Delorme S, L.H., Poitras et al, *Pre-,intra-, and postoperative 3D evaluation of AIS.* J Spinal Disorders, 2000 **13**: p. 93-101.

152. Dubousset J, H.T., Shaffelbarger H, *The crankshaft phenomenon.* Journal of Pediatric Orthopedics, 1989. **9**: p. 541-550.

153. Wittek, *Operative Behandlung der Skoliose, Zeitschrift fur Orthopadische.* Chirurgie, 1924. **44**: p. 226-235.

154. Nachlas, I.W. and J.N. Borden, *The cure of experimental scoliosis by directed growth control.* J Bone Joint Surg Am, 1951. **33**(1): p. 24-34.

155. Smith A., Von Lackum W., and W. R., *An operation for stapling vertebral bodies in congenital scoliosis.* J Bone and Joint Surgery, 1954. **36**: p. 342-348.

156. Roaf, R., *The treatment of progressive scoliosis by unilateral growth-arrest.* J Bone and Joint Surgery, 1963. **45B**: p. 637-651.

157. Carpintero P., et al., *Scoliosis induced by asymmetric lordosis and rotation: an experimental study.* Spine, 1997. **22**(19): p. 2202-2206.

158. Rumpf C., Lang R., and Gotz M., *Evaluation of four different laser systems for a minimally invasive scoliosis treatment.* J of Selected Topics in Quantum Electronics, 1999. **5**(4): p. 1067-1071.

159. Newton P, et al., *Multilevel Spinal Growth Modulation with an Anterolateral Flexible Tether in an Immature Bovine Model.* Spine, 2005. **30**(23): p. 2608-2613.

160. Newton, P.O., et al., *Asymmetrical flexible tethering of spine growth in an immature bovine model.* Spine, 2002. **27**(7): p. 689-93.

161. Braun, J.T., et al., *Experimental scoliosis in an immature goat model: a method that creates idiopathic-type deformity with minimal violation of the spinal elements along the curve.* Spine, 2003. **28**(19): p. 2198-203.

162. Betz R, et al., *Vertebral body stapling procedure for the treatment of scoliosis in the growing child.* Clinical Orthopaedics and Related Research, 2005. **434**: p. 55-60.

163. Betz, R.R., et al., *An Innovative Technique of Vertebral Body Stapling for the Treatment of Patients with Adolescent Idiopathic Scoliosis: A Feasibility, Safety and Utility Study.* Spine, 2003. **28**(20S): p. 255-265.

164. Newton, P.O., et al., *Spinal growth modulation with use of a tether in an immature porcine model.* J Bone Joint Surg Am, 2008. **90**(12): p. 2695-706.

165. Schmid, E.C., et al., *A novel fusionless vertebral physeal device inducing spinal growth modulation for the correction of spinal deformities.* Eur Spine J, 2008. **17**(10): p. 1329-35.

166. Newton, P.O., et al., *Effects of intraoperative tensioning of an anterolateral spinal tether on spinal growth modulation in a porcine model.* Spine (Phila Pa 1976), 2011. **36**(2): p. 109-17.

167. Braun JT., et al. *Fussionless scoliosis correction using a shape memory alloy staple in the anterior thoracic spina of the immature goat*. in *Scoliosis Research Society Annual Meeting*. 2000. Carns, Australia.

168. Guille J, Andrea L, and Betz R, *Fussionless treatment of scoliosis.* Orthop Clin North Am, 2007. **38**: p. 541-545.

169. Braun John, J.W., Ephraim A, Darrel B, and Kent B, *Fussionless Scoliosis Correction Using a Shape Memory Alloy Staple in the Anterior Thoracic Spine of the Immature Goat.* Spine, 2004. **29**: p. 1980-1989.

170. Bylski-Austrow, D.I., et al., *Spinal hemiepiphysiodesis decreases the size of vertebral growth plate hypertrophic zone and cells.* J Bone Joint Surg Am, 2009. **91**(3): p. 584-93.

171. Bylski-Austrow D, et al. *In Vivo Compressive Stresses In The Intervertebral Disc*. in *North American Congress on Biomechanics*. 2008. Ann Arbor, Michigan.

172. Lowe T., et al., *A posterior tether for fusionless modulation of sagittal plane growth in a sheep model.* Spine, 2005. **30**(17S): p. S69-S74.

173. Newton P, et al., *Spinal Growth Modulation with an Anterolateral Flexible Tether in an Immature Bovine Model.* Spine, 2008. **23**(7): p. 724-733.

174. Braun, J.T., et al., *Three-dimensional analysis of 2 fusionless scoliosis treatments: a flexible ligament tether versus a rigid-shape memory alloy staple.* Spine, 2006. **31**(3): p. 262-8.

175. Borodic, G.E., *Non-surgical modulation of spinal curvature in vertebrates - partic. for children, by injecting acetyl:choline transmission inhibitor which mimics effects of botulinum toxin*, BORODIC G E (BORO-Individual).

176. Betz, R., T. Drewry, and M.C. Sherman, *Apparatus for use in the correction of spinal deformities*. 1999, SDGI HOLDINGS INC (SDGI-Non-standard): US.

177. Guille J., et al., *The feasibility, safety, and utility of vertebral wedge osteotomies for the fusionless treatment of paralytic scoliosis.* Spine, 2003. **28**(20S): p. S266-S274.

178. Braun, J.T., et al., *Bone anchor for spinal stabilization system has head extended from proximal end of anchor body and positioned outside vertebra if anchor body engages to vertebra by engaging thread form of anchor body with undisturbed bone of vertebra*, BRAUN J T (BRAU-Individual) MOLZ F J (MOLZ-Individual) DREWRY T D (DREW-Individual) SHERMAN M C (SHER-Individual) SDGI HOLDINGS INC (SDGI-Non-standard) WARSAW ORTHOPEDIC INC (WARS-Non-standard).

179. Dodge, G.R. and J.R. Bowen, *Bone growth arresting device for e.g. leg, has power source for generating current, and lead in electrical communication with power source for applying current to electrode that applies current to preset location of bone*, DODGE G R (DODG-Individual) BOWEN J R (BOWE-Individual).

180. Braun, J.T., et al., *Implant for treatment of curved spinal column segment, has body that distracts spinal column segment along concavely curved surface toward straightened configuration while permitting motion of spinal column segment*, BRAUN J T (BRAU-Individual) MOLZ F J (MOLZ-Individual) JUSTIS J R (JUST-Individual) SDGI HOLDINGS INC (SDGI-Non-standard) WARSAW ORTHOPEDIC INC (WARS-Non-standard).

181. Blain, J., *Spinal disorder treating device for treating spinal disorders, comprises prosthesis with two faces*, BLAIN J (BLAI-Individual) QUANTUM ORTHOPEDICS (QUAN-Non-standard).

182. Kiester, P.D., *Spine`s scoliotic curve correcting method, involves producing controlled force by expansion of the rod over at extended time period, and stretching curve between*

selected portions using force until desired curve is obtained, KIESTER P D (KIES-Individual).

183. Serhan, H.A., et al., *Spinal anchoring system for treatment of spinal deformities e.g. scoliosis has low profile spinal anchoring device that maintains flexible elongate tether in fixed position*, DEPUY SPINE INC (DEPU-Non-standard).

184. Hudgins, R.G., M.E. Lancial, and H.D. Hestad, *Facet implant for use in treating e.g. scoliosis, has facet bearing body between opposing facets, and fixation tab fixable to one vertebra, where band provides restraining force to control relative movement of opposing facets*, ZIMMER SPINE INC (ZIMM-Non-standard).

185. Tebbe, S., M. Altarac, and D.H. Kim, *Interspinous spacer device for treatment of e.g. human spine, has actuator shaft disposed within body with distal end configured such that distal motion of actuator shaft contacts tips at proximal ends*, VERTIFLEX INC (VERT-Non-standard).

186. Altarac, M., S. Tebbe, and C.J. Flaherty, *Spinal motion segment stabilizing device for arthrodesis treatment has actuator shaft which contacts tips of proximal ends of superior and inferior U shaped sections through distal motion so that U shaped sections are rotated*, VERTIFLEX INC (VERT-Non-standard).

187. Flaherty, J.C., M. Altarac, and S. Tebbe, *Device for stabilizing spinal motion segment, has expandable spacer comprising deployed configuration and undeployed configuration, and axial and radial dimensions for positioning between spinous processes of adjacent vertebrae*, VERTIFLEX INC (VERT-Non-standard) FLAHERTY J C (FLAH-Individual).

188. Kim, R.C., *Magnetic spinal implant device has magnet coupled to implant piece, which exerts repelling or attracting magnetic force on another magnet coupled to another piece*, KIM R C (KIMR-Individual).

189. Betz, R.R., et al., *Spinous process implant for treating e.g. back pain, has elastomeric cuffs sized and configured to encase minor portions of two different spinous processes, where cuffs are attached to one another*, SPINEMEDICA CORP (SPIN-Non-standard).

190. Bruneau, A., et al., *Spinal stabilization system comprises bone anchor assemblies; and connecting element including support portion between anchor engaging end portions, and stabilizer extending between and engaged to supporting elements of support portion*, SDGI HOLDINGS INC (SDGI-Non-standard).

191. Jahng, T., J. Yim, and B.S. Bowman, *Flexible connection unit for use in spinal fixation device, has spacer provided between end portions of rod, and cladding separating spacer from portions and wire so that spacer do not rub against with portions and wire*, JAHNG T (JAHN-Individual) YIM J (YIMJ-Individual) BOWMAN B S (BOWM-Individual).

192. Zucherman, J.F., et al., *Spinal implant for use during extensive implantation procedure, has binder positioned around spinous processes, and guides positioned adjacent to one of*

two wings such that guides are spaced from each other, ST FRANCIS MEDICAL TECHNOLOGIES LLC (SFRA-Non-standard).

193. Campbell, R.M., *Expandable vertical prosthetic rib - has rib shaft fitting adjustably in sleeve and has integral attachment ends, allowing growth adjustments*, CAMPBELL R M (CAMP-Individual).

194. Wall, E.J., D.I. Bylski-Austrow, and J.E. Reynolds, *Spinal staple used for treating scoliosis, has fastener retaining portion provided to end of bridge in manner in which it will have one side facing one side of fastener retaining portion of adjacent staple*, WALL E J (WALL-Individual) BYLSKI-AUSTROW D I (BYLS-Individual) WALL M D E J (WALL-Individual) CHILDREN'S HOSPITAL MEDICAL CENT (CHIL-Non-standard) REYNOLDS J E (REYN-Individual).

195. Gaines, R.W., *System for anterolateral surgical correction of such conditions such as scoliosis, involves using an improved surgical implant spinal staple having tines for fastening and anchoring staple to vertebral body*, GAINES R W (GAIN-Individual).

196. Sybert, D.R., et al., *Repairing spinal disorder, e.g. kyphosis, comprises affixing biocompatible osteogenic band to vertebra*, OSTEOTECH INC (OSTE-Non-standard) SYBERT D R (SYBE-Individual) SHIMP L A (SHIM-Individual) BOYCE T M (BOYC-Individual) BOYLE J W (BOYL-Individual).

197. Lieberman, I.H., *Correction apparatus for spinal deformity, e.g. scoliosis, has anchor which includes helical spikes having tip portions at distal ends which penetrate into vertebral body as platform is rotated*, CLEVELAND CLINIC FOUND (CLEV-Non-standard).

198. Zhang, H., et al., *Anterior spinal instrumentation method for treating spinal deformities, involves inserting cancellous screws into cephalad and caudal end vertebrae at anterior portion of convex side of deformity through spinal plates*, TEXAS SCOTTISH RITE HOSPITAL CRIPPLED (TEXA-Non-standard) SDGI HOLDINGS INC (SDGI-Non-standard) ZHANG H (ZHAN-Individual) JOHNSTON C E (JOHN-Individual) PIERCE W A (PIER-Individual) ASHMAN R B (ASHM-Individual) TEXAS SCOTTISH RITE HOSPITAL FOR CHILDRE (TEXA-Non-standard).

199. Carl, A.L., D. Sachs, and M. Rosenberg, *Spine implant system for treatment of pain associated with spine, has reinforcement system to support implant device coupled to spinous protrusion*, VERTECH INNOVATIONS LLC (VERT-Non-standard) CARL A L (CARL-Individual) SACHS D (SACH-Individual).

200. Carl, A.L., D. Sachs, and M. Rosenberg, *Spine implant, has joint prosthesis exerting distraction force between facets of facial joint, and ball bearing providing bearing surface for motion of facets, and posts that are screwed in facets*, CARL A L (CARL-Individual) SACHS D (SACH-Individual) ROSENBERG M (ROSE-Individual).

201. Lim, R.K., M.C. Sherman, and R. Lim, *Interspinous spacer for use during laminectomy, has anchoring plates securing spacer to vertebra, and two saddles disposed on superior arch and inferior arch to receive spinous process of superior vertebrae and inferior vertebrae*, SDGI HOLDINGS INC (SDGI-Non-standard).

202. Bruneau, A., et al., *Expandable spinal rod used in surgical treatment of spinal disorder e.g. scoliosis, fracture has intermediate section expandable between first and second size to space first and second rod ends apart*, WARSAW ORTHOPEDIC INC (WARS-Non-standard) BRUNEAU A (BRUN-Individual) LANGE E C (LANG-Individual) ALLARD R N (ALLA-Individual) ANDERSON K M (ANDE-Individual).

203. Justis, J.R. and H.H. Trieu, *Expandable spinal rod used in surgical treatment of spinal disorder e.g. scoliosis, fracture has rails preventing interior cavity from collapsing axially along longitudinal axis during insertion of spinal rod into patient*, WARSAW ORTHOPEDIC INC (WARS-Non-standard) SDGI HOLDINGS INC (SDGI-Non-standard).

204. Dawson, J., *Implantable orthopedic system for stabilizing spinal column comprises bone anchors having head portion including cord receiving portion and clamping mechanism to secure cord to anchor; and incompressible spacer with cord receiving channel*, ZIMMER SPINE INC (ZIMM-Non-standard).

205. Dipoto, G., A.E. Shluzas, and G.P. Dipoto, *Spinal stabilization apparatus for treating adjacent level degenerative disc disease, has spacer device intermittently interacting with adjacent spinal level, and having spacer to be inserted between spinous processes of vertebras*, ENDIUS INC (ENDI-Non-standard).

206. Malandain, H.F., A.A. Edidin, and A.C. Kohm, *Implant expansion apparatus for treatment of spinal condition such as spinal stenosis has rod with portion disposed within shaft and distal end portion configured to releasably engage interspinous implant*, KYPHON INC (KYPH-Non-standard) MALANDAIN H F (MALA-Individual) EDIDIN A A (EDID-Individual).

207. Aubin CE (S-L, C., et al., *Fusionless Vertebral Physeal Device and Method*. 2009: United States.

208. Lalonde, N.M., et al., *Biomechanics of the intra-operative lateral decubitus position for the scoliotic spine: effect of the pelvic obliquity.* Stud Health Technol Inform, 2010. **158**: p. 95-100.

209. Stokes I and Gardner-Morse M, *Muscle activation strategies and symmetry of spinal loading in the lumbar spine with scoliosis.* Spine, 2004. **1**(19): p. 2103-2107.

210. Meir A., et al., *High pressures and asymmetrical stresses in the scoliotic disc in the absence of muscle loading.* Scoliosis, 2007. **2**: p. article 4.

211. Stokes I.A., *Axial Rotation Component of Thoracic Scoliosis.* Journal of Orthopaedic Research, 1989. **7**: p. 702-708.

212. Aronsson D., et al., *Surgical correction of vertebral axial rotation in adolescent idiopathic scoliosis: prediction by lateral bending films.* Journal of Spinal Disorders, 1996. **9**(3): p. 214-219.

213. Wojcik A., Webb J., and Burwell R., *Harrington-Luque, Cotrel-Dubousset instrumentation for idiopathic thoracic scoliosis: a postoperative comparison using segmental radiologic analysis.* Spine, 1990. **15**(5): p. 424-431.

214. Mahar, A.T., et al., *Biomechanics of cantilever "plow" during anterior thoracic scoliosis correction.* Spine J, 2006. **6**(5): p. 572-6.

215. Lenke, L.G., *Lenke classification system of adolescent idiopathic scoliosis: treatment recommendations.* Instr Course Lect, 2005. **54**: p. 537-42.

216. Gremion, G., et al., *[Tomodensitometry measurements of proximal tibia and acceleration in marathon athletes].* Rev Med Suisse Romande, 2004. **124**(2): p. 77-9.

217. Cann, C.E. and H.K. Genant, *Precise measurement of vertebral mineral content using computed tomography.* J Comput Assist Tomogr, 1980. **4**(4): p. 493-500.

218. Nault ML, et al., *Spine Morphologic Differences at First Visit between Non Evolutive and Evolutive Adolescent Idiopathic Scoliosis* Stud Health Technol Inform, 2010. **7**: p. 189.

219. Beaudette, K., et al., *Towards a handheld probe based on optical coherence tomography for minimally invasive spine surgeries.* Stud Health Technol Inform, 2010. **158**: p. 49-54.

220. McLain, R.F., S.A. Yerby, and T.A. Moseley, *Comparative morphometry of L4 vertebrae: comparison of large animal models for the human lumbar spine.* Spine (Phila Pa 1976), 2002. **27**(8): p. E200-6.

221. Cotterill, P.C., et al., *An anatomical comparison of the human and bovine thoracolumbar spine.* J Orthop Res, 1986. **4**(3): p. 298-303.